INFORMATION TO USERS

This reproduction was made from a copy of a manuscript sent to us for publication and microfilming. While the most advanced technology has been used to photograph and reproduce this manuscript, the quality of the reproduction is heavily dependent upon the quality of the material submitted. Pages in any manuscript may have indistinct print. In all cases the best available copy has been filmed.

The following explanation of techniques is provided to help clarify notations which may appear on this reproduction.

1. Manuscripts may not always be complete. When it is not possible to obtain missing pages, a note appears to indicate this.

2. When copyrighted materials are removed from the manuscript, a note appears to indicate this.

3. Oversize materials (maps, drawings, and charts) are photographed by sectioning the original, beginning at the upper left hand corner and continuing from left to right in equal sections with small overlaps. Each oversize page is also filmed as one exposure and is available, for an additional charge, as a standard 35mm slide or in black and white paper format.*

4. Most photographs reproduce acceptably on positive microfilm or microfiche but lack clarity on xerographic copies made from the microfilm. For an additional charge, all photographs are available in black and white standard 35mm slide format.*

***For more information about black and white slides or enlarged paper reproductions, please contact the Dissertations Customer Services Department.**

Darsillo, Michael Steven

THE PHOTOCHEMISTRY AND PHOTOCATALYTIC REACTIONS OF IRON CARBONYLS ADSORBED ONTO POROUS VYCOR GLASS

City University of New York PH.D. 1986

PLEASE NOTE:

In all cases this material has been filmed in the best possible way from the available copy. Problems encountered with this document have been identified here with a check mark __✓__.

1. Glossy photographs or pages _____
2. Colored illustrations, paper or print _____
3. Photographs with dark background __✓__
4. Illustrations are poor copy _____
5. Pages with black marks, not original copy _____
6. Print shows through as there is text on both sides of page _____
7. Indistinct, broken or small print on several pages __✓__
8. Print exceeds margin requirements _____
9. Tightly bound copy with print lost in spine _____
10. Computer printout pages with indistinct print _____
11. Page(s) _____ lacking when material received, and not available from school or author.
12. Page(s) _____ seem to be missing in numbering only as text follows.
13. Two pages numbered _____. Text follows.
14. Curling and wrinkled pages _____
15. Dissertation contains pages with print at a slant, filmed as received _____
16. Other _____

_____

_____

University
Microfilms
International

THE PHOTOCHEMISTRY AND PHOTOCATALYTIC REACTIONS OF IRON CARBONYLS ADSORBED ONTO POROUS VYCOR GLASS

by

MICHAEL S. DARSILLO

A dissertation submitted to
the Graduate Faculty in Chemistry
in partial fullfillment of the
requirements for the degree of
Doctor of Philosophy, the City
University of New York

1986

This manuscript has been read and accepted for the Graduate Faculty in Chemistry in satisfaction of the dissertation requirement for the degree of Doctor of Philosophy.

1/21/86
date

Harry D. Gafney
Chairman of Examining Committee

1/21/86
date

A. M.
Executive Officer

Richard Pasternack
Arthur T. Baker

Supervisory Committee

The City University of New York

Abstract

A Study of the Photochemical and Photocatalytic Reactions of Iron Carbonyls Adsorbed Onto Porous Vycor Glass

by

Michael S. Darsillo

Advisor: Professor Harry D. Gafney

$Fe(CO)_5$ and $Fe_3(CO)_{12}$ physisorb onto PVG without significant change in their electronic or vibrational spectra, however, $Fe_2(CO)_9$ undergoes disproportionation upon adsorption to yield $Fe(CO)_5$ and $Fe_3(CO)_{12}$. UV photolysis of $Fe(CO)_5$(ads) in vacuo leads to formation of the tetracarbonyl with a quantum yield of unity. The tetracarbonyl rapidly reacts with the PVG surface and chemisorbed water to form the spectrally distinct, oxidative addition products H-$Fe(CO)_4$-OSi and H-$Fe(CO)_4$-OH. These primary photoproducts undergo secondary photolysis to form, depending on the intial loading, either elemental iron or the trimeric cluster, $Fe_3(CO)_{12}$. Diffuse reflectance FTIR spectroscopy, recorded after cw or pulsed laser excitation, establish the presence of dimeric and trimeric intermediates. Trapping experiments with CO and trimethylphosphine indicate a photochemically driven, stepwise reaction sequence in which the intermediates leading to cluster formation are more highly unsaturated intermediates, principally $Fe(CO)_3$.

Diffuse reflectance FTIR spectra, recorded after cw excitation of $Fe(CO)_5$(ads) under 100 torr of olefin, establish the presence of of a host of monomeric and dimeric catalytically active iron carbonyl-olefin complexes. The photocatalyzed isomerization of 1-pentene by the $Fe(CO)_5$-PVG hybrid system occurs with a quantum yield of 155 ± 2.0, indicating photogeneration of species which are extremely efficient alkene isomerization catalysts at ambient temperature. The trans/cis ratio for the reaction differs from that found in fluid solution and is similar to the product distribution observed for iron carbonyl complexes containing bulky ligands in their coordination sphere.

UV photolysis of $Fe_3(CO)_{12}$(ads) results in CO evolution along with H_2 and CH_4 evolution. Periodic analysis of the gaseous effluent surrounding the photolyzed sample, in conjunction with spectral analysis, indicate that CH_4 evolution is mediated by an irreversibly oxidized iron species. The formation of photoinduced high resolution optical density changes using the $Fe(CO)_5$-PVG system has also been investigated.

Acknowledgements

I would like to express my appreciation to my thesis mentor, Professor Harry D. Gafney, for his supervision in directing this thesis work and for making my graduate education a rich and rewarding experience.

To Dr. Michael S. Paquette, who provided his knowledge, talents and ideas in contributing to this work, and to his family for the kindness and generosity shown to me during my stay in Michigan. Thanks to Professor Arthur D. Baker and Professor Thomas C. Strekas whose helpful discussions during our group meetings aided in this work. To Ottmar Safferling, who not only fixed my broken glassware, but provided many cups of free coffee and hours of enjoyable conversation.

Thanks to my many friends, in particular Bill Uliano and Carl Arriaga, who throughout the years offered their support and encouragement, thereby making the darkest days of graduate school a little lighter.

Most of all, I would like to thank my parents who provided me with all the love, kindness and understanding a son could ask for, and whose contributions cannot be put into simple words.

TABLE OF CONTENTS

List of Tables

List of Figures

Introduction

A. Introduction

To most chemists the word "catalyst" simply conjurs up memories of the definition learned in introductory chemistry courses: "A catalyst increases the rate of a chemical reaction without affecting the equilibrium by lowering the energy of activation between reactants and products". Indeed, chemists are aware of the important role catalysts play in the chemical industry. From the large scale oil refineries and plastic manufacturers down to the synthetic chemist in the pharmaceutical laboratory producing minute amounts of biologically active drugs, catalysts have become increasingly salient in every part of the chemical industry. In recent years, the rapidly diminishing supply of available petroleum feedstocks has focused attention on development of more highly selective and efficient catalysts which produce gaseous and liquid hydrocarbon fuels and other organic chemicals from non-petroleum sources (eg., coal). Another challenging goal is the development of catalysts which can activate stable chemical bonds such as those in molecular nitrogen, carbon dioxide, or the C-C and C-H bonds in alkanes. If the bond in molecular nitrogen could be economically cleaved to produce nitrogen compounds suitable for fertilizers (nitrogen fixation), or C-C and/or C-H bonds

could be selectively broken to form valuable derivatives, the economic returns could be enormous. While catalytic systems have been developed for these reactions, none of them are currently economically viable. Given the state of the world's dwindling energy resources, and the vast profits attainable, continued research into development of new catalytic systems is necessary.

Generally, catalysts have been divided into two distinct classes, homogeneous and heterogeneous catalysts. A heterogeneous catalyst is immiscible with the gaseous or liquid reaction mixture as compared with a homogeneous catalyst which is soluble in the reaction mixture. There are distinct advantages and disadvantages associated with the use of both types of catalysts. The advantages of using heterogeneous catalysts include the ability to easily recover the catalyst from the reaction mixture, acceptable thermal and mechanical stability, and high activity for a wide range of reactions. However, the fact that the reaction can only occur on the limited surface of the catalyst is a major disadvantage. In addition, characterization of the active species is often difficult, hindering catalyst design and improvement. Finally, reactions using heterogeneous catalysts are often run under severe and costly conditions (eg., high temperatures and pressures). In contrast, the dispersion of a homogeneous catalyst throughout the reaction mixture

offers a level of efficiency not obtainable in heterogeneous systems since the entire catalyst is operational, not just the surface. Additional advantages of homogeneous catalysts are their high selectivity in complex organic reactions due to their activity under mild reaction conditions, and their amenability to study by conventional instrumentation. The major disadvantage associated with homogeneous systems is the inability to easily separate the reaction products from the catalyst. With volatile products distillation offers an easy solution. However, separation of less volatile products from thermally sensitive catalysts is considerably more difficult.

B. Hybrid Catalysts

One approach to the separation problem associated with homogeneous systems is to immobilize a catalytic species that is ordinarily soluble onto an insoluble catalyst support. Such hybrid systems, as pointed out by Baily and Langer, combine advantages of both homogeneous and heterogeneous catalysts (1). The immobilization of transition metal carbonyls onto organic and inorganic supports is of particular interest since the carbonyls of many catalytically active metals are known and are either commercially available or readily synthesized (2). Additional incentives for supporting metal carbonyls

include their well characterized structure and bonding, and their ability to form polynuclear cluster compounds which can catalyze reactions like nitrogen hydrogenation and alkane isomerization that require several active metal sites (3). Finally, catalyst preparation is often simplified since most metal carbonyls are sufficently volatile to allow their deposition directly onto the support from the gas phase. Less volatile metal carbonyls can also be supported via solution impregnation using low boiling organic solvents.

The choice of a support for immobilization of transition metal carbonyls is dependent upon satisfying several basic requirements. The support should be inert to the reaction mixture, be able to withstand the required reaction conditions, and possess an acceptable surface area. Due to the complex nature of surface reactions, an additional requirement is that the support be amenable to spectroscopic techniques so that a fundamental understanding of the nature of reactive, catalytic intermediates can be aquired. Recent advances in surface spectroscopy, (eg., rapid scanning diffuse reflectance FTIR spectroscopy), have allowed characterization of surface confined transient intermediates with subsecond time resolution. Both organic and inorganic supports have been used in supporting metal carbonyls. Typical organic supports

include styrene and acrylic polymers, poly(amino) acids, and crosslinked dextrans, while glass, silica, alumina, zeolites and clays are among the most commonly used inorganic supports (4). Disadvantages of organic supports are their low thermal stability (ca. 433 K), and their tendency to swell when used in organic media. Since diffusion of reactants and products to and from the catalytically active site is often the rate limiting step in hybrid systems, some swelling might be desirable to increase the diffusion rate. However, extensive swelling of the organic polymeric support must be controlled in order to avoid disruption of the catalytically active sites. Inorganic support materials have received the most industrial attention due to their higher thermal stability (ca. 1000 K), and their rigid structure which does not permit swelling. Transport of reactants and products to and from the catalytically active site in inorganic supports occurs by diffusion through the pore structure of the support which allows for preselection of diffusional characteristics under most reaction conditions.

Whether in solution or confined to a support, the catalytic activity of metal carbonyls requires either vacant or labile reaction sites where the substrate can bind and undergo chemical transformation (5-8). In most cases, particularly involving hybrid systems, the

precursor complex is thermally activated generating a highly reactive subcarbonyl species. Since transition metal carbonyls possess a rich photochemistry, the photoactivation of a surface confined complex is an alternate route to catalytically active species (9). Photoinduced ligand dissociation, metal-metal bond cleavage, oxidative addition, and reductive elimination are processes which may lead to catalytically active species (10-12). However, the opacity of many traditional support materials drastically reduces the efficency of any photochemical process due to a nearly complete loss of useful light due to scattering and reflection or to competitive absorption by the support. Even under monolayer coverage, absorption by the support can be the dominant process. Due to the difficulties associated with photochemical activation of hybrid catalysts, the bulk of the literature on hybrid catalysts, particularly that involving iron carbonyl systems, involves thermal activation. The following summarizes the thermal activation of iron carbonyls on a variety of inorganic supports.

C. Thermally Activated Iron Carbonyl Systems.

The interest in supporting iron carbonyl complexes stems from their known ability to homogeneously catalyze carbon monoxide and olefin reactions in which more

economically desirable, complex organic molecules are produced (2,13). Interaction between the surface functionality of the support and the adsorbed iron carbonyl complex often results in changes in the thermal reactions of the surface confined species from those observed in the gas phase or in fluid solution (1). In addition to the chemical nature of the support surface, recent work has emphasized the role of surface dimensionality in the reactions of surface confined species (14,15). The surfaces of many of the currently used supports are not characterized by regular translationally invariant lattices. Rather, these highly irregular surfaces possess a dilation symmetry and are characterized by a fractal or Hausdorff dimension. The latter, which can be less than the dimensionality accessable to a molecule in the gas phase or fluid solution, can impose further constraints on the reactivity of a surface confined molecule. Pieffer and Avnir point out that these geometric factors may outweigh chemical factors in determining the kinematics of surface confined species.

The thermal decomposition of iron carbonyls adsorbed onto zeolite supports has been investigated by several groups. Interesting properties associated with zeolites include their variable cavity sizes, inner electrostatic fields, and acidic and redox properties which allow

introduction of transition metal centers in sites of varying accessibilities. Nagy, van Eenoo, and Derouane (16) have investigated the adsorption, binding, and reactions of $Fe(CO)_5$ on HY zeolite at 400 °C by ^{13}C-NMR spectroscopy. The interaction between the zeolite surface and the adsorbed $Fe(CO)_5$ molecule was determined to be weak as evidenced by the small ^{13}C chemical shift of the carbonyl group of the adsorbed complex (209.9 ppm at 293 K) versus the tabulated value of 209.0 ppm which characterizes pure liquid $Fe(CO)_5$. Additional evidence for the weak interaction of the $Fe(CO)_5$ molecules with the zeolite surface results from the temperature dependence of the NMR linewidth from which the heat of adsorption was calculated to be only 2.0 kcal/mole. Thermal decomposition of the adsorbed complex results in a decrease of the intensity of the ^{13}C line attributed to the carbonyl groups until a CO/Fe ratio of slightly less than unity is observed. In addition, the linewidth was observed to increase from intially 50 Hz value to approximately 140 Hz while the resonanace progressively shifts downfield from 209.9 ppm at 20 °C to 214 ppm after thermal decomposition at 70 C. These investigators propose that the thermal decomposition of $Fe(CO)_5$ supported on HY zeolites occurs stepwise, and leads to dispersed, zerovalent, atomic Fe. The progressive decrease in spectral intensity reflects the progressive loss of CO, while the increase in linewidth shows an

increasing, (although still weak), interaction with the zeolite surface. The absence of an NMR signal when the decomposition has been fully completed, coupled with the appearance of a room temperature ferromagnetic resonance signal, has led these authors to conclude that the thermal decomposition of $Fe(CO)_5$ on this support results in 100% dispersed atomic Fe.

Ballivet-Tkatchenko and Coudurier (17) have also investigated the adsorption and thermal decomposition of iron carbonyls adsorbed on dehydrated HY type zeolite. The thermal decomposition under vacuum was monitored by infrared and mass spectroscopy and gas evolution studies. Although no CO evolution was detected, adsorption of $Fe_3(CO)_{12}$ onto the HY zeolite was accompanied by a spectral change where the visible band that occurs at 605 nm in fluid solution shifts to 630 nm. In spite of the shift in electronic spectrum, the IR spectrum of the adsorbed complex is consistent with the spectrum of $Fe_3(CO)_{12}$ in solution where a threefold axis of symmetry is proposed (18). Nevertheless, modifications in the IR spectrum of the zeolite framework, coupled with the low frequency shifts of the bridging CO stretches, suggests formation of a Lewis acid type adduct formed through interaction of the bridging CO's of $Fe_3(CO)_{12}$ with the surface hydroxyl groups located in the supercage of the zeolite support. In contrast, adsorption of $Fe(CO)_5$ and

$Fe_2(CO)_9$ results in a slight evolution of CO and identical IR spectra for the two adsorbed complexes. The IR spectra have been assigned to that of $Fe(CO)_5$(ads) superimposed with that of a monosubstituted $Fe(CO)_4$ species (19). Thus, the surface reaction upon adsorption results in dissociation of $Fe_2(CO)_9$ and $Fe(CO)_5$ via substitution of one carbonyl ligand by a lattice oxygen on the support. The zeolite, due to the presence of its surface hydroxyl groups, is capable of stabilizing the unsaturated $Fe(CO)_4$ species allowing its IR characterization.

The progressive thermal decomposition of the $Fe_3(CO)_{12}$/HY zeolite system from 60 to 250 °C under vacuum leads to gradual decarbonylation of the adsorbed complex. At the final temperature, 250 °C, approximately 12 moles of CO hve been evolved per mole of $Fe_3(CO)_{12}$ adsorbed. At 200 °C, H_2 and CO_2 are simultaneously evolved, while at 250 °C the formation of CH_4 is observed. H_2 evolution, indicative of a redox reaction between the metal and surface hydroxyl groups of the support, is evidence that the decarbonylated iron species undergoes oxidation (20). The IR spectrum obtained following adsorption of NO (21) and CO (22) onto the thermally decomposed sample clearly indicates that the iron is in a +2 oxidation state. Evacuation of the $Fe(CO)_5$-$Fe_2(CO)_9$/HY zeolite systems for one hour at 60 °C resulted in the evolution of 1 ± 0.3 moles

of CO/mole of adsorbed complex, with the sample visibly turning green (λ max = 630 nm). In addition, the infrared spectra were observed to change with time to yield spectra identical to that of the $Fe_3(CO)_{12}$ sample. The formation of a Lewis Acid type adduct, $Fe_3(CO)_{12}$-HO-Z, identical to that obtained directly from adsorption of $Fe_3(CO)_{12}$, was interpreted as resulting from the thermally induced migration and aggregation of the $Fe(CO)_4$ moieties formed on adsorption of these complexes onto the support. The subsequent thermal decomposition of these samples was identical to that observed for the $Fe_3(CO)_{12}$/HY zeolite system.

Phillips, Clausen and Dumesic (23) have used Mossbauer spectroscopy to study the production of small, metallic iron particles formed via thermal decomposition of $Fe(CO)_5$ adsorbed on a high surface area, oriented graphite support (Grafoil). The use of graphite as a support for metallic particles stems from its unique electronic and structural properties compared with other catalyst supports such as silica or alumina (24-27). Being a conductor, graphite may show significant electron transfer with the supported catalyst particles, and the morphology of the support surface may be altered through appropriate pretreatment. Comparison of the Mossbauer spectrum of $Fe(CO)_5$ adsorbed on graphite at 77 K with the room temperature spectrum indicates that $Fe(CO)_5$ is

physisorbed on this support. This is further confirmed by the small quadrupole splitting observed in the spectrum of the adsorbed complex relative to that observed for solid $Fe(CO)_5$, which is consistent with a displacement of CO groups out of the equatorial plane (28). This suggests that there is a weak interaction between $Fe(CO)_5$ and graphite, which leaves the $Fe(CO)_5$ structure altered by only a slight displacement of the equatorial CO groups. Thermal decomposition of the physisorbed complex for 1 hour at 378 K results in a six-peak spectral pattern characteristic of metallic iron. Transmission electron microscopy indicates that the metallic iron is formed preferentially at edges or other dislocations on the graphite surface. Extended heating at 450 K caused sintering and possible formation of iron carbide species.

Basset and coworkers (29) have investigated the reactivity of $Fe_3(CO)_{12}$ and $Fe(CO)_5$ with the surface hydroxyl groups of silica, alumina, magnesia, and zinc oxide. The adsorption of $Fe_3(CO)_{12}$ on silica was determined to be a reversible process since the cluster can be quantitatively extracted from the silica surface by washing with hexane. The adsorption of $Fe(CO)_5$ was also determined to be reversible since no IR bands attributed to the adsorbed complex could be detected following vacuum treatment at room temperature. This

reflects the low reactivity of the silanol groups of silica toward the carbonyl ligands of the monomer or metallic frame of the cluster. This is in contrast to the behavior of the silanol groups of silica towards $Ru_3(CO)_{12}$ or $Os_3(CO)_{12}$ where an oxidative addition reaction of a surface silanol group with the metal cluster occurs (30-34). The adsorption of $Fe_3(CO)_{12}$ and $Fe(CO)_5$ on alumina, magnesia, and zinc oxide was determined to be irreversible as the result of the formation of the anionic hydrido cluster, $HFe_3(CO)_{11}^-$, which was characterized by infrared, ^1H NMR, and UV-Vis spectroscopy. Since this species is observed on supports that do not contain molecular water, its formation was postulated as occuring by nucleophilic attack of the basic surface hydroxyl groups of these supports on $Fe_3(CO)_{12}$.

Basset and coworkers (35) have also studied the thermal decomposition and catalytic properties in Fisher-Tropsch synthesis of $Fe_3(CO)_{12}$, $HFe_3(CO)_{11}^-$, and $Fe(CO)_5$ on these highly divided inorganic oxide supports. Characterization of the supported complexes before and after decomposition was carried out using ferromagnetic resonance (FMR), Mossbauer spectroscopy, electron microscopy and gas phase analysis. The behavior of the precursor iron carbonyl complex was observed to be strongly dependent on the water content of the support

before impregnation. Thermal decomposition of $Fe_3(CO)_{12}$ supported on dehydroxylated MgO and Al_2O_3 supports at 393 K under vacuum resulted in a ferromagnetic resonance signal attributed to zerovalent iron atoms (36). The decrease of the magnetization with increasing temperature, obtained by double integration of the FMR signal, indicated a superparamagnetic behavior of the iron particles. In FMR experiments, superparamagnetism is observed for iron particles < 35 A in diameter (37). The appearance of a single line in the Mossbauer spectrum, instead of the six line spectrum usually observed for metallic iron, is also consistent with the formation of small superparamagnetic iron particles (38,39). Analysis of the gas phase following thermal decomposition revealed no significant evolution of H_2. These results indicate that on dehydroxylated supports $Fe_3(CO)_{12}$ retains its zerovalent oxidation state after decarbonylation at 393 K to yield very small iron particles. Thermal decomposition above 473 K resulted in a dynamic migration of zerovalent iron to form particles of higher sizes. As previously mentioned, on hydroxylated MgO and Al_2O_3 supports the $Fe_3(CO)_{12}$ cluster is quantitatively converted into the anionic hydrido cluster, $HFe_3(CO)_{11}^-$. Subsequent thermal decompostion under vacuum resulted in the appearance of an FMR signal characteristic of both zerovalent iron particles and iron in a +3 oxidation state. The smaller linewidth of the

FMR signal indicates formation of iron particles of slightly larger sizes (40). Analysis of the gas phase following the thermal decomposition revealed significant H_2 evolution due to the oxidation of zerovalent iron by the surface hydroxyl groups of the support.

The activity of these catalysts in Fisher-Tropsch synthesis was also investigated by this group (35). Thermal activation was carried out in a flow reactor under CO + H_2, ($CO:H_2$ = 1:1; P = 10 atm.), for ca. 90 hours in the temperature range 180-270 C. A high selectivity for olefins (> 50%) was observed with a product distribution showing a sharp maximum for C2-C3 hydrocarbons. By comparison, impregnation of the same supports with $Fe(NO)_3$, followed by calcination in air and reduction under H_2, exhibited a completely different product distribution with a minimum selectivity for C2-olefins and a wide range of hydrocarbons extending as far as C-16. In addition, the selectivity towards olefinic compounds was only 38%. The selectivity for low molecular weight olefins observed for the iron carbonyl catalysts was found to decline slowly with time, and near the end of the catalytic reaction, hydrocarbons of higher molecular weight are obtained. Electron microscopy indicates the presence of large iron particles (ca. 200-500 Å) at the end of the run. These results seem to indicate that low molecular weight hydrocarbons are

produced when small iron particles are present whereas a broader molecular weight distribution may be associated with larger particles of iron.

Brenner and Hucul (41) have studied the temperature-programmed decomposition of $Fe(CO)_5$, $Fe_2(CO)_9$, and $Fe_3(CO)_{12}$ surface bonded to alumina. Temperature programmed decomposition, (TPDE), an experimental technique in which the evolution of gases is monitored during the thermal activation of a catalyst, has revealed information regarding the stoichiometric reactions which occur between an adsorbed complex and a support. Their results indicate that the nuclearity of the precursor carbonyl affects the chemistry of the surface bound material. While formation of primarily zerovalent subcarbonyl species was observed for activation at temperatures below 423 K, hydrogen evolution above 573 K indicates extensive iron oxidation caused by reaction between the carbonyls and surface hydroxyl groups of the support. The evolution of 3.0 CO's/mole of $Fe(CO)_5$ adsorbed may indicate the existence of an $Fe(CO)_2$(ads) species following activation at 393 K. No other stable subcarbonyl species were detected. Because the surface-bonded carbonyls decompose over a wider range of temperatures than do bulk carbonyls, it was proposed that a major role of the alumina was to stabalize subcarbonyl species over a broad range of temperatures. Carbon

monoxide chemisorption studies indicated that surface-bonded iron carbonyls could be used to prepare metal catalysts which were at least an order of magnitude more dispersed than conventional catalysts prepared via impregnation with iron salts followed by high temperature calcination and reduction. The higher dispersion was attributed to omission of the high temperature calcination and reduction of Fe^{+3} which often leads to sintering and/or production of difficult to reduce iron compounds on the surface.

Brenner (42) has investigated (using TPDE) the dependence of methane formation on the nuclearity of alumina supported iron carbonyls. The amount of methane evolved by $Fe(CO)_5$, $Fe_2(CO)_9$, and $Fe_3(CO)_{12}$ during TPDE to 600 °C did not change significantly, although the average amount of methane increased ca. 30 fold. Methane formation was observed to vary linearly with metal carbonyl loading and was independent of the carrier gas flow rate indicating methanation at mononuclear sites and only involving adsorbed species. These results suggest that methane formation is formed by direct hydrogenation of the carbonyl ligands by the surface hydroxyl groups of the support. A catalytic scheme was proposed which involved oxidation of mononuclear sub-carbonyl species with the surface hydroxyl groups to form methane, the role of the H_2 being to reduce the metal again. The

hydrogenation of subcarbonyl intermediates was attributed to the requsite thermal stability of supported subcarbonyl species compared with the lower temperature decomposition of the bulk carbonyls.

McVicker and Vannice (43) have prepared well-dispersed, highly promoted K-Fe catalysts by impregnation of alumina and silica with precursor K-Fe carbonyl complexes (eg., K_2-$Fe(CO)_4$-C_4H_8O), followed by thermal decomposition of the supported complexes under hydrogen. The presence of Group IA metals, especially K and Rb, is well known to promote Group VIII metals for the Fisher-Tropsch reaction. Since potassium and iron are in intimate contact in the precursor complexes, the deposition and subsequent thermal decomposition of such complexes on a support facilitates K-Fe metal contact and maximizes the promotional effects of potassium. Infrared spectroscopy indicated that the precursor K-Fe carbonyl complexes are relatively stable on partially dehydrated alumina surfaces in the absence of oxygen. When subjected to hydrogen reduction, reduced iron metal species are formed on the surface since chemisorption of CO occurs and infrared bands from the organic portion of the precursor complexes are no longer present. An estimate of the iron crystallite size obtained by X-ray diffraction measurements indicates the presence of 40-50 Å particles. Carbon monoxide chemisorption studies

indicate that thermal decomposition of $K_2Fe(CO)_4$ complexes yields either a more highly dispersed or a more reducible (or both) iron phase than supported iron catalysts prepared by conventional methods. However, CO chemisorption and X-ray results suggest that iron is less well dispersed on silica than on alumina, presumably due to differences in the surface hydroxyl groups. As with catalysts derived from other surface-bonded iron carbonyls, these catalysts showed higher activity and higher olefin selectivity than conventionally prepared catalysts.

D. Photoactivation of Iron Carbonyl Systems.

The photochemical reactivity of metal carbonyls has been recognized for some time (9). In fluid solution, optical irradiation causes CO dissociation and formation of coordinatively unsaturated species which are known intermediates in thermally activated homogeneous catalytic systems (5-8). In addition, photoactivation may provide a route to new catalytic species, and since the system can be activated with a light pulse of short duration, i.e., < 1 usec, photoactivation may offer additional insight into catalytic cycles. A key advantage of photocatalyzed reactions is that they can be run at low temperatures, whereas thermal activation of the same catalyst precursor often requires use of high temperatures to sustain catalytic activity. For example,

coordinatively unsaturated metal carbonyl species can undergo oxidative addition and β-hydride elimination which are two reactions important in thermally activated catalytic systems. It may be possible to gain better understanding of these processes by photogeneration of the coordinatively unsaturated intermediate at temperatures where there is not sufficent thermal activation available to affect these reactions. In addition, spectroscopic detection of catalytically active intermediates not observable at higher temperatures is possible. Photogeneration of catalysts also offers a level of control not accessible through conventional thermal activation since the primary photoprocesses of organometallic complexes show a strong wavelength dependence. The ensuing discussion will include descriptions of the geometric and electronic structures of the iron carbonyls investigated, and detail the photochemistry of these complexes under a variety of physical and chemical conditions.

1. Geometric Structure of Iron Carbonyls.

The geometric structures of the commonly available iron carbonyls, $Fe(CO)_5$, $Fe_2(CO)_9$ and $Fe_3(CO)_{12}$ are shown in Figure 1. In each of these complexes the iron atom is formally in a zero oxidation state. In both the solid and liquid state, the geometry of $Fe(CO)_5$ has been

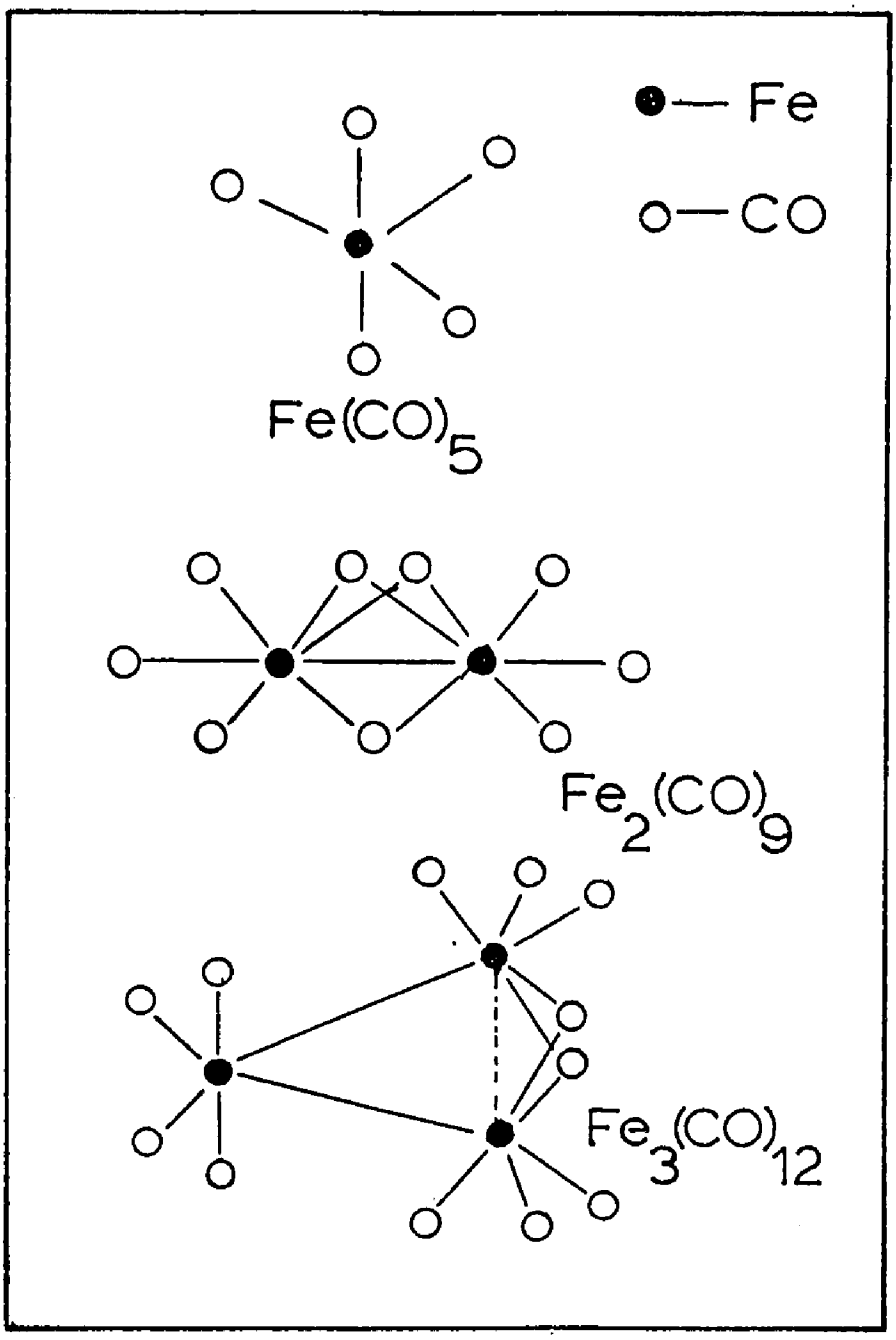

Figure 1. Geometric Structures of Iron Carbonyls.

established by electron diffraction studies (44) and infrared spectroscopy (45) to be trigonal bypyramidal, (D_3h symmetry). Of importance is the fact that $Fe(CO)_5$ contains only terminal CO groups. In contrast, $Fe_2(CO)_9$ contains three bridging CO in addition to six terminal CO groups. The structure of this complex, which also has D_3h symmetry, was determined by X-ray diffraction studies (46). Additional evidence for this structure was obtained from the infrared spectrum of the solid which shows a strong band at 1828 cm^{-1} indicative of bridging CO groups (45). The determination of the molecular structure of $Fe_3(CO)_{12}$ in solution has been complicated by an inability to correlate the solution infrared spectrum with that of the solid state structure determined by X-ray photographic analysis. The molecular configuration of this complex in the solid state has C_2v symmetry and can be considered as being formed from the insertion of a cis-$Fe(CO)_4$ group at one of the three bridging carbonyl positions of $Fe_2(CO)_9$ (47). The infrared spectrum of $Fe_3(CO)_{12}$ in low temperature matrices is consistent with the solid state C_2v structure, however, the spectrum in n-hexane solution is different and suggests a different molecular configuration (48). Of particular interest is the presence of only very weak bands in the bridging CO region at ca. 1867 and 1838 cm^{-1}. Recent work has suggested the presence of three isomeric forms of

$Fe_3(CO)_{12}$ in solution (49). Rotation of the Fe3 triangle in the solid state structure by 30° about the C_2 axis results in a second isomeric form possessing D_3 symmetry in which all the CO groups are equivalent and terminally bonded. Further rotation about the same axis, (or either of the other two equivalent C_2 axes), generates a third isomeric form in which the two bridging CO groups occupy positions above and below the Fe3 triangle. This is in contrast to the edge-bridging CO groups found in the solid state structure. Further rotation by 30° sequentially regenerates the other two isomeric forms. The two isomeric forms found in solution not only follow naturally from the rotation of the Fe3 triangle within the CO-icosahedron, but also provide a reasonable explanation of the infrared solution spectrum. For a molecule with D_3 symmetry, six terminal carbonyl absorptions are ir-active ($2A_2 + 4E$) and of these, the four E modes are expected to be broad. The band at 2103 cm^{-1} and the broad, unresolved terminal CO absorptions in the region 2050-2000 cm^{-1} are taken as evidence that ca. 95% of the trimer exists as the second isomeric form in fluid solution, and the weak bands at 1867 and 1838 cm^{-1} are attributed to small amounts of the solid state structure and/or the third isomeric form.

2. Electronic Structure.

The electronic absorption spectrum of $Fe(CO)_5$ in n-hexane exhibits strong absorption in the UV with shoulders at 282 and 250 nm (50). Electronic spectral data for $Fe(CO)_5$ and $Fe_3(CO)_{12}$ are listed in Table 1, and the d-orbital ordering for D_3h symmetry is shown in Figure 2. The lowest energy absorption maximum for $Fe(CO)_5$ has been assigned to the d_{xy}, $d_{x2-y2} \longrightarrow d_{z2}$ transition (50,51). The d_{z2} orbital is σ-antibonding to all ligands in the coordination sphere but particularly for ligands on the z-axis. The intense UV absorption is associated with unresolved MLCT and intraligand transitions.

Due to the insolubility of $Fe_2(CO)_9$ in organic solvents, very few data are available concerning its electronic spectrum. The single crystal spectrum shows only a rising absorption into the UV with no bands of appreciable intensity in the visible region (52). The trinuclear $Fe_3(CO)_{12}$ cluster shows two visible electronic absorption bands with maxima at 602 and 437 nm. These bands have been assigned on the basis of single crystal electronic absorption polarization data to be $\sigma \longrightarrow \sigma^*$ (602 nm) and $\sigma^{*\prime} \longrightarrow \sigma^*$ (432 nm) transitions, respectively (52). The lowest energy one-electron excited states involve population of orbitals that are

TABLE 1.

Electronic Spectral Features of Iron Carbonyl Complexes.

Iron Carbonyl Complex	Absorption Maxima, nm, (ε)
$Fe(CO)_5$	285 (3800)
	240 (40,000)
$Fe_3(CO)_{12}$	603 (2900)
	440 (2400)
	315 (12,400)
	275 (17,700)
	192 (>70,000)

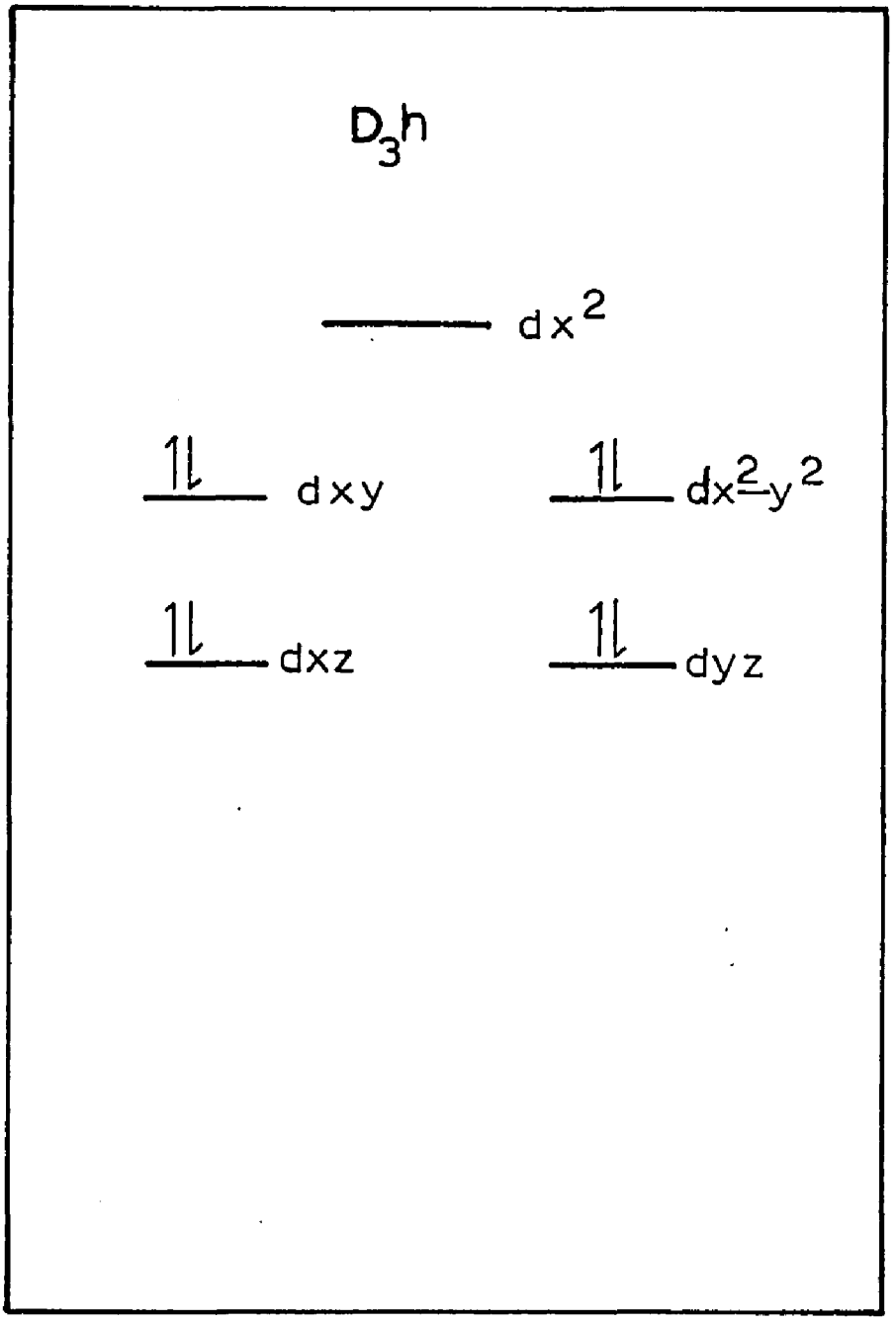

Figure 2. D-orbital ordering for D_{3h} symmetry.

strongly σ-antibonding with respect to the metal-metal bonds. The intense UV absorption has been assigned to a MLCT transition.

3. Photoreactions.

The photochemistry of $Fe(CO)_5$ has been studied extensively during the last two decades. The primary photoprocess has been determined to be dissociative loss of CO from $Fe(CO)_5$ to yield $Fe(CO)_4$ according to reaction 1 (53). In condensed phases, the quantum yield of this photoprocess is on the order of unity (54).

(1). $Fe(CO)_5 \longrightarrow Fe(CO)_4 + CO$

In the presence of added ligands, photosubstitution takes place as in reaction 2, provided the substituted complex is stable under the reaction conditions. Coordinatively unsaturated intermediates formed via photolysis of $Fe(CO)_5$ are also susceptible to oxidative addition. The oxidative addition of tri-alkyl silane to photogenerated $Fe(CO)_4$, for example, is shown in reaction 3 (55).

(2). $Fe(CO)_4 + L \longrightarrow Fe(CO)_4L$

(3). $Fe(CO)_4 + R_3Si\text{-}H \longrightarrow cis\text{-}Fe(CO)_4(SiR_3)(H)$

In the absence of added nucleophiles, photolysis of $Fe(CO)_5$ as a neat liquid, in noncoordinating solvents, and in the gas phase leads predominately to the formation of $Fe_2(CO)_9$ as the dominant reaction product (55-58). This presumbably occurs by a secondary thermal reaction between photogenerated $Fe(CO)_4$ and another $Fe(CO)_5$ molecule. The net reaction, shown in reaction 4, is the earliest known photoreaction of a metal carbonyl.

(4). $2Fe(CO)_5 \longrightarrow Fe_2(CO)_9 + CO$

In contrast to the photochemistry observed in the absence of nucleophiles where the dominant photoproduct is $Fe_2(CO)_9$, photolysis in the presence of weak ligands, such as pyridine, leads to formation of $Fe_3(CO)_{12}$ (59,60). The absence of $Fe_2(CO)_9$ is explained by its instability under these conditions since $Fe_2(CO)_9$ dissociates in solution in the presence of a weak ligand to yield $Fe_3(CO)_{12}$ and $Fe(CO)_5$. It appears that the unstable, monosubstituted $Fe(CO)_4L$ complexes, formed in reactions 1 and 2, act as intermediates in this thermal reaction to form $Fe_3(CO)_{12}$ (61-63).

The results obtained following UV irradiation of $Fe(CO)_5$ in the gas phase are at variance with the presumption that absorption of a photon by a $Fe(CO)_5$ molecule results solely in formation of $Fe(CO)_4$ and CO. Photolysis of mixtures of $Fe(CO)_5$ and PF_3 with a KrF laser (248 nm) results in sequential fragmentation of the $Fe(CO)_5$ molecule following absorption of a single photon to yield $Fe(CO)_2(PF_3)_3$, $Fe(CO)_3(PF_3)_2$ and $Fe(CO)_4(PF_3)$ (64). These stable products were quantitatively analyzed by gas chromotography. The primary photochemical yields at 248 nm for these fragments were determined to be 0.55, 0.35, and 0.10, respectively, with a net total quantum yield of approximately unity. The difference in photochemical behavior between the isolated, gas phase $Fe(CO)_5$ molecule and that observed in solution is attributed to a closer interaction with the enviroment in condensed phases, which prevents further fragmentation of the intially generated $Fe(CO)_4$ by efficent removal of excess internal excitation, i.e. enhanced nonradiative decay.

Further confirmation of the formation of highly coordinatively unsaturated species was obtained by recording the transient infrared absorption spectrum following pulsed UV photolysis of $Fe(CO)_5$ in the gas phase (65). Four spectral features were observed in the carbonyl stretching region and were assigned by reference

to low temperature matrix and chemical trapping data to $Fe(CO)_4$, $Fe(CO)_3$, and $Fe(CO)_2$. In the absence of added CO, more than the initial photolyzed quantity of $Fe(CO)_5$ was removed from the system due to reaction of $Fe(CO)_5$ with the photogenerated coordinatively unsaturated species to yield polynuclear iron carbonyl complexes. Even with a 3000-fold excess of CO, all $Fe(CO)_5$ is not regenerated implying that the reactions leading to polynuclear complexes are exceedingly efficent. The kinetics of reaction of photolytically generated $Fe(CO)_x$ (x = 2, 3, 4) with CO was investigated (66). Under 100 torr CO both $Fe(CO)_2$ and $Fe(CO)_3$ react very rapidly to generate $Fe(CO)_4$, which then reacts more slowly to regenerate $Fe(CO)_5$. This observation is consistent with the hypothesis that 12 and 14-electron species are more reactive than 16-electron species. Another possible factor contributing to the slower rate of reaction between $Fe(CO)_4$ and CO is that $Fe(CO)_4$ is predicted to have a triplet C_2v ground state, thus requiring both a spin change and a large geometry change to form $Fe(CO)_5$.

The use of matrix isolation techniques has proven invaluable in characterizing the photochemistry of metal carbonyl complexes (67). In the form discussed here, unstable species are prepared by photolysis of a stable molecule, trapped in a large excess of inert solid at low temperature (eg., solid Ar at 20 K). Once prepared the

unstable fragments can be studied spectroscopically, usually by infrared and UV-Vis spectroscopy. Of particular importance is that the concentration of metal carbonyl in the matrix can be controlled, resulting in formation of coordinatively unsaturated species in dilute matrices and polynuclear complexes in more concentrated matrices.

UV photolysis of $Fe(CO)_5$ in dilute nitrogen, argon and methane matrices (1:8000) at 20 K leads to progressive loss of CO and formation of $Fe(CO)_4$, $Fe(CO)_3$ and $Fe(CO)_2$ (68). Infrared spectra of ^{13}C enriched complexes indicate that $Fe(CO)_4$ has C_2v geometry and $Fe(CO)_3$ is a pyramidal molecule possessing C_3v symmetry (69). The magnetic circular dichroism (m.c.d.) spectrum of matrix isolated $Fe(CO)_4$ is temperature dependent which confirms that the ground state is paramagnetic (70,71). The electronic spectrum of $Fe(CO)_4$ exhibits a UV absorption band (λ max = 325 nm) and a far-red-near-i.r. absorption band (λ max = 770 nm) due to d--d electronic transitions (68,71). Excitation of the latter transitions promotes addition reactions with reactants available in the matrix forming $Fe(CO)_4Q$ species where Q = CH_4, Xe, and N_2. The electronic spectra of the addition products are different from that of uncomplexed $Fe(CO)_4$. These molecules exhibit a broad absorption in the region of 375 nm and no near-i.r. absorptions

(69,70). Prolonged UV photolysis of $Fe(CO)_5$ in dilute matrices (1:8000) at 20 K results in progressive loss of CO and formation of atomic iron in small yields (72). The first derivative, electronic absorption spectrum obtained following prolonged photolysis shows a series of sharp but rather weak bands superimposed upon a rising UV absorbance. The positions of these bands are extremely close to that reported for iron vapor co-condensed with nitrogen at 4 K (73). Thus the result of prolonged UV photolysis appears to be the stripping of all five CO ligands from $Fe(CO)_5$ leaving the "naked" metal atom. In contrast to the photoproducts formed in dilute matrices, UV photolysis of $Fe(CO)_5$ in moderately concentrated methane matrices (1:1000) results in the matrix turning a faint green color, and the appearance of infrared bands in both the terminal and bridging CO regions which were assigned to the polynuclear complexes $Fe_2(CO)_8$ and $Fe_3(CO)_{12}$. Upon annealing the matrix, infrared bands assigned to $Fe_2(CO)_9$ were observed.

Excited state reactions of $Fe_2(CO)_9$ and $Fe_3(CO)_{12}$ include both substitution and declusterification. Near-UV photolysis of $Fe_2(CO)_9$ in low temperature matrices results in intial loss of a bridging CO group to generate $Fe_2(CO)_8$ (74). Analysis of the infrared spectrum indicates this structure possesses C_2v symmetry with a 'double' bond between the two iron atoms. Prolonged

photolysis leads to a second form of $Fe_2(CO)_8$ which does not contain bridging CO groups. Although the exact structure of this species was not confirmed, a D_3d structure formed by replacement of an axial CO ligand on $Fe(CO)_5$ with $Fe(CO)_4$ was suggested. In the presence of nucleophiles, L, near-UV photolysis of $Fe_2(CO)_9$ results in formation of mononuclear $Fe(CO)_nL_{5-n}$ complexes. A mechanism has been proposed which involves intial loss of CO to form $Fe_2(CO)_8$. This reactive species rapidly scavenges L to form the mono-substituted, dimeric $Fe_2(CO)_8L$. Subsequent decomposition of this unstable species results in formation of $Fe(CO)_4L$ and $Fe(CO)_4$ which then reacts with another L. The absence of declusterification reactions involving metal-metal bond cleavage is attributed to the presence of the bridging CO groups which may preclude efficent cleavage of the Fe-Fe bond.

Visible irradiation of $Fe_3(CO)_{12}$ in the presence of CO (75) and 1-pentene (76,77) results in the formation of $Fe(CO)_5$ and $Fe(CO)_4$(1-pentene), respectively. The primary photoreaction appears to be Fe-Fe bond cleavage (rxn. 5) with the resulting fragment undergoing unimolecular thermal processes to yield final products. The disappearance quantum yields are fairly low, (ca. 0.02 for 550 nm excitation), probably reflecting efficent reformation of the Fe-Fe bond to regenerate $Fe_3(CO)_{12}$.

4. Photocatalytic Reactions.

Numerous reports have appeared in recent years concerning the photogeneration of catalysts using precursor iron carbonyls. Examples of catalyzed isomerizations, hydrosilations, hydroformylations, and metathesis reactions of olefins mediated by photoactivated homogeneous iron carbonyl complexes illustrate the broad diversity of reacting systems (78-82). The term photocatalysis has been defined by Wrighton to be the photogeneration of a catalyst from a thermally inert precursors such that substrate transformations result which are both catalytic with respect to the number of photons absorbed and with respect to the actual catalyst (83). Figure 3 illustrates the various photochemical and thermal steps involved in a photocatalytic reaction.

Several points are to be noted concerning photocatalytic reactions. First, since the only excited state chemistry is the primary act of catalyst formation, the photogenerated catalyst has the potential to be unique with respect to thermal activation of the same precursor complex. Secondly, the photogenerated catalyst behaves as a thermal catalyst thereby leading only to thermal reactions of the substrate. Third, catalytic activity begins only upon photolysis and continues after

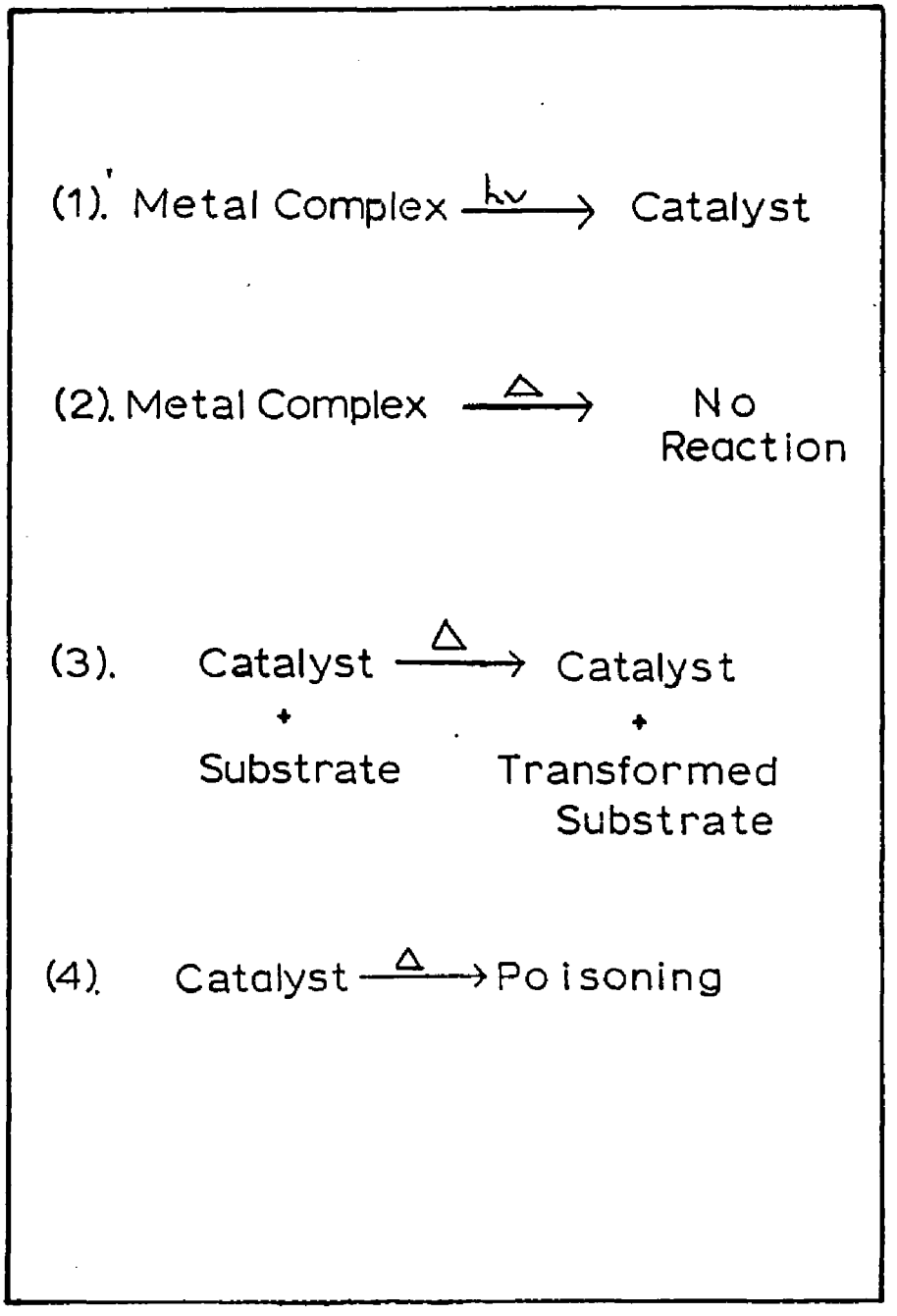

Figure 3. Photochemical and thermal steps in a photocatalytic system.

cessation of photolysis until poisoning processes have removed or inhibited the catalyst. Since photocatalyzed olefin isomerization and hydrogenation reactions have received the most attention, the following discussion will be limited to these two reactions.

Wrighton and Schroeder (79) have investigated the photocatalyzed solution phase isomerization and hydrogenation reactions of olefins by $Fe(CO)_5$. Near-UV irradiation of $Fe(CO)_5$ in the presence of 1-pentene resulted in isomerization to both cis and trans 2-pentene. It was observed that a common equilibrium mixture of pentenes was formed, regardless of the starting pentene isomer. This value was found to be very close to the thermodynamic ratio of alkenes previously measured (84). The intial isomerization rates appear to show a short induction period where the rate increases as a function of irradiation time. The observed quantum efficiency is far in excess of unity, approaching 500 in neat 1-pentene. This implies that the role of the light is to generate a thermally active catalyst. A mechanism for pentene isomerization was proposed, Figure 4, which involves generation of a coordinatively unsaturated $Fe(CO)_3$(alkene). This complex was proposed to undergo an oxidative addition reaction to form the catalytically active π-allylhydride intermediate, $HFe(CO)_3(\pi\text{-allyl})$.

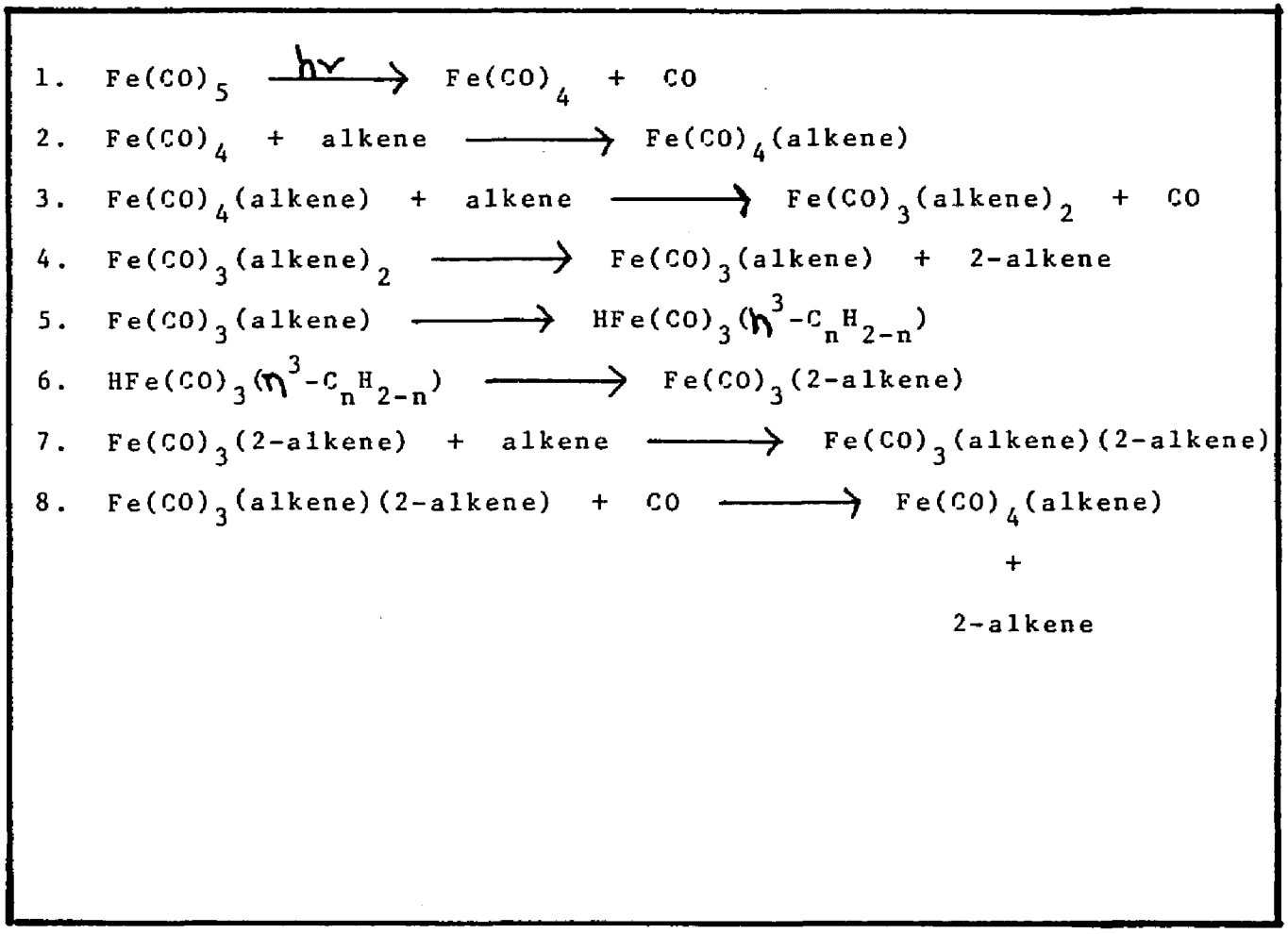

Figure 4. Mechanism for $Fe(CO)_5$ photocatalyzed 1-pentene isomerization.

The 1-pentene isomerization reaction was also investigated using $Fe_3(CO)_{12}$ as the precursor complex (85). Since $Fe_3(CO)_{12}$ has lower energy electronic transitions relative to $Fe(CO)_5$, it has the advantage of being activated by visible light. This is particularly important when organic substrates absorb too strongly in the UV to allow use of $Fe(CO)_5$. Based on the identical product ratios (trans-2-pentene/cis-2-pentene) for both monomer and trimer, it appears the trimer fragments upon visible irradiation to yield monomeric iron carbonyl-olefin complexes which react according to Scheme II.

Near-UV irradiation of $Fe(CO)_5$ in the presence of olefin and H_2 (1 atm) results in olefin hydrogenation at room temperature or below (79). The reaction was selective in that the more sterically unhindered alkenes were most effectively hydrogenated. As with the isomerization reaction, the observed quantum efficiency exceeds unity indicating that hydrogenation proceeds catalytically with respect to the number of incident photons. Substantial fractions of neat alkenes (> 20%) were hydrogenated using 0.001 M $Fe(CO)_5$ showing that the turnover number with respect to iron exceeds 10^3. A mechanism was proposed in which the key catalytic species was again $Fe(CO)_3$, as was proposed for the photocatalyzed isomerization reaction.

In homogeneous catalysis, it is well established that ligands in the coordination sphere of a metal centered catalyst can influence the rate and selectivity of a reaction (5,7,86-88). An understanding of the influence of various ligands on the rate and product distribution of a reaction will allow for design of more efficent and selective catalysts in the future, i.e., catalysts tailored for a given reaction (89). Phosphorous ligands have been extensively studied since they exhibit a wide range of steric and electronic properties and are capable of stabilizing many metal complexes. Wrighton (90) has investigated the influence of various phosphine based ligands on the photocatalyzed 1-pentene isomerization reaction. All phosphine substituted complexes were capable of moving high concentrations of 1-pentene toward the thermodynamic ratio of pentenes. In addition, high turnover numbers ($> 10^3$) and quantum yields exceeding unity were observed. The intial ratio of trans/cis-2-pentene was found to be strongly dependent on the nature of the phosphorus ligand bonded to the iron carbonyl catalyst. As the steric bulk of the phosphorus ligand increased, a larger kinetic preference for the less stable cis-2-pentene isomer was observed. While the electronic properties of the phosphorus ligands may be contributory, it was concluded that the electronic effects on the intial rate of formation of the 2-pentenes are minor compared with the

steric effects of the phosphorus ligands. These results demonstrate that the product distribution of photocatalyzed reactions can be 'tuned', in this case by changing the steric bulk of the phosphorus ligand.

Clark and Swartz (91) have studied the effects of trifluorophosphine substitution in the photocatalyzed 1-pentene isomerization reaction. Increasing PF_3 content in $Fe(PF_3)_x(CO)_{5-x}$, where x = 1-4, causes these species to become progressively less effective photochemical catalysts. Suprisingly, although PF_3 substitution incrementally influences the isomerization, total substitution caused the isomerization to cease. These authors also demonstrated that the (1-pentene)$Fe(PF_3)_4$ complex has a PF_3 group that is photochemically active, yet photocatalytic isomerization did not occur. It was proposed that higher PF_3 substituted iron carbonyls do not react by the Schroeder-Wrighton mechanism given in Scheme II. Rather, a labile, multiply bonded, bridged dimeric iron species was postulated as the active catalytic intermediate. This is consistent with the photochemical data obtained which show a lack of catalytic activity for the totally substituted iron carbonyl complex. The indispensable role of CO in the isomerization reaction was attributed to the ability of CO to act as a bridging ligand between metal atoms whereas PF_3 is unable to do so.

The pulsed-UV laser isomerization and hydrogenation reactions of olefins were investigated by Grant and co-workers in both solution (92) and gas phases (93). The time dependence of the isomerization reaction was qualitatively identical with results previously obtained with $Fe(CO)_5$ and other iron carbonyl catalyst precursors (79,85,91). The reaction exhibits an induction period, during which the rate of the reaction increases with time, followed by a steady state period in which the rate decreases monotonically as the system approaches the equilibrium substrate concentrations. The observed quantum yield for the solution phase isomerization reaction exceeds 1000, which is substantially higher than the value of 400 obtained using steady-state irradiation. Thus a substantial efficiency advantage exists when pulsed rather than continuous irradiation is used to intiate photocatalysis. Turnover numbers for the system regularly exceed 10^4, indicating that the catalyst reverts to a catalyst precursor capable of reactivation. In neat 1-pentene the quantum efficiency of the system was observed to increase with decreasing laser repetition rate, indicating the laser pulses are irradiating catalytic intermediates. However, below 4 Hz the quantum efficiency was independent of the laser repetition rate, allowing an estimation of the lifetime of the active catalyst under these conditions to be 0.2 seconds. The time dependence of the hydrogenation reaction was

similiar to that observed for isomerization. The observed quantum yields for hydrogenation (P_H = 800 torr) ranged from 2 to 4, which is in agreement with previous studies showing isomerization to be the more efficent reaction. Hydrogenation apparently competes with isomerization for the same catalytically active intermediates since the isomerization rate decreases with increasing H_2 pressure. Pulsed-UV laser irradiation of gas phase $Fe(CO)_5$ in the presence of 1-pentene leads to quantum yields which approach 400 for the isomerization reaction, indicating a lower efficiency relative to liquid phase photocatalytic isomerization. However, a higher efficiency for gas phase hydrogenation is observed since quantum yields approach 20, whereas the quantum yield of hydrogenation in the liquid phase rarely exceeds unity under any conditions.

Mitchener and Wrighton (94) have used a cw Ar ion laser as their excitation source to provide very high light intensity in studying the photocatalyzed 1-pentene isomerization using $Fe(CO)_5$ and $Fe_3(CO)_{12}$ as catalyst precursors. The use of high light intensity excitation allows the catalyst turnover rate, not the actual photogeneration of the catalyst, to become the rate-limiting feature. The reaction was monitored by near-infrared absorption spectroscopy which allows for quantitative analysis of reactants and products on a

faster time scale than gas chromotography. Flash photolysis followed by monitoring the decline of the 1330 nm band of 1-pentene showed that catalysis persists for < 5 secs. after irradiation is terminated. In all cases, the observed disappearance quantum yields for 1-pentene exceeded unity and the lower limits of the turnover rates generally exceeded 1000. The photolysis of $Fe(CO)_5$ or $Fe_3(CO)_{12}$ was observed to yield exceedingly active catalysts which are not excited state species since the excited state lifetimes of $Fe(CO)_5$ and $Fe_3(CO)_{12}$ are too short to effect catalysis. Rather, the time resolution of these experiments confirms the catalytically active species are ground state species, photoproduced by loss of CO from $Fe(CO)_5$ or Fe-Fe bond cleavage.

Chase and Weigert (95) have measured the catalyst lifetime in the $Fe(CO)_5$ photocatalyzed 1-pentene isomerization reaction by Fourier Transform Infrared Spectroscopy. Operation of the interferometer in the rapid scan mode allows simultaneous monitoring of many absorption bands during a single experiment with a temporal resolution of < 1 second. Both disappearance of 1-pentene and appearance of cis and trans 2-pentenes show an induction period suggesting that the active catalyst is not formed directly from $Fe(CO)_5$ by a one quantum process. The lifetime of the active catalyst was determined by adding the absorption changes in both the

olefin and carbonyl bands from the time irradiation from the 2000-W Xenon lamp is terminated to the end of data aquisition. By assuming a first order decay process, the measured catalyst lifetimes was determined to vary from 7 to 28 seconds depending on the concentration of 1-pentene present when the light is turned off. The dependence of catalyst lifetime on 1-pentene concentration suggested that the catalyst lifetime is determined by olefin dissociation from $Fe(CO)_3$(olefin) to yield a fragment which rapidly decomposes to catalytically inactive species.

The low temperature photochemistry of $Fe(CO)_4$(olefin) complexes (olefin = ethylene, propylene, 1-pentene, 3,3-dimethyl-1-pentene, 4-pentadiene) and the IR spectroscopic characterization of several intermediates involved in the $Fe(CO)_5$ photocatalyzed isomerization of alkenes has recently been reported by Mitchener and Wrighton (96). The photoproducts observed for the $Fe(CO)_4$(olefin) complexes were found to be dependent on whether or not the olefin posesses allylic hydrogens. For olefins containing no allylic hydrogens the only observable product observed following irradiation (200-W high pressure Hg lamp) of matrix isolated $Fe(CO)_4$(olefin) in alkane at 77 K were the 16-electron $Fe(CO)_3$(olefin) complexes formed by dissociative loss of CO. In contrast, irradiation of complexes

containing allylic hydrogens resulted exclusively in formation of π-allyl hydride complexes at temperatures as low as 77 K. In all cases CO extrusion, not loss of olefin is the major excited state reaction of $Fe(CO)_4$(olefin) complexes. Irradiation of $Fe(CO)_4$(olefin) at 77 K in a matrix containing significant uncomplexed olefin results in the formation of a strong feature at ca. 1930 cm^{-1} attributable to trans-$(Fe(CO)_3(olefin)_2$. No significant isomerization occurs up to 195 K, but at the softening point of the matrix the 1930 cm^{-1} band disappeared and new features grew in at 1972 and 2048 cm^{-1}. At 195 K the species responsible for these bands was inert, but further warming of the sample to 298 K resulted in extensive olefin isomerization (> 30%) along with regeneration of significant amounts of $Fe(CO)_4$(olefin). It was proposed that the species responsible for the latter bands is $Fe_2(CO)_6(olefin)_2$, a derivative of the known $Fe_2(CO)_8$. This species has been shown to be very catalytically active; addition of 1.0 mL of 1-pentene at 25 C to 1.0 mL of 10^{-2} M $Fe_2(CO)_6(C_2H_4)_2$ in methylcyclohexane yielded ca. 60% isomerization to 2-pentene in < 10 seconds giving 600 turnovers per $Fe_2(CO)_6(C_2H_4)_2$ unit and a turnover rate of at least 3600 per minute.

E. Photochemically Activated Hybrid Systems

As previously mentioned, the opacity of many supports has hindered photochemical preparation of hybrid catalysts, due to the nearly complete loss of useful light to scattering and reflection or to absorption by the support. In addition, spectroscopic characterization of the immobilized species, its catalytic forms, and its catalytic chemistry is often difficult. Yet, such information is vital to understanding and realizing the advantages of hybrid catalysts. The following discussion serves to summarize the available literature on the photochemical and photocatalytic reactions of iron carbonyls immobilized on both organic and inorganic supports.

De Paoli and Marco (97) have used the polymer matrices polytetrafluorethylene (PTFE) and polyethylene (PE) to study the ambient temperature photochemistry and olefin substitution reactions of $Fe(CO)_5$. Such polymer matrices are suitable for studying photoinduced metal carbonyl reactions for two reasons. First, they do not absorb the radiation used to induce the photochemical process which would hinder the reaction and might lead to polymer degradation. Second, they are transparent to infrared radiation in the terminal and bridging carbonyl stretching region (2200 - 1800 cm^{-1}) allowing spectroscopic characterization of photoproducts. $Fe(CO)_5$

was adsorbed into these matrices by soaking the polymer in a 10% solution of the complex in degassed hexane. After impregnation, no inert atmosphere was necessary since exposure of the sample to air did not result in detectable iron oxidation during the time frame of these experiments. The infrared spectrum of adsorbed $Fe(CO)_5$ exhibited two bands at 2020 and 1998 cm^{-1}, indicating that substituted mononuclear or polynuclear iron carbonyl complexes were not formed by adsorption onto the support. Following three minutes of broad-band UV irradiation two new absorptions were observed at 2063 and 1973 cm^{-1}, while the band at 1998 cm^{-1} (mainly due to $Fe(CO)_5$) grew in intensity relative to the 2020 cm^{-1} band before photolysis. The bands at 1973 and 1998 cm^{-1} were assigned to the photofragment $Fe(CO)_4$, while the 2063 cm^{-1} band was tentatively assigned to the more highly coordinatively unsaturated $Fe(CO)_3$ fragment. In order to study the photoinduced olefin substitution reactions of $Fe(CO)_5$, the polymer films pretreated with $Fe(CO)_5$ were saturated with the desired olefin. This was accomplished by either solution impregnation or vapor phase deposition. The iron carbonyl-olefin complexes formed following irradiation included dieneirontricarbonyl complexes and monosubstituted $Fe(CO)_4L$ complexes (L = ethylene, acetylene, and methylacrylate). The reactivity of the unstable, coordinatively unsaturated species in these polymeric matrices is an advantage over the use of

low temperature matrices where the cage effect of the frozen matrix often permits efficent recombination of photodissociated CO with the coordinatively unsaturated species to regenerate the parent molecule (98).

Jackson and Trusheim (99) have studied the ambient temperature photochemistry of silica-adsorbed $Fe(CO)_5$. UV irradiation of $Fe(CO)_5$ at surface coverages below monolayer with a N_2 laser yields $Fe_3(CO)_{12}$ as the dominant photoproduct. This cluster was identified by its characteristic infrared and electronic spectrum. The formation of $Fe_3(CO)_{12}$ on silica gel is in contrast to the photoproducts formed in solution and in the gas phase, where, in the absence of nucleophiles, UV irradiation of $Fe(CO)_5$ yields predominately $Fe_2(CO)_9$. Sublimation of $Fe_2(CO)_9$ onto silica gel resulted in a disproportionation reaction yielding $Fe_3(CO)_{12}$ and $Fe(CO)_5$. The participation of surface silanol groups as weak ligands provides a rationale for the photochemistry observed on silica gel since photolysis of $Fe(CO)_5$ in the presence of weak ligands also yields $Fe_3(CO)_{12}$ (59-60). The absence of $Fe_2(CO)_9$ is explained by its instability in the presence of weak ligands, where it dissociates to yield $Fe(CO)_5$ and $Fe_3(CO)_{12}$. UV irradiation of $Fe(CO)_5$ at surface coverages greater than monolayer coverage did, however, result in formation of $Fe_2(CO)_9$. This observation is consistent with the argument that the

surface silanol groups participate as weak ligands since these overlayers are not intimately associated with the silica surface. A mechanism for $Fe_3(CO)_{12}$ formation was postulated which involves initial formation of surface-bound $Fe(CO)_4$, which undergoes subsequent thermal trimerization on the silica surface.

In an effort to understand the secondary thermal processes leading to formation of $Fe_3(CO)_{12}$, Jackson and Trusheim have examined the photochemistry of silica-adsorbed $Fe(CO)_5$ at reduced temperatures (100). The only significant photoproduct observed by IR spectroscopy following irradiation with the second harmonic of a Nd:Yag laser (355 nm) at temperatures between 200 and 300 K is $Fe_3(CO)_{12}$: no $Fe_2(CO)_9$ was detected. The photochemistry of silica supported $Fe_3(CO)_{12}$ was also examined. This cluster was found to be photochemically inert since irradiation at 100 and 300 K at integrated laser exposures two times higher than those used in the $Fe(CO)_5$ experiments produced no observable loss of $Fe_3(CO)_{12}$. Following photolysis of $Fe(CO)_5$ at 200 K, the IR spectrum which exhibits bands attributed to both $Fe_3(CO)_{12}$ and $Fe(CO)_5$, was observed to undergo the following spectral changes upon warming the sample to room temperature. An increase in the intensity of the $Fe(CO)_5$ bands at the expense of the $Fe_3(CO)_{12}$ bands confirmed that a slow thermal reversal of the overall

photoprocess occurs at temperatures above ca. 200 K. Irradiation of silica-adsorbed $Fe(CO)_5$ at 100 to 150 K also yields $Fe_3(CO)_{12}$. However, the appearance of bands in the terminal CO streching region at 1960 and 1940 cm^{-1} indicate another major photoproduct is formed as well. The species exhibiting these bands has been assigned to $Fe(CO)_4(SiO_2)$, which denotes a species formed upon addition of a silica surface hydroxyl group or siloxane bridging oxo group to the primary photoproduct, $Fe(CO)_4$. In photolyses performed at 10 and 50 K, these bands are weak or absent. However, two new bands in the bridging carbonyl region are noted at 1860 and 1820 cm^{-1}. The latter band has been assigned to $Fe_2(CO)_9$ while the former band, due to poor resolution and peak broadening, remained unassigned. Changes in the intensities of these bands are observed upon warming a sample photolyzed at 10 K. At 50 K the 1860 cm^{-1} band has diminished in intensity, accompanied by a growth of the band at 1820 cm^{-1}. This trend continues on warming further to 100 K, where the 1860 cm^{-1} band is no longer observed. Except for the growth in the 1820 cm^{-1} band noted above, no further spectral changes were observed upon warming the sample to 250 K. Increasing the temperature to 300 K, however, leads to loss of the 1820 cm^{-1} band along with an increase in the bands assigned to $Fe_3(CO)_{12}$ and $Fe(CO)_5$. A new mechanism consistent with these observations was proposed, Figure 5, which involves

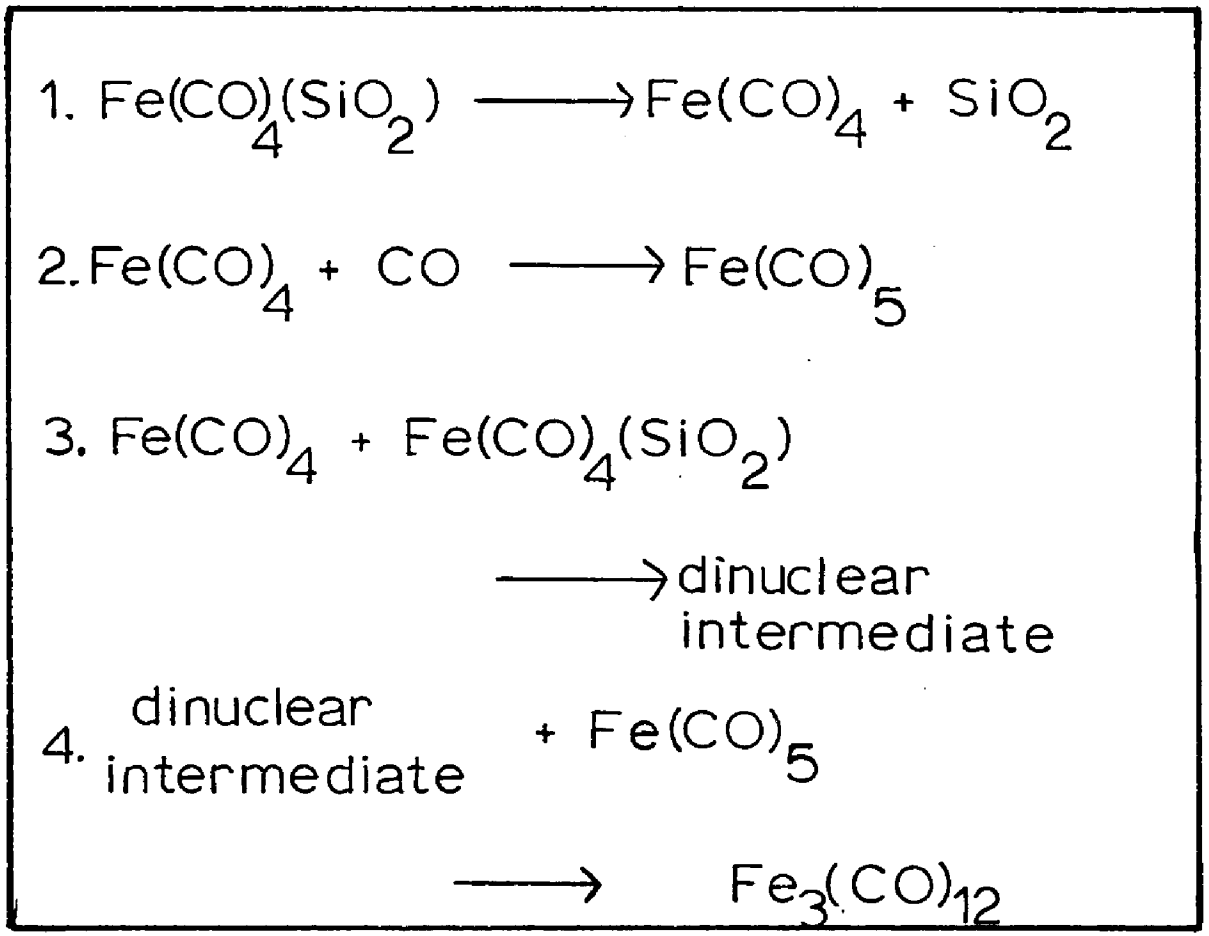

Figure 5. Mechanism for $Fe_3(CO)_{12}$ formation via photolysis of silica-adsorbed $Fe(CO)_5$.

formation of a short-lived dinuclear intermediate, formed thermally by reaction of uncomplexed $Fe(CO)_4$ with $Fe(CO)_4(SiO_2)$. The chemical identity of the dinuclear intermediate is uncertain, although, obvious candidates include the 18-electron species $Fe_2(CO)_8(SiO_2)$ and the 16-electron species $Fe_2(CO)_8$. The reactive dinuclear intermediate was then postulated to react thermally with adsorbed $Fe(CO)_5$ to form $Fe_3(CO)_{12}$.

Two reports investigating the photocatalyzed 1-pentene isomerization reaction using hybridized $Fe(CO)_5$ systems have been published in the literature. Wrighton and coworkers (101) have used the 1-pentene isomerization reaction as their probe reaction in comparing the photocatalytic activity of suspensions of polymer-anchored $Fe(CO)_n$ (n = 3,4) species with the homogeneous model complexes $Fe(CO)_4(PPh_3)$ and $Fe(CO)_3(PPh_3)_2$. The polymer, a 200-400 mesh styrene-1% divinylbenzene microporous resin, contains a triarylphosphine group which serves as the "anchor" for the iron carbonyl species. Infrared spectra in the carbonyl bridging region, following thermal displacement of CO by the polymer attached phosphine ligands, indicate that the predominant species surface-bonded to the polymer are $Fe(CO)_4$ and $Fe(CO)_3$. Near-UV irradiation of the model complexes established that loss of CO, not loss of phosphine, is the dominant photoreaction of phosphine

substituted $Fe(CO)_5$ complexes. The observed quantum yields for the polymer-anchored system, while substantially lower than the homogenous systems, exceed unity for each catalyst precursor. This finding confirms the photogeneration of a catalyst which effects a number of turnovers before requiring reactivation with light. The retention of the triarylphosphine ligand in the coordination sphere during catalysis is reflected in the intial ratio of trans/cis 2-pentene which varies for each catalyst precursor. While the catalytic chemisty is qualitatively the same for the polymer suspensions and for the homogeneous complexes, these results indicate the potential for designing photostable anchors which can exert some control over catalysis product distribution.

The photocatalytic isomerization of 1-pentene using $Fe(CO)_5$ supported on the surface of small-pore zeolites and absorbed in the supercages of large-pore zeolites was studied by Suib and coworkers (102). The interaction of $Fe(CO)_5$ with the zeolite surface was dependent on the extent of hydration of the zeolite. While dehydrated zeolites allowed the coordination sphere of $Fe(CO)_5$ to remain intact, hydrated zeolites caused decomposition of $Fe(CO)_5$ to an oxidized form, to another cluster ($Fe_3(CO)_{12}$), or to combinations of the above. The choice of zeolite and solvent in the photolysis experiments was critical since use of hydrated zeolites and benzene

resulted in significant leaching of iron into the solution. For this reason 1% $Fe(CO)_5$/dehydrated zeolites were used with isooctane as the solvent during the photolysis experiments. Analysis of the solution after several hours of photolysis verified no leaching of iron into solution occured and that heterogeneous catalysis was indeed taking place. The use of different zeolite supports in the isomerization reaction clearly alters the percent conversion and the trans/cis-2-pentene ratio as compared to those for homogeneous reactions. The trans/cis ratio was found to vary from about 2.7 to 4.4 depending on the zeolite used. Cation effects were also evident since lithium and cesium ion-exchanged zeolites yield greater percent conversions and a higher trans/cis ratio. It was suggested that cation effects are due to a modification of the electrostatic field that iron carbonyl species encounter on the zeolite surface. The larger percent conversions noted for large pore zeolites relative to use of small pore zeolites were attributed to the enhanced stability of the photogenerated subcarbonyl species adsorbed in the supercages of the zeolite rather than on the surface.

The transparency of Corning code 7930 Porous Vycor glass, PVG, to visible and near-UV light circumvents the difficulties associated with photoactivation of surface confined species on opaque supports since scattering and

absorption of light is negligible at wavelengths $\geq$ 350 nm. Characterization of the photoproducts by spectroscopic techniques based on the transmission of light, (UV-visible, Raman spectroscopy), is also possible. These advantages have provided the incentives for studying the photochemistry of iron carbonyls adsorbed on this support. Morse, Borelli, and Schreurs (103) have investigated the photochemical reactions of organometallic compounds adsorbed onto PVG. Impregnation of PVG with $Fe(CO)_5$, followed by exposure to light and subsequent heating in air, resulted in high resolution optical density changes in the glass. The photoreaction involves the breaking of one or more iron-carbon bonds leading to a coordinatively unsaturated species, which reacts with the hydroxyl groups on the glass surface. Heating had the effect of removing the unreacted $Fe(CO)_5$ by volatilization, and stabilizing the photolyzed product through formation of an iron oxide. The magnetic properties of the iron oxide were investigated, and it was found that both superparamagnetic and ferrimagnetic particles were present, with the single domain particles having an exceedingly high coercive force. While an identification of the magnetic phase has not been made, since the phase is ferrimagnetic only two distinct possibilities exist within the iron-oxide system, i.e.; Fe_3O_4, and Fe_2O_3 or solid solutions of the two. Electron microscopy indicates the distribution of iron-oxide

particles is relatively uniform over the radius range 50-100 Å, and the depth of adsorption is ca. 100 micrometers. The resolution which could be attained has been shown to be < 1 micrometer, illustrating the potential of these materials to be used for high UV transmitting, durable, low-expansion photomask applications.

This doctoral research has exploited the transparency of PVG in characterizing the photochemical and photocatalytic reactions of iron carbonyls adsorbed onto this support. In order to interpret the role of the support in photochemically activated hybrid systems, an understanding of the nature of the interaction between support and adsorbate is essential. This requires a detailed understanding of the surface properties of the support used. The following discussion will detail the surface properties of Corning Code 7930 Porous Vycor Glass.

F. Properties of Porous Vycor Glass.

Porous Vycor Glass is obtained as an intermediate in the process used for the manufacture of 96% silica glass (104,105). First, a glass in the borosilicate system is melted and fabricated by standard glass manufacturing techniques at comparatively low temperatures. Following fabrication, it is subjected to a heat treatment that

causes the glass to separate into a boron-rich and a silica-rich phase. Subsequent treatment with weak acids and/or alkalies causes the soluble boron-rich phase to leach out, leaving a porous silica glass which retains its original shape, even on consolidation. The final product, consisting of 96% SiO_2, 3% B_2O_3, and 1% Na_2O and Al_2O_3, is a transparent, surface hydroxylated silica, which contains a myriad of randomly dispersed, interconnected pores (106-115). Samples containing $1.2 \pm 0.3 \times 10^{18}$ pores/gram with a pore diameter of 70 ± 21 Å, have a surface area of 130 meter^2/gram . The surface of PVG is anionic since it develops a zeta potential of -26 $\pm$ 2 mV in distilled water at 25 $\pm$0.1 C (116). This is consistent with previous studies in this laboratory which indicate that cationic and neutral complexes are readily adsorbed while anionic complexes show no significant adsorption. Adsorption of various indicator dyes onto PVG, and their subsequent color changes, suggest that the surface pH of PVG is between 4 and 5 (117).

Since PVG consists of 96% silica, it would seem reasonable to conclude that its surface properties would be analgous to those of a slightly impure silica gel. Although the surfaces of silica gel and PVG have many similiar features, numerous studies have shown that there are differences in both surface functionality and dimensionality between these two supports. Hair and

Chapman (118) have studied the adsorption of ammonia onto PVG in order to probe the surface heterogeneity of this support. Infrared spectra recorded following adsorption of ammonia at room temperature reveal the presence of both physisorbed and chemisorbed ammonia. A comparison of the NH_3 vibrations of the chemisorbed species with those of a NH_3-BF_3 complex confirms that these bands are due to NH_3 molecules coordinatively bonded to Lewis-acid type sites on the surface. Quantitative work by the same authors indicates that ca. one third of the PVG surface consists of B_2O_3 Lewis-acid type sites which are not present on purified silica gels. More recent work has shown the dimensionality of the PVG surface to be significantly lower than that of silica gel. The Hausdorff dimension of silica gel is 2.94 ± 0.06, whereas Jortner and coworkers (119) report that of PVG is 1.76 ± 0.12. Both of these factors, while not affecting the primary photoprocess, may influence the secondary thermal and photochemical reactions of an adsorbate on PVG so that the observed reaction products differ from those formed on silica gel.

The transparency of PVG to visible and near-UV light, together with the previously discussed advantages associated with more traditional inorganic supports, make it ideal for studying the photoinduced surface reactions of immobilized metal carbonyls. Since

scattering and absorption of light by PVG at wavelengths > 300 nm is minimal, the efficiency of the photochemical processes is large relative to the use of more opaque organic and inorganic supports. In addition, determination of quantum yields for the photoprocesses are possible since scattering and absorption of incident radiation by PVG can be virtually neglected. The use of PVG as a support also enables characterization of the adsorbed species by spectroscopic techniques not available to the surface scientist studying reactions on opaque supports. Previous work in our laboratory (120) has established the viability of using UV-Vis and Raman spectroscopy as well as flash photolysis techniques in characterizing surface species.

In the discussion detailing the thermal and photochemical reactions of iron carbonyls immobilized on various supports, we have seen numerous examples where interaction of the photogenerated subcarbonyl species with the support imparts additional stability to these reactive species. Given their transient existence in ambient temperature fluid solution (< 1 usec), the enhanced stability provided through interaction with the support aids in their spectroscopic characterization and eludication of thermal and photochemical reaction pathways. The kinetic stabilization of photogenerated intermediates adsorbed onto PVG has been previously

demonstrated by Kubokawa and Anpo (121). Work in this laboratory has focused on studying the photochemical and photocatalytic reactions of metal carbonyls adsorbed onto PVG. The use of PVG as a convenient alternative to low temperature matrices for isolation and characterization of group 6 pentacarbonyls has been reported by Simon, Morse and Gafney (122). Adsorption of $M(CO)_6$ (where M = Cr, Mo and W) onto PVG does not disrupt the primary coordination sphere, and in all cases the complexes are physisorbed onto this support. Near-UV photolysis of the physisorbed $M(CO)_6$ complexes results in subsequent generation of the corresponding pentacarbonyls, designated $M(CO)_5(ads)$. These photogenerated subcarbonyls have spectroscopically quantitated lifetimes of $\geq$ 48 hours in vacuo at room temperature. The similarity of the UV-visible spectra of the $W(CO)_5(ads)$ with spectra of $W(CO)_5L$ species, where L is an O-donor ligand, indicates that the vacated coordination site is occupied by a silanol group or adsorbed water on the support. The unusually long lifetimes of $M(CO)_5(ads)$ is attributed to a weak interaction between the absorbate and the support. However, stability does not occur at the expense of subsequent thermal reactivity since exposure of $M(CO)_5(ads)$ to various ligands results in rapid quantitative formation of $M(CO)_5(ads)$. The activation energy of the reactions of $W(CO)_5(ads)$ with added CO confirm that the $W(CO)_5$-PVG interaction is weak

($\leq$ 7 kcal/mole) (123). Dieter and Gafney (124) have reported that adsorption of $Ru_3(CO)_{12}$ onto PVG results in oxidative addition of a silanol group across a Ru-Ru metal bond, forming H-$Ru_3(CO)_{10}$-OSi. Characterization of the chemisorbed complex was by gas phase analysis, UV-visible and diffuse reflectance FTIR spectroscopy. While adsorption of $Ru_3(CO)_{12}$ onto PVG followed by evacuation resulted in formation of H-$Ru_3(CO)_{10}$-OSi, the thermal reaction appeared to be slow, requiring several days at room temperature. In contrast, in vacuo near-UV irradiation of physisorbed $Ru_3(CO)_{12}$ resulted in formation of the oxidative addition product in a few minutes.

The very nature of the support and precursor catalysts provide the impetus for studying the photochemistry of iron carbonyl complexes adsorbed onto PVG. The choice of iron carbonyls as photochemical precursors is based on the extensive characterization of their photophysical, photochemical, and thermal reactions and their known ability to photocatalyze diverse organic transformations of industrial significance (78-82). The transpareny and unique surface properties of PVG have spurred its use as a support in these studies. Particular emphasis was placed on eludicating, on a molecular level, the interaction of the support with the photogenerated products. The objectives of this doctoral

research are two-fold; 1) to investigate the photochemical and secondary thermal reactions of iron carbonyl complexes adsorbed onto PVG, and 2) to explore the potential for creating novel, more efficent catalysts via photoactivation of hybrid catalysts using iron carbonyl precursors.

EXPERIMENTAL SECTION

A. Materials.

$Fe(CO)_5$ (Pressure Chemical Company) was vacuum distilled and stored in a freezer under an inert atmosphere. Absorption and IR spectra of the distilled complex were in excellent agreement with the published spectra. $Fe_2(CO)9$ and $Fe_3(CO)_{12}$ (Pressure Chemical Company) were used as received since their absorption and IR spectra were in excellent agreement with published spectra. $Fe(CO)_4$(pyridine) was prepared photochemically (125). 12.4 millimoles pyridine and 14.9 millimoles of $Fe(CO)_5$ were dissolved in 300 mls. n-hexane in a pyrex roundbottom flask equipped with a rubber septum. The solution was degassed by nitrogen bubbling for 15 minutes and then photolyzed at 310 nm for one hour. The solvent was removed in a Roto-evaporator at room temperature under reduced pressure. The resulting air stable, dark orange crystals decompose on melting at 65 °C. The IR spectrum of the complex in n-hexane, shown in Figure 6, exhibits bands in the carbonyl stretching region at 2050, 1964 and 1939 cm^{-1} which are in excellent agreement with the literature spectrum of the complex. The UV-visible spectrum of the complex in n-hexane, Figure 7, exhibits a strong MLCT transition at 220 nm and a d---d ligand field transition which appears as a shoulder at 270 nm. The

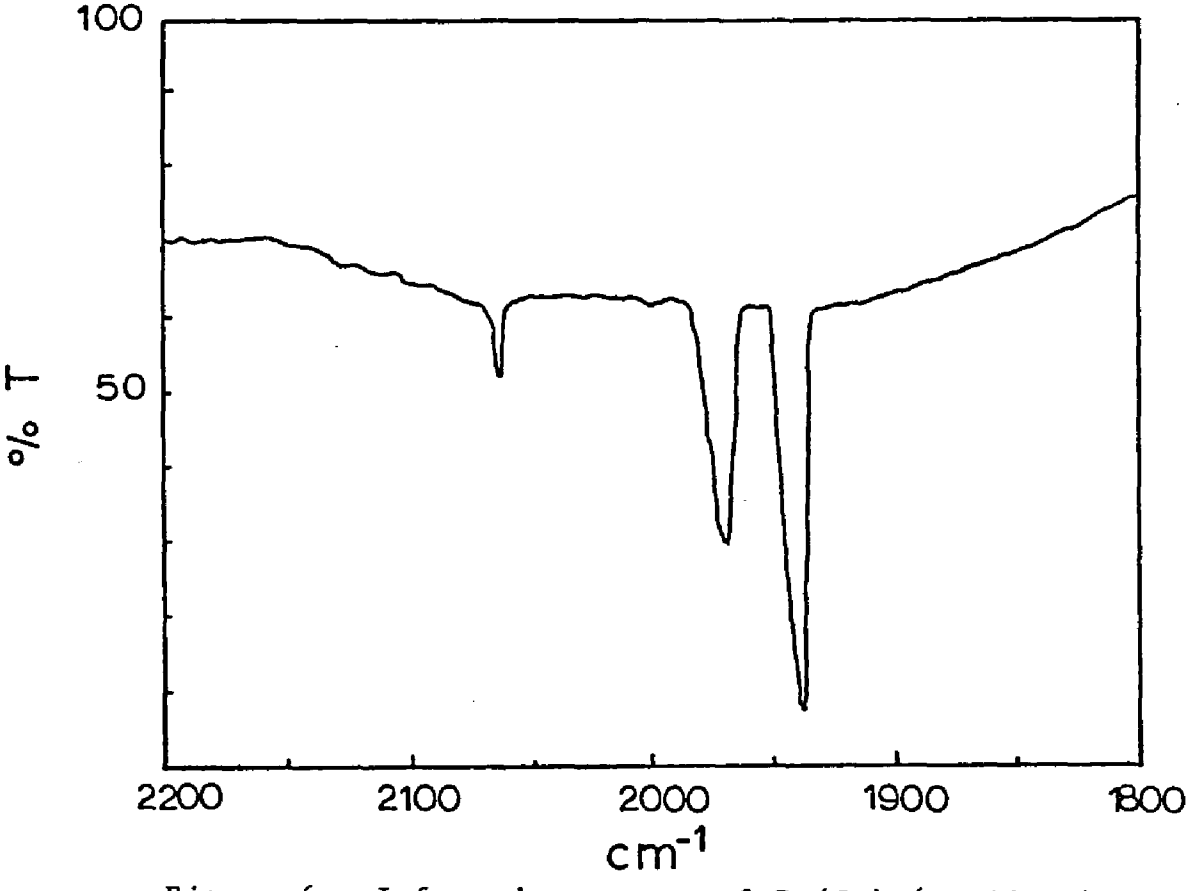

Figure 6. Infrared spectrum of $Fe(CO)_4$(pyridine) in hexane.

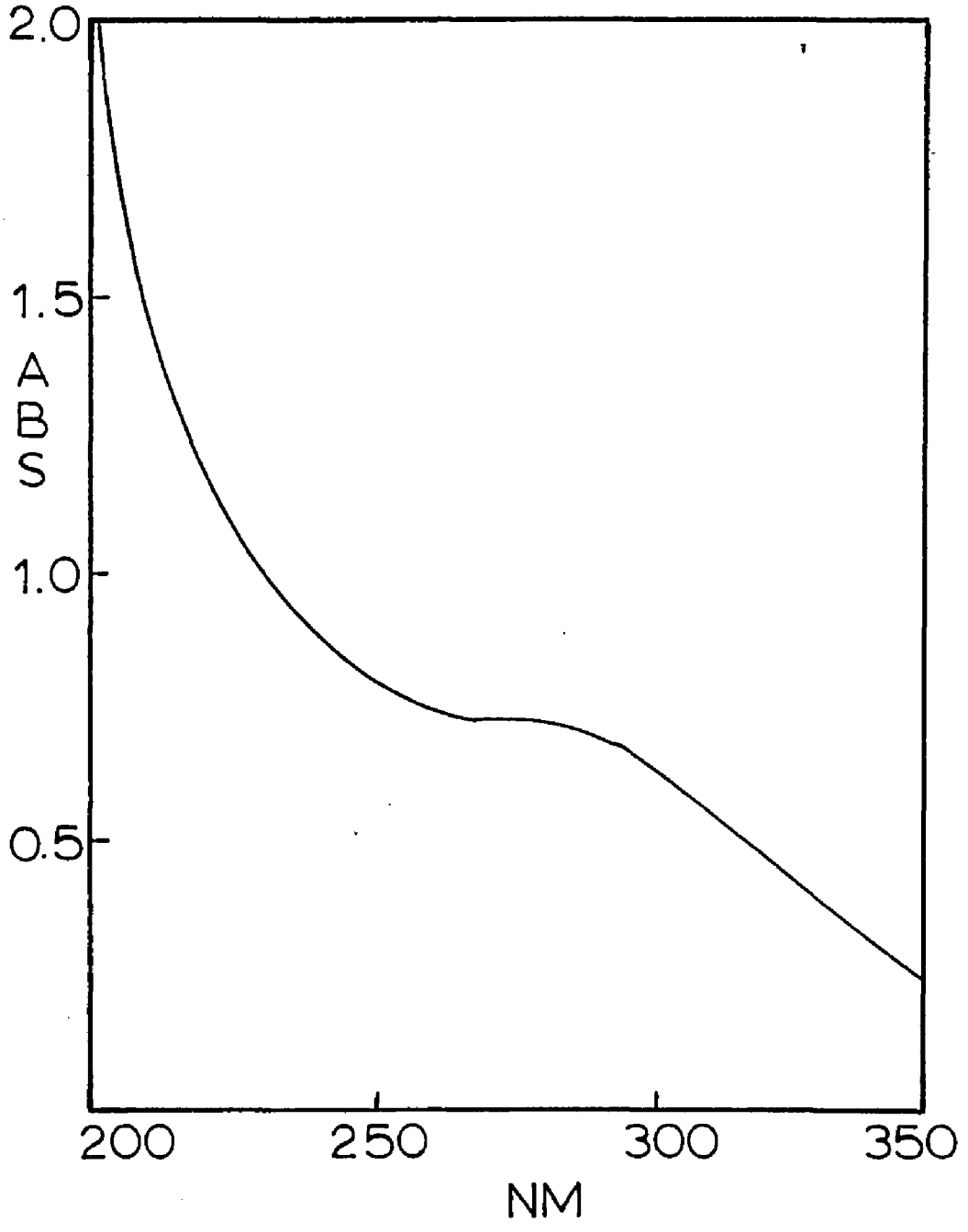

Figure 7. Electronic Absorption Spectrum of $Fe(CO)_4$(pyridine) in hexane.

complex also exhibits a tail-end absorption extending into the visible region characteristic of the spectra of mono-substituted $Fe(CO)_4L$ complexes, where L is a weak ligand. Both 1-pentene (Fluka) and trimethylphosphine (Strem) were used as received since their IR spectra agreed with literature spectra. Ethylene (Matheson) and Carbon Monoxide (Linde or Matheson, CP grade) were used as received. Spectral grade solvents were distilled over CaH_2 and stored over molecular sieves prior to use.

Code 7930 Porous Vycor Glass containing 70 ± 21 Å diameter cavities was obtained from the Corning Glass Works. To insure reproducibility, the PVG was subjected to a standardized pretreatment procedure. Pieces (25 mm x 19 mm x 4 mm) were continuously extracted with distilled water for 24 hours, and then dried at 60 °C under reduced pressure ($p \leq 10^{-4}$ torr). The dried samples were calcined in air at 550 °C for at least 24 hours and stored at this temperature until needed. For diffuse reflectance FTIR (DRIFT) experiments, extracted, dried pieces of PVG were crushed to a 325 mesh powder ($\leq$ 45 microns). The powder was calcined at 550 °C for 12 hours, and then transferred while hot to tightly capped vials which were stored in an oxygen and water free glove box. For Ferromagnetic Resonance (FMR) experiments, pretreated plates of PVG were coasely ground and stored at 550 °C until needed.

B. Sample Impregnation.

Impregnation with $Fe(CO)_5$ was by vapor deposition where the number of moles adsorbed was determined by differential pressure measurements (126). After removal from the oven, the PVG was transferred in air to a 1 cm x 2.2 cm x 4 cm rectangular quartz cell. The sample was mounted upright in the cell with teflon holders, and a pyrex top attached by means of a 7.62 cm o.d. O-ring joint. The top possessed a 2 mm high vacuum valve with a 10/30 ground glass joint through which the entire cell apparatus, illustrated in Figure 8, could be connected to a pyrex vacuum line. Before impregnation, the optical spectrum of the PVG was recorded versus an untreated piece of PVG to establish a baseline. The pyrex vacuum line was equipped with MKS Baratron Models 315, BHS-1000 and 315 BHS-1 capacitance pressure sensors and a MKS Baratron Model 170 monitor. The line was evacuated to a pressure of $\leq 10^{-6}$ torr, and $Fe(CO)_5$ vapor from the previously degassed aliquot was allowed to expand into the line. The pressure in the line was recorded and the vapor was allowed to expand onto the cell. Equilibration occurred in < 5 min, and the pressure drop was recorded. Measurements were also performed without the PVG sample to correct for adsorption onto other surfaces, and the moles of $Fe(CO)_5$ adsorbed onto the PVG sample were calculated from the corrected pressure drop. Following

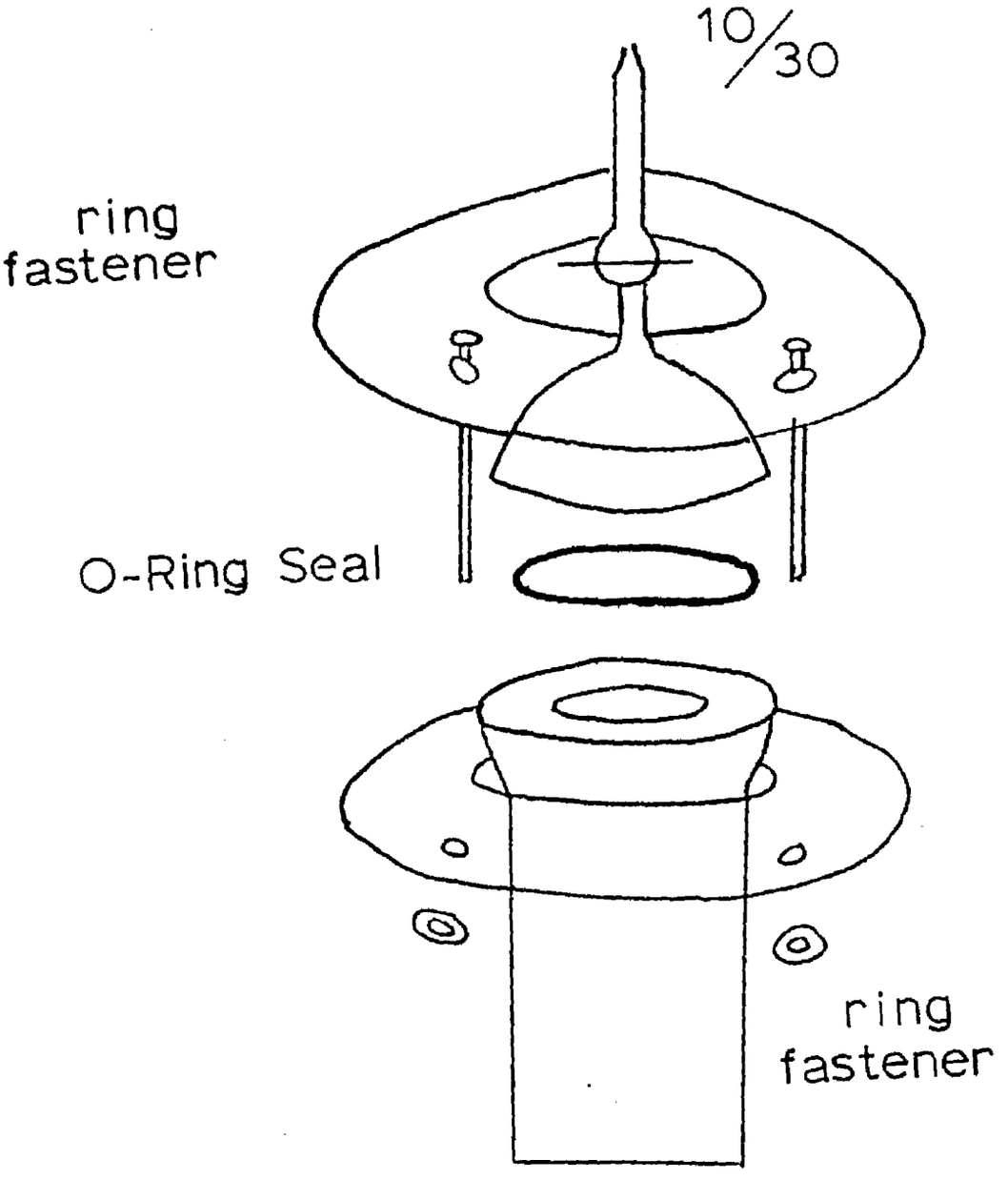

Figure 8. Cell apparatus.

equilibration, the optical spectrum of the impregnated sample was recorded. A number of samples containing from 2.0×10^{-8} to 2.0×10^{-5} moles of $Fe(CO)_5$(ads) /gm of PVG were prepared in this manner. The measured absorbance was corrected for absorbance due to PVG, which was determined from the PVG spectrum prior to impregnation, and calibration plots, Figures 9 and 10, of the moles of complex adsorbed versus the optical density of $Fe(CO)_5$(ads) at 350 and 400 nm, respectively, were constructed. The number of moles of complex adsorbed onto subsequent samples was determined from these plots, and their measured optical density. Because of an inherent spectroscopic uncertainity of $\leq$ 8%, due to light scattering by the random internal pore structure of PVG, there is an uncertainity of ca. 10% in the moles adsorbed determined by this spectroscopic technique. Samples prepared by adsorption of $Fe(CO)_5$ vapor contained, as determined by optical measurements, from 10^{-7} to 10^{-4} moles of $Fe(CO)_5$(ads)/gm. of PVG. In the FMR experiments, the coarsely crushed PVG was removed from the oven and placed in a quartz EPR tube equipped with a 19/22 ground glass male joint which allowed attachment of a 2 mm high vacuum valve equipped with a 10/30 joint, Figure 11. Following evacuation at room temperature for 0.5 hours, the PVG was impregnated in the same manner described above.

Figure 9. Calibtration Plot: Moles $Fe(CO)_5$(ads.)/gm. PVG vs. optical density at 350 nm.

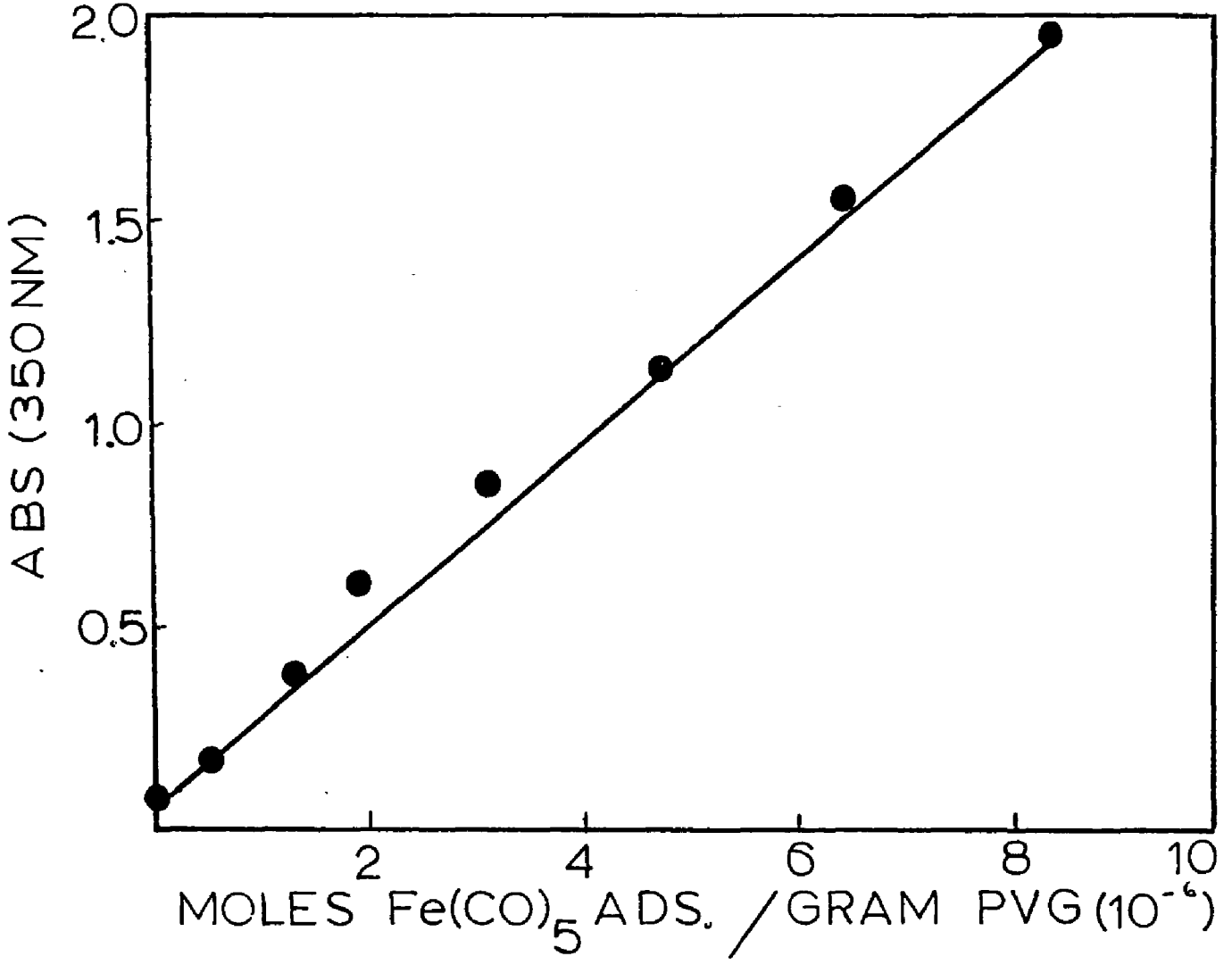

Figure 10. Calibration Plot: Moles $Fe(CO)_5$(ads.)/gm. PVG vs. optical density at 400 nm.

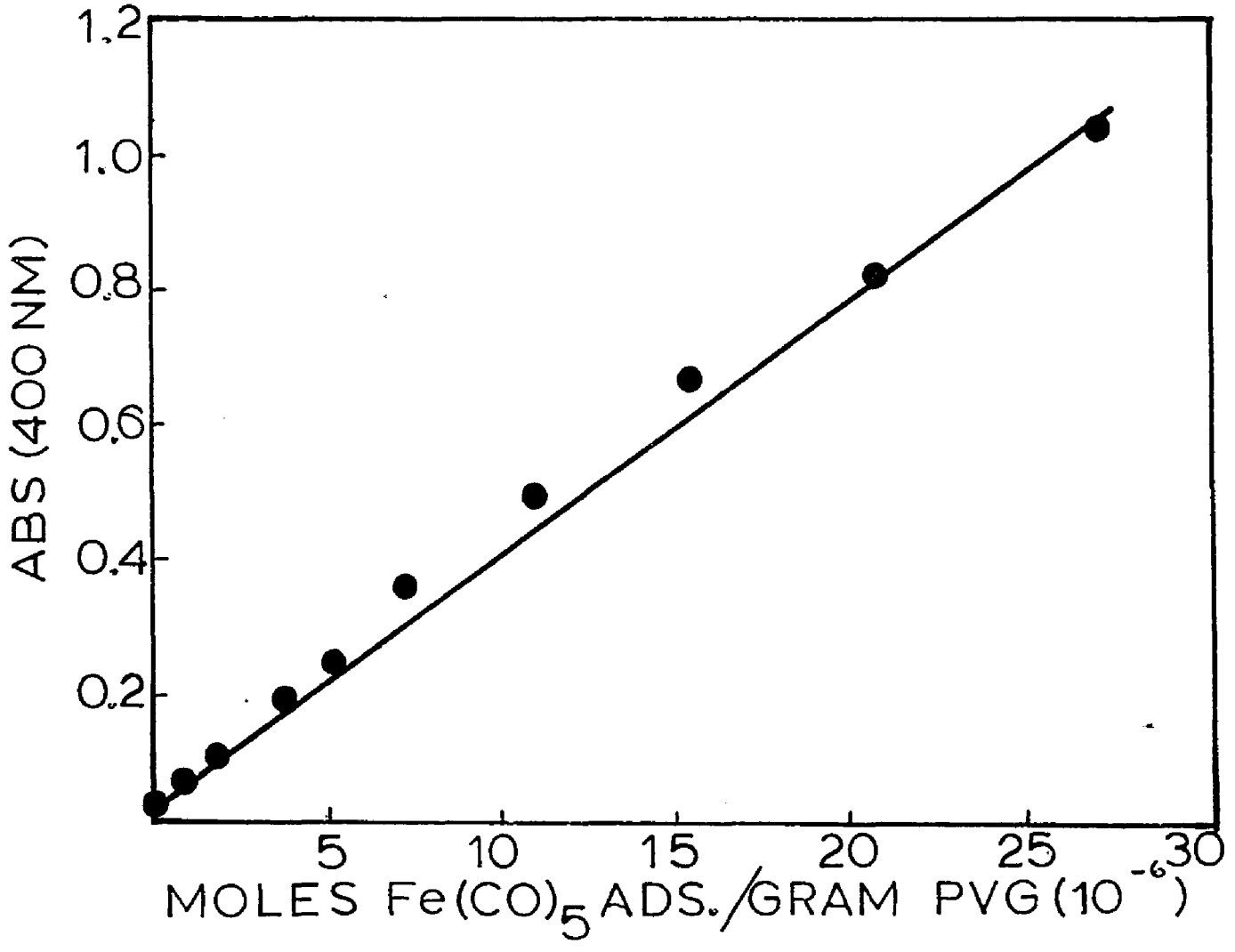

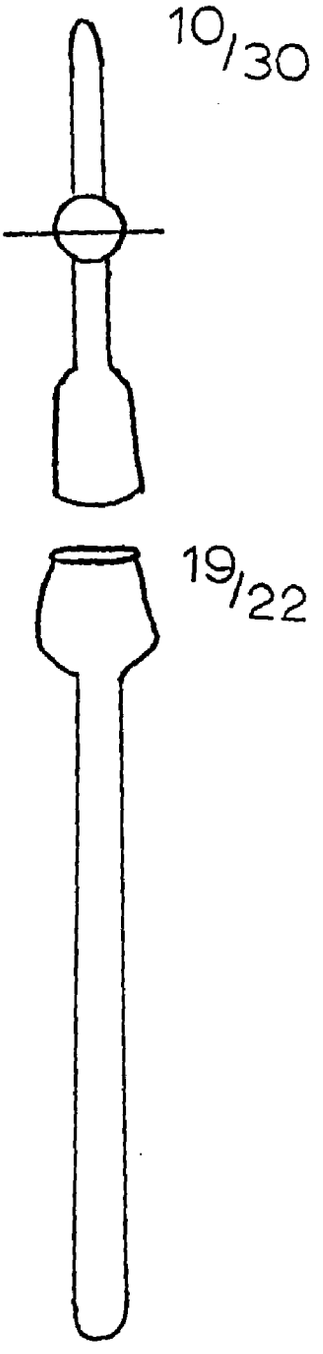

Figure 11. EPR apparatus.

Impregnation with $Fe_3(CO)_{12}$ was by solution or sublimation techniques, whereas impregnation with $Fe_2(CO)_9$, due to the low solubility of the complex, was either by dry mixing $Fe_2(CO)_9$ with crushed PVG under an inert atmosphere or by sublimation techniques. Solution impregnation of PVG was accomplished by mounting clean, dry pieces of PVG upright in an Eastman Kodak developing jar (catalogue number 13265) followed by addition of 50 ml of a degassed n-hexane solution of $Fe_3(CO)_{12}$. Both the molarity of the solution and the soaking time were varied, depending on the surface coverage desired. The absorbance of the solution phase was monitored during adsorption and the number of moles of complex adsorbed was calculated from the absorbance change at 605 nm. Following impregnation, the excess solvent and air were removed under vacuum. A number of samples ranging from 10^{-8} to 10^{-6} moles $Fe_3(CO)_{12}$ adsorbed/gm. of PVG were prepared in this manner, and a calibration curve, Figure 12, of the moles of complex adsorbed versus the optical density of $Fe_3(CO)_{12}$(ads) at 605 nm was constructed. In the FMR experiments, impregnation of PVG with $Fe_3(CO)_{12}$ was by soaking the coarsely ground PVG in a degassed n-hexane solution of the complex. Following adsorption, the impregnated crushed glass was filtered off, and the moles adsorbed determined from the decrease in absorbance of the solution phase at 605 nm. Sublimation of the complexes onto PVG was accomplished using the sublimation

Figure 12. Calibtation Plot: Moles $Fe_3(CO)_{12}$(ads.)/gm. PVG vs. optical density at 605 nm.

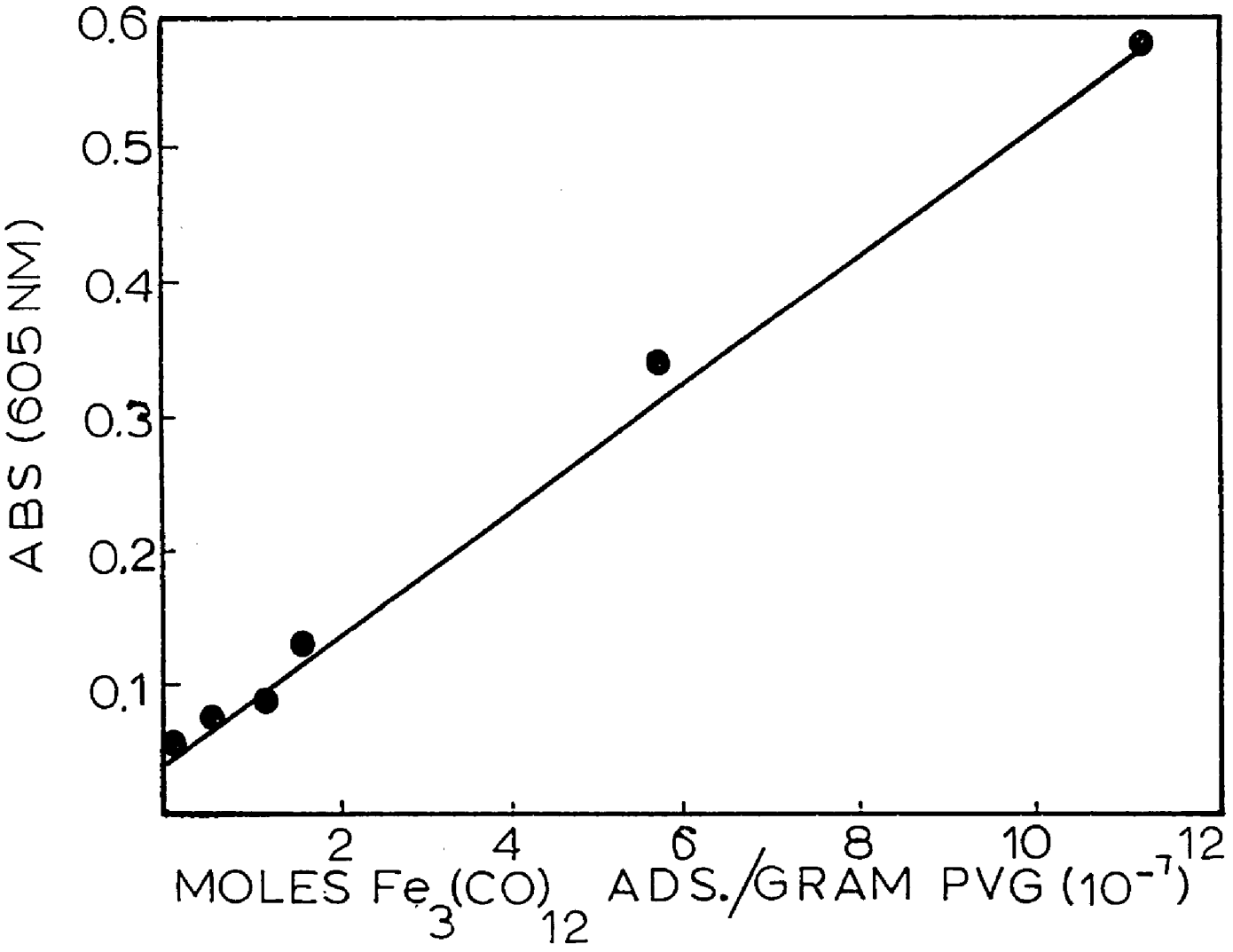

apparatus shown in Figure 13. Both plate and powdered samples of PVG were suspended above the solid complex, the chamber was evacuated, and the complex sublimed onto the support under vacuum at 60 °C.

C. Adsorption Isotherms.

Adsorption isotherms for $Fe(CO)_5$ on both plate and crushed (325 mesh) PVG were determined at room temperature, 26±1 °C, using standard differential pressure measurements (126). The adsorption isotherm on plate PVG, shown in Figure 14, was measured using the previously described rectangular quartz cell and pyrex vacuum line system. A sample of clean, calcined plate PVG was mounted in the cell which was then attached to the vacuum line. Outgassing due to the sample was minimized by evacuating the cell for several hours ($p \leq 10^{-6}$ torr) at room temperature. $Fe(CO)_5$ vapor from a previously degassed aliquot was allowed to expand into the line and the pressure recorded. The pressure following expansion of $Fe(CO)_5$ vapor into the cell containing the sample was recorded after equilibration, and the moles adsorbed calculated from the pressure drop. Additional points were determined in the same manner. The adsorption isotherm on crushed PVG, shown in Figure 15, was measured by loading 0.28 grams of PVG into a high vacuum diffuse reflectance cell (Harrick KKK model) under

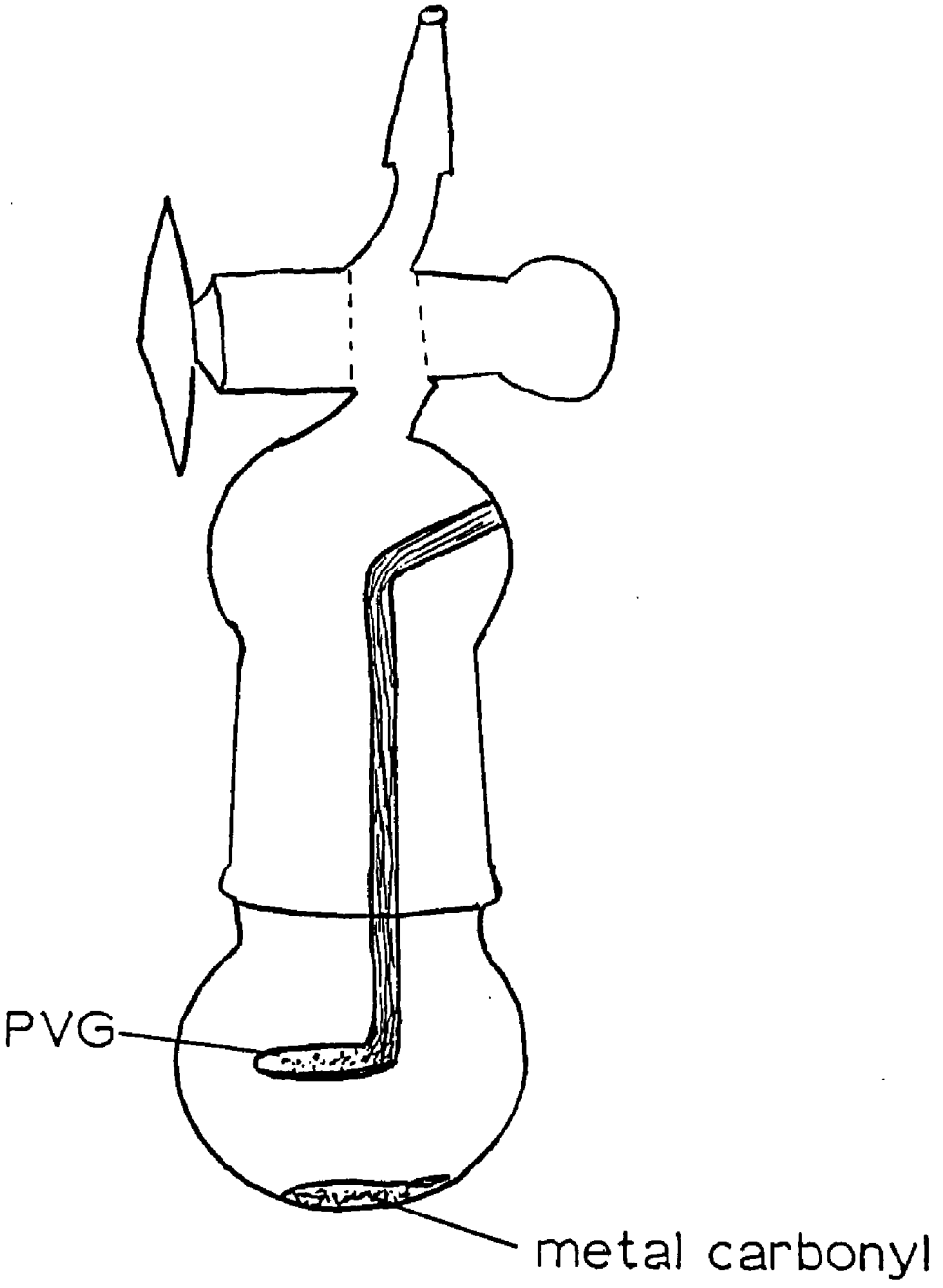

Figure 13. Sublimation apparatus.

Figure 14. Adsorption isotherm for $Fe(CO)_5$ On Plate PVG (26 C).

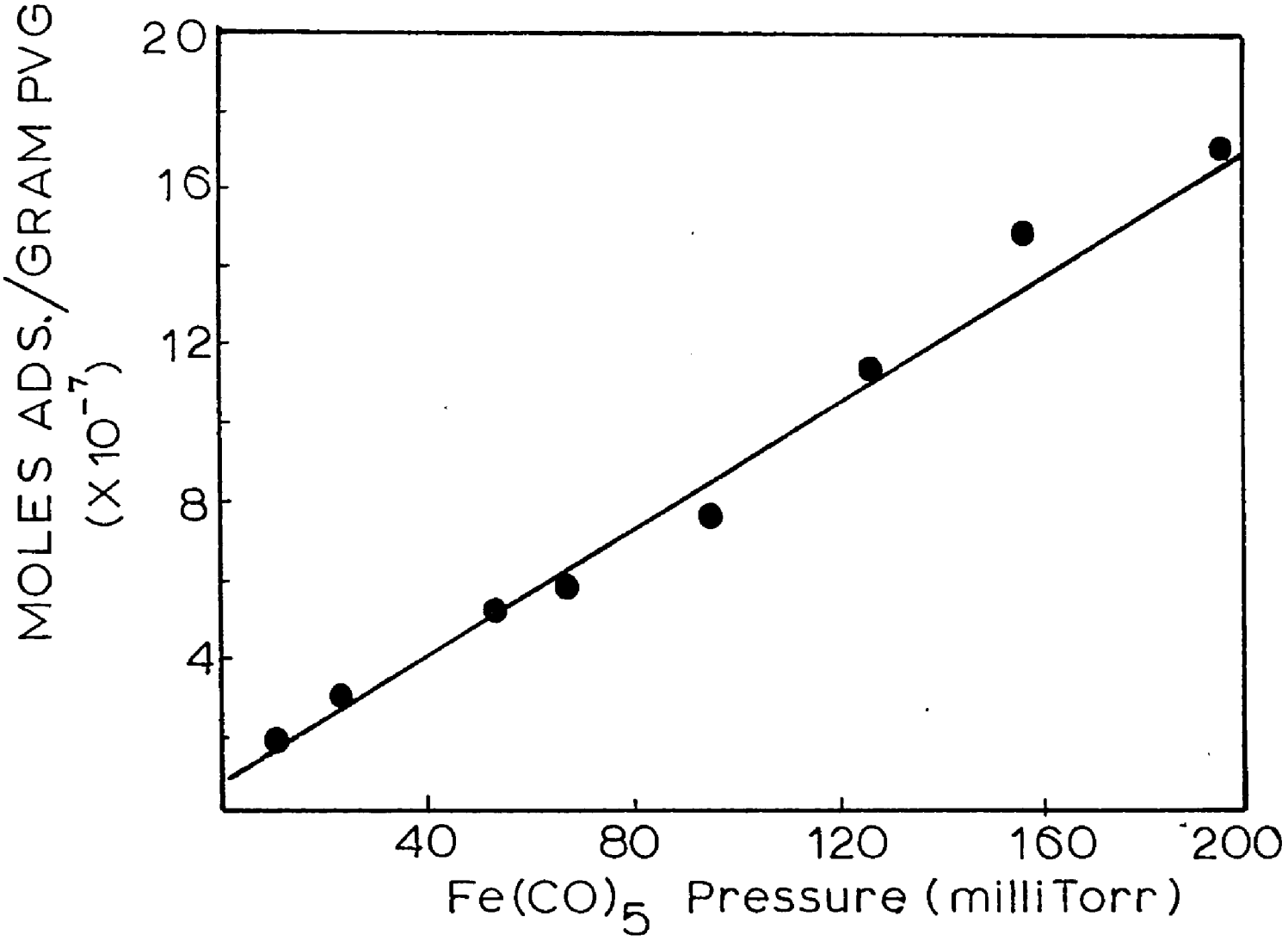

Figure 15. Adsorption isotherm for $Fe(CO)_5$ on Crushed PVG (26 C).

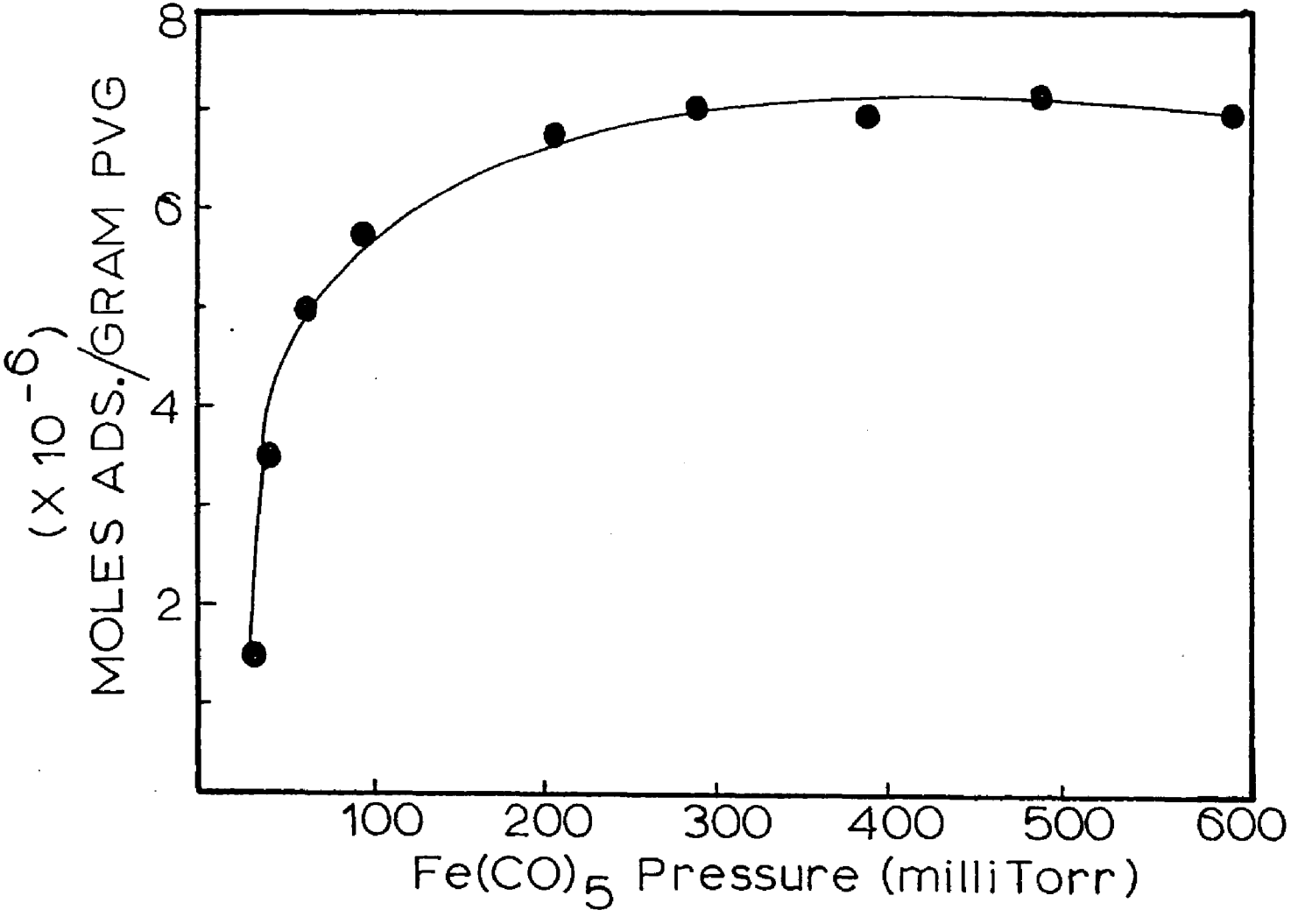

an inert atmosphere. The cell was then sealed and transferred to the FTIR sample compartment where it was attached to the metal vacuum system (see below) and evacuated for several hours ($p \leq 2 \times 10^{-6}$ torr) at room temperature. The cell was closed off and $Fe(CO)_5$ vapor allowed to expand into the vacuum manifold. The moles of complex adsorbed following equilibration was determined as described previously for the plate samples.

D. Photolysis Procedures.

Calcined pieces of PVG where transferred while hot to the previously described rectangular quartz cell. The cell was attached to the vacuum line and evacuated ($p \leq 10^{-4}$ torr) while the sample cooled to room temperature, 22 ± 1 °C. The sample was exposed to $Fe(CO)_5$ which had been degassed by three freeze-pump-thaw cycles, allowed to equilibrate, and then re-evacuated to remove $Fe(CO)_5$ remaining in the vapor phase. Tests with the empty cell showed that adsorption onto the cell walls was spectrally undetectable, and the moles of complex adsorbed onto PVG was determined from its optical density and the above calibration plot. The number of moles of $Fe_3(CO)_{12}$ adsorbed following solution impregnation was also determined in this manner. Prior to photolysis, excess solvent and air were removed by evacuating the rectangular cell, or in the case of the FMR exeriments,

the quartz EPR tube. $Fe(CO)_5$ and $Fe_3(CO)_{12}$ impregnated samples were irradiated in a Rayonet photochemical reactor (Southern New England Ultraviolet Co.) equipped with either 350, 310, or 254-nm bulbs. The excitation intensity was determined by ferrioxalate actinometry (127) and was typically 2×10^{-9} Einsteins/sec-cm^2. However, quantum yield measurements were limited to 350-nm excitation since competitive adsorption of PVG is negligible at this wavelength. UV-visible and FMR spectra of the adsorbed complexes and photoproducts were recorded periodically to monitor the consumption of the starting material and photoproduct formation. UV-visible spectra were recorded on a Cary 14 spectrophotometer whose sample compartment was modified to hold the rectangular cells. Difference spectra, indicative of only the adsorbates, were recorded by placing an unimpregnated piece of PVG in the spectrophotometer reference compartment. FMR spectra of products generated on coarsely ground PVG were recorded at room temperature, $22 \pm$ °C, on an IBM-Bruker Model ER200E-SCR spectrometer equipped with a X-band microwave source which was calibrated using a strong pitch standard. No resonance was detected from the unimpregnated PVG.

In the time resolved diffuse reflectance FTIR (DRIFT) experiments, spectra of the adsorbed species were recorded on a Nicolet Model 60SX FTIR equipped with a

narrow band MCT detector. A diffuse reflectance beam condensor (Harrick Scientific Model DRA-PMN) mounted in the sample compartment was modified to accept a custom designed diffuse reflectance microreactor, illustrated in Figure 16. The microreactor, which has a 26 mm x 3 mm x 2 mm sample bed, was loaded with previously calcined, 325 mesh PVG in a dry, inert atmosphere box. A BaF_2 window, which is transparent to UV, visible, and infrared radiation, was attached above and in contact with the 325 mesh sample. This arrangement allowed the recording of adsorbate spectra without interference from reagents in the gas phase. The microreactor was then mounted on a translational stage that allowed 3 mm diameter spots to be sampled along the entire length of the sample bed. The sample compartment of the spectrophotometer was modified to pass electrical, gas flow, vacuum, liquid flow, and auxilary purge lines to the microreactor as well as a shaft for positioning the translational stage. Quartz windows were installed in the sample compartment to admit the exciting radiation. These windows were masked during all manipulations to prevent unplanned photochemistry prior to the experiment.

The lines attached to the microreactor were connected to a vacuum system consisting of a forepump (Edwards Model E2M5), diffusion pump (Edwards Model E01), trap, metal lines and fittings (Cajon Ultratorr), bellows

Figure 16. Diffuse reflectance microreactor.

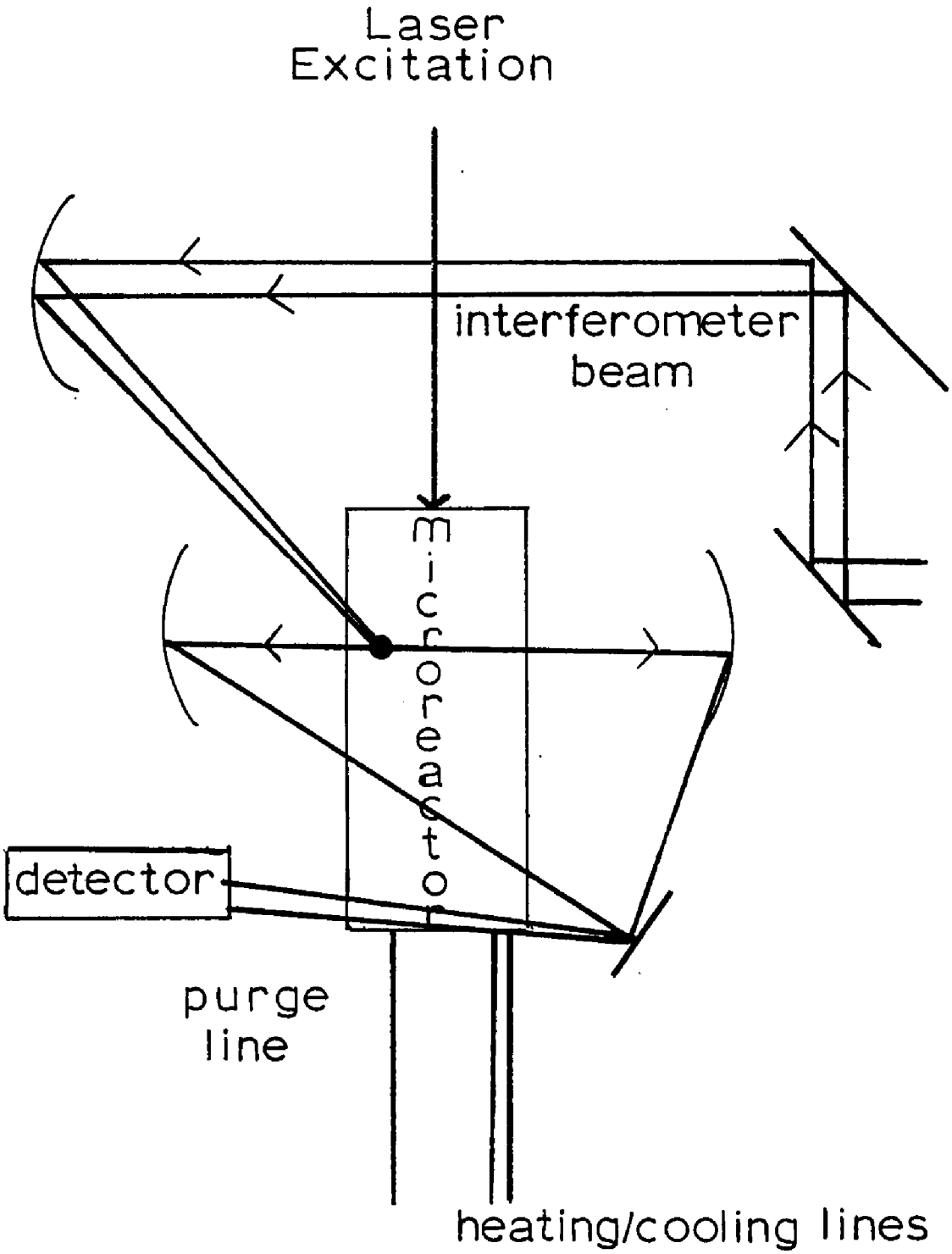

sealed valve (Nupro), and capacitance pressure sensors (MKS Baratron Models 315BHS-1000 and 315 BHS-1) and monitiors. An auxilary gas manifold equipped with needle valves and a Penning sensor (Edwards Model CP25) and controller (Edwards Model 8) was used to evacuate the microreactor to a pressure of 2×10^{-6} torr. Gas samples were then prepared in this line (total volume 102 ml) and were admitted to the microreactor cell in the FTIR sample compartment through narrow bore tubing (total volume 1.5 ml). The powdered PVG was impregnated with $Fe(CO)_5$ by expanding a set quantity, generally 5 torr in 102 ml, into the microreactor cell. After equilibration, the cell was closed off and and the manifold re-evacuated. The surface loading using this procedure was calculated to be 3×10^{-4} moles of $Fe(CO)_5$/gm. of PVG. Following evacuation of the manifold, other gases such as CO, $P(CH_3)_3$, ethylene, and 1-pentene were admitted to the reactor and the desired pressure established.

In a typical DRIFT experiment, background spectra, i.e., spectra of the unimpregnated PVG in the evacuated microreactor, were recorded in each sampling position. $Fe(CO)_5$ was expanded into the cell and after equilibration the desired gas was added. Initial spectra were recorded at each sampling position and then the samples were irradiated at 350 nm with a Kr ion laser (Coherent Model CR3000K) or at 355 nm with the second

harmonic from a Q-switched (Quanta Ray Model DCR-2) Nd:YAG laser. In the cw experiments the laser intensity was measured with a Coherent Model 210 power meter, and the laser output was adjusted to provide 500 milliwatts to an area, 0.13 cm^2, slightly larger than the FTIR sampling area. The exposure time of the cw irradiation was controlled with a (Newport Research Model 880) electronic shutter, timed to open between the spectometer data acquisition periods and to close a predetermined time later. The Nd:YAG laser intensity was adjusted to provide 50 mJ (40 MW/cm^2) of Q-switched radiation to the same sample area. The laser flashlamps were synchronized with the spectrometer data acquisition rate and the Q-switch was fired between the spectrometer scans. In most cases, a second program was intiated immediately after excitation which acquired spectra over a longer time interval. For different exposure times or pulse configurations, the sample was moved to a new position with the translational mount where it was spectroscopically verified that no chemistry had occured. After completion of the data acquisition for a given set of experiments, the interferograms were transformed, co-added, and ratioed against the appropriate background spectra. The reflectance spectra were then converted into Kubelka Munk spectra for evaluation.

E. Physical Measurements.

Infrared spectra of solutions or mulls were recorded on a Perkin-Elmer 1330 spectrophotometer, calibrated against polystyrene, and equipped with a Model 1660 data station. Gaseous photoproducts were collected with a Toepler pump, Figure 17, and analyzed with a Gow Mac Model 69-100 gas chromatograph equipped with a Re-W thermal conductivity detector and a 6' x 1/4" stainless steel column containing 5A (80/100 mesh) molecular sieve (Supelco) packing. Calibration experiments in which a known amount of gas in the photolysis cell was transferred to the G.C. indicated the error involved in collecting the gaseous photoproducts using the Toepler pump was $\leq$ 3%. The gas chromatographic conditions employed were an oven temperature of 100 °C, a flow rate of 40 ml/min, and a detector current of 150 mA. CP grade Helium (Matheson Gas Products) was used as the carrier gas to quantitate CO evolution whereas Argon (CP grade, Matheson Gas Products) was used as the carrier gas for the simultaneous detection of CO, H_2, and CH_4. The detector response, calibrated by injecting a known pressure and volume of each gas (CP grade CO, H_2, CH_4; Linde) into the gas chromatograph, was displayed on a Shimadzu R-111 millivolt recorder. The resulting calibration curves, illustrating the integrated peak area versus the number of moles of gas, are shown in Figures

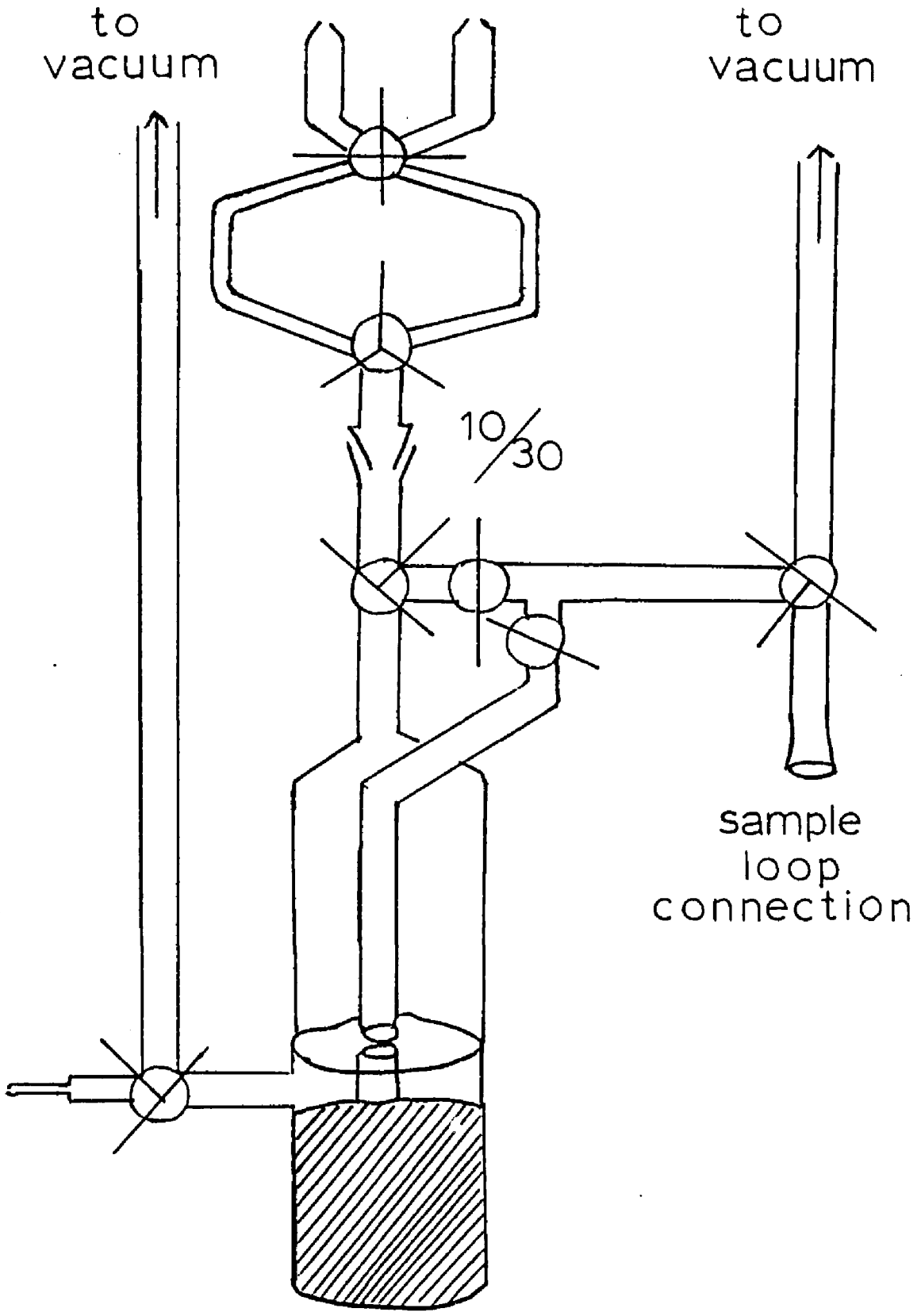

Figure 17a. Toepler pump.

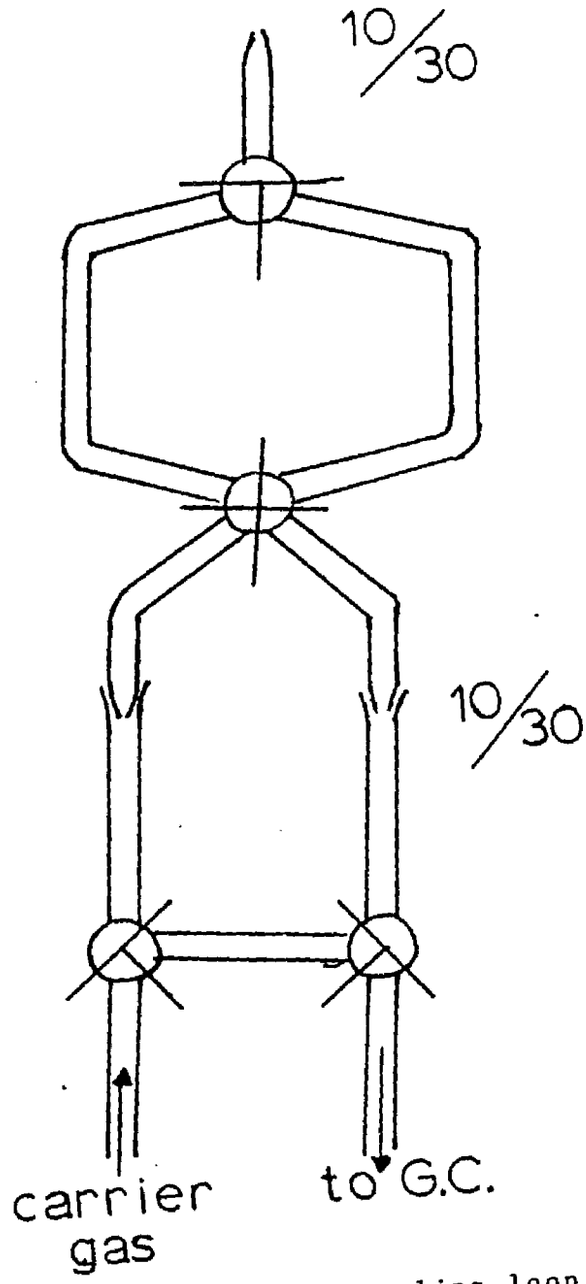

Figure 17b. Gas sampling loop.

18-20. Retention times for the various gases are summarized in Table 2, and a typical chromatogram is displayed in Figure 21.

In photocatalyzed olefin reactions, the gaseous photoproducts were collected in a gas tight syringe (Hamilton Company) and analyzed on a Varian Series 2400 gas chromatograph equipped with a flame ionization detector. Separation of the various olefins was accomplished using a 2 meter x 1/8" O.D. stainless steel column packed with 80/100 Carbopack c/o 19% picric acid (Supelco). The detector response was calibrated for 1-pentene by filling the photolysis cell with a known pressure of the olefin and injecting various volumes into the G.C. The calibration curve obtained is shown in Figure 22. Gas Chromatographic conditions employed were an oven temperature of 50 °C, a detector temperature of 130 °C, and a N_2 flow rate of 20 ml/min. A typical chromatogram obtained under these conditions is illustrated in Figure 23.

F. Formation of High Resolution Optical Patterns.

Samples of pretreated, polished plate PVG (25.4 x 25.4 x 1mm) were placed in a copper wire basket and suspended over liquid $Fe(CO)_5$ in a 100 ml beaker. The beaker was covered with a watch glass to minimize diffusion of toxic $Fe(CO)_5$ vapor into the atmosphere.

Figure 18. CO calibration curve.

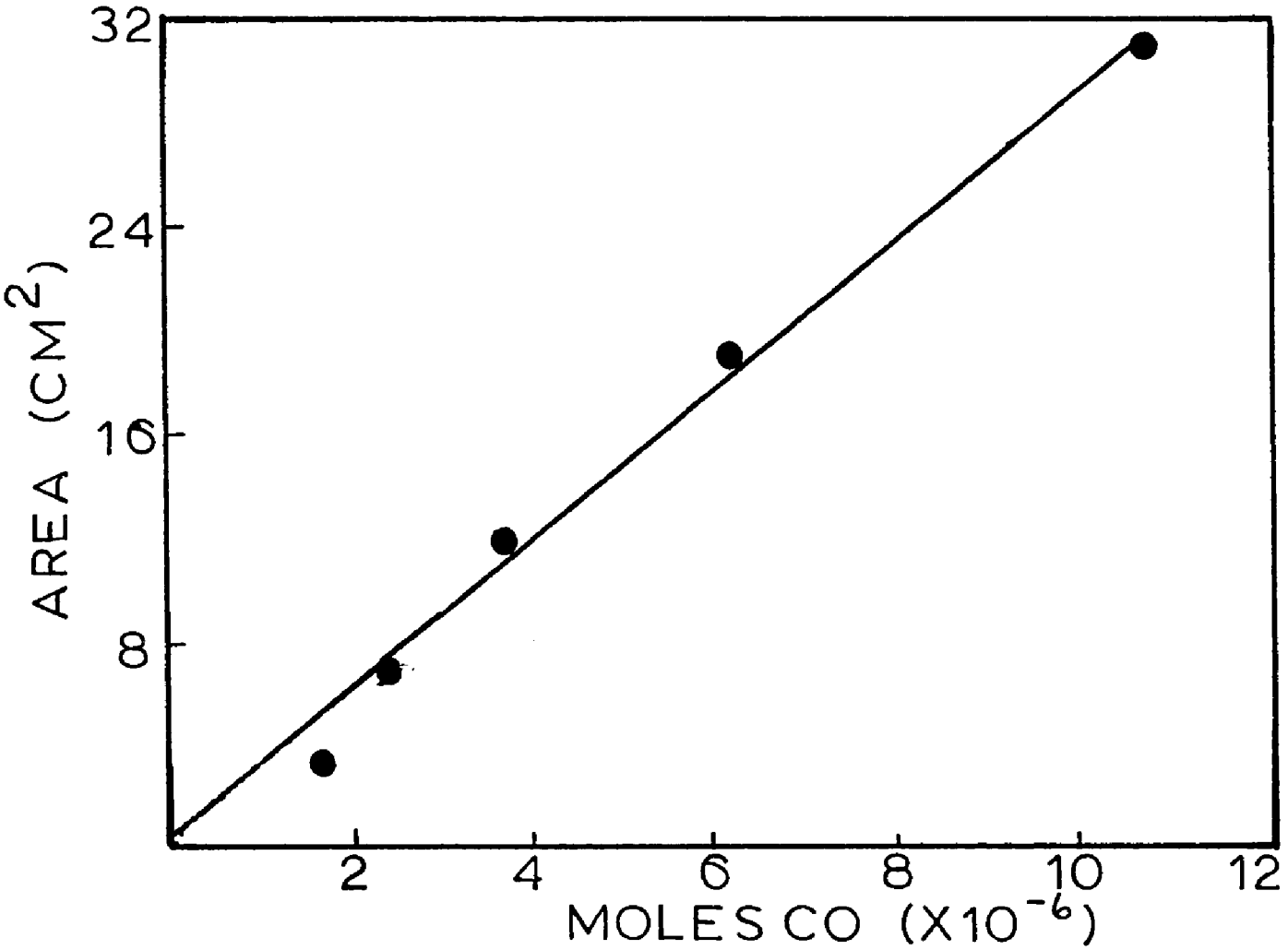

Figure 19. Hydrogen calibration curve.

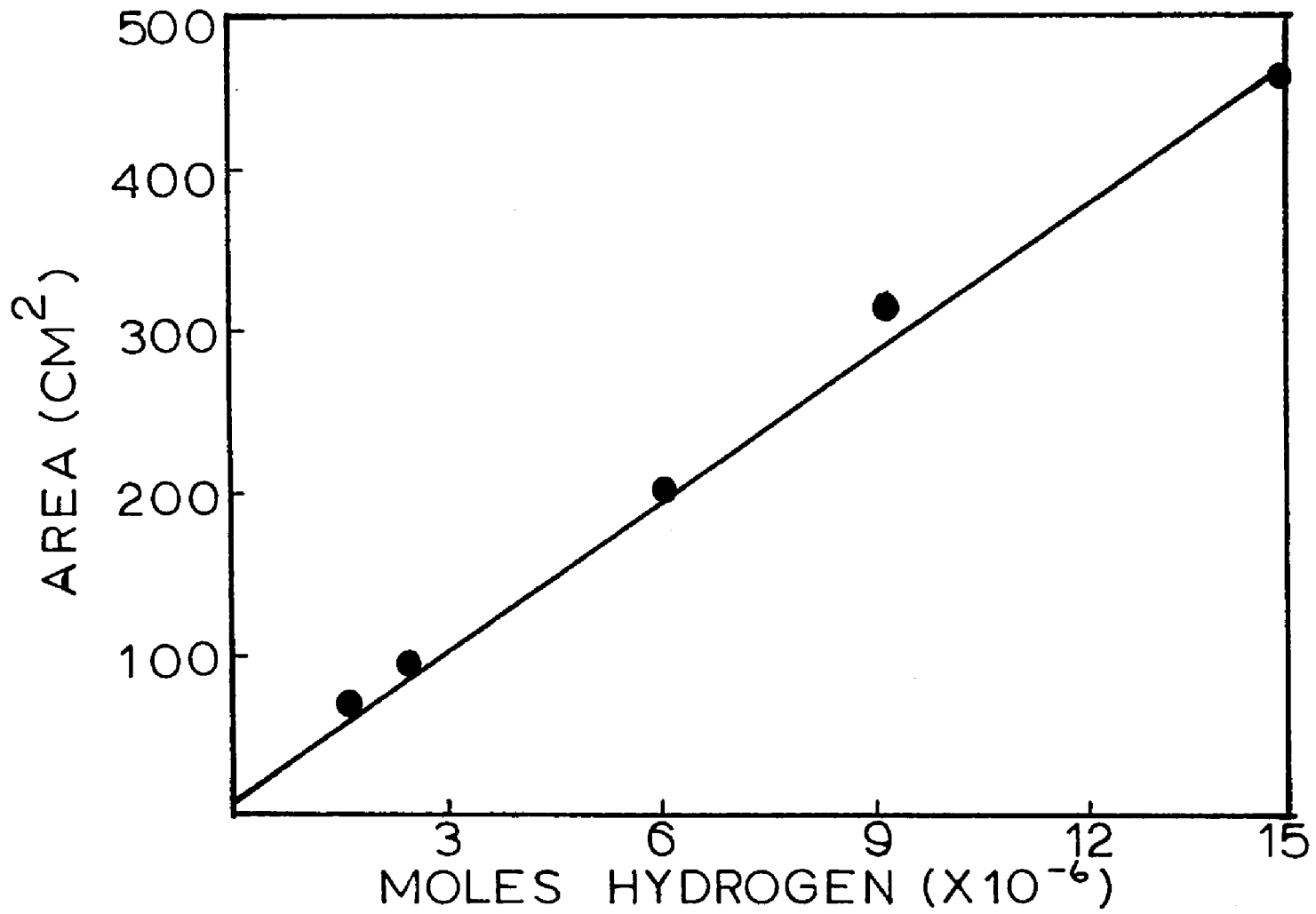

Figure 20. Methane calibration curve.

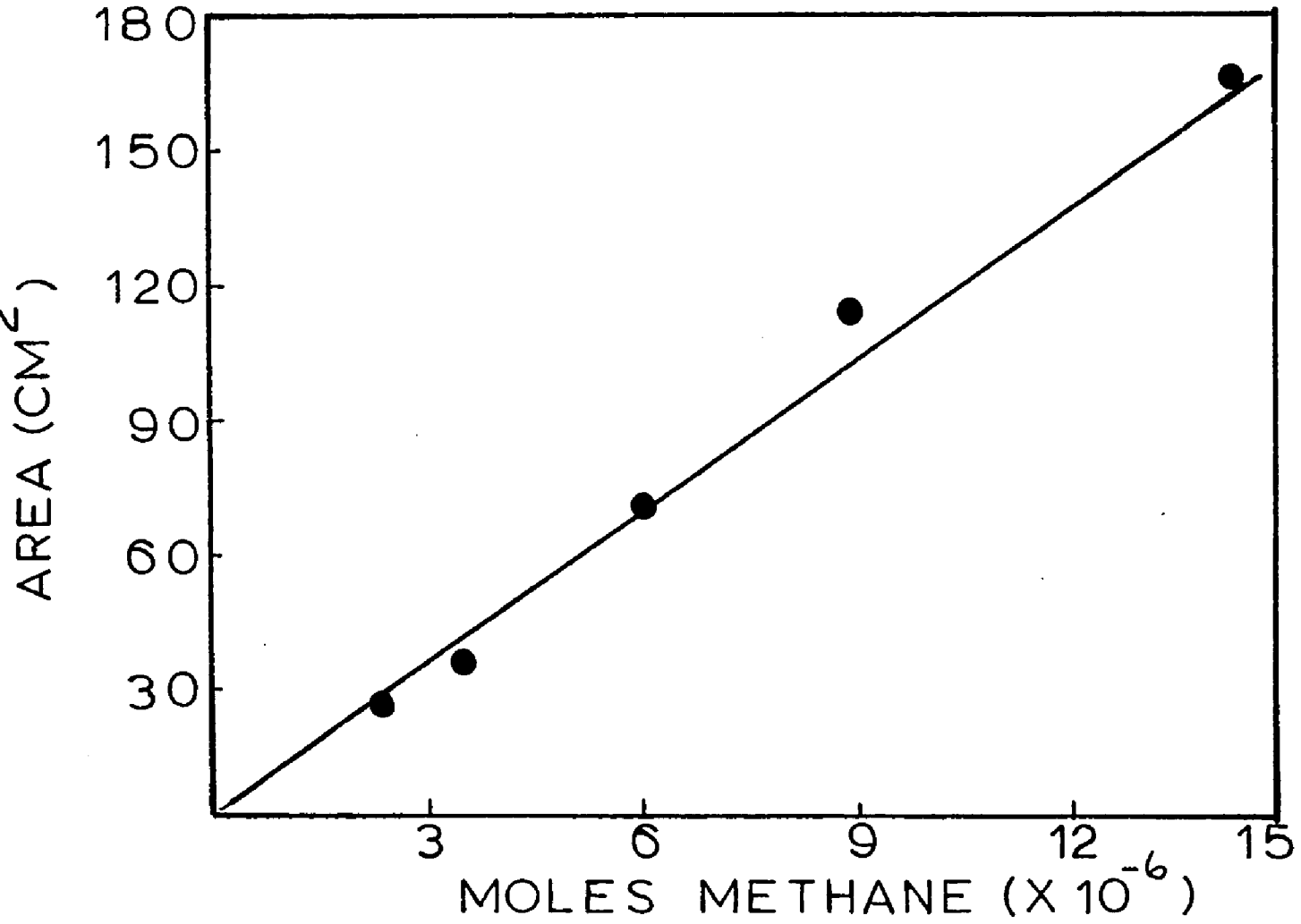

TABLE 2.

Thermal Conductivity Detector Response for H_2, CH_4, and CO in He and Ar Carrier Gases.

He Carrier Gas

Gas	Slope of Calibration Curve	Retention Time (mins.)
CO	2.23×10^6	4.75

Ar Carrier Gas

H_2	4.90×10^7	1.7
CH_4	1.15×10^7	4.2
CO	3.28×10^6	5.8

Figure 21. Gas Chromatogram showing separation and simultaneous detection of CO, H_2 and CH_4.

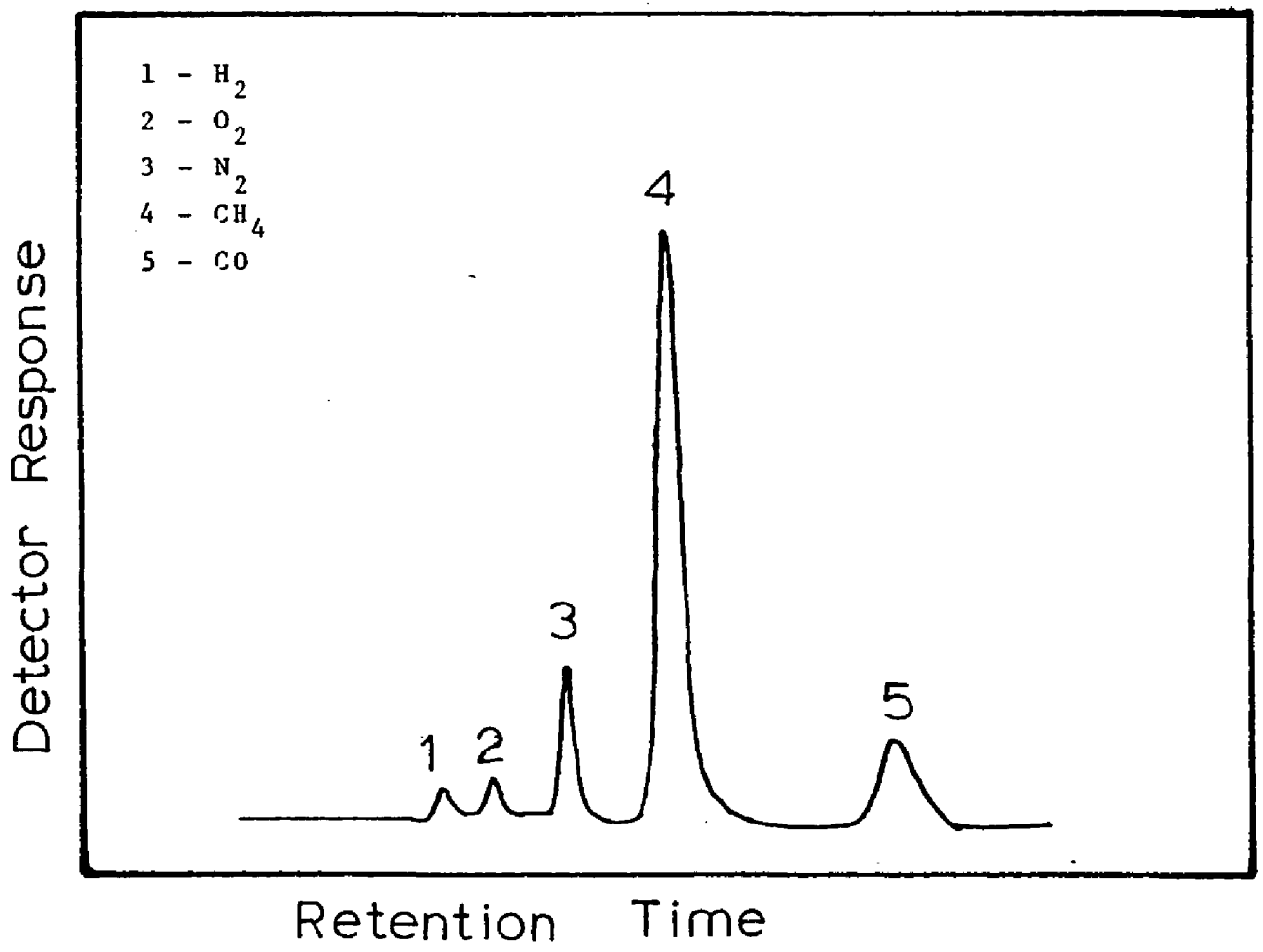

Figure 22. 1-pentene calibration curve.

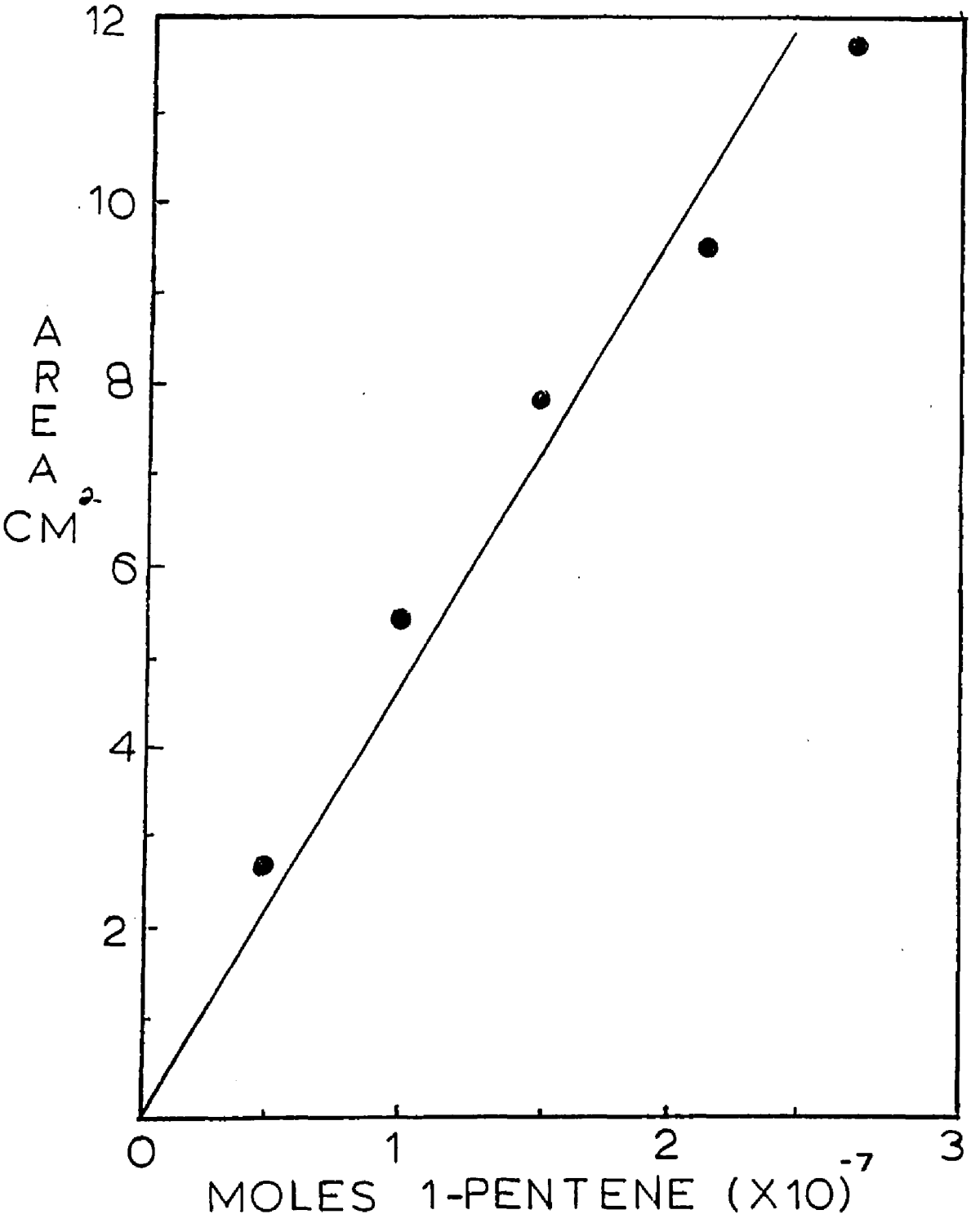

Figure 23. Gas Chromatogram showing separation of 1-pentene and cis and trans-2-pentenes.

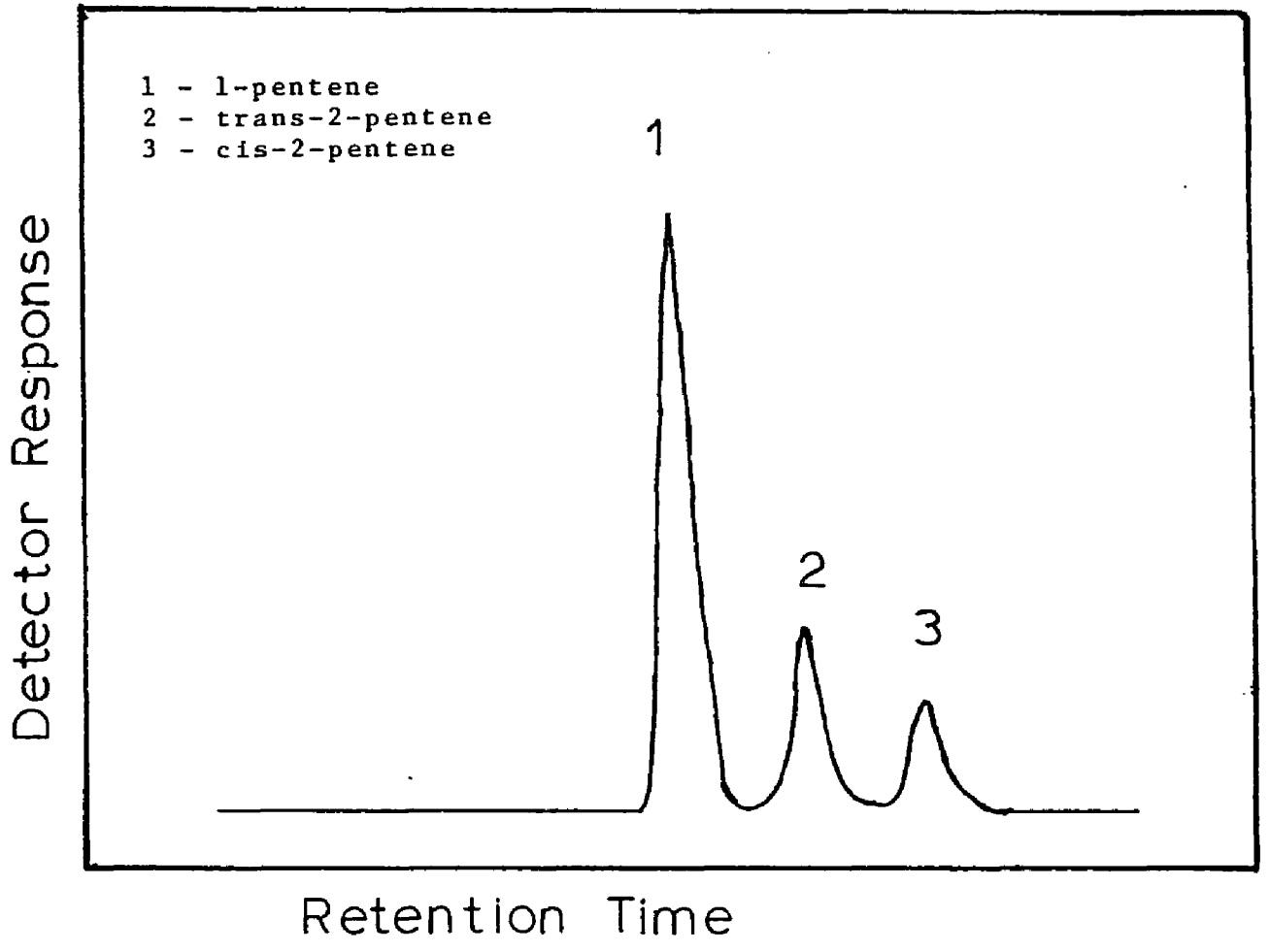

Exposure time of the PVG samples to $Fe(CO)_5$ varied from 2 to 3 minutes. After impregnation, the samples were transferred in air to a slide holder where they were mounted. The desired pattern was made by standard photolithographic techniques. A collimated light beam from a 100 Watt Xenon lamp was passed through a 35 mm plastic slide containing the pattern and focused onto the PVG. The plastic slide limited the excitation to wavelengths > 300 nm. After photolysis, the samples were placed in a muffler oven and slowly heated in air to 900 °C. The samples were maintained at 900 °C for 12 hours and allowed to cool to room temperature in air.

Results

A. Adsorption of Iron Carbonyls.

Thermal gravimetric analysis of PVG, indicates the presence of both bulk and chemisorbed water. As shown in Figure 24, bulk water desorbs at 100-120 °C while chemisorbed water desorbs slowly up to the point of consolidation, *ca.* 700 °C. Dispersed in Fluorolube, the IR spectrum of crushed PVG before calcination, Figure 25, exhibits a broad, intense adsorption due to water centered at 3500 cm^{-1}. In addition, the spectrum exhibits a band at 3744 cm^{-1} with a shoulder at 3665 cm^{-1} which have been assigned to free and hydrogen bonded silanol groups, respectively (128). The DRIFT spectrum of uncalcined PVG is essentially identical to the spectrum of PVG dispersed in Fluorolube, except that as shown in Figure 26, the spectrum is more resolved. Comparison of the DRIFT spectra of uncalcined 60-200 mesh silica gel, Figure 27, and uncalcined plates of PVG confirms that the surfaces of these two supports are quite similiar. Both DRIFT spectra reveal the presence of free and hydrogen bonded silanol groups in addition to significant amounts of chemisorbed water. DRIFT spectra of PVG recorded under flowing helium as a function of temperature show that the intense, broad adsorption due to water declines, and at 550 °C the spectrum, Figure 28,

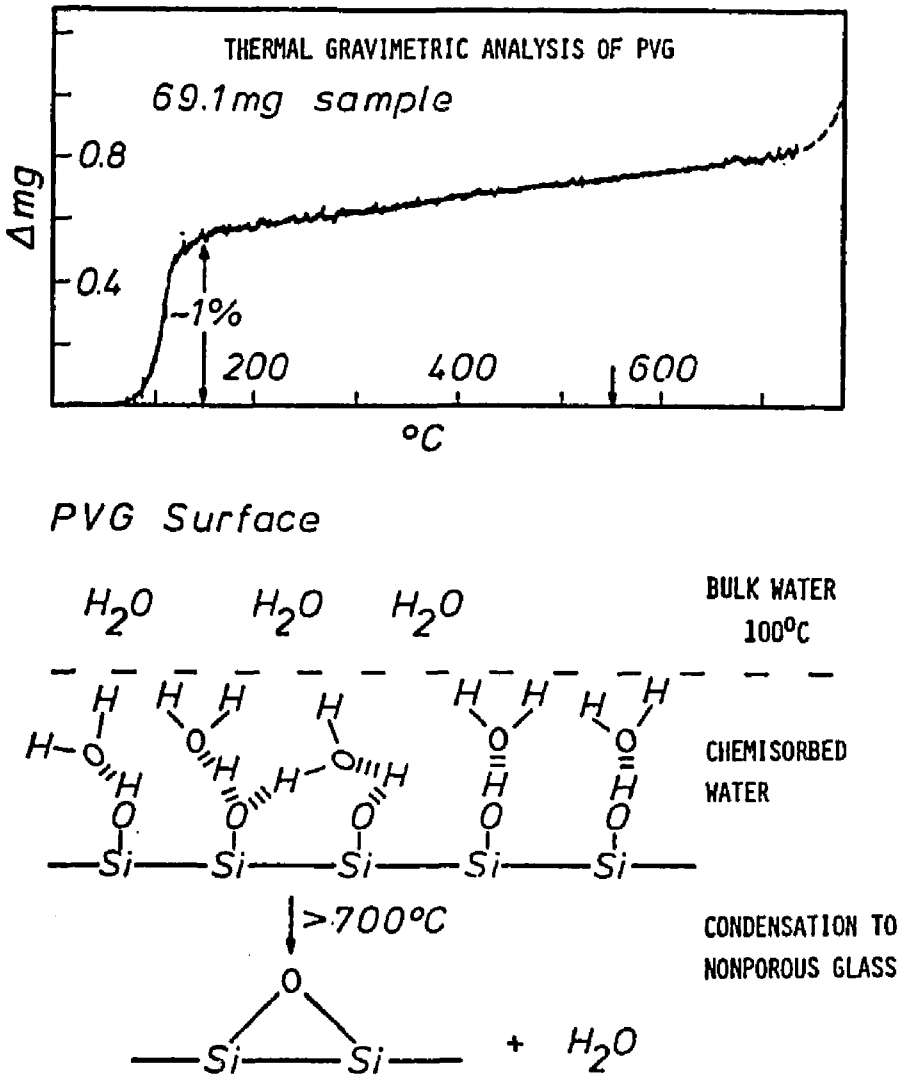

Figure 24. Thermal gravimetric analysis of PVG.

Figure 25. Infrared Spectrum of PVC in Fluorolube.

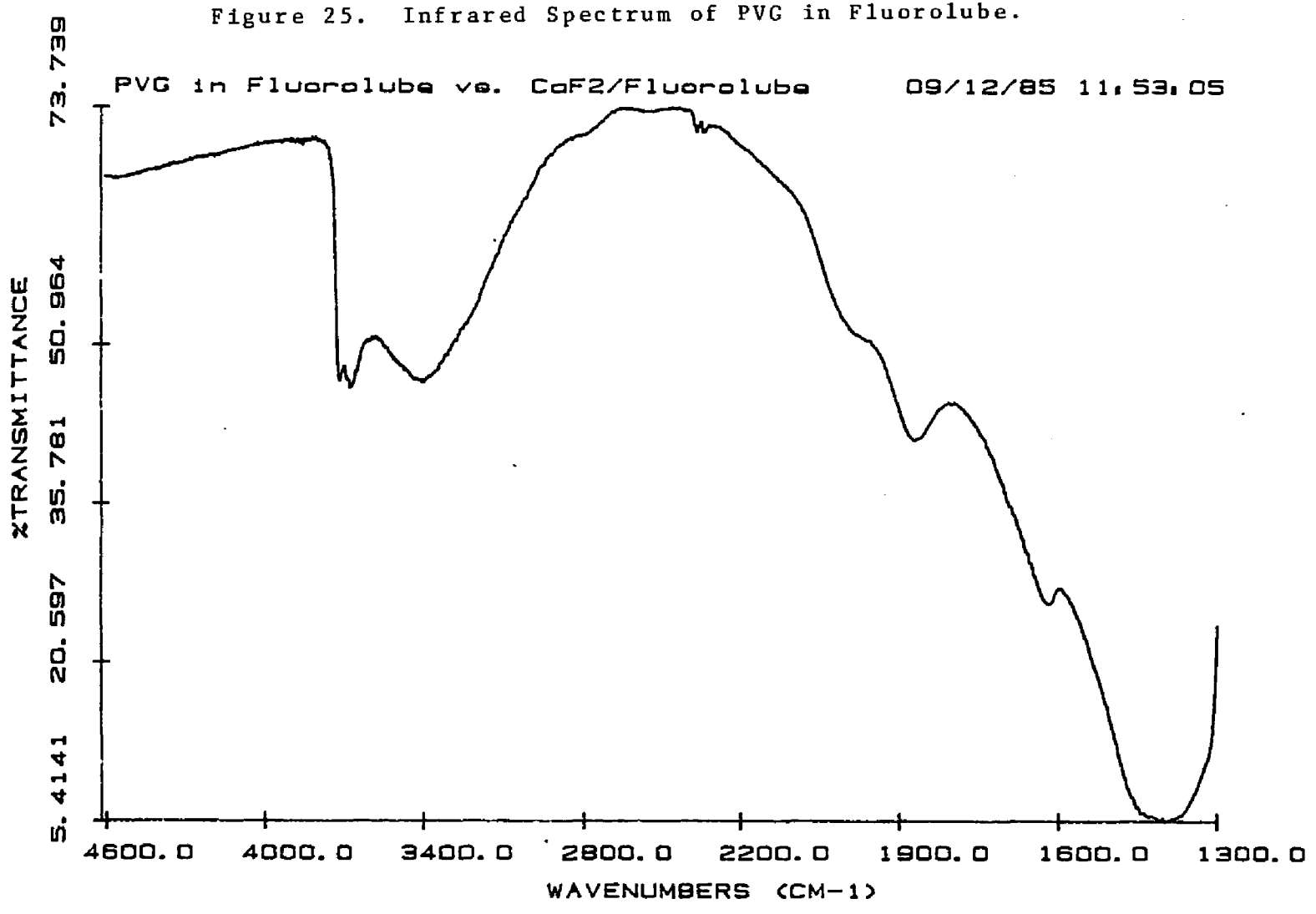

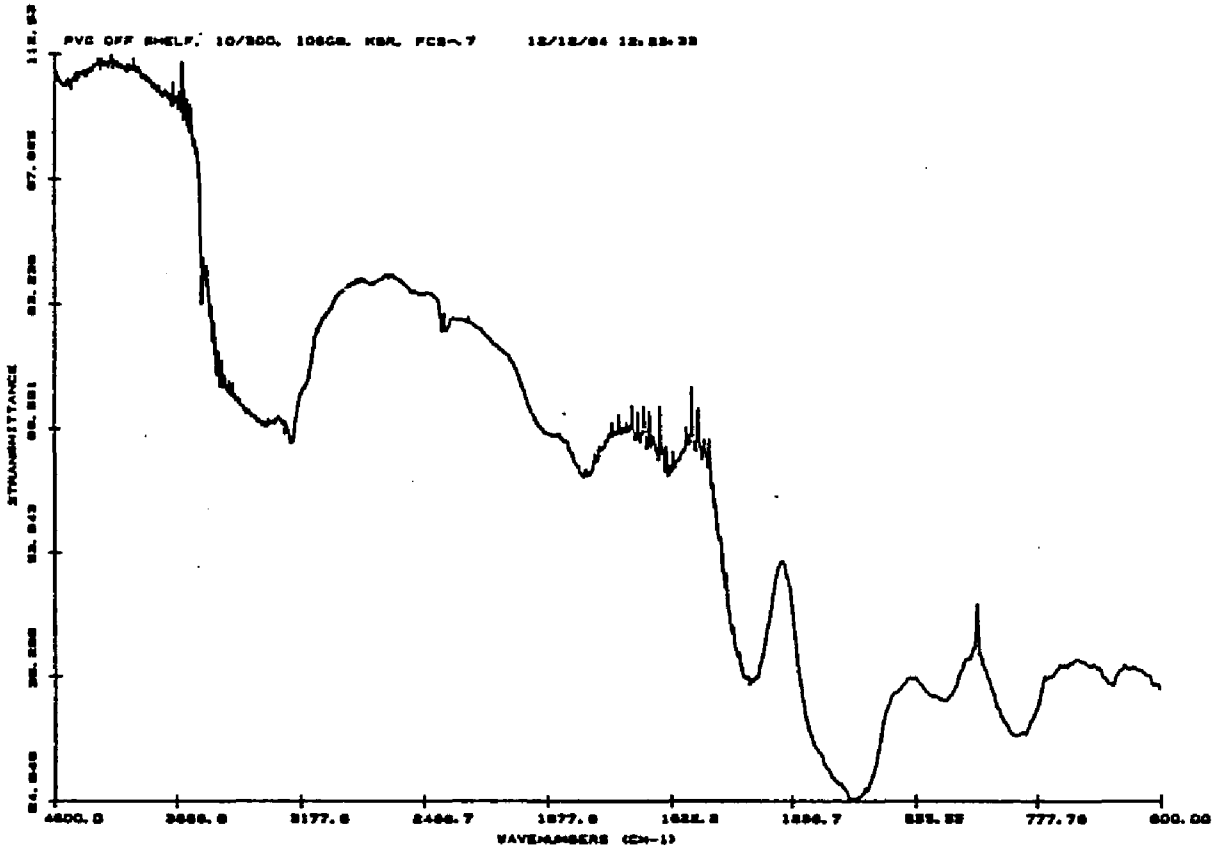

Figure 26. DRIFT spectrum of uncalcined PVG.

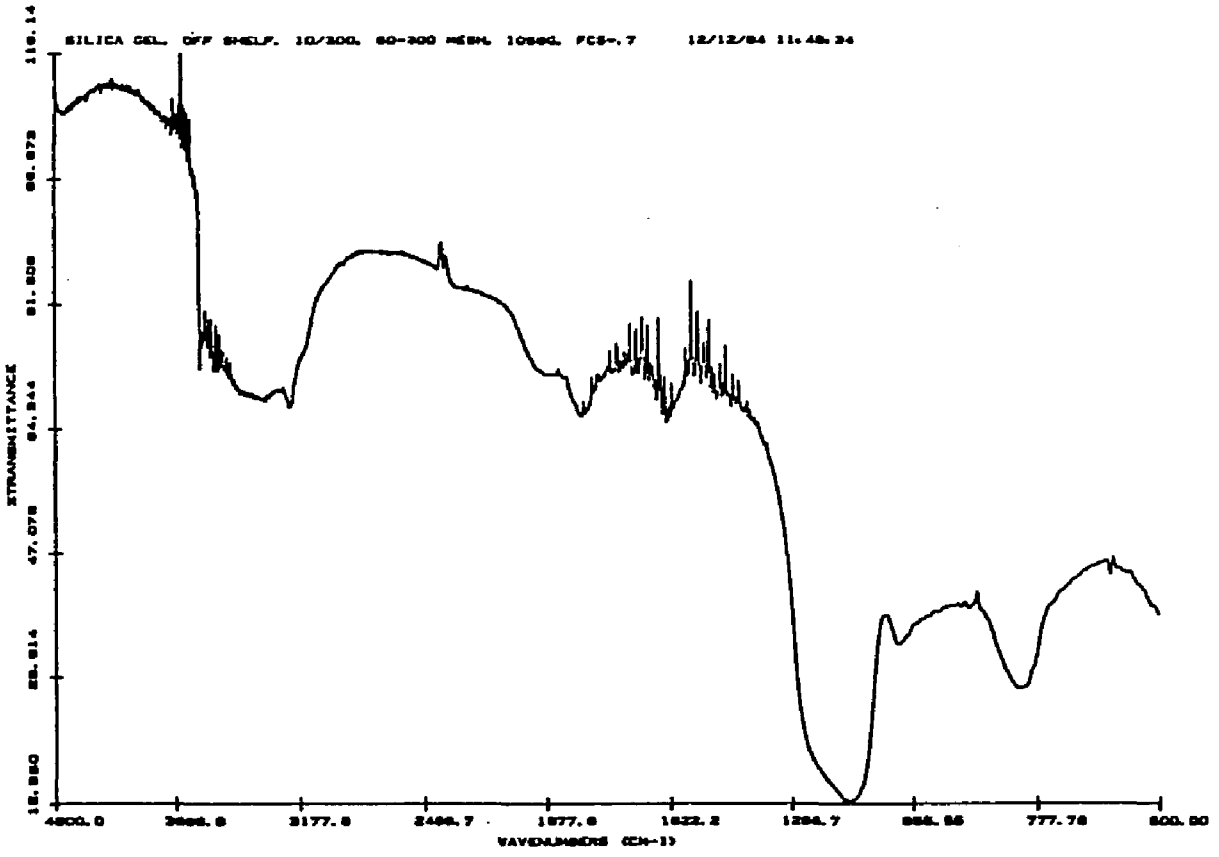

Figure 27. DRIFT spectrum of uncalcined silica gel.

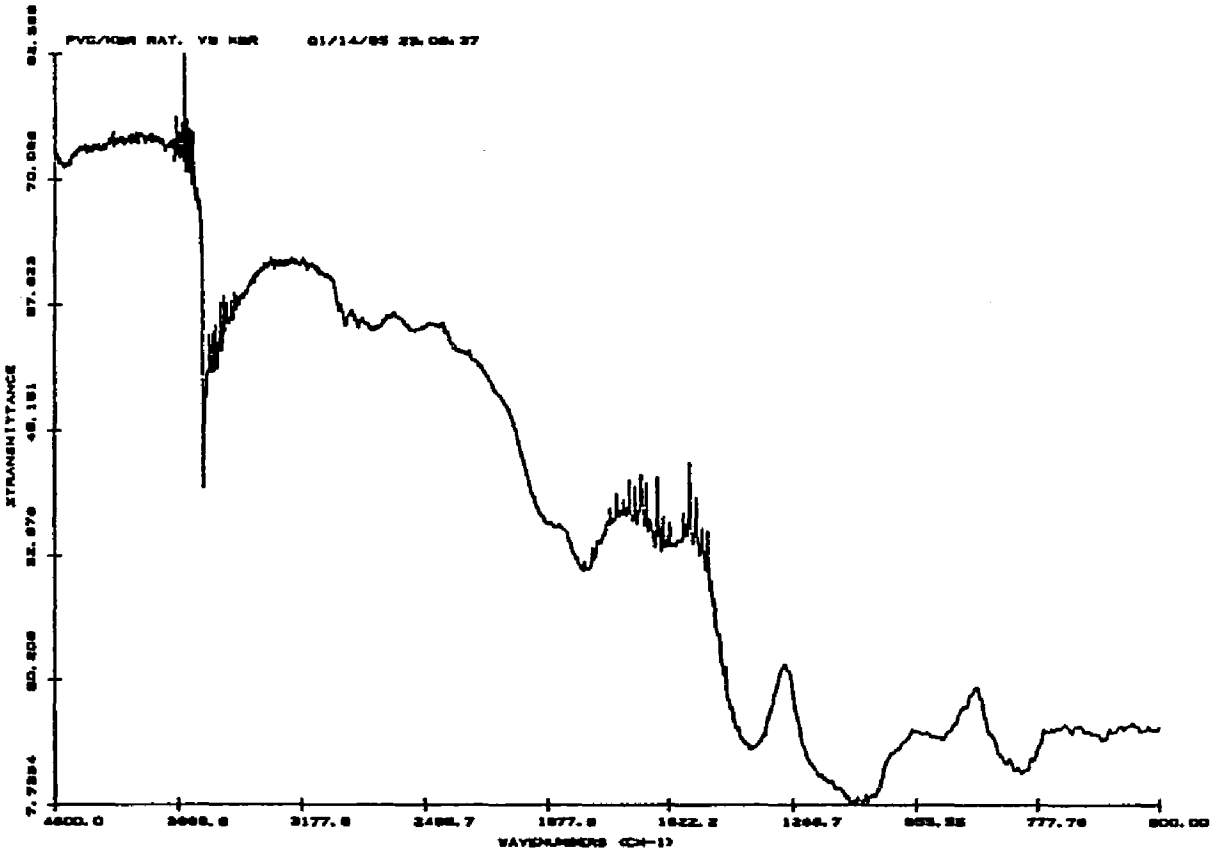

Figure 28. DRIFT spectrum of calcined PVG.

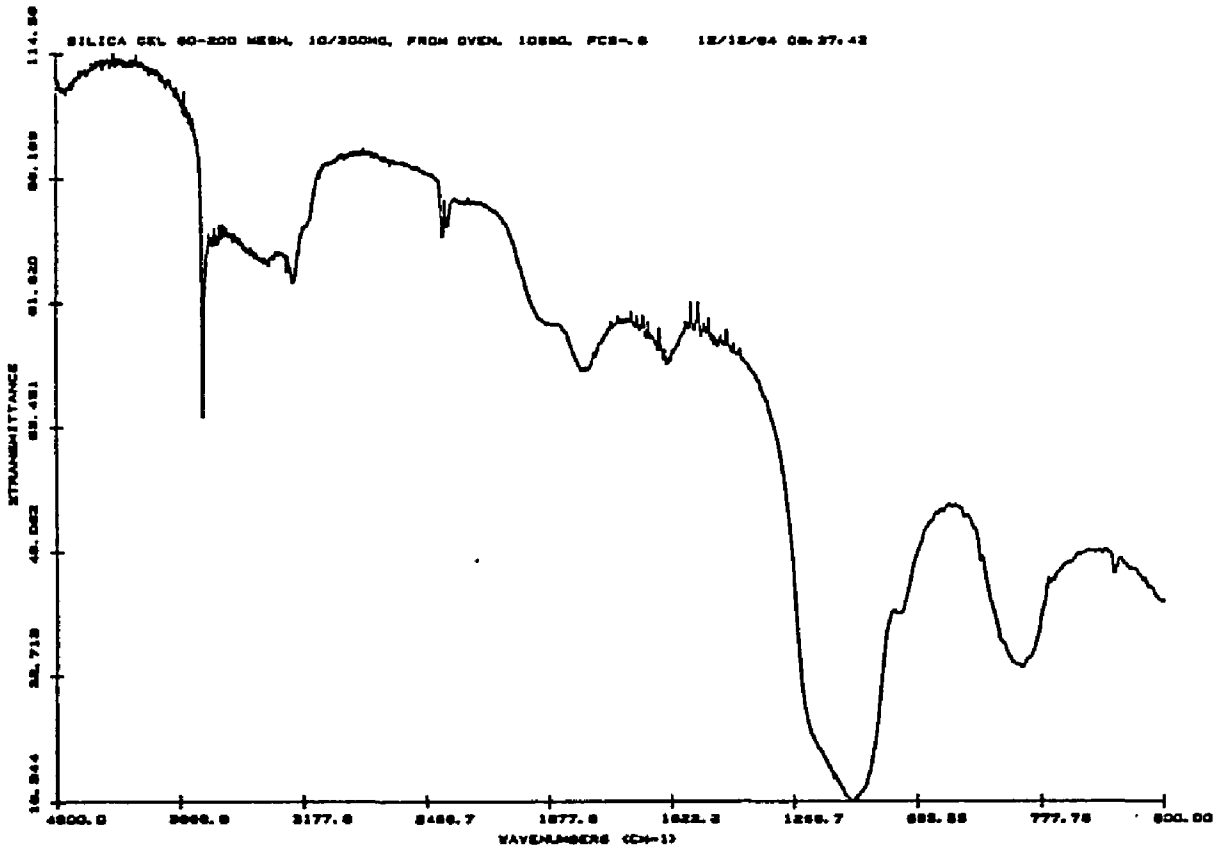

Figure 29. DRIFT spectrum of calcined silica gel.

exhibits a sharp, intense band at 3744 cm^{-1} which has been assigned to free silanol groups and a shoulder at 3665 cm^{-1} which has been assigned to hydrogen bonded silanol groups. However, a weak band due to small amounts of chemisorbed water remains. The intensity of this band varies from sample to sample, but after calcination is always $\leq$15% of that of the 3744 cm^{-1} silanol band. The DRIFT spectrum of silica gel following calcination at 550 °C, Figure 29, shows identical spectral changes, i.e., a decline in bands due to adsorbed H_2O and a resolution of the bands due to free and associated silanol groups.

Adsorption of $Fe(CO)_5$ onto plate PVG is a linear function of pressure over the range 0.125 to 2.04 torr, and the isotherm measured at 26 °C, shown in Figure 14, resembles that reported for adsorption of the complex onto silica gel (99). Approximately 35 to 40% of the $Fe(CO)_5$ admitted into the quartz cell was adsorbed relatively independent of the $Fe(CO)_5$ pressure. Regardless of the moles of $Fe(CO)_5$ adsorbed, however, the complex does not penetrate throughout the entire pore volume. Breaking samples containing 2×10^{-5} moles/gram shows that $Fe(CO)_5$ penetrates 0.5 ± 0.1 mm into PVG, and as found with other complexes (116,120,122), impregnates volumes of PVG adjacent to the outer geometric surfaces of the sample. Since the adsorbate does not uniformly

distribute throughout the entire pore volume, surface coverage on an irregular, porous support, such as PVG, cannot be uniquely defined. Rather, a lower limit is calculated where it is assumed that that surface area within the impregnated volume of PVG corresponds to that measured by N_2 adsorption at low temperature, 130 m^2/gram of PVG; the latter penetrates throughout the entire pore volume. Taking the area occupied by $Fe(CO)_5$(ads) to be 0.3 nm^2, the samples prepared in these experiments, which range from $<10^{-7}$ to $2.0\pm0.2 \times 10^{-5}$ moles of $Fe(CO)_5$/gram of PVG, correspond to fractional surface coverages of $\leq$0.15% to 3.0%. The calculated values are approximations, however, and are used in a relative, rather than absolute sense.

The adsorption isotherm, measured at 26 °C for $Fe(CO)_5$ on the finely crushed PVG used in the DRIFT experiments, is shown in Figure 15. The isotherm exhibits a Langmuir dependence with saturation of the surface occuring at higher pressures. Adsorption was more extensive on the powder than on the plate PVG, since of the $Fe(CO)_5$ admitted into the cell, only 1.5% remained in the gas phase. Regardless of whether plate or powdered samples are used, the adsorption of $Fe(CO)_5$ onto PVG is reversible. However, the rates of desorption of the complex differ. The IR bands of $Fe(CO)_5$ adsorbed on powdered PVG, 3×10^{-4} moles/gram, disappear within 5

minutes at room temperature when the DRIFT microreactor is evacuated, whereas desorption from the plate samples is considerably slower. Evacuation of a quartz cell containing a plate sample impregnated with $4.0\pm0.4 \times 10^{-6}$ moles of $Fe(CO)_5$/gram causes a steady decline in the UV spectrum, Figure 30, but optical density attributable to the adsorbed complex is discernible after several hours. The difference in desorption rates is thought to reflect differences in penetration depth, i.e., adsorption onto powdered PVG, because of its larger outer surface area, is principally limited to the outer surfaces of the particles whereas adsorption onto the plate samples, as described above, leads to limited impregnation of interior pores.

B. Spectral Properties Of Adsorbed Fe Compounds.

i. $Fe(CO)_5$.

The electronic spectrum of a sample containing 5×10^{-7} moles/gram of $Fe(CO)_5$ and corrected for absorption due to PVG is shown in Figure 31. The spectrum consists of a strong featureless absorption in the UV associated with MLCT and ligand localized transitions resembles that of the complex in fluid solution (50,51). However, the lower energy ligand field transitions, which appear as shoulders at 245 and 285 nm in the fluid solution spectrum, Figure 32, are not discernible. Ligand field

Figure 30. Optical density of $Fe(CO)_5$(ads.) at 350 nm. vs. evacuation time.

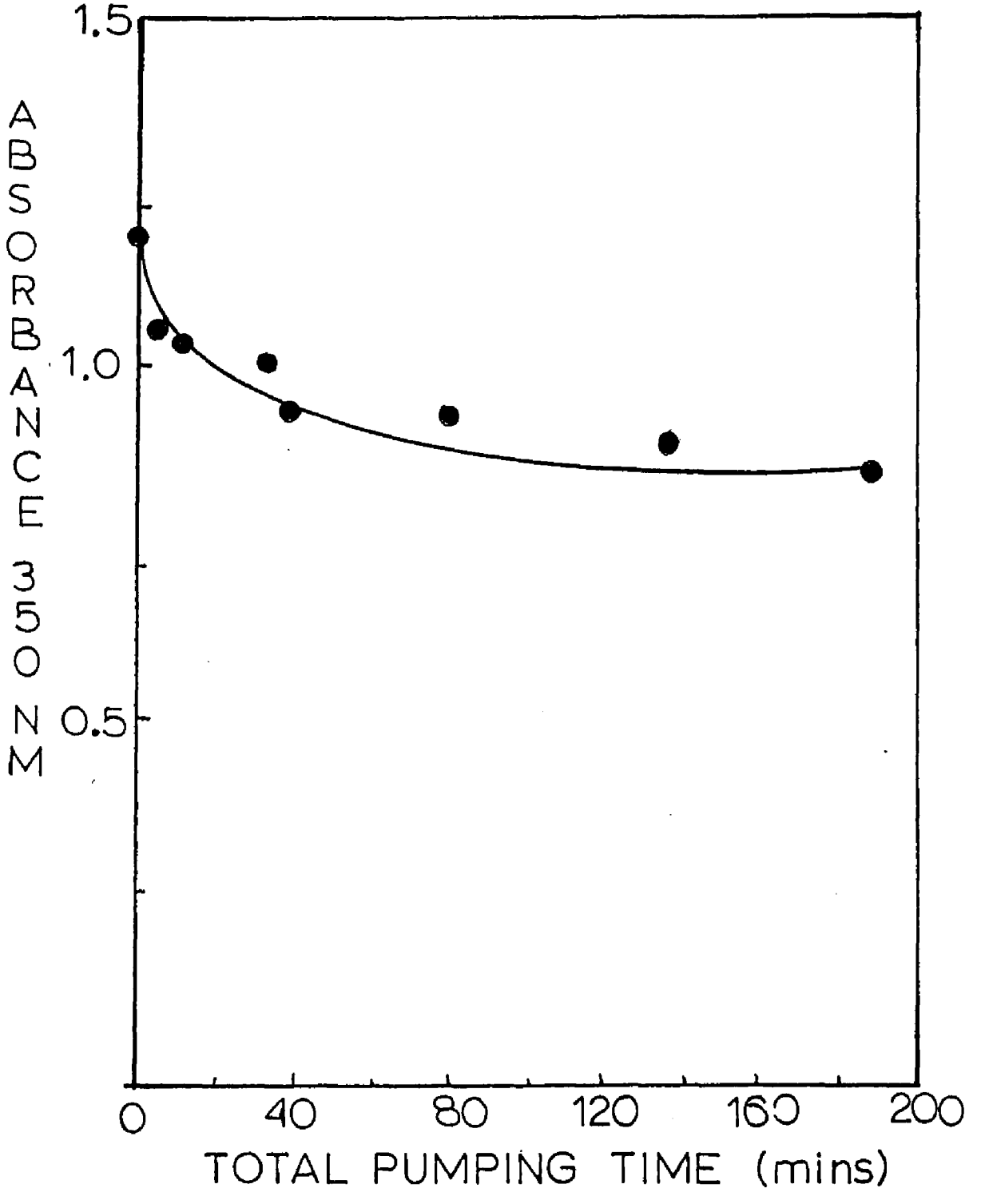

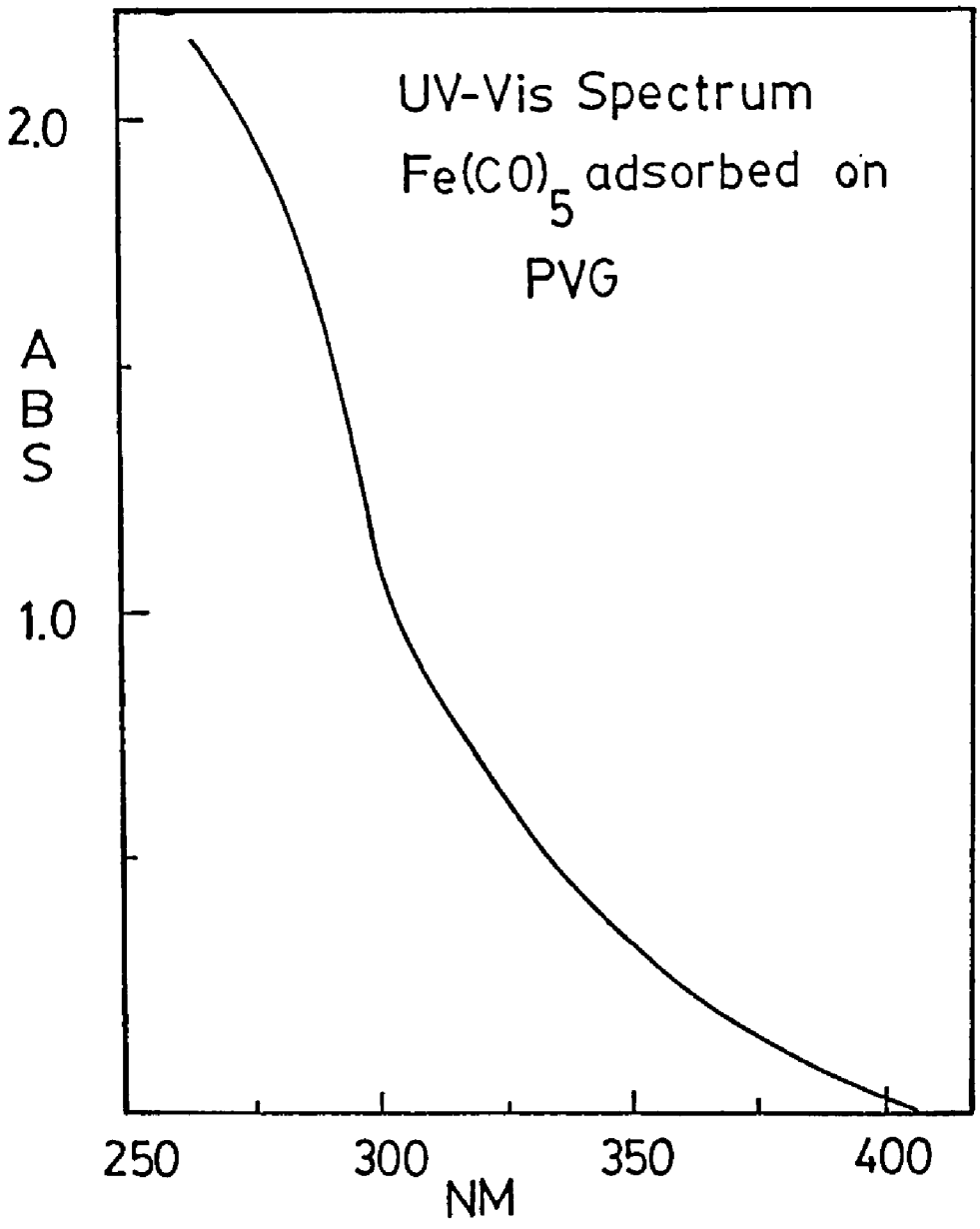

Figure 31. Electronic Absorption spectrum of $Fe(CO)_5$(ads.)

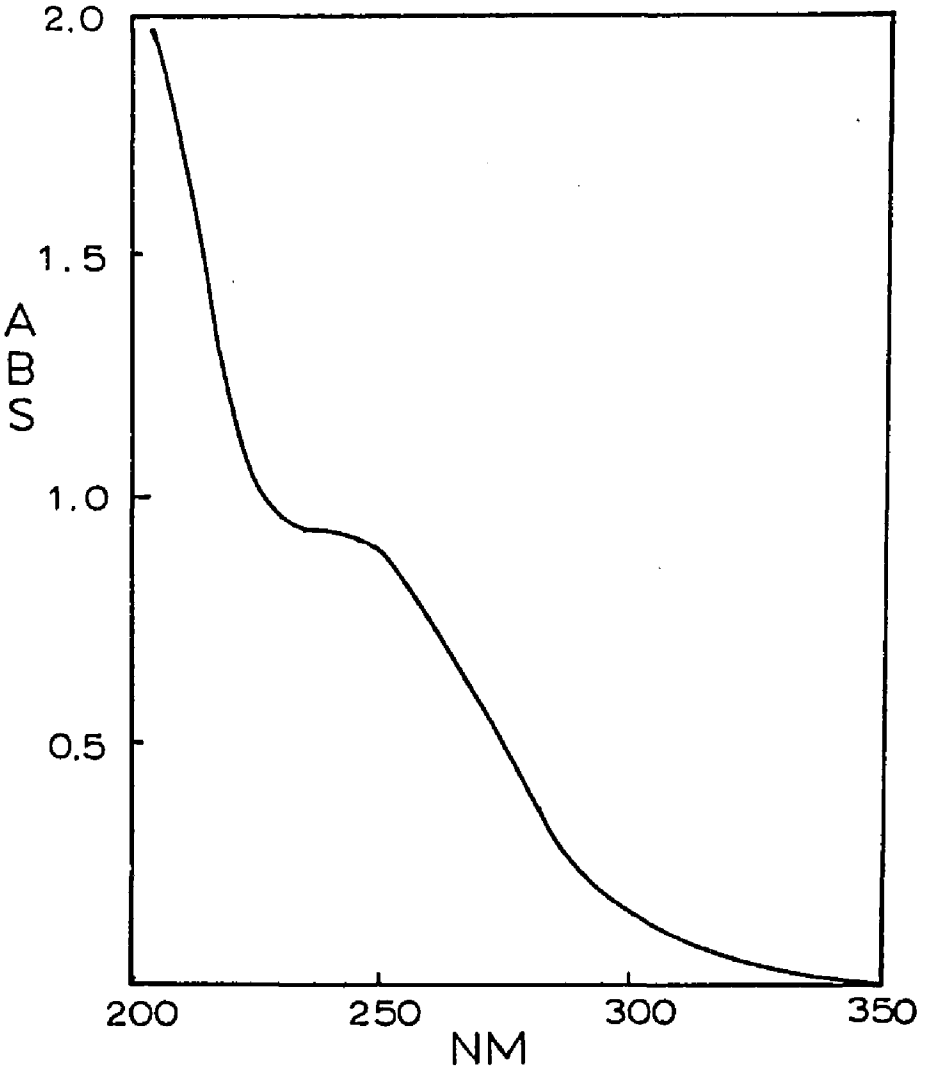

Figure 32. Electronic Absorption spectrum of $Fe(CO)_5$ in n-hexane.

transitions indicative of ligand substitution or agglomerization are not observed.

The DRIFT spectrum of the adsorbed complex, plotted in Kubelka Munk absorbance units, is shown in Figure 33. The complex exhibits intense bands at 2004 and 2026 cm^{-1} and a weak band at 2114 cm^{-1}. Other than increases in band intensity, the spectrum is independent of the moles adsorbed, but the bands are red shifted relative to the IR spectrum of $Fe(CO)_5$ in the vapor phase where the major CO bands occur at 2012 and 2033 cm^{-1}. Also, the intensities of the bands are inverted relative to the vapor phase spectrum and observed to vary depending on the pretreatment conditions of the PVG. Changes in the relative shapes and intensities of the bands are observed upon exposure of PVG to moist air, or aging of the PVG. The weak band at 2114 cm^{-1}, which is not observed in the vapor or solution phase spectrum of the complex, Figure 34, is assigned to the symmetric v_1 mode (19a). The latter occurs at 2116 cm^{-1} in the Raman spectrum of liquid $Fe(CO)_5$, and appears as a weak band at 2115 cm^{-1} in the IR spectrum of crystalline $Fe(CO)_5$ due to lower site symmetry, C_2, in the crystalline state (19b). Bein and Jacobs (129) assign weak bands in the 2115 cm^{-1} region of the spectrum of $Fe(CO)_5$ adsorbed on zeolites to the v_1 mode, and suggest that perturbations imposed by the adsorbent reduce the molecular symmetry of the

Figure 33. Kubelka Munk Spectrum of $Fe(CO)_5$(ads.).

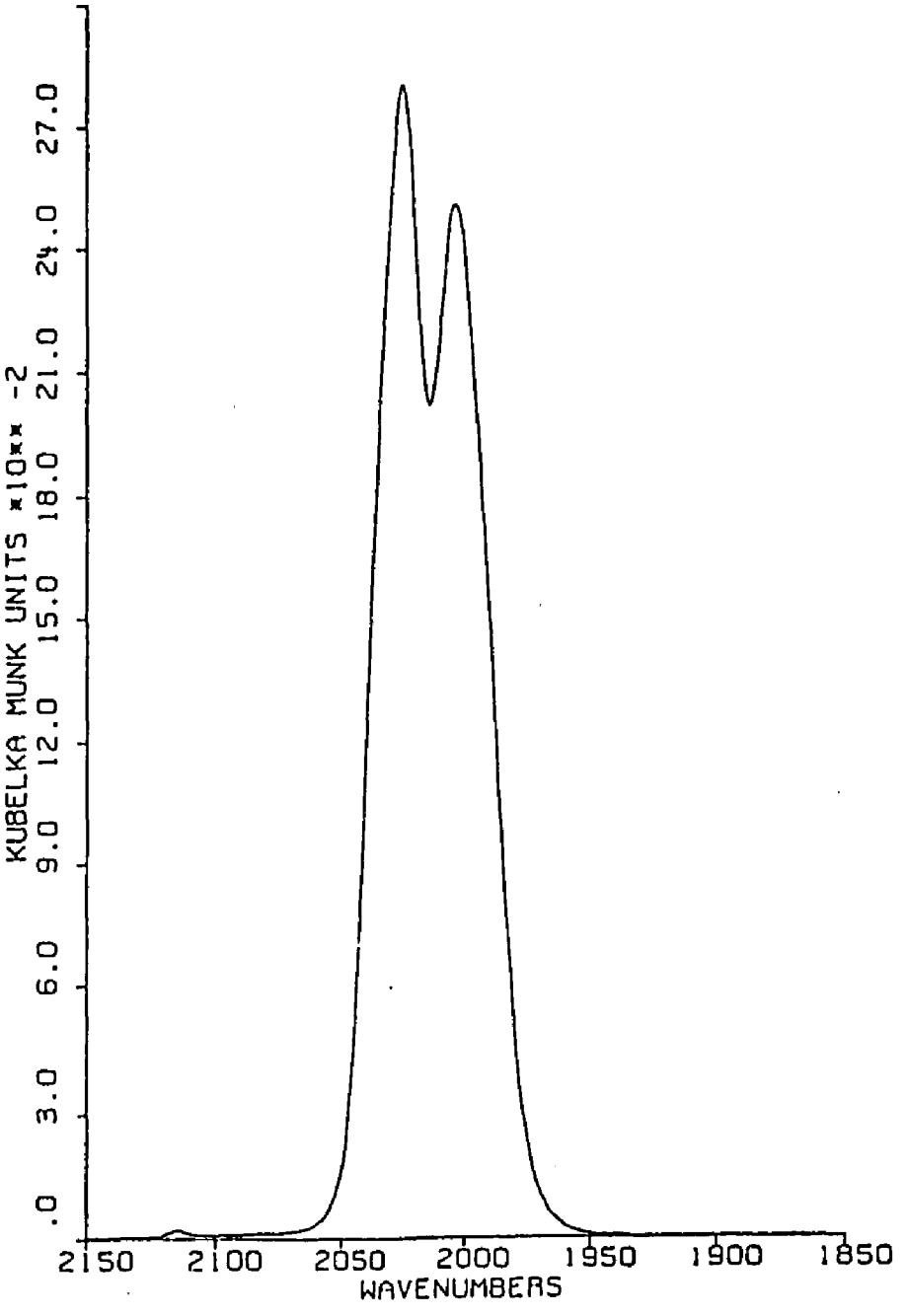
KUBELKA MUNK UNITS *10** -2
.0
3.0
6.0
9.0
12.0
15.0
18.0
21.0
24.0
27.0
2150
2100
2050
2000
1950
1900
1850
WAVENUMBERS

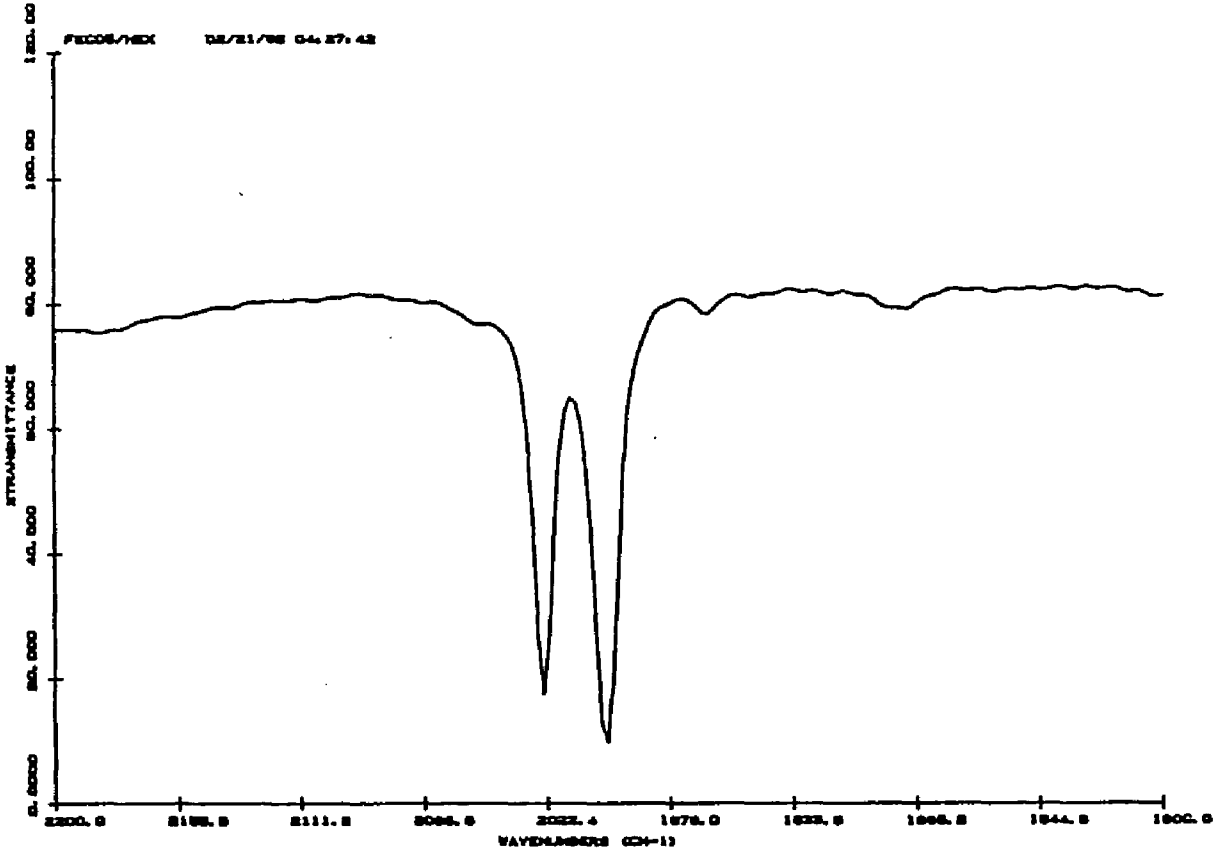

Figure 34. Infrared spectrum of $Fe(CO)_5$ in n-hexane.

adsorbate. The appearance of the v_1 mode, albeit weak, when $Fe(CO)_5$ is adsorbed on PVG suggests that some distortion occurs. However, the similarity of the electronic and DRIFT spectra of the adsorbed complex with vapor and solution phase spectra, as well as the ability to desorb the intact complex, establish that the complex physisorbs onto PVG without disruption of its primary coordination sphere.

ii. $Fe_2(CO)_9$.

The UV-visible spectrum recorded following vacuum sublimation of $Fe_2(CO)_9$ onto PVG at 44 °C, exhibits intense UV absorption with weak ligand field bands at 605 and 440 nm. The presence of the 605 nm band, which is absent in the spectrum of $Fe_2(CO)_9$ in Fluorolube, Figure 35, indicates disproportionation of the adsorbed complex to $Fe_3(CO)_{12}$ and $Fe(CO)_5$. The IR spectrum of $Fe_2(CO)_9$ in Fluorolube, Figure 36, exhibits broad adsorptions in the carbonyl stretching region centered at 2015 cm^{-1} and 1820 cm^{-1}, which is in sharp contrast with the DRIFT spectrum of PVG loaded with $Fe_2(CO)_9$ (from mixing powdered solids) where the major absorptions occur at 2051, 2028, 2005, and 1878 cm^{-1}. It is clear that the 2028 and 2005 cm^{-1} bands are due to $Fe(CO)_5$ while the 2051 cm^{-1} absorption can be attributed to $Fe_3(CO)_{12}$. The bridging carbonyl band at 1878 cm^{-1} is not due to $Fe_2(CO)_9$, but cannot be

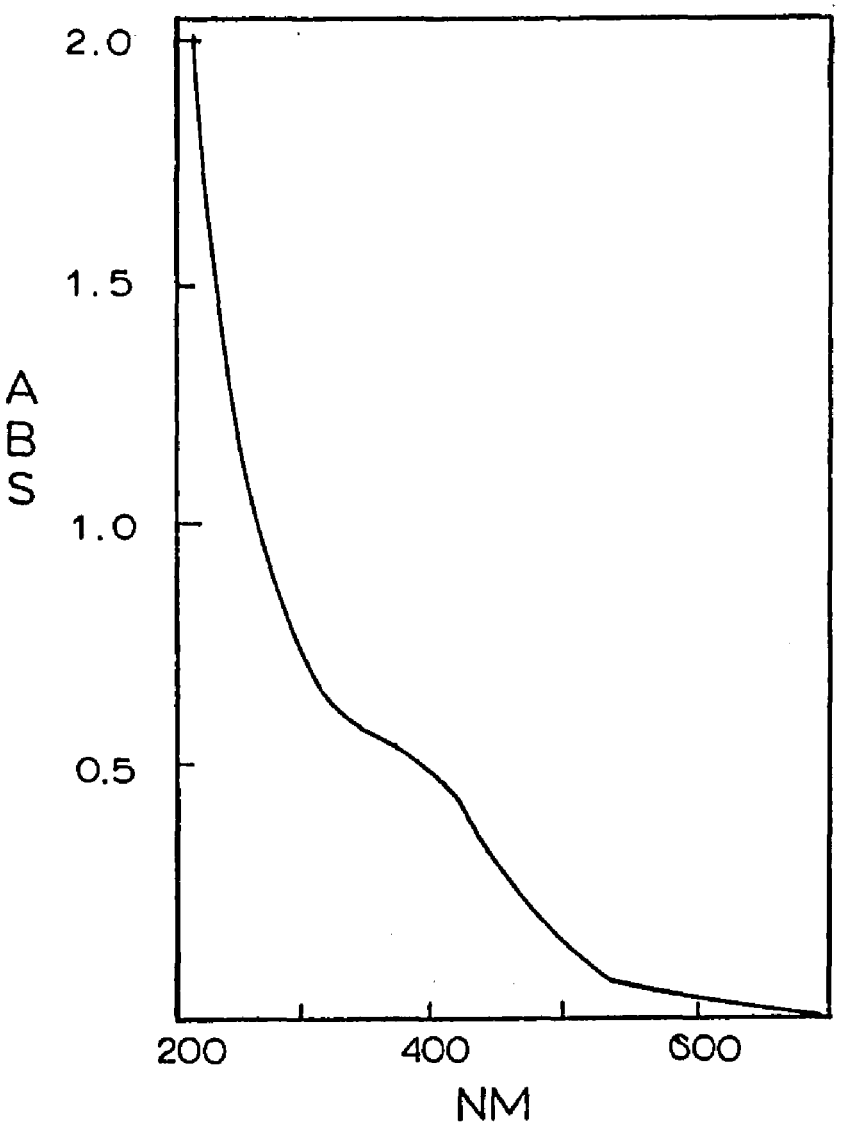

Figure 35. Electronic Absorption spectrum of $Fe_2(CO)_9$ in Fluorolube.

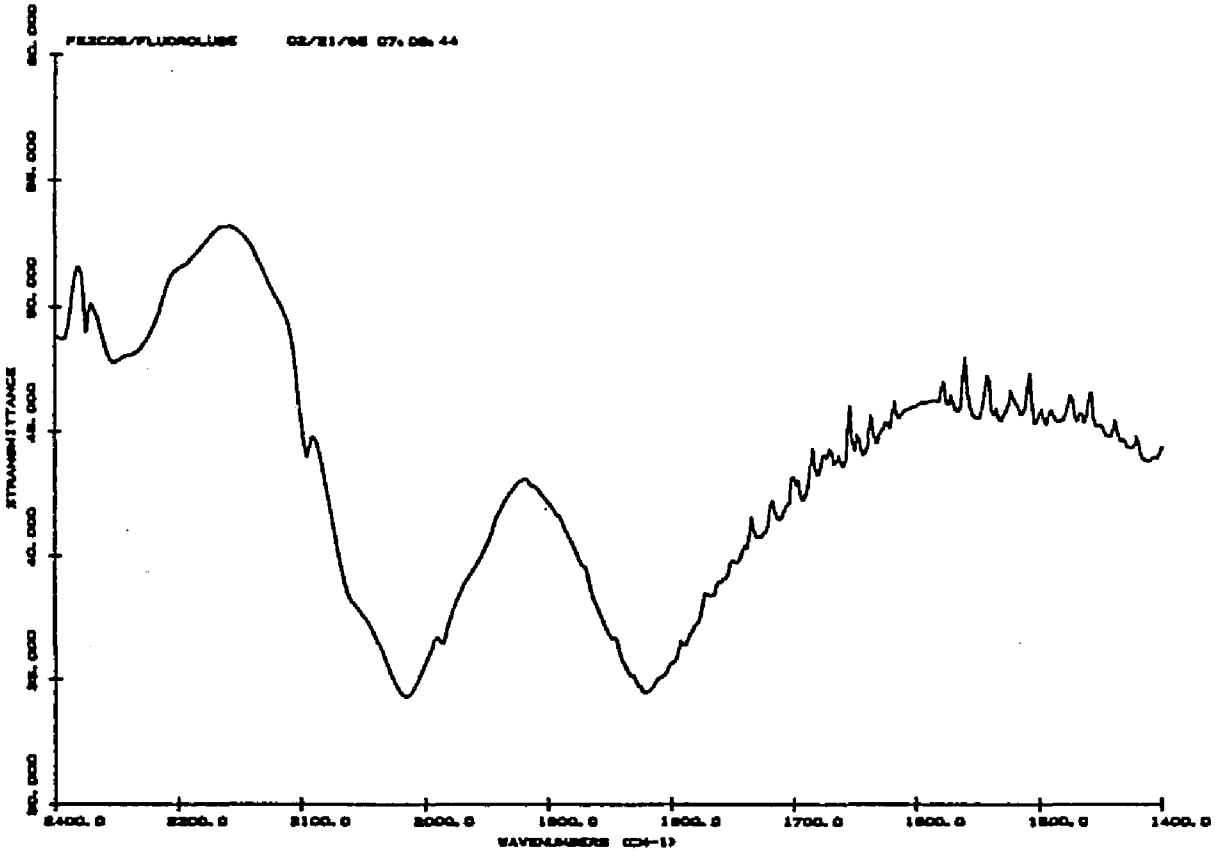

Figure 36. Infrared spectrum of $Fe_2(CO)_9$ in Fluorolube.

assigned to a specific molecular entity. The electronic and spectral evidence indicates a disproportionation of $Fe_2(CO)_9$ to $Fe_3(CO)_{12}$ and $Fe(CO)_5$ when adsorbed onto PVG. Disproportionation also occurs when $Fe(CO)_5$ is adsorbed on silica gel (99) and in solutions containing weak ligands at room temperature (59,60).

iii. $Fe_3(CO)_{12}$.

PVG is impregnated with $Fe_3(CO)_{12}$ via solution impregnation techniques and the UV-visible spectrum of adsorbed $Fe_3(CO)_{12}$ is shown in Figure 37. The spectrum exhibits an intense MLCT UV absorption with well resolved bands in the visible region at 605 and 440 nm due to $\sigma^* \longrightarrow \sigma^*$ and $\sigma \longrightarrow \sigma^*$ transitions, respectively (52). The spectrum is similiar to that obtained in fluid solution, Figure 38, and a comparison of the ratio of the relative extinction coefficents of the 605 and 440 nm bands for the adsorbed complex, with that in fluid solution, are within experimental error. The adsorbed complex appears to be relatively stable for hours when stored under vacuum at room temperature. After several days, however, some thermal decomposition does occur. The intensity of the 605 nm band declines slightly and analysis of the gas phase indicates a slight evolution of CO. The decomposition is accelerated in the presence of air, with the sample apparently forming an iron oxide.

Figure 37. Electronic Absorption Spectrum of $Fe_3(CO)_{12}$(ads.).

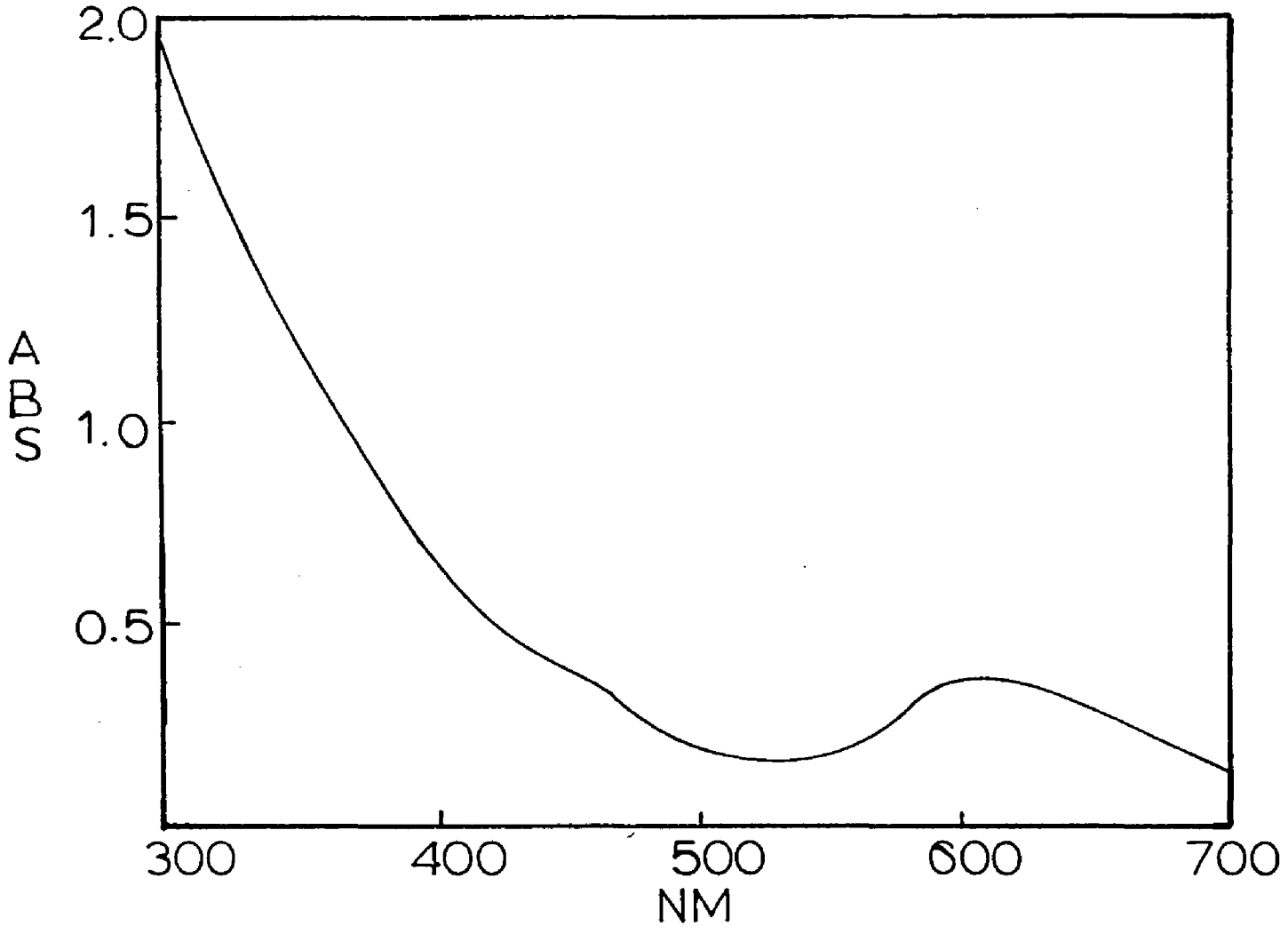

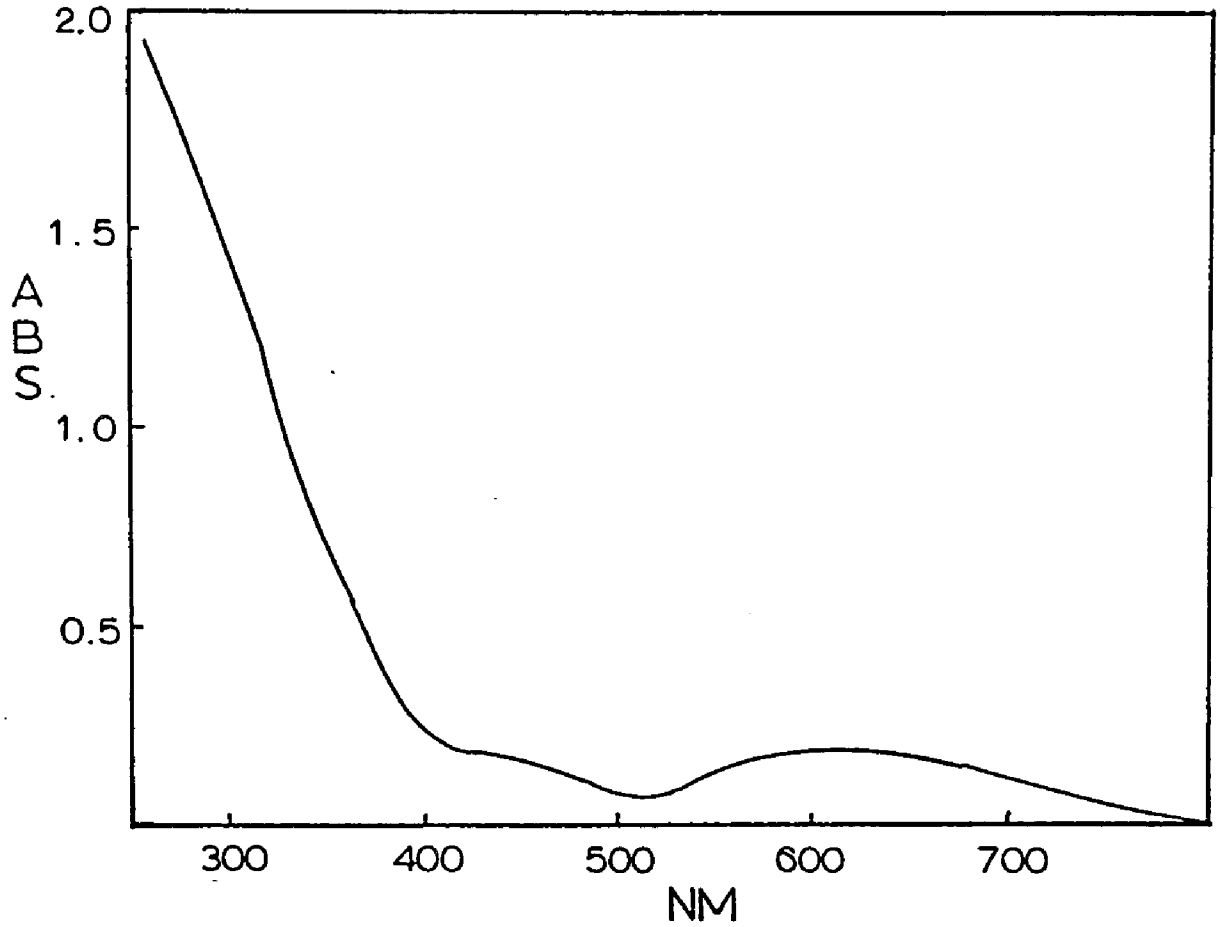

Figure 38. Electronic Absorption spectrum of $Fe_3(CO)_{12}$ in n-hexane.

The adsorption of $Fe_3(CO)_{12}$ on PVG, like that of $Fe(CO)_5$, is reversible since soaking a sample containing $5.2\pm0.1 \times 10^{-6}$ moles/gram in n-hexane for several hours results in decolorization of the previously green sample. The UV-visible spectrum of the extracting solution indicates $Fe_3(CO)_{12}$, which confirms the complex leaches out of the PVG into solution intact.

The DRIFT spectrum of $Fe_3(CO)_{12}$ sublimed onto PVG, Figure 39, is similar to the IR spectrum of the complex in n-hexane, shown in Figure 40. In the latter solvent, IR bands at 2047 and 2026 cm^{-1} occur, whereas $Fe_3(CO)_{12}$(ads) exhibits a single major absorption at 2053 cm^{-1} with a broad shoulder at 2032 cm^{-1}. No absorptions in the bridging CO region are observed in either spectrum. The similarity of the spectra as well as the ability to desorb the complex intact establishes that $Fe_3(CO)_{12}$ physisorbs onto PVG with no declusterification or substitution of the complex occuring.

2. Photochemical Reactions of $Fe(CO)_5$(ads).

i. Low Surface Coverage Experiments.

The photochemistry of $Fe(CO)_5$(ads) on PVG exhibits a pronounced dependence on loading. Photolysis of samples containing $\leq 10^{-6}$ moles/gram in vacuo with 350, 310, or 254-nm light causes a decline in the UV absorbance, characteristic of $Fe(CO)_5$(ads) and a concurrent growth of

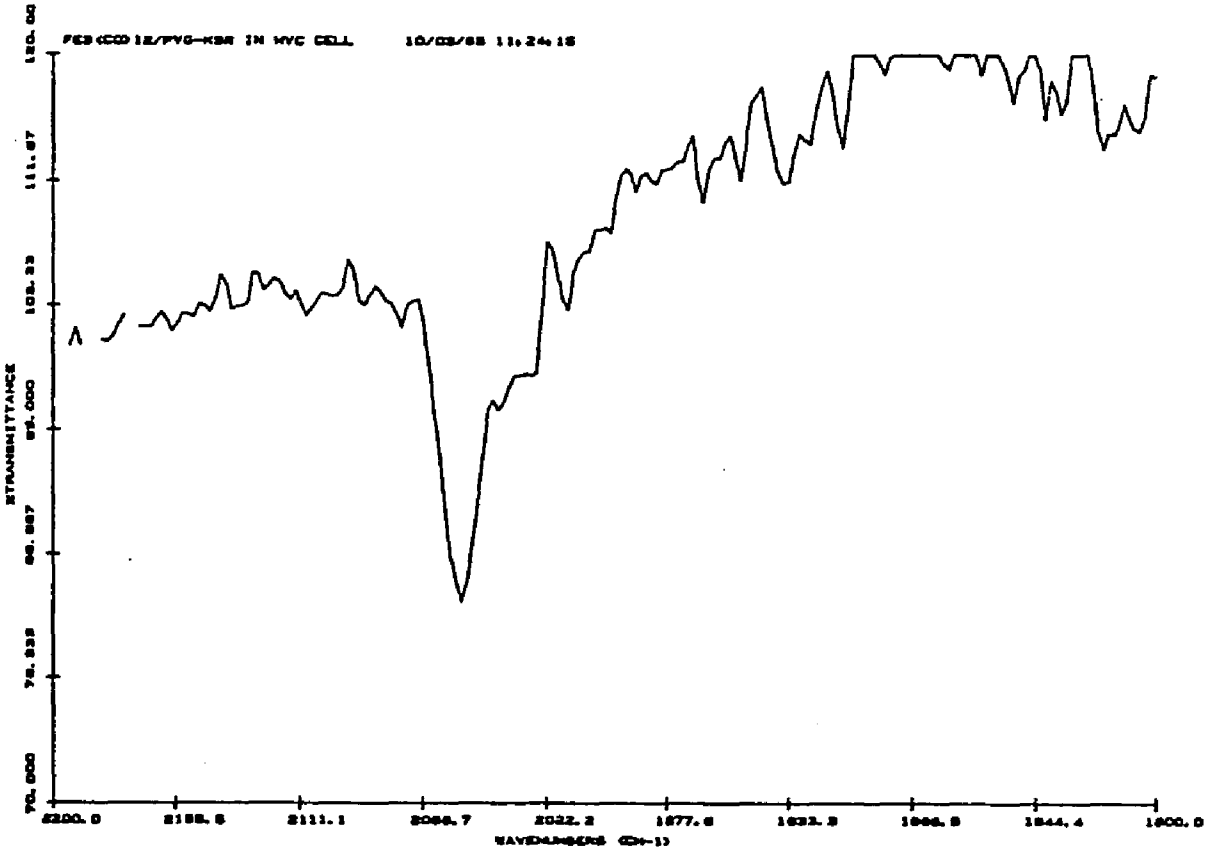

Figure 39. DRIFT spectrum of $Fe_3(CO)_{12}$(ads.)

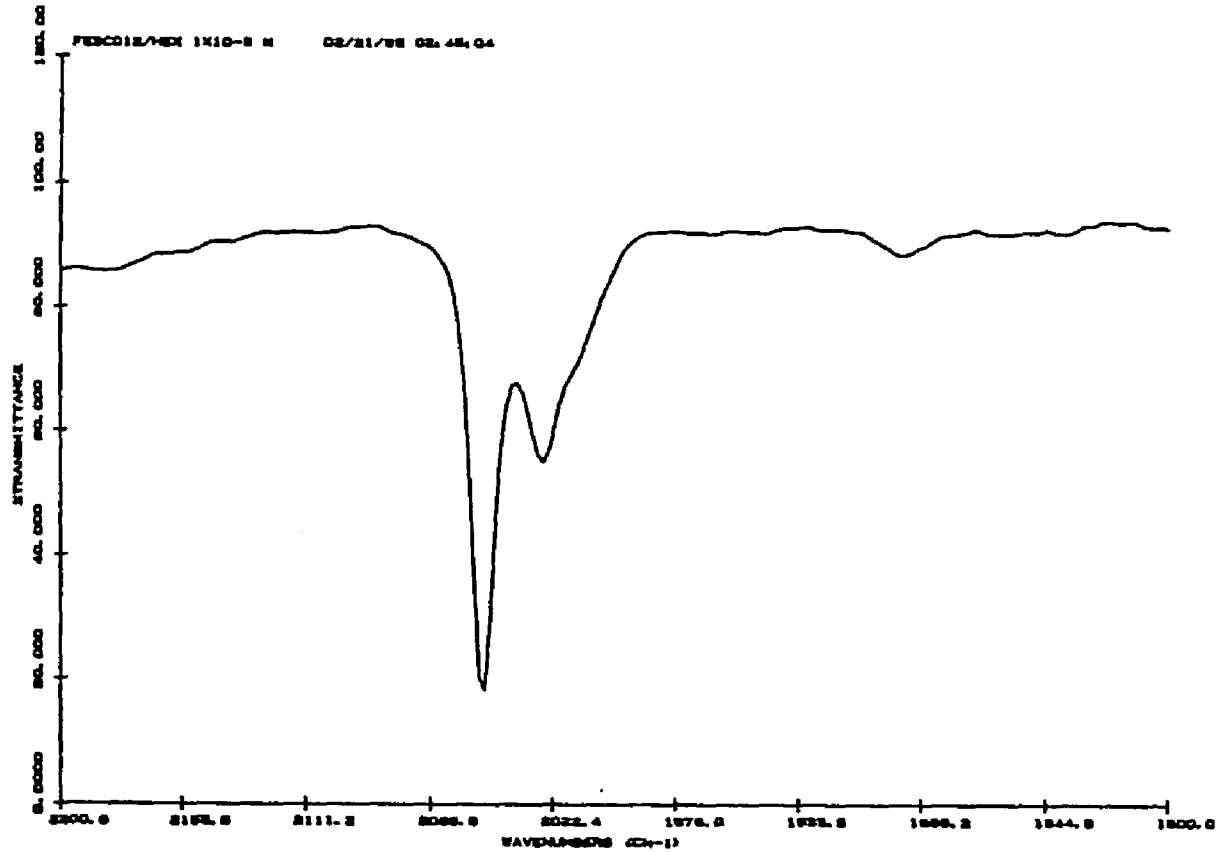

Figure 40. Infrared spectrum of $Fe_3(CO)_{12}$ in n-hexane.

a broad absorption centered at 370 nm as shown in Figure 41. An isosbestic point at 285 nm is maintained during short irradiation times, and exposing the photoproduct to 1 atm of CO causes spectral changes corresponding to recovery of $\geq$97% of the original pentacarbonyl. The similarity of the photoproduct spectrum with that of $Fe(CO)_4$ generated in low temperature matrices (68) indicate that the primary photoreaction is

1.) $$Fe(CO)_5(ads) \longrightarrow Fe(CO)_4(ads) + CO$$

The stability of the tetracarbonyl, which exists for hours in vacuo at room temperature is attributed to an interaction with the PVG surface. The absence of a near-IR absorption characteristic of free $Fe(CO)_4$ (69,70), and the presence of absorption in the near-UV characteristic of $Fe(CO)_4L$ complexes, i.e., $Fe(CO)_4$(pyridine), suggests that the vacant coordination site of the surface bound tetracarbonyl, $Fe(CO)_4$(ads), is occupied by either a silanol group or chemisorbed water. Reaction 1 is independent of excitation wavelength, i.e., 350, 310 or 254 nm. However, quantum yield measurements were limited to 350 nm where competitive absorption by the support is negligible. As shown in Figure 42, plots of ϕ_{obs} vs. irradiation time extrapolate to a limiting yield, 0.96 ± 0.05, within experimental error of unity. This high efficiency is an experimental difficulty since the

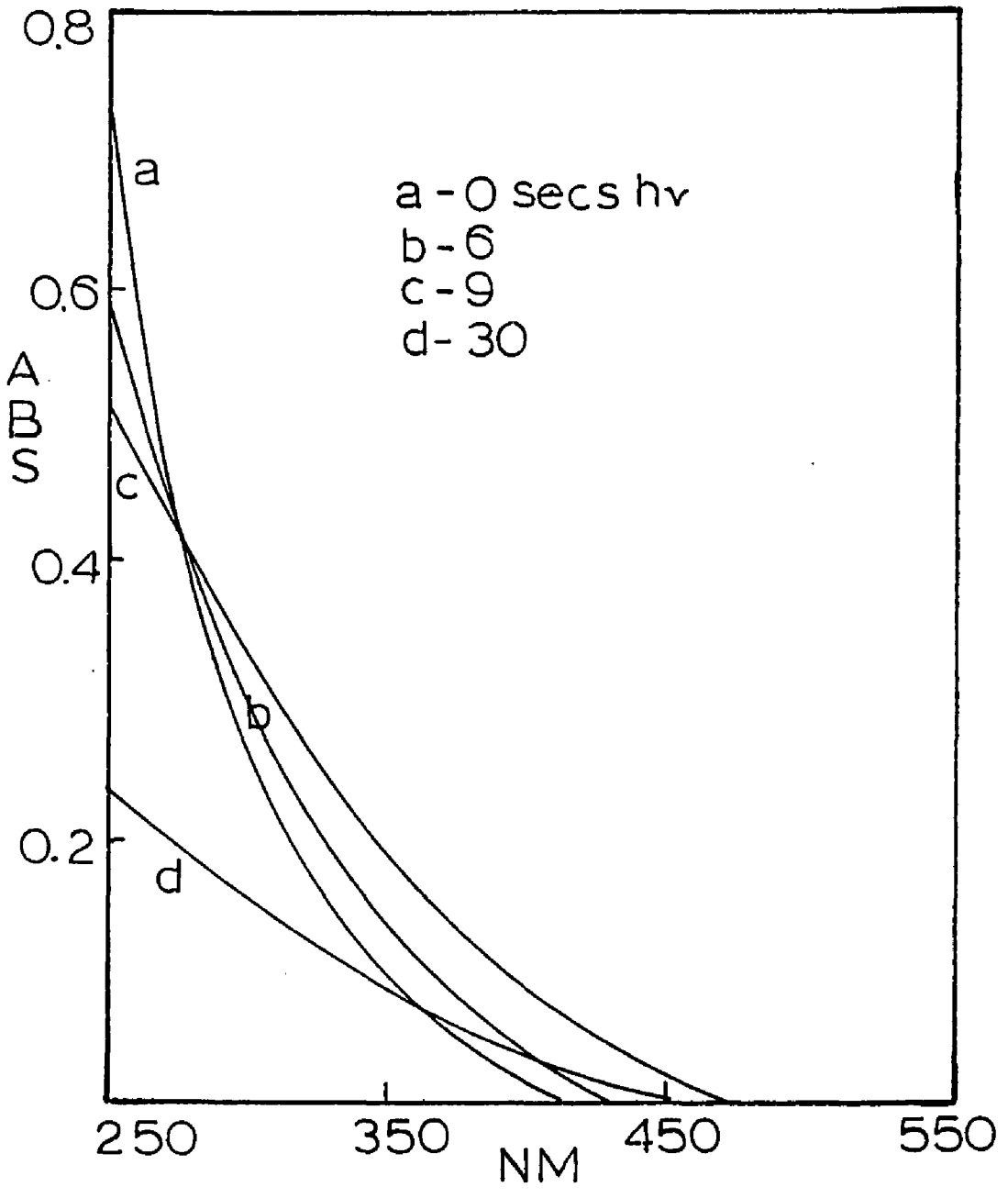

Figure 41. Electronic Absorption Spectra following UV photolysis of $Fe(CO)_5$(ads.) at low surface coverage.

Figure 42. Quantum yield of $Fe(CO)_5$(ads.) disappearance.

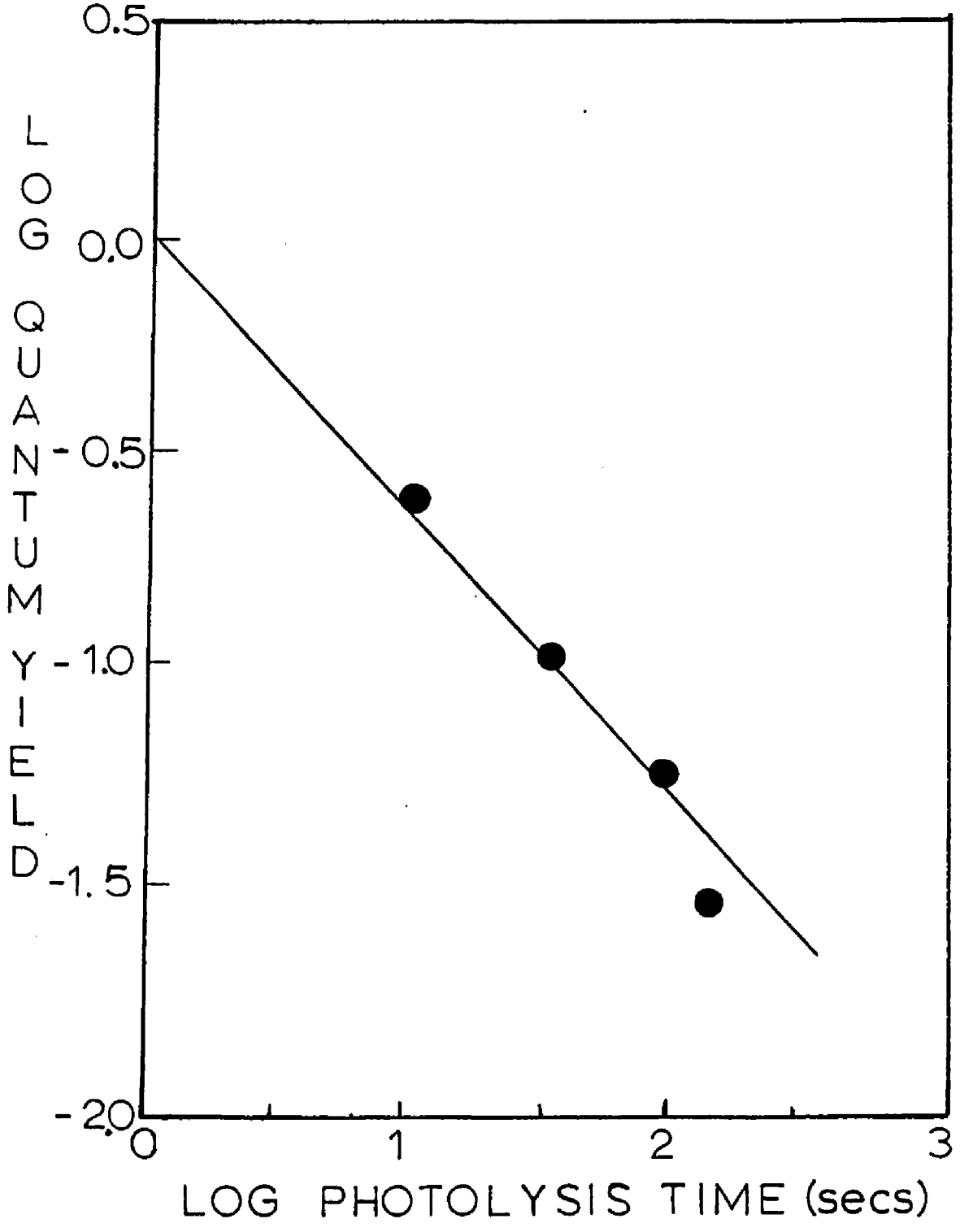

product forms rapidly and undergoes secondary photolysis with similar facility.

Continued photolysis, particularly with 254-nm light, leads to the evolution of 4.9±0.2 moles of CO/mole of $Fe(CO)_5$(ads). UV-visible spectra recorded periodically during photolysis, however do not reveal absorptions due to dimeric or trimeric species. At 280 nm, for example, the relative absorptivity of $Fe_3(CO)_{12}$ is 4.8 times that of $Fe(CO)_5$ both in solution (85) and adsorbed onto PVG. Hence, formation of $Fe_3(CO)_{12}$ from three molecules of $Fe(CO)_5$ should result in an increase in the UV absorbance. Yet, the spectral changes consist of a general decline throughout the UV region. H_2 evolution, indicative of metal oxidation is not detected (20), <0.02 moles of H_2/mole of $Fe(CO)_5$(ads), and exposing the photoproduct to 1 atm of O_2 free CO rapidly regenerates the absorbance at 370 nm assigned to surface-bound $Fe(CO)_4$(ads). The tetracarbonyl then undergoes a slower reaction to $Fe(CO)_5$(ads). In a number of experiments, the final spectrum, Figure 43, consisted of a series of sharp bands superimposed on a rising UV background. The spectrum closely resembles that reported for atomic iron generated via UV photolysis of $Fe(CO)_5$ in dilute low temperature matrices (72), and the band maxima, listed in Table 3, agree closely with the reported values.

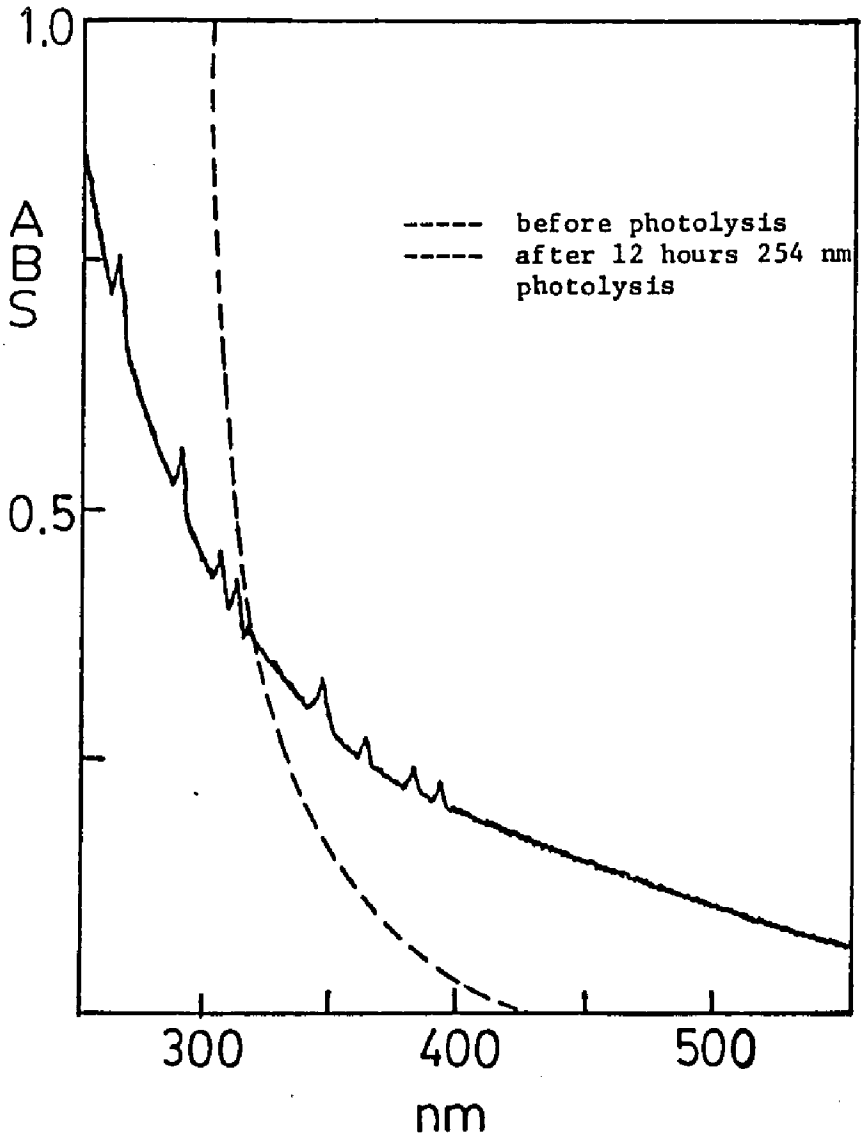

Figure 43. Electronic spectrum of Atomic Iron on PVG.

Table 3.

Positions (nm) of UV Absorption Bands of Matrix Isolated Iron Atoms.

PVG	nitrogen	argon	krypton
389			
380			
	367.9		368.0
362	360.1		
	354.4	358.9	
345			
315	329.8	333.6	333.5
		326.0	
311			
305			
	296.5	298.0	300.1
	292.4	294.5	297.1
288	287.7	288.5	
		286.5	289.5
		268.2	268.9
262	264.8	263.0	
	245.5	246.5	249.6
	241.3	241.4	244.3
		240.0	
		237.5	
		213.0	

FMR spectra recorded at room temperature, 22±1 °C, after a 12 hour, 254-nm photolysis of $Fe(CO)_5$(ads), Figure 44, show a broad asymmetric resonance with g = 2.07±0.01, and a line width of 5.0±0.5 x 10^3 G. The g value is shifted with respect to that reported for bulk iron, 2.15±0.04 (130). The line shape closely resembles that reported by Basset and coworkers (36) for zerovalent iron particles formed by the thermal decomposition of $Fe_3(CO)_{12}$ on hydroxylated Al_2O_3 and MgO supports. The latter, which are ≤ 15Å particles, exhibit line widths at 300 K of 250 G and 2250 G on MgO and Al_2O_3, respectively. The larger line widths found in our experiments on PVG, by analogy with the results obtained with Ni (131), are consistent with the formation of smaller iron particles. However, the experimental factors which control atomic iron formation are not immediately obvious. Although GC analyses of the vapor phase consistently indicated the evolution of 4.9±0.2 moles of CO/mole of $Fe(CO)_5$(ads) and FMR spectra of the adsorbed photoproduct exhibited broad resonances suggestive of small iron particles, the band spectrum of atomic iron was not obtained with every sample. In most experiments, the final spectrum consists of nondescript, increasing absorbance in the UV region. The role of surface dimensionality in these experiments, which may differ from sample to sample, particularly on a molecular scale, appears to be a critical determinant of the level of agglomerization of the photogenerated Fe.

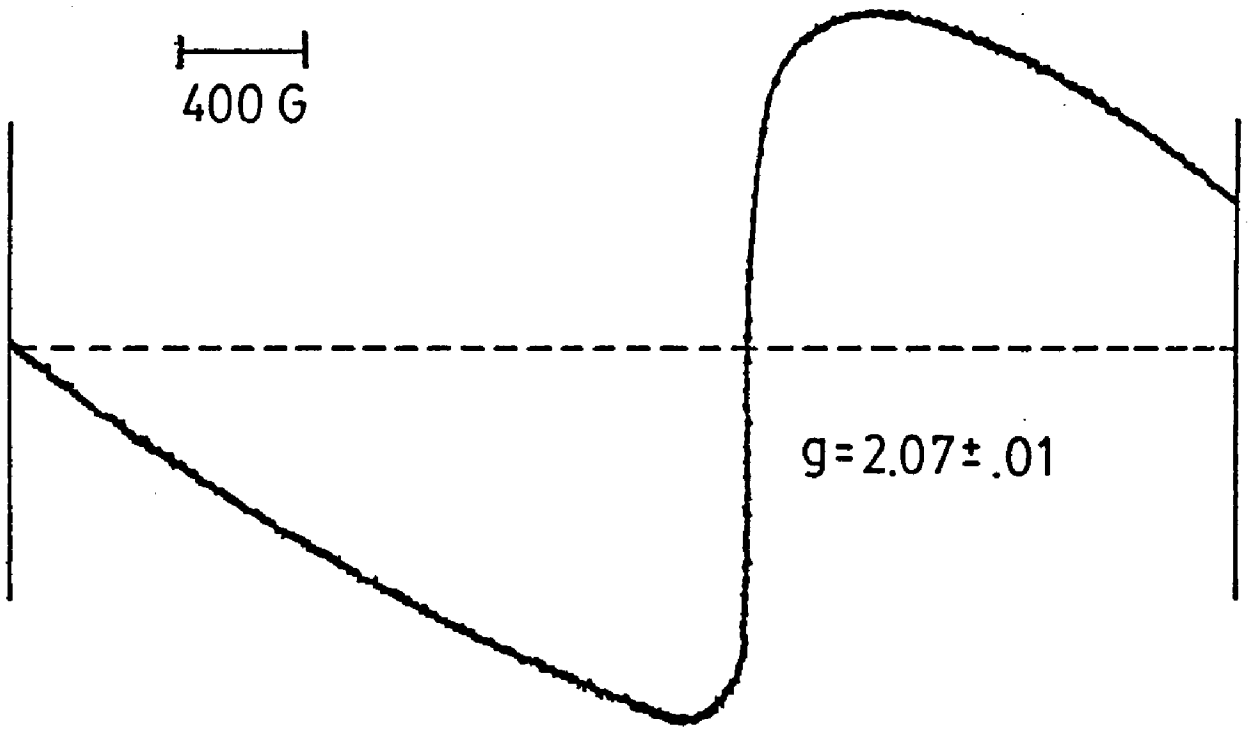

Figure 44. FMR spectrum of Atomic Iron on PVG.

ii. Higher Surface Coverage Experiments.

Photolysis of a PVG sample containing > 10^{-6} moles of $Fe(CO)_5$(ads)/gram in vacuo at 22±1 C with 254, 310, or 350-nm radiation causes an immediate growth in absorption at 605 nm, Figure 45. This band, which agrees exactly with that observed in the visible spectrum of $Fe_3(CO)_{12}$(ads), establishes formation of the trimer. The stoichiometry of the reaction and the quantum yield of trimer formation, however, indicate a complex reaction sequence. As shown in Figure 46, GC analysis of the vapor phase reveals considerably more CO evolved than the theoretical yield assuming that 3 moles of CO are evolved/mole of $Fe_3(CO)_{12}$ formed. The latter being determined by comparison of the photogenerated absorbance at 605 nm with that of PVG samples containing known amounts of $Fe_3(CO)_{12}$(ads).

The quantum yield of trimer formation, ϕ_T, shows a marked dependence on irradiation time. As shown in Figure 47, samples containing from 3.7 x 10^{-6} to 2.5 X 10^{-5} moles of $Fe(CO)_5$/gram exhibit an induction period which suggests that formation of the trimer arises from secondary reaction(s) of the primary photoproduct. The electronic spectrum of $Fe_3(CO)_{12}$, both in solution and adsorbed onto PVG, exhibits a well resolved shoulder at 440 nm. However, the 440-nm shoulder of the trimer could not be resolved in the photoproduct spectrum. Rather, a

Figure 45. Electronic Absorption Spectra following UV photolysis of $Fe(CO)_5$(ads.) at higher surface coverages.

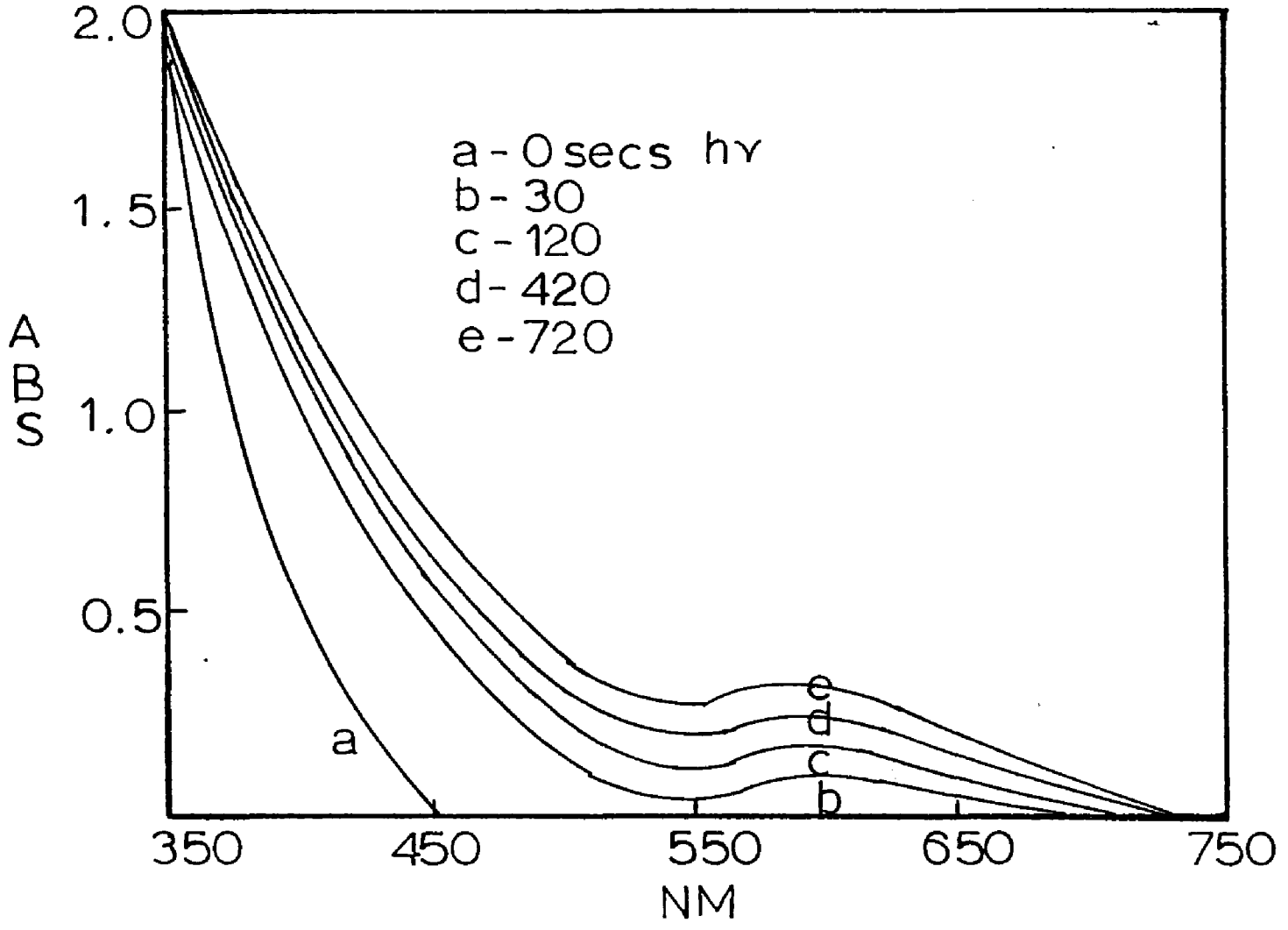

Figure 46. Moles of CO evolved following UV photolysis of $Fe(CO)_5$(ads.) vs. moles of $Fe_3(CO)_{12}$ formed.

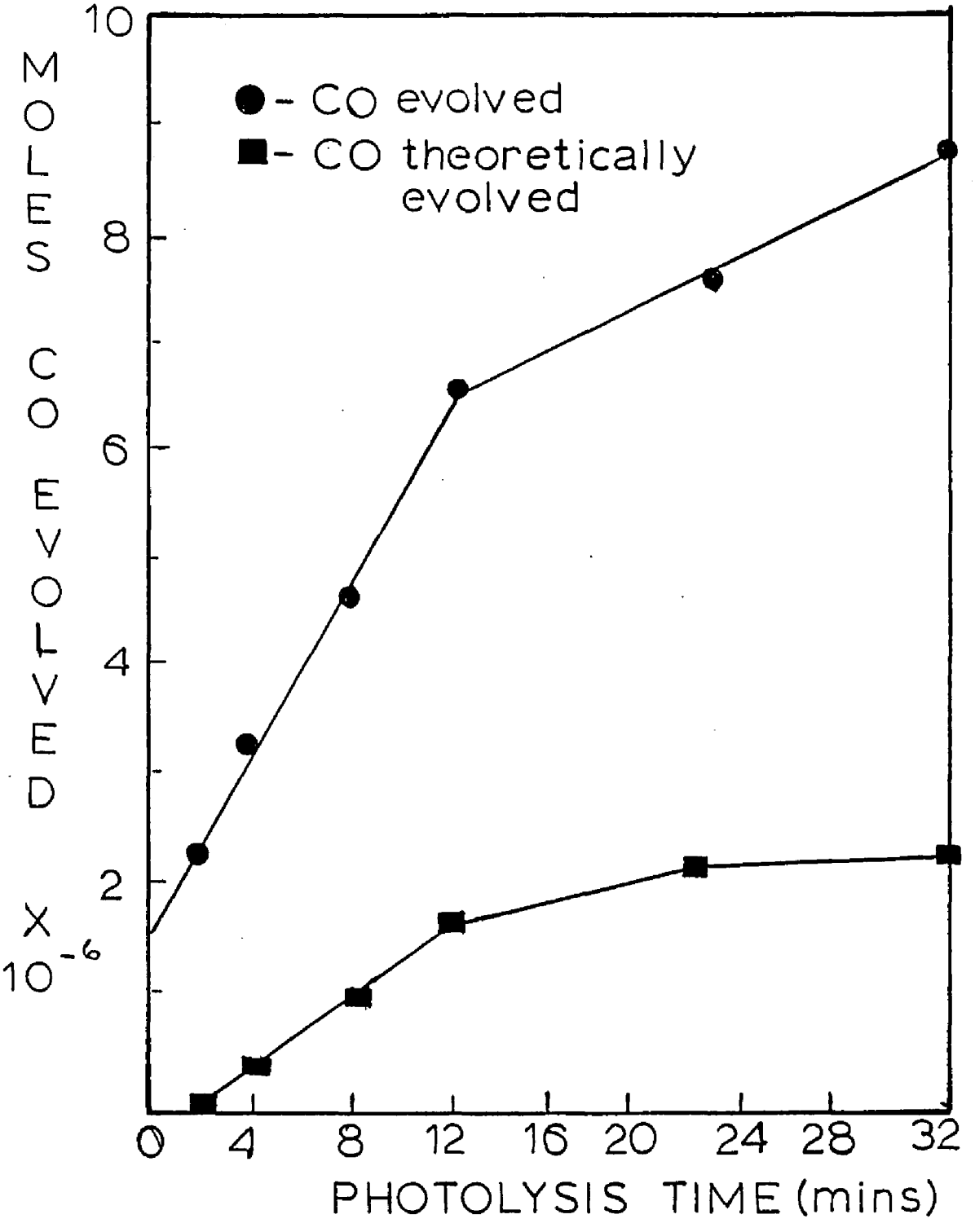

Figure 47. Quantum yield of $Fe_3(CO)_{12}$ formation vs. photolysis time.

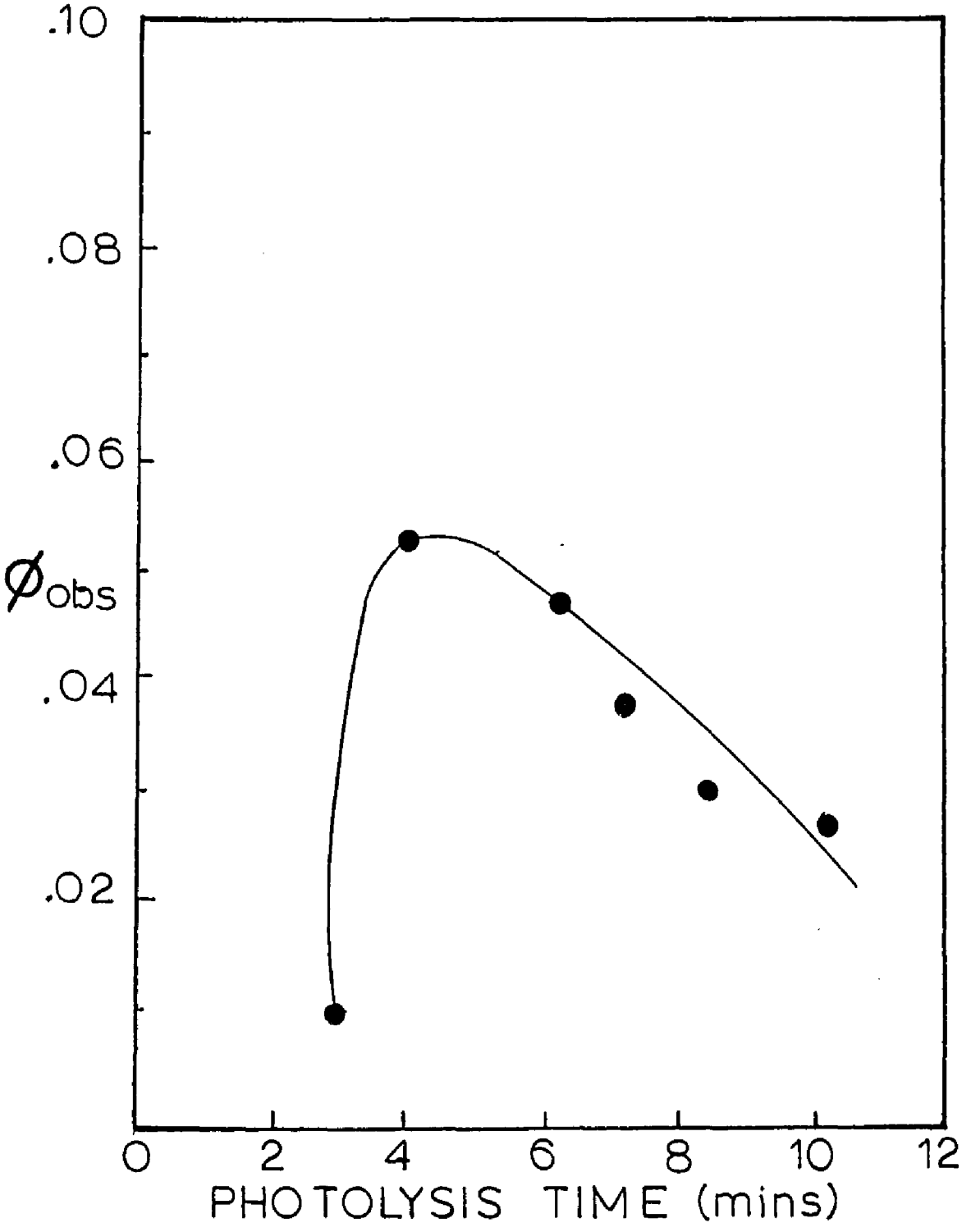

broad adsorption centered at ca. 400 nm occurs, and comparison of the relative intensities found in the photolyzed sample at 605 and 440 nm with those of a known sample of $Fe_3(CO)_{12}$(ads) indicated the presence of additional photoproducts. Subtracting the relative absorbance due to $Fe_3(CO)_{12}$ in the 350-450 nm region, based on its absorbance at 605 nm, yields a spectrum with a maximum at 370-380 nm that closely resembles that of $Fe(CO)_4$(ads). There is no spectral evidence of the formation of $Fe_2(CO)_9$, and exposure to 1 atm of CO causes a rapid decline in absorbance in the near-UV while that at 605 nm remains unchanged. Futhermore, the absorption at 605 nm characteristic of the trimer does not appear when $Fe(CO)_5$(ads) is photolyzed under pressures of CO ranging from 400 torr to 1 atmosphere. Photolysis develops a yellow color which quickly disappears in the time required to move the cell from the Rayonet reactor to the spectrophotometer. These results suggest that photolysis leads intially to surface bound $Fe(CO)_4$(ads) which, at sufficently high loadings, undergoes further reactions leading to the trimer. Indeed, diffuse reflectance FTIR reveals a number of species.

3. Diffuse Reflectance FTIR Experiments.

As previously described, powdered samples (325 mesh) containing 3 x 10^{-4} moles of $Fe(CO)_5$/gram of PVG were irradiated in a microreactor in the sample compartment of an FTIR. The microreactor was mounted on a translational stage that allowed as many as six separate experiments on the same sample. The samples were irradiated with either 350-nm light from a Kr ion laser ($4W/cm^2$) or 355-nm light from a Nd:YAG laser (50 mj, 7nsec fwhm). The spectrum recorded at the specified times after pulsed excitation is shown in Figure 48. Excitation causes significant loss of $Fe(CO)_5$ band intensity and the appearance of two higher energy absorptions at 2073 and 2048 cm^{-1}. Figure 49, displays five spectra from a period less than 1.5 seconds after the pulse. The $Fe(CO)_5$ bands at 2026 and 2004 cm^{-1} are observed to return to their original intensity within this time. Since the latter occurs without detectable change in the photoproduct band intensity, it is not due to a thermal backreaction of the photoproducts with photoejected CO. Rather, rapid regrowth of the pentacarbonyl band intensity is attributed to replenishment of the surface depleted $Fe(CO)_5$ by diffusion through the powdered PVG in the microreactor. Consequently, $Fe(CO)_5$(ads) spectra are subtracted from spectra acquired at later times to reveal minor changes in the photoproduct spectrum. Figure 50

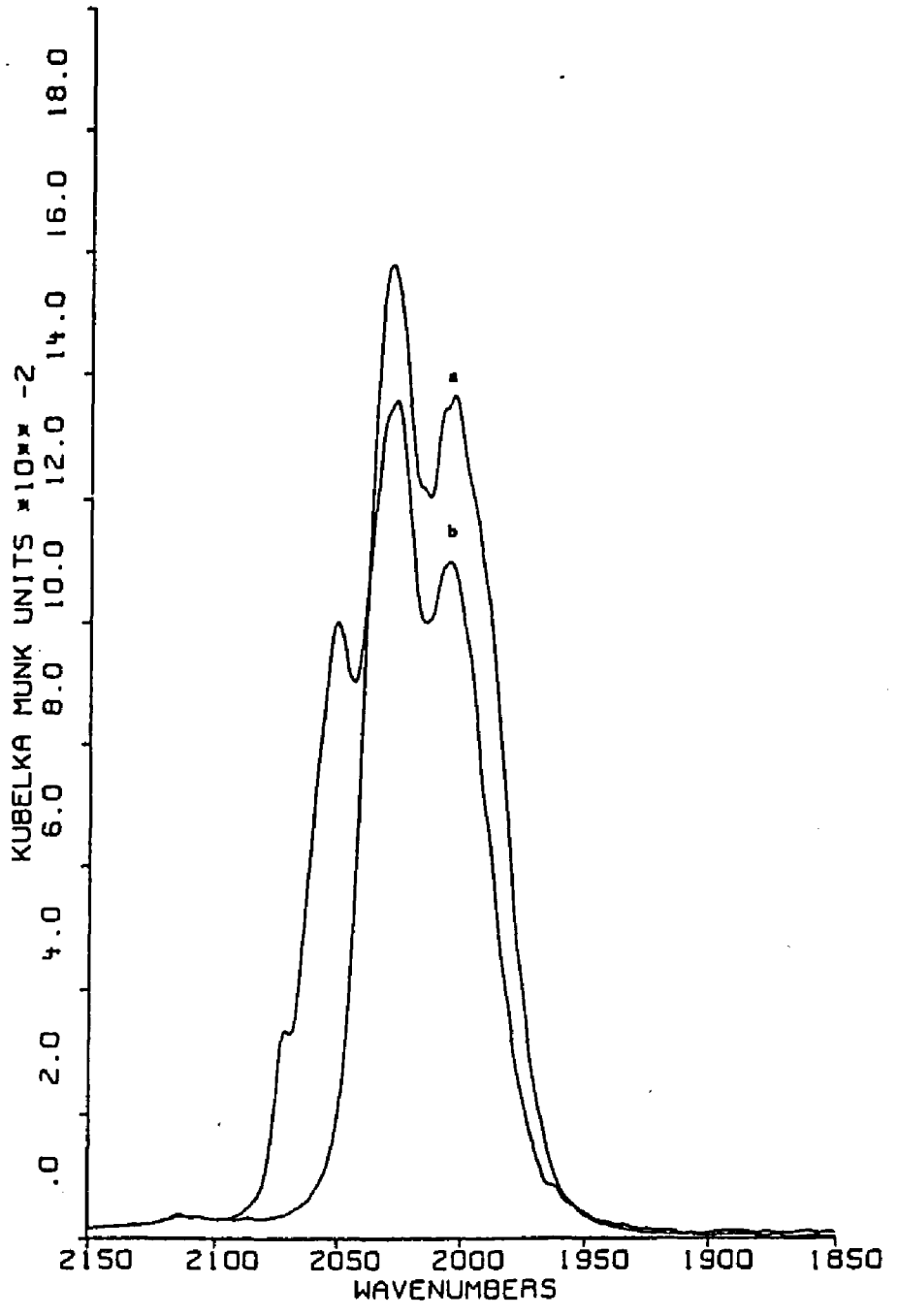

Figure 48. Kubelka Munk spectra of $Fe(CO)_5$(ads.)
a) before and b) after 1 pulse from a Nd:YAG laser.

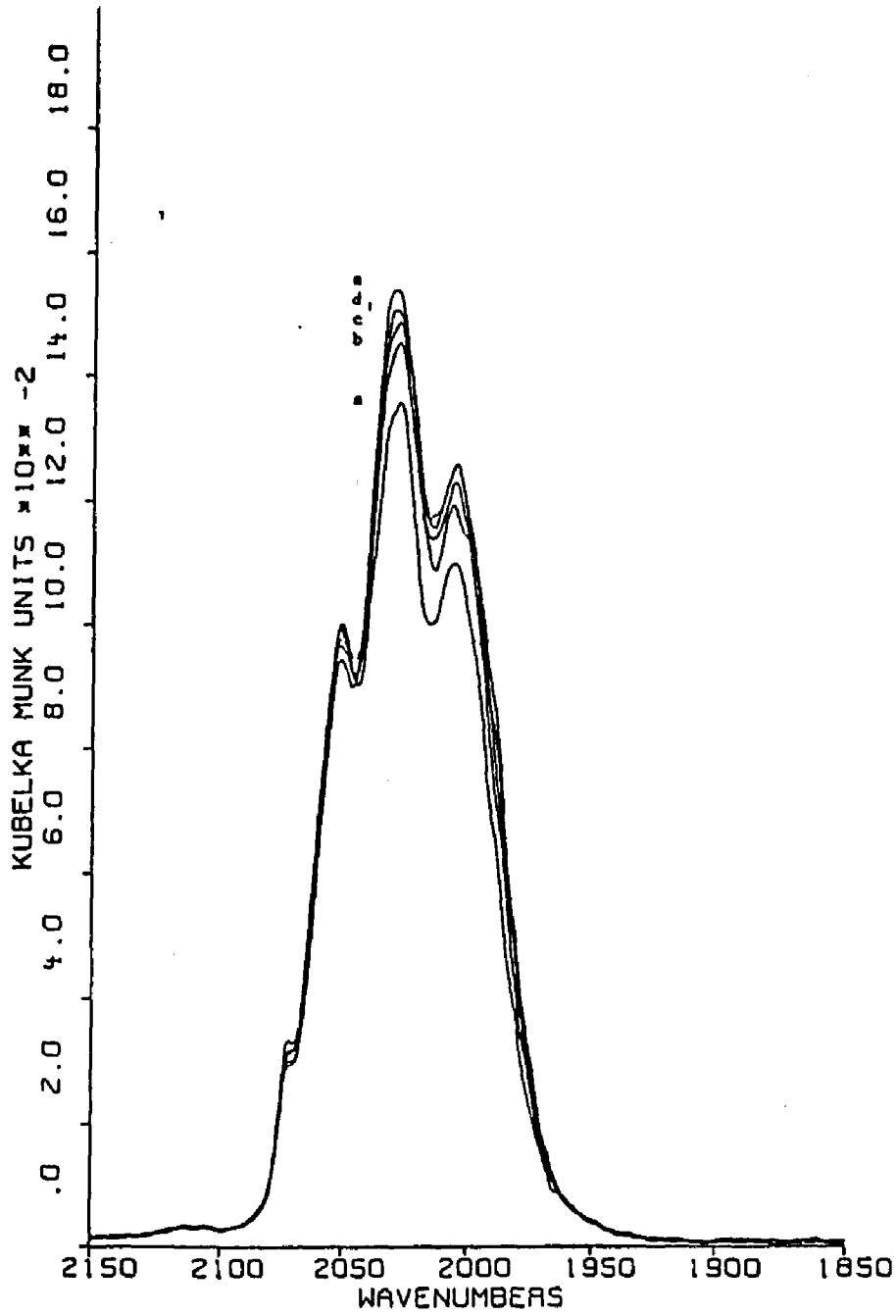

Figure 49. Kubelka Munk spectra of $Fe(CO)_5$(ads.) after 1 laser pulse (Nd:YAG) showing regrowth of $Fe(CO)_5$ a) 0 b) 0.14 c) 0.27 d) 0.41 e) 1.22 sec. after laser pulse

illustrates difference spectra following two pulse (50mJ, 7 nsec fwhm) excitation of powdered PVG containing 3 x 10^{-4} moles of $Fe(CO)_5$/gram in vacuo. The top spectrum represents the difference between the $Fe(CO)_5$(ads) spectrum and those recorded immediately after excitation. The subsequent spectra are the difference between that recorded immediately after excitation and that recorded at the specified later times. Difference spectra highlight features which have decayed (positive bands) or grew in (negative bands) during the indicated time intervals. These spectra reveal that the spectral features exhibit only minor changes over the 540 second analysis time. The first feature to decay is the high frequency shoulder at 2073 cm^{-1}. Most of its decay occurs during the first 40 seconds and is accompanied by loss of a shoulder at 2048 cm^{-1}. These bands are assigned to a single species since both decay at the same rate. A low intensity band in the bridging carbonyl region, 1790 cm^{-1}, also appears and decays during this time interval. At longer times, i.e., 400 seconds after excitation, decay of the intense 2056 cm^{-1} dominates the spectral change. This decay continues beyond the times shown in Figure 50, but at a much slower rate. The spectral changes depicted in Figure 50 follow two pulse excitation. Similar results occur with single pulse excitation except that less product is formed, and the second pulse favors formation of the 2056 cm^{-1} absorption

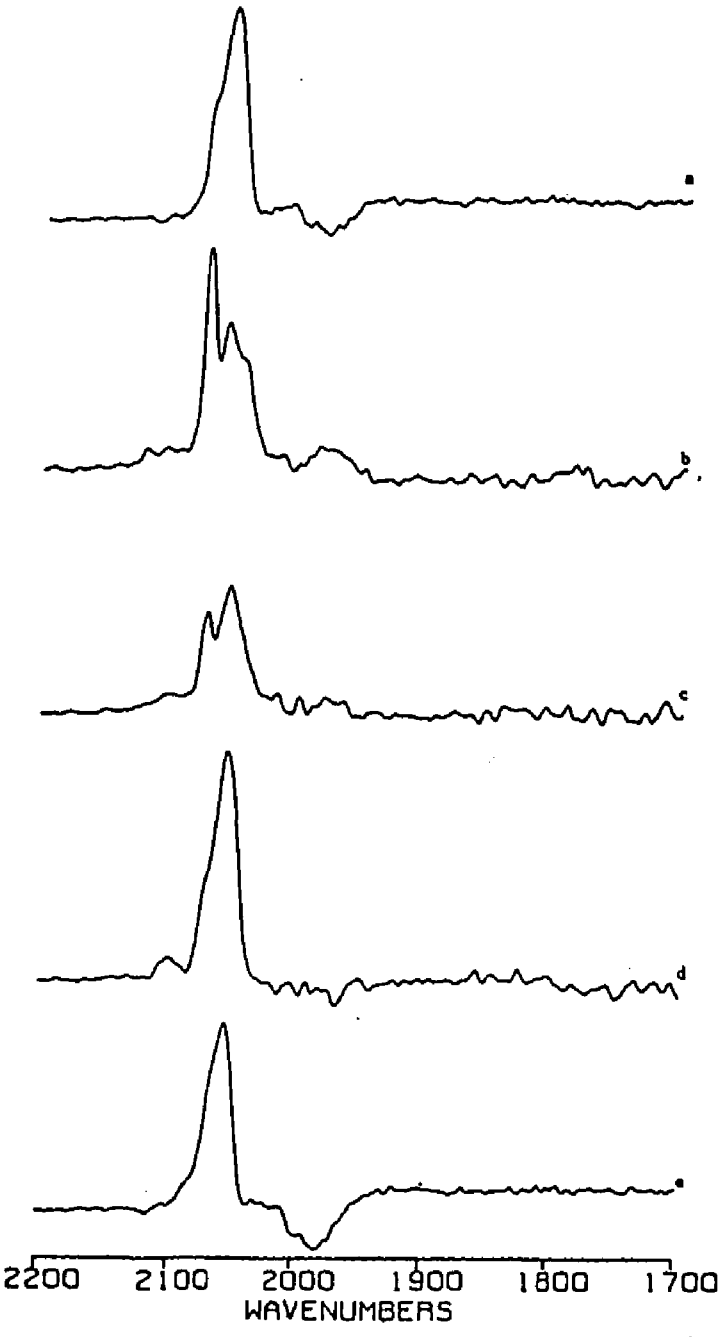

Figure 50. Difference spectra of $Fe(CO)_5$(ads.) following 2 laser pulses (Nd:YAG)
a) intial difference b) difference during next 40 secs.
c) difference during next 100 secs.
d) difference during next 400 secs.
e) final difference after 540 secs.

over an increase in the 2073 cm^{-1} absorption. In addition, a weak absorption arises in the bridging carbonyl region at 1823 cm^{-1}.

Although of somewhat higher frequency, bands in the 2053-2059 cm^{-1} region are indicative of a trimeric cluster. The Kubelka Munk spectrum of $Fe_3(CO)_{12}$(ads), Figure 39, displays a major absorption at 2053 cm^{-1} with a broad shoulder at 2032 cm^{-1} and a weak absorption at 2109 cm^{-1}. Since absorptions in the bridging carbonyl region are not detected in the $Fe_3(CO)_{12}$(ads) spectrum, their occurence in spectra after excitation may be indicative of the formation of dimeric adsorbates. Poliakoff and Turner (69,70,74) report that $Fe_2(CO)_9$ and $Fe_2(CO)_8$ in low temperature matrices exhibit bands in the bridging carbonyl region at 1820 and 1790 cm^{-1}, respectively. The appearance and rapid decay of weak absorptions at 1790 and 1823 cm^{-1} following two pulse excitation of $Fe(CO)_5$(ads) suggests formation of unstable, dimeric intermediates on PVG at room temperature.

In contrast to pulsed excitation, which produces a grayish spot, 0.1 to 1.6 second cw excitation (350 nm, $4W/cm^2$) produce a pale green color similiar to that observed when $Fe_3(CO)_{12}$ is formed on the plate samples. Difference spectra recorded after excitation reveal bands in the bridging carbonyl region as well as somewhat

different absorptions in the terminal carbonyl region. Weak bands are observed in the bridging carbonyl region at 1790 and 1820 cm^{-1} along with an intense band in the terminal CO stretching region at 2066 cm^{-1}. The band intensities in the bridging ν_{CO} region increase with increasing the irradiation time, without a change in their decay rates, whereas band intensities in the terminal ν_{CO} region exhibit a more complex dependence. Figure 51 is representative of the spectral changes following 0.1 second excitation. Immediately after excitation, the spectrum after subtraction of absorptions due to $Fe(CO)_5$(ads) exhibits an intense absorption at 2059 cm^{-1} with a discernible high frequency shoulder. During the first 100 seconds after excitation, difference spectra show that a severe decline in the intensities of the bridging carbonyl absorptions at 1790 and 1820 cm^{-1} is accompanied by loss of intensity at 2066 cm^{-1}. The intensities of these bands continue to decline during the next 100 seconds during which time the decay of the bands at 2073 and 2048 cm^{-1} becomes apparent. At later times, the bridging carbonyl absorptions and the band at 2066 cm^{-1} disappear and the 2073 and 2048 cm^{-1} bands dominate the decay. The latter decay to a spectrum exhibiting a single absorption at 2059 cm^{-1} which closely resembles that observed immediately after excitation.

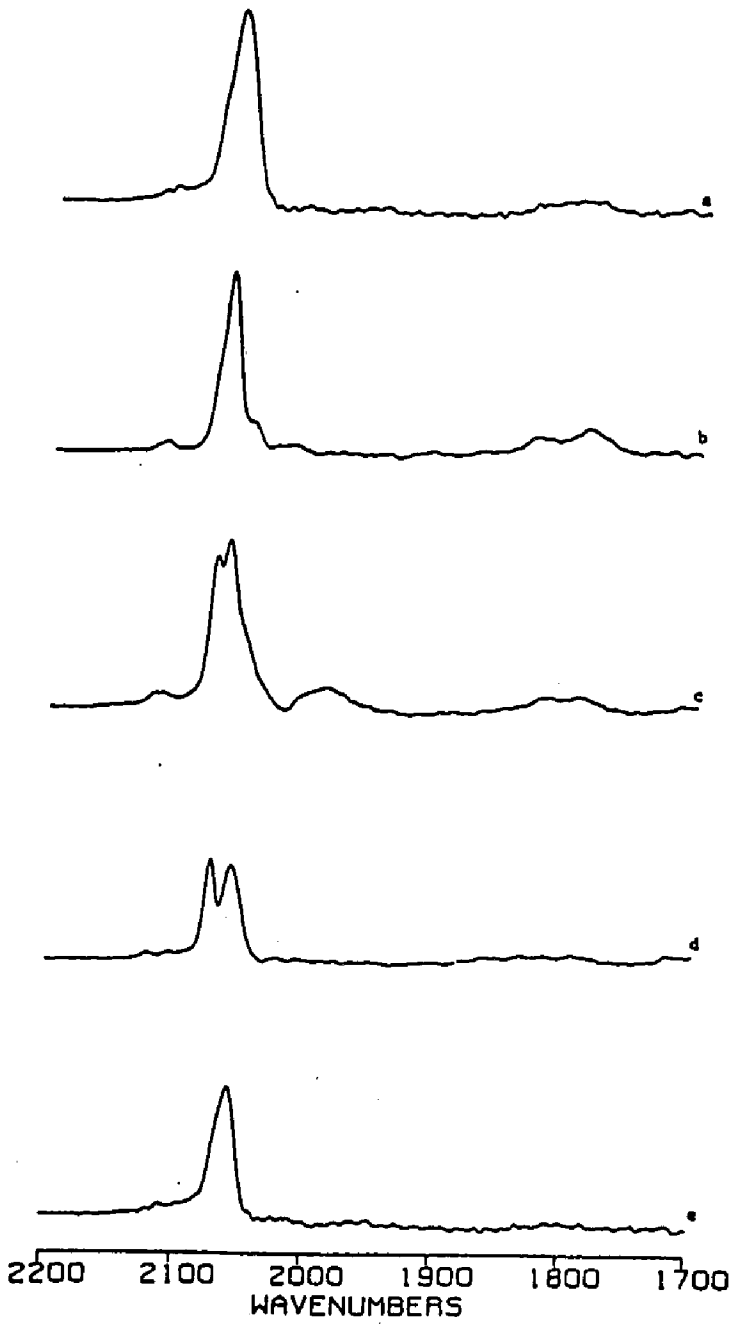

Figure 51. Difference spectra of $Fe(CO)_5$(ads.) following 0.1 second laser irradiation (Kr ion,500 mW)
a) intial difference b) difference during next 100 secs.
c) difference during next 100 secs.
d) difference during next 400 secs.
e) final difference after 600 secs.

In both cw and pulsed excitation experiments, the 2048 cm^{-1} band accompanies the appearance of the 2073 cm^{-1} band. The band intensities correlate well in the different experiments and both decay at the same rate. Thus both bands are assigned to a single species whose decay characteristics suggest that it is an intermediate common to the decay and formation of other transients. For example, the rate of decay of the species responsible for the 2073 and 2048 cm^{-1} bands is much slower following cw excitation than it is following pulsed excitation. This suggests that the 2073-2048 cm^{-1} transient is a product of the decay of secondary photoproducts. In addition, cw excitation produces a strong absorption at 2066 cm^{-1} which decays before the 2073-2048 cm^{-1} decay is apparent. This suggests that the species exhibiting the 2066 cm^{-1} band converts into the species displaying the 2073-2048 cm^{-1} bands, perhaps balancing its decay. Futhermore, spectra recorded at 80 millisecond intervals during 1.0 second cw excitation show that an early growth of a 2073 cm^{-1} absorption is followed by a later growth of a strong 2063 cm^{-1} band. The latter comprises the quickly decaying 2066 cm^{-1} band and the slower decaying 2058 cm^{-1} band.

Pulsed and cw excitations liberate CO during photolysis and consume it during the thermal back reactions. Experiments were performed under CO pressures

ranging from 0.04 to 400 torr to further probe the transients observed in vacuo. Spectra recorded during 0.4 second irradiations (350 nm, 500 mW) under different CO pressures show that the intial formation of the 2073 and 2050 cm^{-1} bands is followed by the rapid growth of the 2062 cm^{-1} band. Longer irradiation times and high CO pressures of 40 or 400 torr enhance the formation of the rapidly decaying 2062 cm^{-1} band. The order of product appearance, i.e., the 2073-2050 cm^{-1} bands appear first followed by the 2062 cm^{-1} band, and positions of the band maxima closely resemble that found in CO free experiments. In contrast to the CO free experiments, however, where photoproduct decay occurs over hundreds of seconds, Figures 50 and 51, the presence of CO accelerates the thermal dark reactions. The relative rate of photoproduct decay increases by approximately an order of magnitude when the CO pressure is increased from 4 to 400 torr. Figure 52 displays difference spectra at short times following 0.1 second excitation under 400 torr CO. The 2062 cm^{-1} band disappears first followed by decay of the 2073 and 2050 cm^{-1} bands. The rapid loss of the strong 2062 cm^{-1} absorption is not accompanied by an increase in the 2073 cm^{-1} absorption. These are single scan spectra and the enhanced noise in the 2030-1980 cm^{-1} region is characteristic of strong Kubelka-Munk absorptions due to unreacted $Fe(CO)_5$(ads). Figure 53 shows the decay of photoproducts at later times. This

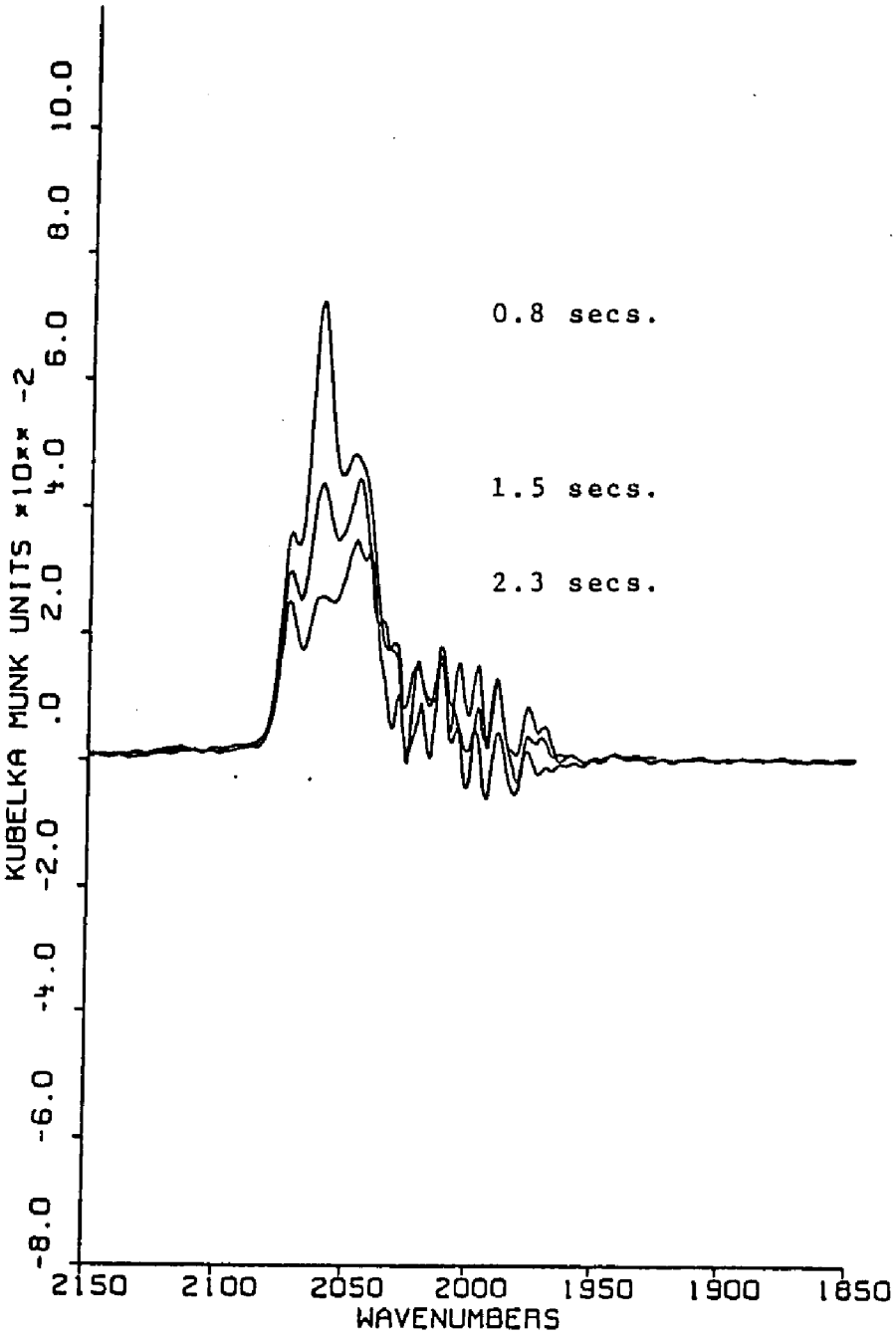

Figure 52. Difference spectra of $Fe(CO)_5$(ads) following 0.4 sec. irradiation (Kr ion) in 400 torr CO. (spectra at 0.8, 1.5, and 2.3 secs. following irradiation).

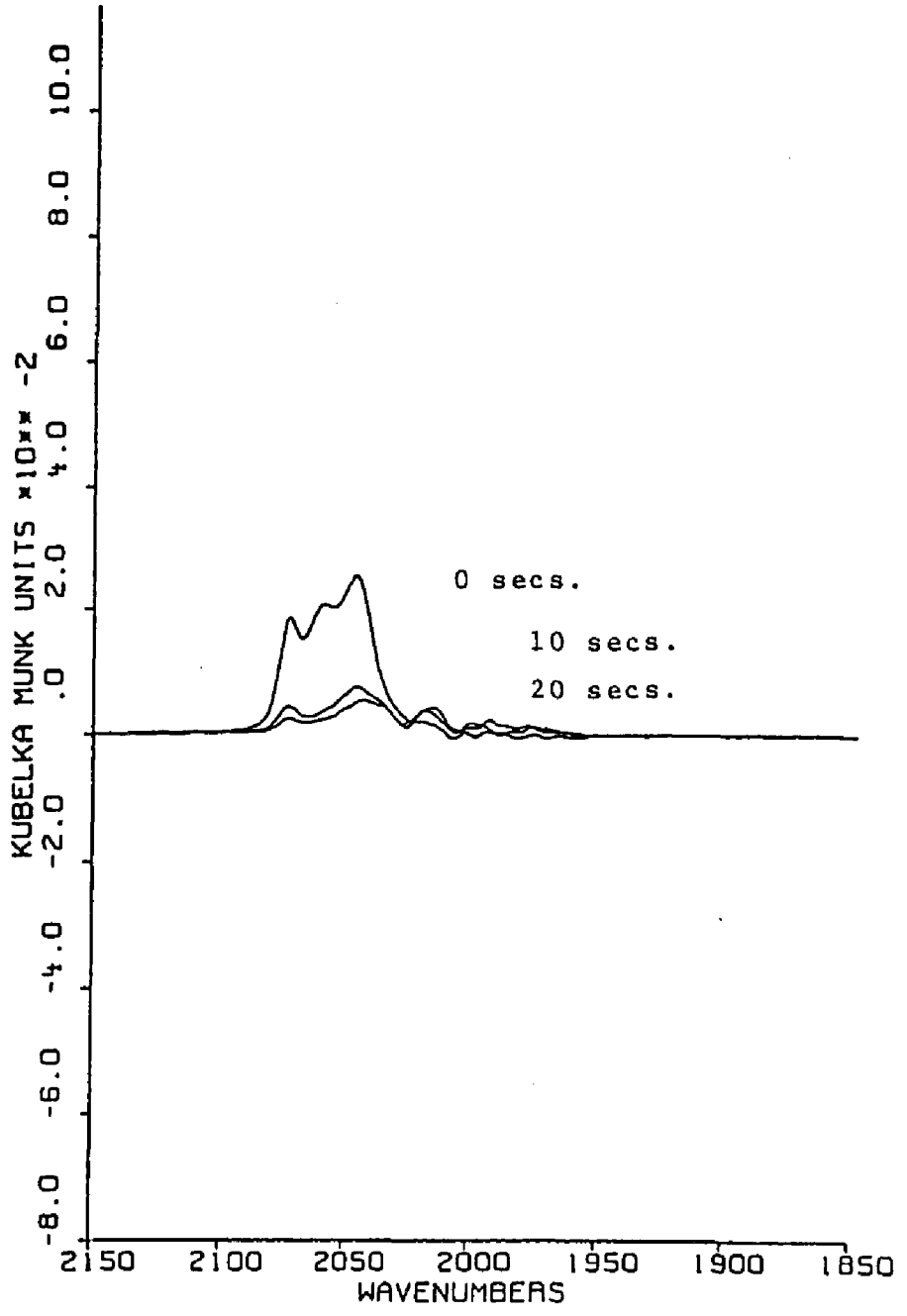

Figure 53. Difference spectra of $Fe(CO)_5$(ads.) following 0.4 sec. irradiation (Kr ion) in 400 torr CO. (spectra at 0, 10 and 20 seconds following irradiation).

decay is nearly complete only 20 seconds following excitation, whereas the decay in vacuo occurs over hundreds of seconds.

Figure 54, displays the short term decay of photoproducts following 0.1 second excitation under only 4 torr of CO. The peak positions are similar to those observed under high CO pressures, but a comparison of Figure 52 and Figure 54 shows that the band shapes differ. Besides the intial decay of the 2062 cm^{-1} band and the later decay of the 2073 cm^{-1} band, Figure 55 shows a broad, slowly decaying band at 2053 cm^{-1} at longer decay times. Although occuring at slightly lower frequency, the 2053 cm^{-1} band resembles the 2058 cm^{-1} band observed in CO free experiments. In addition, at low CO pressures and longer irradiation time, bridging ν_{CO} absorptions at 1820 and 1790 cm^{-1} become detectable. Photolysis of $Fe(CO)_5$(ads) under 40 torr of CO yields results intermediate between those at 4 and 400 torr of CO, whereas results under 0.4 or 0.04 torr of CO resemble CO free experiments.

Experiments in vacuo or under CO reveal the order of photoproduct growth and decay, but in many cases do not reveal the nature of the intermediate. To gain further information regarding the nature of the transients, photolyses under trimethylphosphine, TMP, were examined.

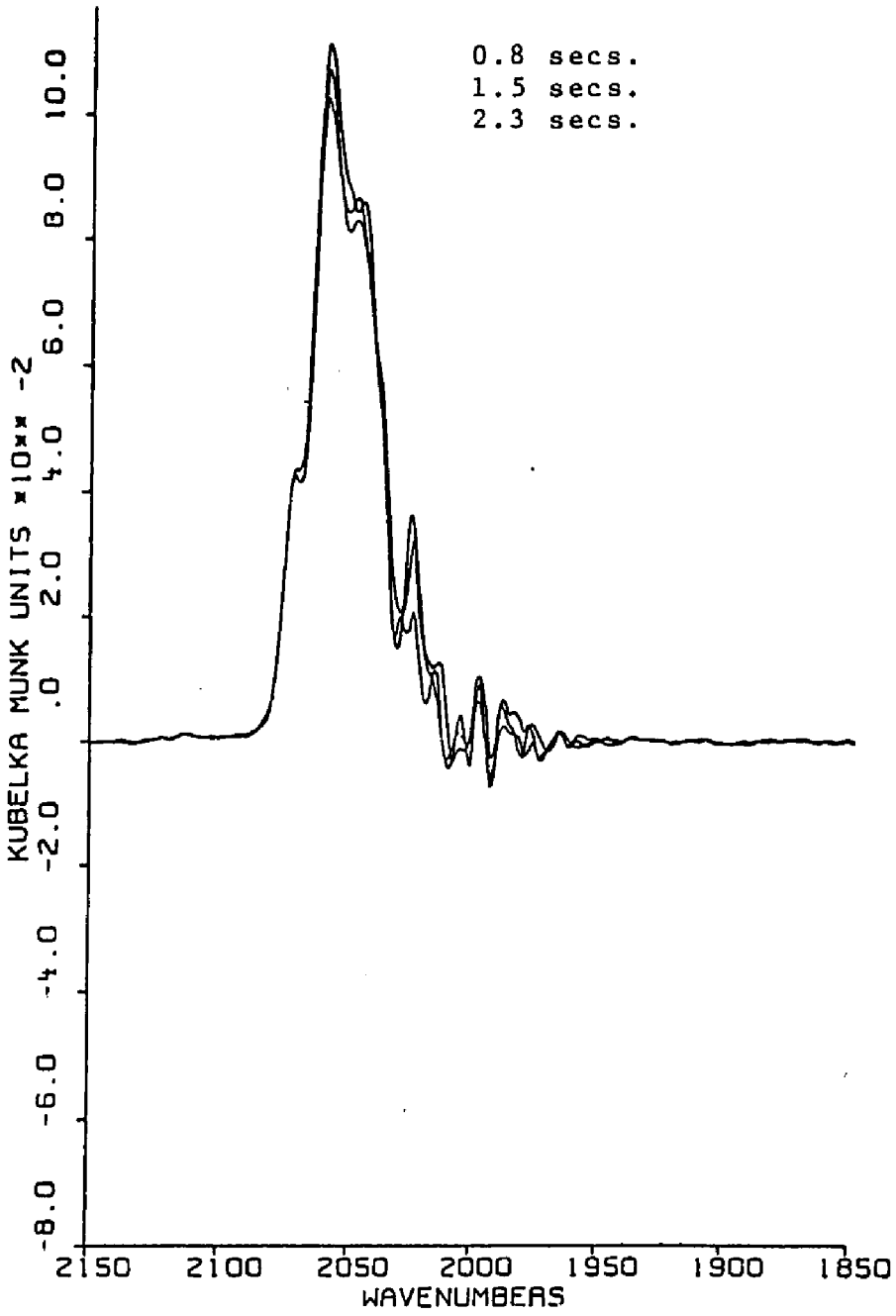

Figure 54. Difference spectra of $Fe(CO)_5$(ads.) following 0.4 sec. irradiation (Kr ion) in 4 torr CO. (spectra taken at 0.8, 1.5 and 2.3 secs. following irradiation).

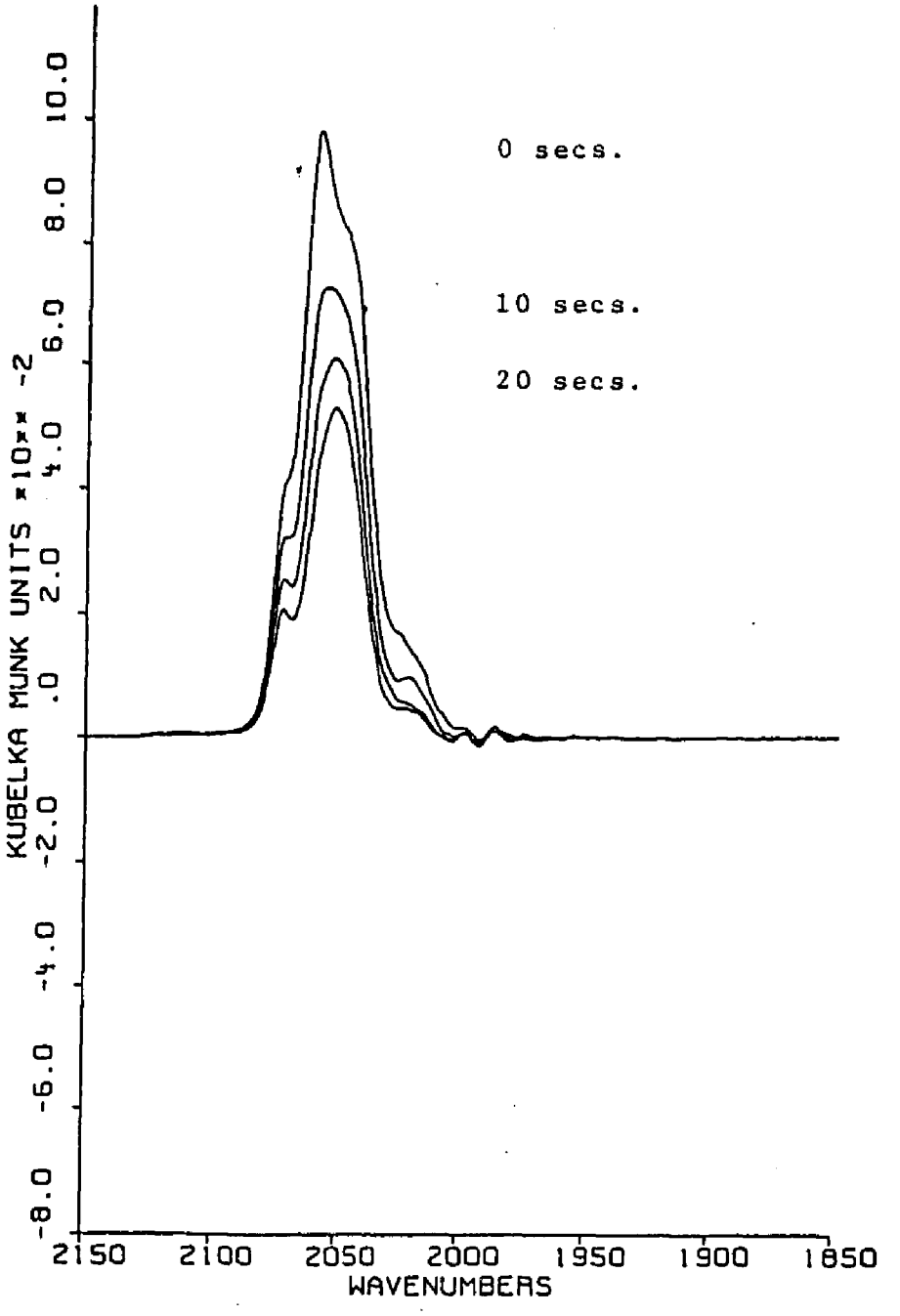

Figure 55. Difference spectra of $Fe(CO)_5$(ads.) following 0.4 sec. irradiation (Kr ion) in 4 torr CO (spectra at 0, 10 and 20 secs following irradiation).

Figure 56 illustrates the spectral changes following successive 350-nm irradiations of $Fe(CO)_5$(ads) under 100 torr of TMP. As photolysis proceeds, lower frequency bands at 1969, 1940, 1885 and 1846 cm^{-1} show a continuous increase in intensity whereas bands at higher frequency exhibit a more complex dependence. During the first 0.4 seconds of irradiation, the bands at 2047, 2020, and 2004 cm^{-1} increase in intensity, but then decline at longer irradiation times. The bands at 1814 and 1790 cm^{-1} are not present in the intial spectra. These bands appear as photolysis proceeds, and the rate of increase in their intensity correlates with the decline in intensity of the higher frequency bands, i.e. those at 2047, 2020 and 2004 cm^{-1}. Continued photolysis also causes changes in peak position and shapes of several major bands. The difference between spectra recorded at later photolysis times show that the change in band shape is due to the growth of absorptions at 1950, 1920 and 1855 cm^{-1} which develop during longer irradiation times.

As found in the other experiments, the spectral changes continue in the dark. Figure 57 shows difference spectra recorded 45 seconds apart following 6.4 second irradiation under 100 torr TMP. These spectra indicate a photoproduct decay sequence where several changes occur at once. For example, difference spectra recorded 45 seconds apart following 6.4 second excitation reveal a

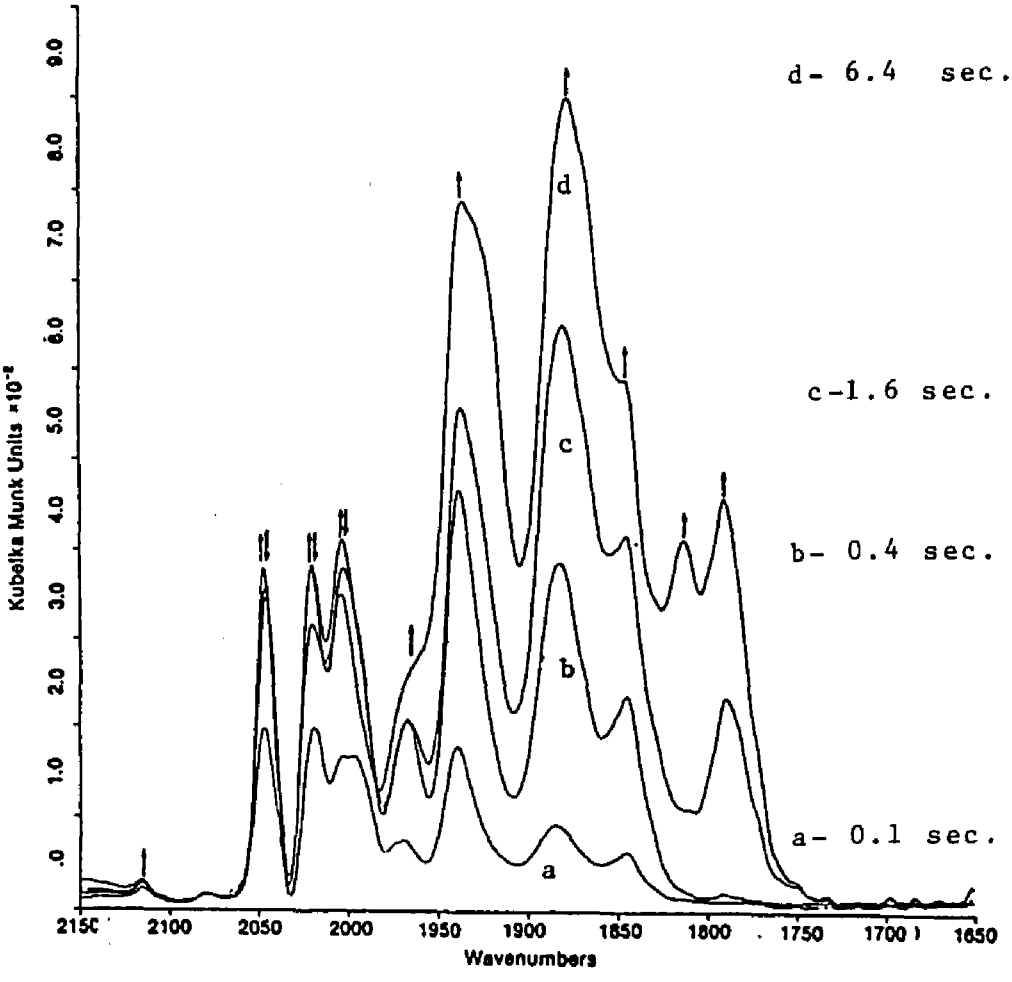

Figure 56. Difference spectra of $Fe(CO)_5$(ads.) following a) 0.1 sec. b) 0.4 sec. c) 1.6 sec. d) 6.4 sec. irradiation (Kr ion) in 100 torr $P(CH_3)_3$ Arrows indicate change with increasing photolysis time.

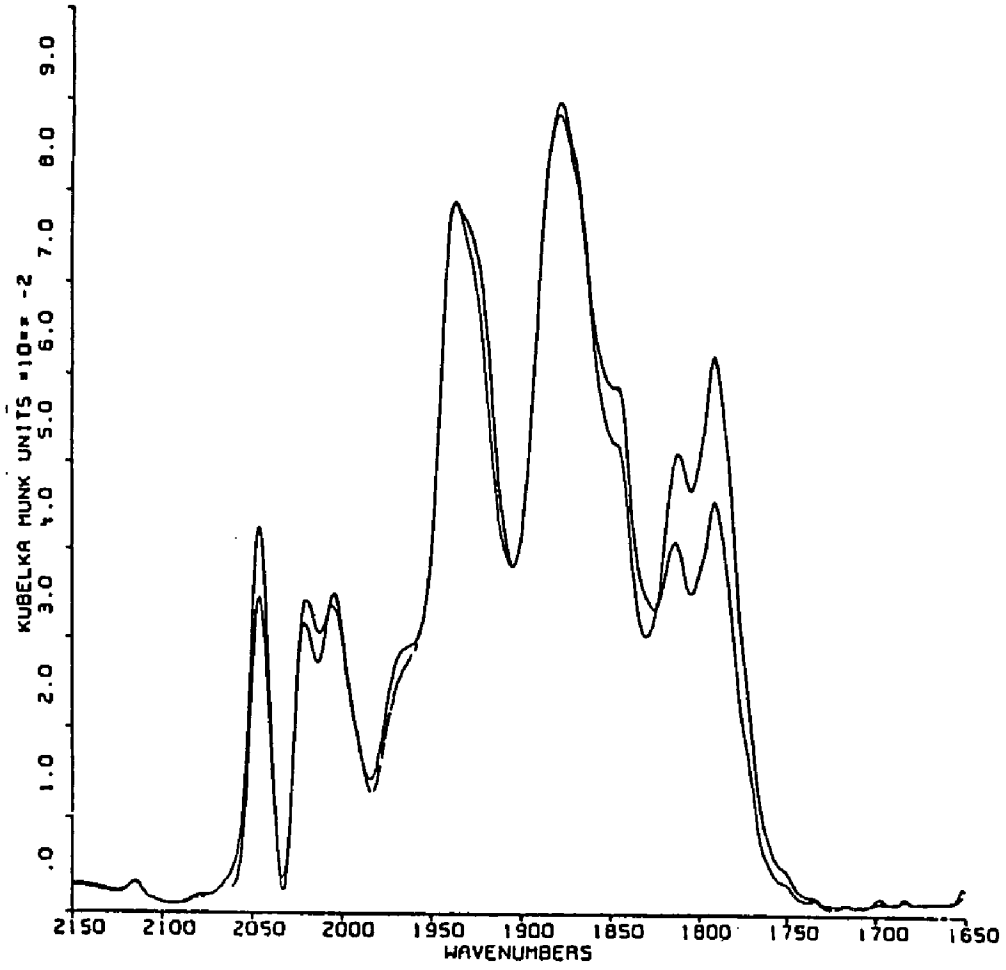

Figure 5 7. Difference spectra 45 secs. apart following 6.4 sec. irradiation (Kr ion) of $Fe(CO)_5$(ads.) under 100 torr $P(CH_3)_3$.

decrease in the intensity of all photoproduct bands with the decay of the 1814 and 1790 cm^{-1} being more pronounced. After these minor perturbations, however, the spectra change no further. The $Fe(CO)_5$(ads) bands do not return to their original intensity and, consistent with the formation of thermally stable phosphine substituted iron carbonyls, prolonged photolysis in the presence of TMP causes significant loss of the starting material.

C. Photochemistry of $Fe_3(CO)_{12}$(ads).

With excitation wavelengths $\leq$ 350 nm, the photochemistry of $Fe_3(CO)_{12}$(ads) is independent of surface coverage. UV-visible spectra recorded following 350-nm irradiation of PVG samples containing from $2.6\pm.2 \times 10^{-8}$ to $2.2\pm.2 \times 10^{-6}$ moles of $Fe_3(CO)_{12}$(ads)/gram in vacuo at $22\pm1\ ^{\circ}C$ show a steady decrease in the 605 and 440 nm bands of the physisorbed trimer with increasing photolysis time. Bands attributable to monomeric or dimeric adsorbates are not detected during photolysis. Rather, the spectral changes consist of a general decline in absorbance throughout the visible and UV regions. As shown in Figure 58, the quantum yield for $Fe_3(CO)_{12}$(ads) disappearance, determined by monitoring the decrease in absorbance of the 605-nm band of the trimer following 350-nm excitation, extrapolates to yield a value of

Figure 58. Quantum yield of $Fe_3(CO)_{12}$(ads.) disappearance.

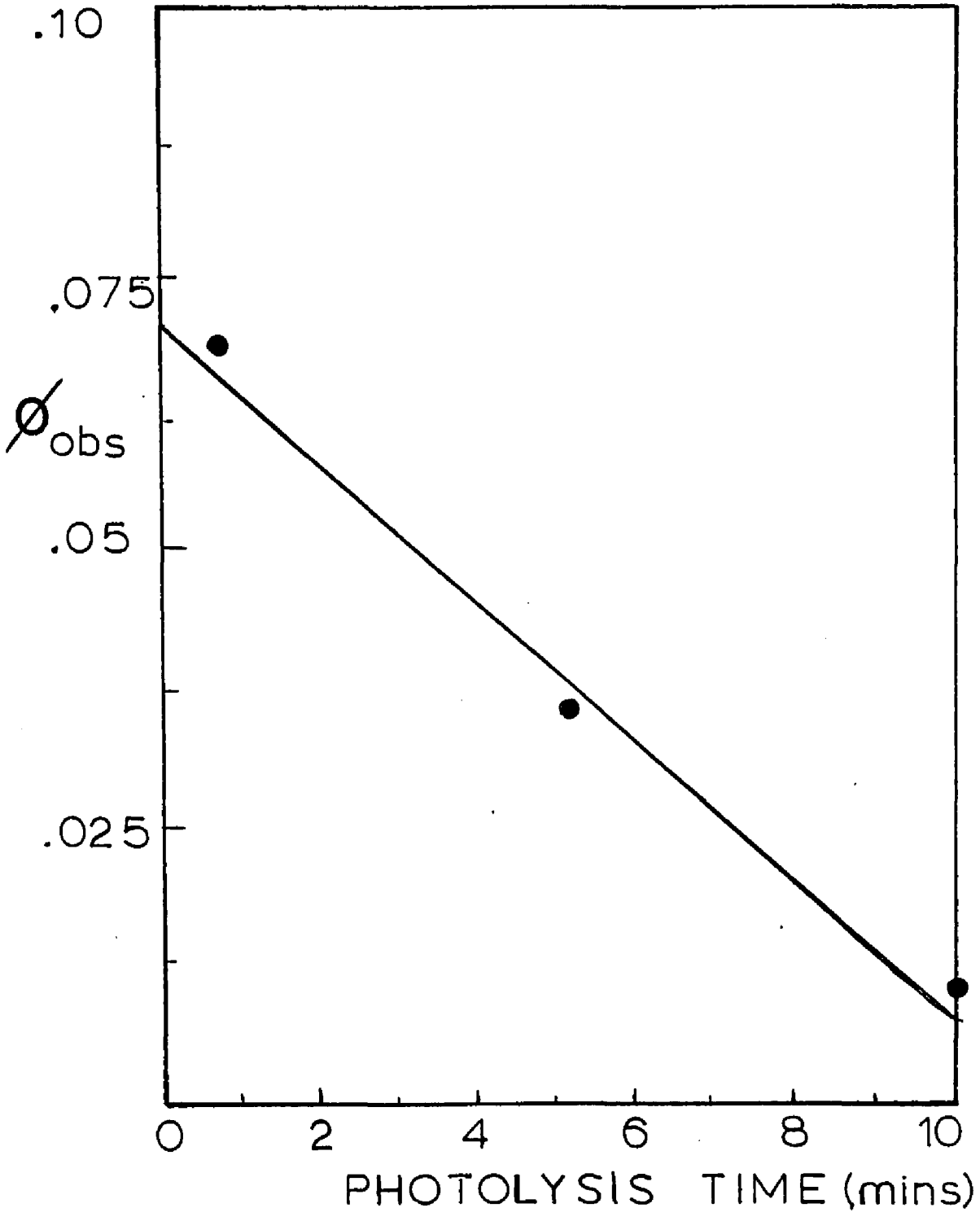

$7.4\pm0.2 \times 10^{-2}$ at $22\pm1\,^{\circ}C$, which is consistent with a value of ca. 0.02 for 550-nm excitation reported by Wrighton (75) for $Fe_3(CO)_{12}$ disappearance in hydrocarbon solution. Since the primary photoprocess for $Fe_3(CO)_{12}$ is thought to be metal-metal bond cleavage (75-77), efficient reformation of the fragmented metal-metal bond could account for the modest quantum yields observed.

Photolysis of a sample with 312 or 254-nm light results in spectral changes identical to those observed following 350-nm irradiation, i.e., the characteristic 605 and 440-nm bands, as well as the UV absorbance, of a sample containing $2.9\pm.3 \times 10^{-7}$ moles of $Fe_3(CO)_{12}$(ads)/gram, decrease with increasing irradiation time. After 1 hour of photolysis, the UV-vis spectrum exhibits a featureless UV absorbance with no lower energy visible absorption bands establishing that cluster decomposition is complete. Gas phase analysis during decomposition indicates CO evolution, but the total amount of CO evolved, ca. 8 CO/mole of cluster decomposed, is well below the expected value of 12 CO/mole of cluster decomposed. Similiar stoichiometries have been reported by Basset and coworkers (36) during the thermal decomposition of unsupported $Fe_3(CO)_{12}$ and $Fe_3(CO)_{12}$ supported on dehydroxylated MgO and Al_2O_3. Following 1 hour of irradiation, 360 torr of CO was added to the sample to examine the ability of the photoproducts

to thermally backreact with CO. A slight increase in the near-UV absorbance, $\leq$ 0.05 absorbance units is immediately observed, however, no further spectral changes are observed after sitting over CO in the dark for 12 hours. The spectral changes observed during the photochemical decomposition of $Fe_3(CO)_{12}$(ads), particularly the absence of new photoproduct bands, and the inability of the photoproducts to react thermally with added CO indicates the presence of irreversibly oxidized Fe species.

Photolysis of a sample containing $2.2\pm.2 \times 10^{-8}$ moles of $Fe_3(CO)_{12}$(ads)/gram with 254-nm excitation for 1 minute results in an immediate decrease in absorbance throughout the UV-vis regions. Analysis of the gas phase reveals simultaneous CO and H_2 evolution. The evolution of H_2 implies oxidation of zerovalent iron by either the surface silanol groups and/or chemisorbed H_2O on the PVG surface; a phenomenon well known following thermal decomposition of $Fe_3(CO)_{12}$ on hydroxylated inorganic oxide supports (17,20,36). UV-vis spectra recorded periodically during a one hour irradiation of the sample show a continuous decline in absorbance throughout the UV and visible regions. Periodic monitoring of the gas phase during this time interval reveals CO evolution along with increasing H_2 evolution. After 1 hour of photolysis the UV-vis spectrum exhibits a featureless UV

absorbance with no lower energy absorption bands. However, analysis of the gas phase reveals in addition to H_2 and CO, significant amounts of CH_4. As shown in Figure 59, increasing amounts of both CH_4 and H_2 are evolved following 1200 minutes of photolysis, however, only a small amount of H_2 is evolved during the next 1800 minute time interval. The sharp decline in H_2 evolution is not accompanied by a similar decline in the amount of CH_4, although a slight decrease in CH_4 evolution is observed. Gas phase analysis of the sample after sitting in the dark at $22\pm1\ ^{\circ}C$ for 72 hours reveals 2.9×10^{-8} moles of H_2 and 7.8×10^{-7} moles of CH_4 are evolved. No other hydrocarbons besides CH_4 are detected.

FMR spectra following 12 hour 254-nm photolysis of $Fe_3(CO)_{12}$ physisorbed on coarsely ground PVG show no resonances due to zerovalent iron particles. This result is consistent with periodic analyses of the gas phase during photochemical decomposition, which reveal that the time dependence of gas evolution is identical to that observed for photolysis of $Fe_3(CO)_{12}$ adsorbed on plate PVG. At photolysis times < 1 hour, H_2 and CO gas are evolved, while more prolonged photolysis results in the evolution of CH_4 in addition to H_2. The absence of a FMR signal due to zerovalent iron and the evolution of H_2 confirms oxidation of the iron atoms.

Figure 59. Gases evolved following UV photolysis of $Fe_3(CO)_{12}$(ads.).

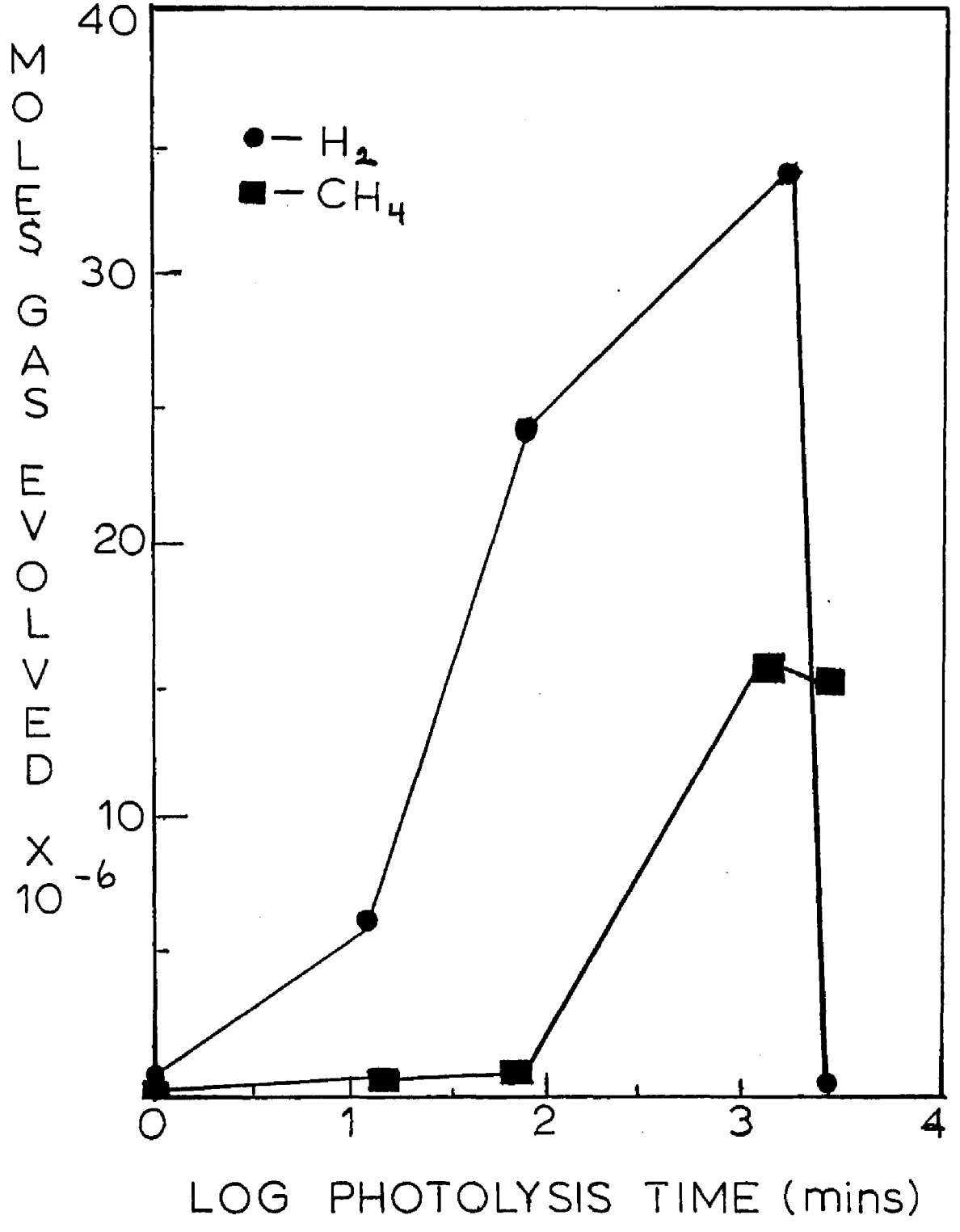

D. Phototoreactions of $Fe(CO)_5$(ads) with Olefin Complexes.

1. Diffuse Reflectance Experiments.

The DRIFT spectrum of PVG under 160 torr of 1-pentene, shown in Figure 60, exhibits strong absorptions in the C-H and C=C stretching regions which are identical to those found in fluid solution. Of particular importance is the decline in intensity of the 3744 cm^{-1} band of the free silanol groups of PVG which indicates adsorption of the olefin onto these sites. The adsorption of olefins onto PVG is reversible since evacuation of the DRIFT microreactor for several minutes results in the subsequent disappearance of the bands due to the physisorbed olefin and reappearance of the 3744 cm^{-1} band. The DRIFT spectrum of $Fe(CO)_5$(ads) exhibits little change following addition of olefins. This confirms that the olefins are not physisorbed onto $Fe(CO)_5$(ads). Rather, they appear to physisorb onto vacant PVG sites and do not affect $Fe(CO)_5$(ads).

When a 350-nm irradiation of $Fe(CO)_5$(ads) is carried out under 100 torr of ethylene, dramatic differences in the spectral features relative to the previous experiment occur. Figure 61 shows the Kubelka Munk spectrum recorded prior to 0.4 second excitation and postpulse spectra recorded at 0, 20, 60 and 100 seconds following excitation. At least three absorption maxima on the high

Figure 60. DRIFT spectrum of 1-pentene on PVG.

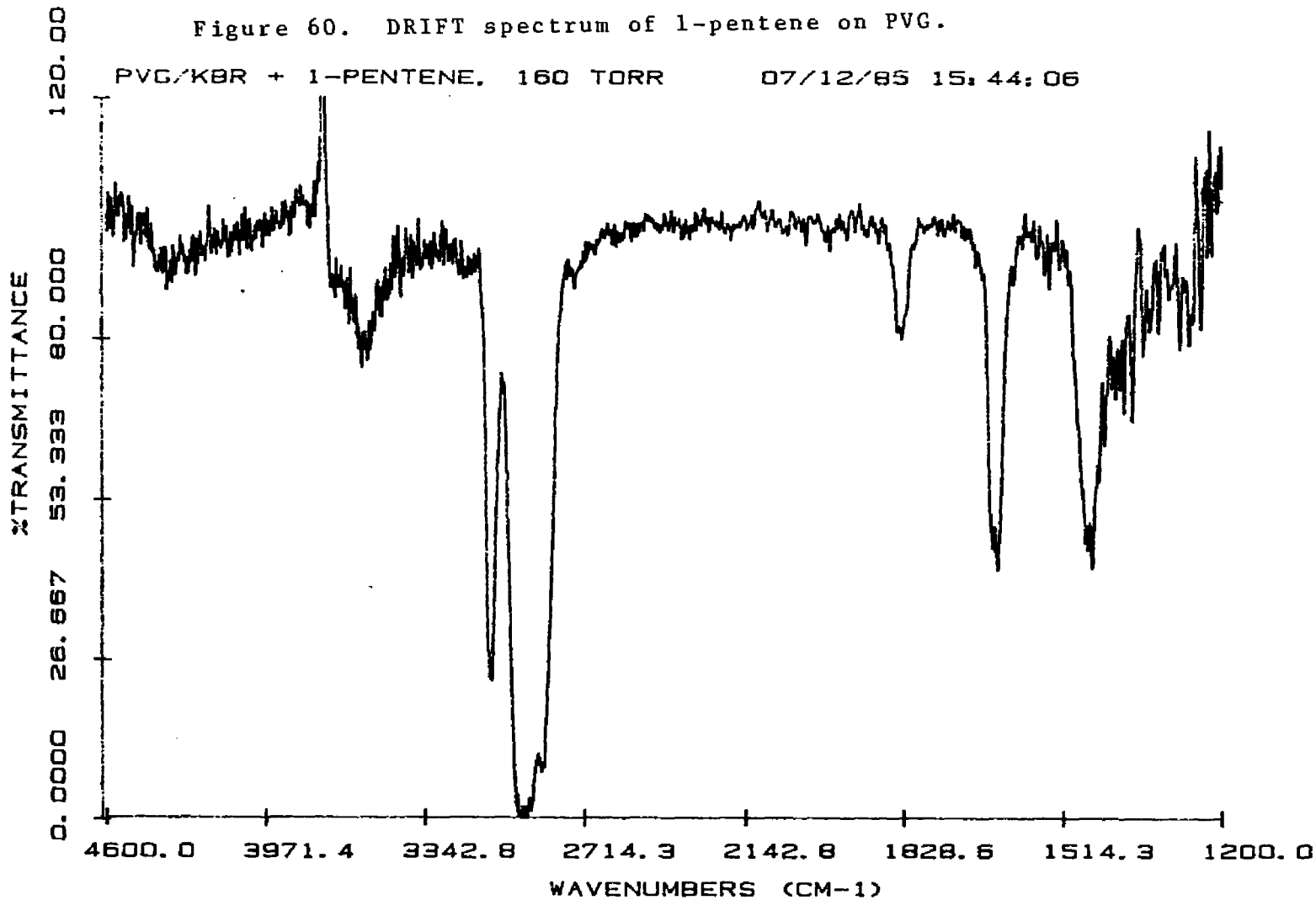

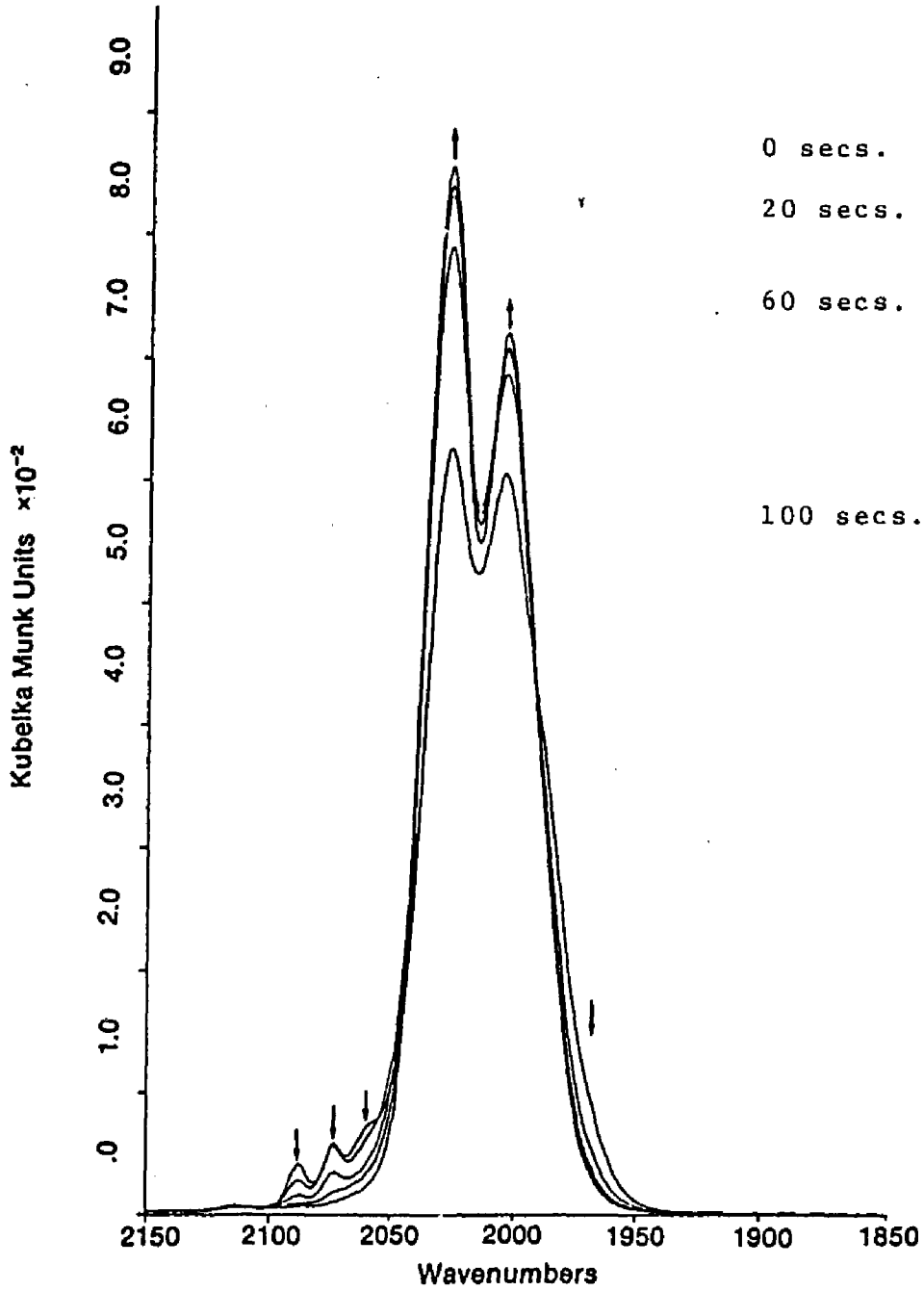

Figure 61. Kubelka Munk spectra of $Fe(CO)_5$(ads.) under 100 torr C_2H_4 before and after 0.4 sec. irradiation (Kr ion). (postpulse spectra recorded at 0, 20, 60 and 100 secs. following irradiation).

frequency side of the major $Fe(CO)_5$(ads) bands are observed, in addition to absorption on the low frequency side. These latter features are consistent with the formulation of the photoproducts as olefin complexes which typically exhibit strong absorptions below 2000 cm^{-1}. For example, Wrighton (96) reports that $Fe(CO)_4$(ethylene) in 3-methylpentane exhibits bands at 2087, 2022, 2007 and 1984 cm^{-1} and trans-$Fe(CO)_3(ethylene)_2$ in a low temperature matrix (77 K) exhibits a single adsorption at 1929 cm^{-1}. The arrows, which illustrate the temporal development of the spectral changes following excitation, indicate a decay of the photoproduct spectrum and an increase in the intensity of the absorption under the $Fe(CO)_5$ bands. Difference spectra, shown in Figure 62, exhibit four peaks to the high frequency side of the major $Fe(CO)_5$(ads) at 2087, 2074, 2059, and 2048 cm^{-1}, and two additional features to the low frequency side at 2015 and 1989 cm^{-1}. The photoproduct decay during the first 20 second interval after excitation is dominated by a very rapid loss of the 2059 cm^{-1} band. Concurrent with this decay is an increase in the 2048 cm^{-1} band intensity. During and after these intial rapid changes, all other photoproduct absorptions decay. The spectral changes during the next 40 second time interval following excitation indicates the 2087 cm^{-1} band is the next feature to disappear. The rate of decay of this band correlates well with the rate

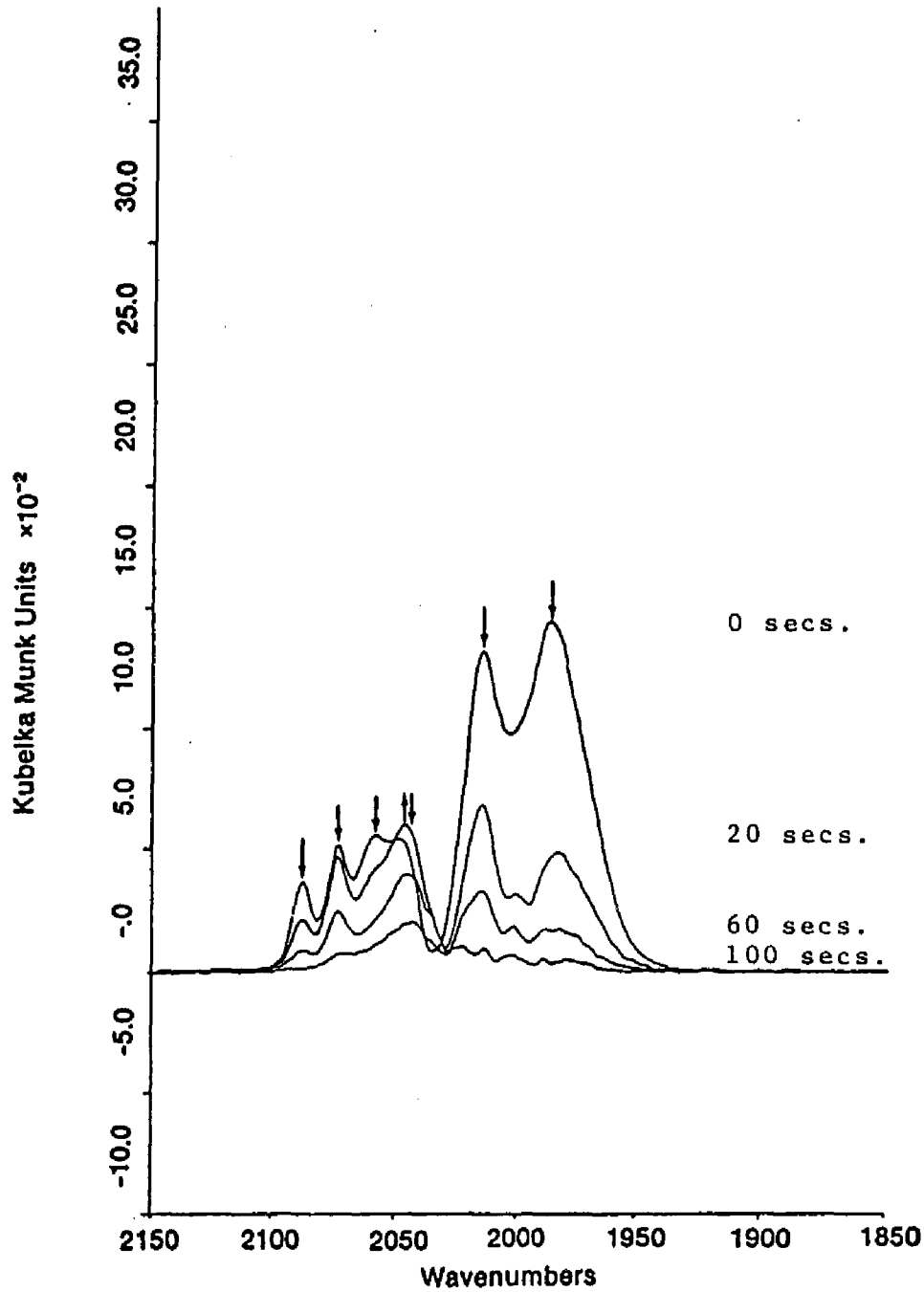

Figure 62. Difference spectra of $Fe(CO)_5$(ads.) following 0.4 sec. irradiation (Kr ion) in 100 torr C_2H_4. (spectra at 0, 20, 60 and 100 seconds following irradiation).

of decay of the bands at 2015 and 1984 cm^{-1}. The 2074 cm^{-1} band, reminiscent of the band observed in both the in vacuo and CO experiments, decays at slightly longer times and its rate of decay appears to correlate with a feature under the 2048 cm^{-1} band, much of which persists as it shifts to 2041 cm^{-1}. Following 1.6 second excitation, the rapidly decaying species which exhibits the 2059 cm^{-1} band is formed in higher proportions. As it decays, one now sees increases in the 2074 cm^{-1} and, to a lesser extent, the 2087 and 2048 cm^{-1} bands. After these longer photolyses, and after shorter (0.1 sec) ones as well, the photoproduct spectrum decays in a similar fashion to that described above. In all three experiments, i.e., after 0.1, 0.4 and 1.6 second irradiations, photoproduct decay was complete within 100 seconds following excitation.

Figure 63 shows Kubelka Munk spectra recorded prior to and following 0.4 second 350-nm irradiation of $Fe(CO)_5$(ads) under 100 torr of 1-pentene. Postpulse spectra, as in the previous experiment, were recorded 0, 20, 60, and 100 seconds following excitation. The spectra again exhibit absorptions at both higher and lower frequencies than the $Fe(CO)_5$(ads) bands. Difference spectra, shown in Figure 64, reveal intial peaks at 2081, 2068, 2051, 2012, and 1973 cm^{-1}. The bands at 2081, 2012, and 1973 cm^{-1} decay in moderate

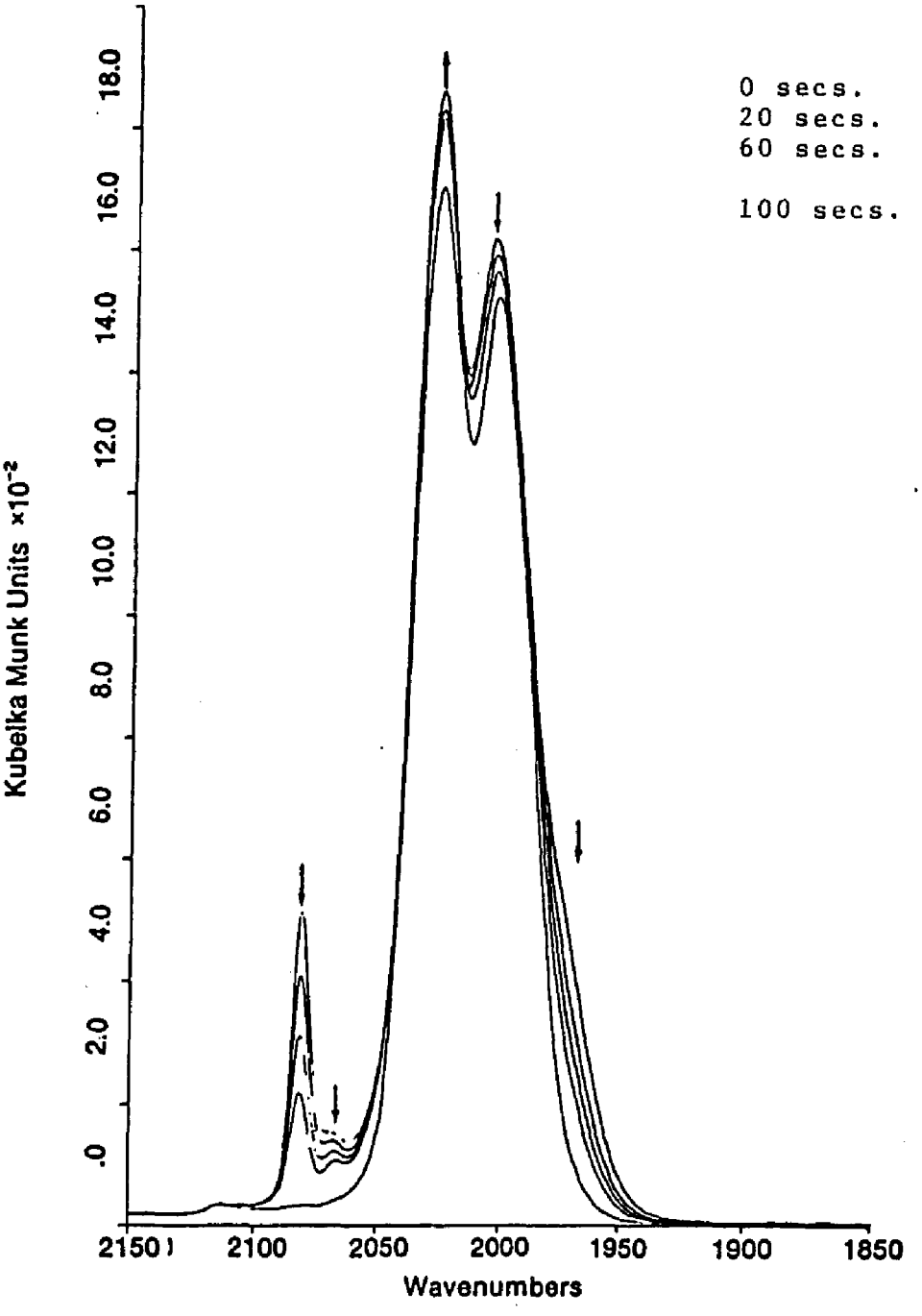

Figure 63. Kubelka Munk spectra of $Fe(CO)_5$(ads.) under 100 torr 1-pentene before and after 0.4 sec. irradiation (Kr ion).
(Postpulse spectra at 0, 20, 60 and 100 secs. following irradiation).

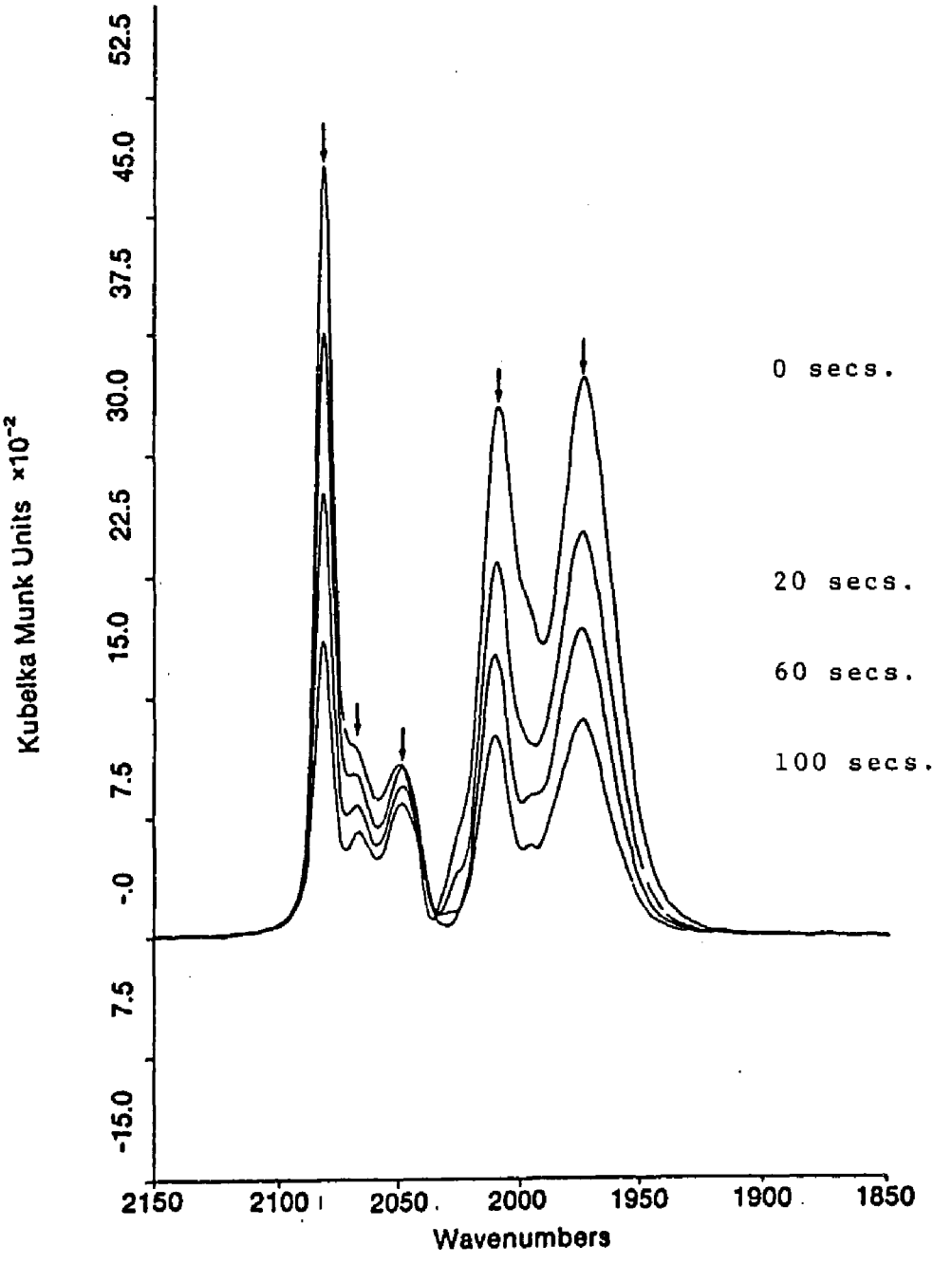

Figure 64. Difference spectra of $Fe(CO)_5$(ads.) following 0.4 sec. irradiation (Kr ion) in 100 torr 1-C_5H_{10}.
(spectra at 0, 20, 60 and 100 secs. following irradiation).

times while the bands at 2068 and 2051 cm^{-1} decay more slowly. The rates of decay of the 2081, 2012, and 1973 cm^{-1} bands correlate well with each other, indicating the presence of a single major component. This is not the case, however, for the 2068 and 2051 cm^{-1} bands, whose different rates of decay suggest the presence of two spectrally distinct species. Formation of the latter species is favored by longer irradiation times. The decays of the 2068 cm^{-1} and 2051 cm^{-1} bands, however, are incomplete after long irradiations, while at short irradiation times, the major component exhibiting bands at 2081, 2012 and 1973 cm^{-1} decays completely. Close examination of a series of difference spectra similar to Figures 50 and 51 for irradiation under 100 torr of 1-pentene, indicates additional components exhibiting absorptions at 2058, 2025, 2006, and 1973 cm^{-1}. These minor components decay rapidly and totally within the first 40 seconds following excitation. Overall, the temporal development of the photoproduct spectrum indicates that four different components are present in this system. While the assignments of chemical identities of the spectral components observed with ethylene and 1-pentene will be discussed later, their presence prompted investigation into the photocatalytic properties of the $Fe(CO)_5$-PVG hybrid system. The results obtained using the photocatalyzed 1-pentene isomerization as a probe reaction are discussed below.

2. Photocatalyzed 1-pentene isomerization reaction.

Gas phase analysis following addition of 100 torr of 1-pentene to a sample containing 1.8±0.2 moles of $Fe(CO)_5$(ads)/gram, indicated no significant isomerization occured after sitting in the dark at room temperature over a period of several hours. Steady state irradiation with 350-nm light resulted in appreciable isomerization of 1-pentene to cis and trans-2-pentenes. UV-visible spectra recorded during photolysis do not exhibit bands attributable to dimeric or trimeric species at irradiation times < 40 minutes, however, at photolysis times > 40 minutes, the sample appeared faint green, and UV-visible spectra exhibit a weak absorption at 605-nm characteristic of the trimer. Relative to samples containing known amounts of $Fe_3(CO)_{12}$, the absorbance at 605 nm indicates $3.5\pm0.2 \times 10^{-8}$ moles $Fe_3(CO)_{12}$(ads)/gm are formed following 60 minutes of irradiation. The time dependence of the photocatalytic isomerization reaction, shown in Figure 65, is qualitatively similiar to that reported by Wrighton (79) and Grant (92,93) in solution and in the gas phase. The reaction first exhibits an induction period during which the rate of the reaction linearly increases with time. This increase in rate of product formation is followed by a steady state period, during which the rate decreases. Examination of the ratio of trans to cis-2-pentenes formed during 60 minutes

Figure 65. Percent 1-pentene conversion vs. photolysis time.

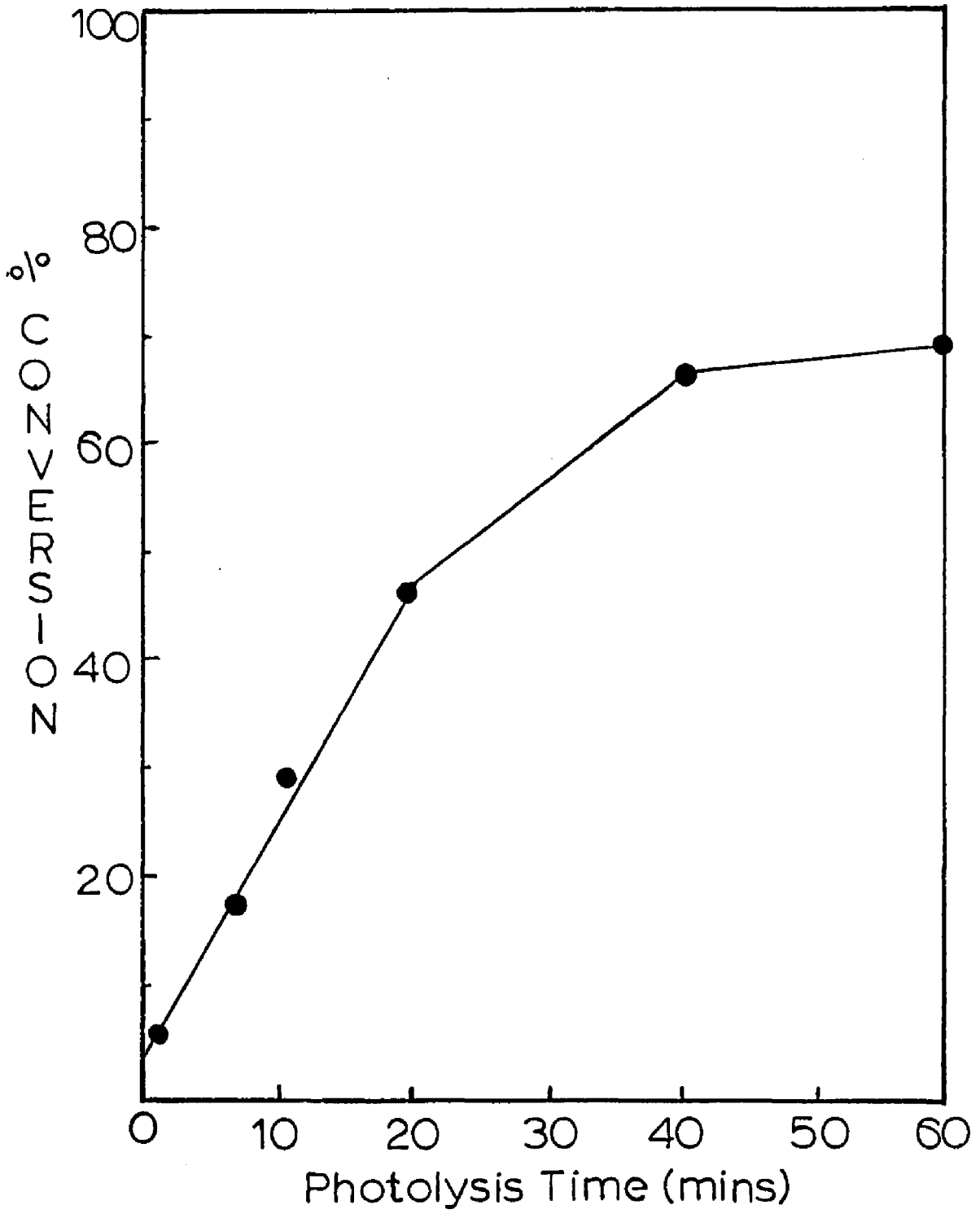

of photolysis time, Figure 66, indicates that the system never reaches the thermodynamic ratio of trans/cis-2-pentene (79% trans, 18.3% cis-2-pentene; trans/cis = 4.32) (84). The trans to cis ratio rapidly increases from 1.58 during the first 5 minutes to 2.67 following 10 minutes of irradiation. After this time period, the rate of the reaction decreases, and a slow increase in the trans/cis ratio is observed until, after 60 minutes, a limiting value of 3.40 is attained. As shown in Figure 67, a plot of log ϕ_{obs} versus log irradiation time over the portion of reaction where the extent of conversion is approximately linear with irradiation time, extrapolates to a quantum yield value of 155$\pm$2.0. The high value of the quantum yield indicates photogeneration of a surface species which is catalytic with respect to the number of photons adsorbed.

E. Photochemically Induced High Optical Density Changes Using $Fe(CO)_5$-PVG.

Exposure of calcined polished 1 mm thick plates of PVG to $Fe(CO)_5$ vapor for 2 to 3 minutes results in the samples turning a pale yellow color. No color change is detected upon exposure of the sample to air in the time required to mount the sample on the slide holder and begin photolysis. Irradiation of the sample with the image produced by focusing a collimated light beam from a

Figure 66. Trans/cis ratio of 2-pentenes vs. photolysis time.

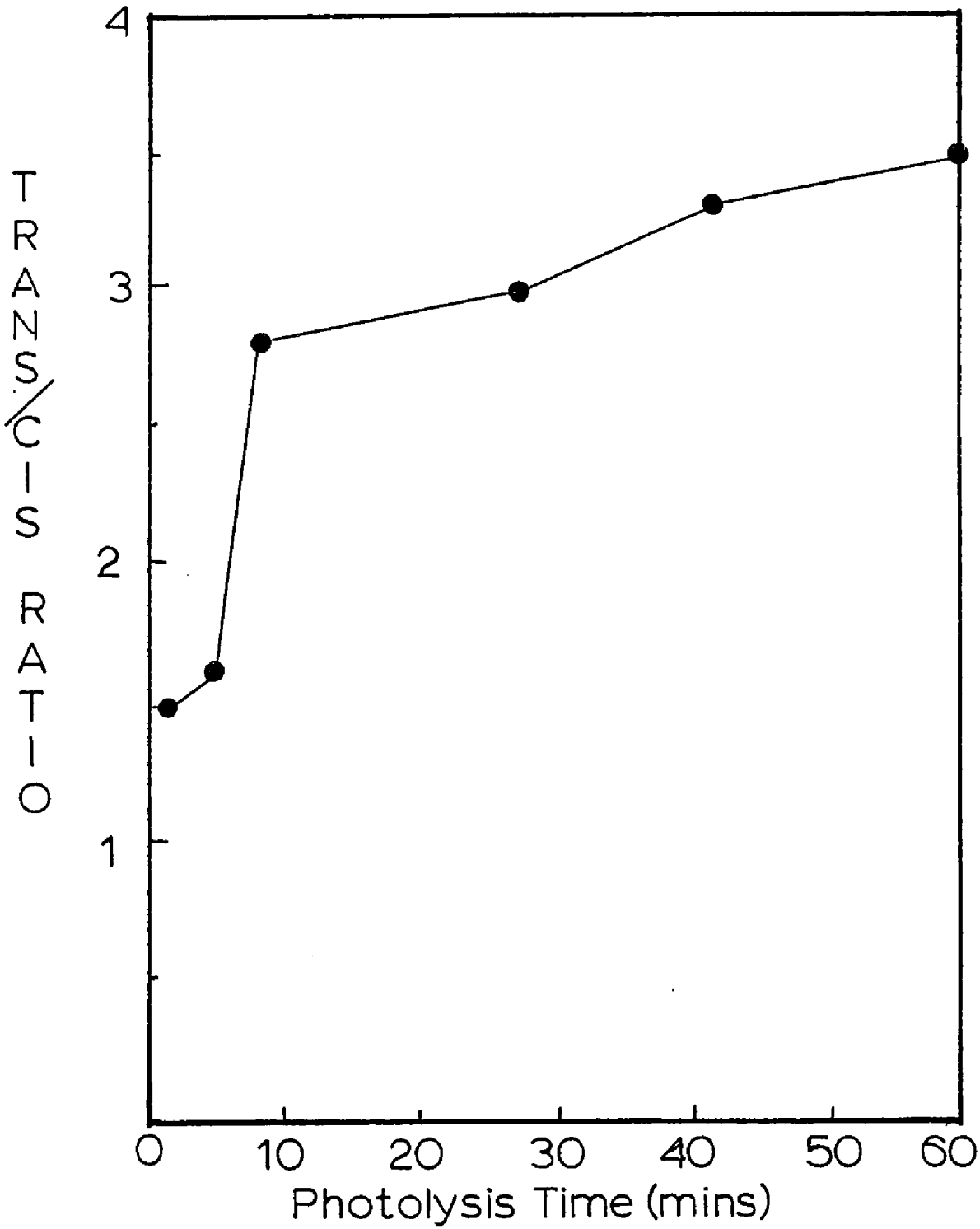

Figure 67. Quantum yield of 1-pentene isomerization.

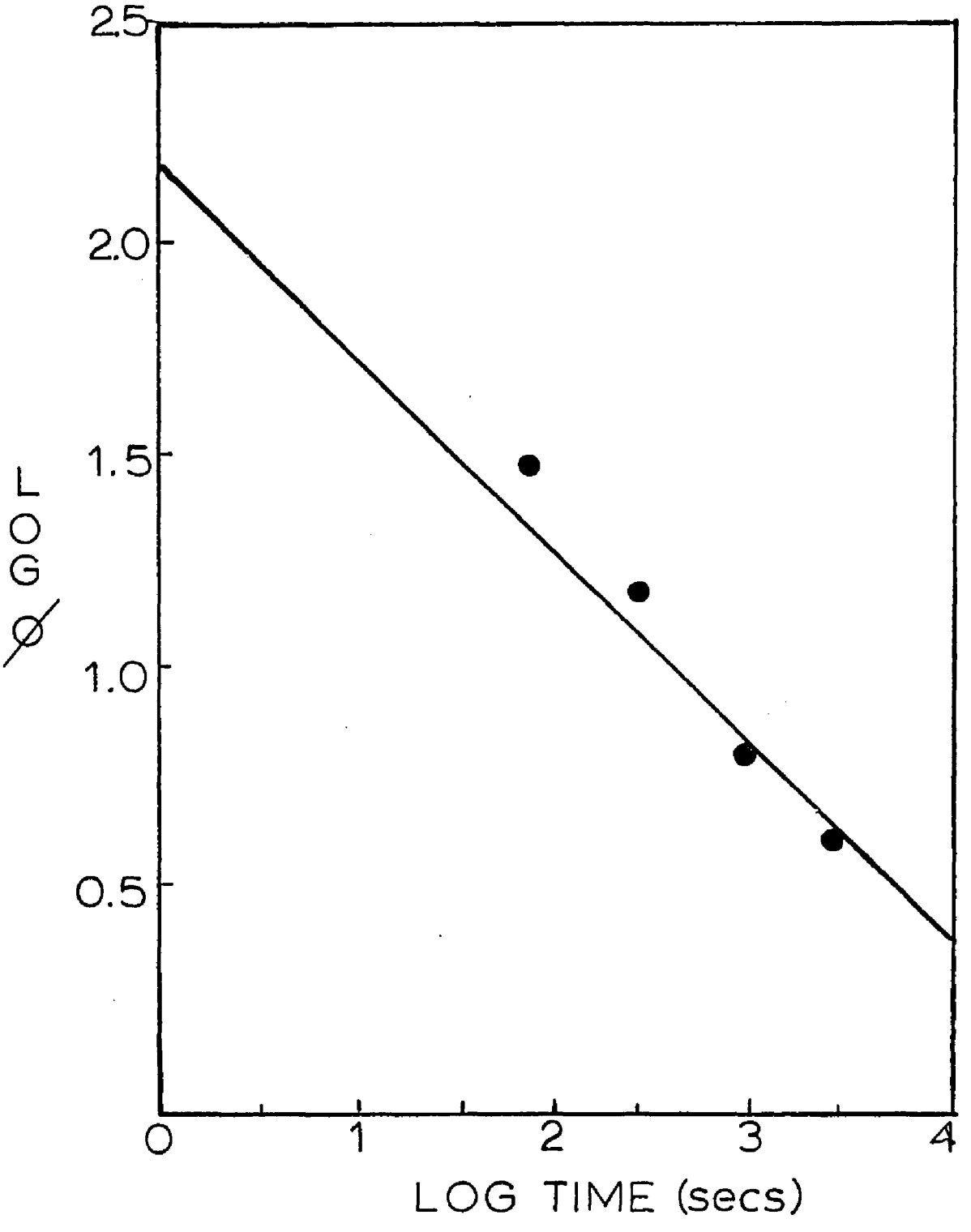

100 W Xenon lamp through a 35 mm plastic slide, however, causes an immediate color change. In the exposed areas, the light causes the sample to become noticeably darker relative to the unexposed pale yellow regions. Gentle heating of the sample in air (ca. 200 °C) results in "fixing" the optical changes, i.e., the optical change becomes permanent and insensitive to futher light exposure. Heating volatilizes the unreacted $Fe(CO)_5$ from the surface and converts the photoproduct to an iron oxide. Heating the PVG sample to 1200 °C consolidates the glass (collapse of its porous structure) producing a 25-30% decrease in sample volume. However, consolidation does not reduce the resolution of the light induced optical pattern. A 30X magnification of an image prepared by these techniques is shown in Figure 68.

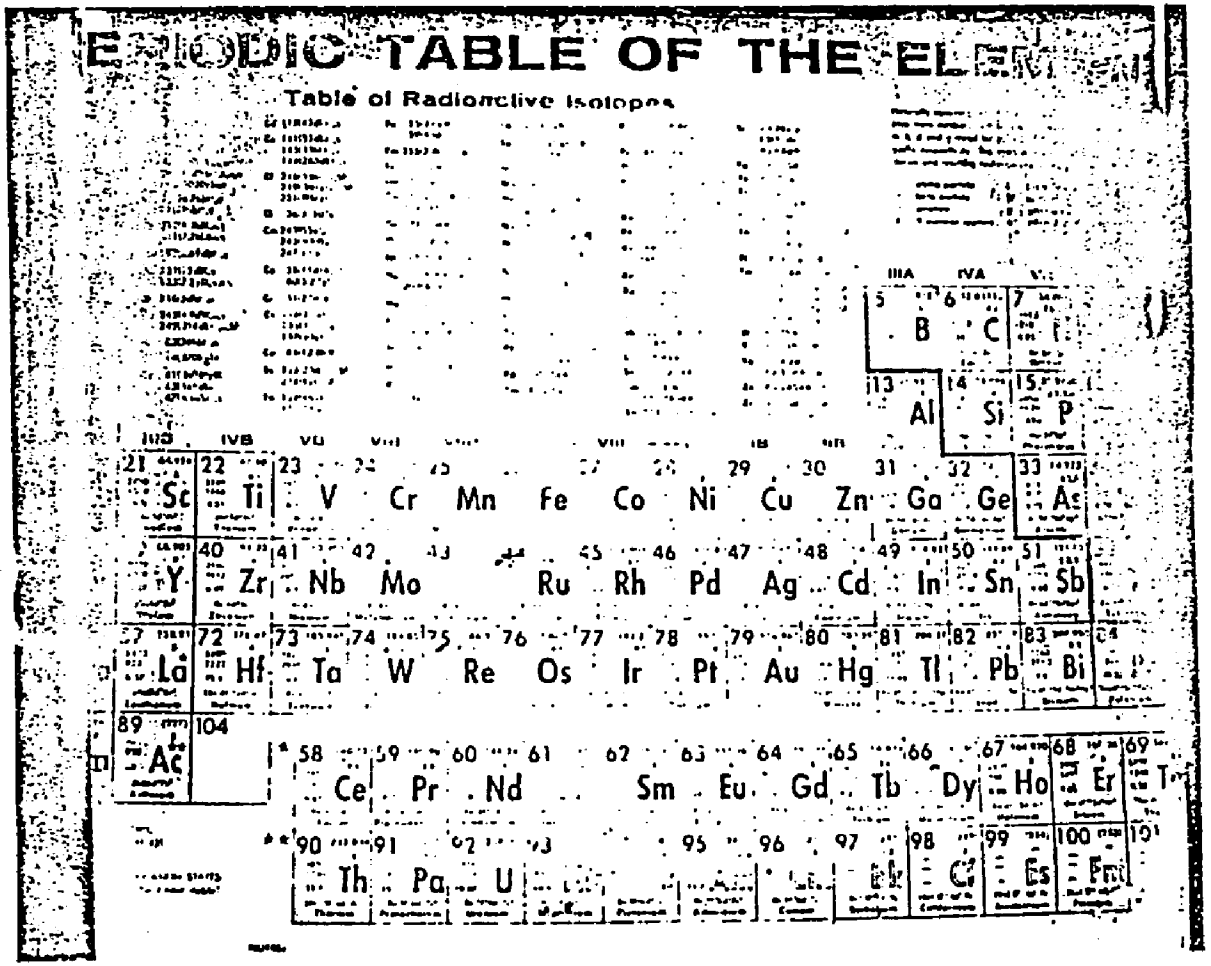

Figure 68. Slide of photoinduced optical pattern.

DISCUSSION

A. Adsorption of Iron Carbonyls.

Vapor deposition of $Fe(CO)_5$ leads to a uniform distribution of $Fe(CO)_5$ on the surface, but not through the cross section of PVG. Regardless of the number of moles adsorbed, which in these experiments ranged from 2×10^{-8} to 2×10^{-5} moles/gram, the complex penetrates 0.5 ± 0.1 mm into the sample and impregnates volumes adjacent to the outer surfaces. Since identical depths occur with different complexes which differ from $Fe(CO)_5$ in both size and mechanism of adsorption, the apparent penetration is taken as a measure of the deviations from surface planarity. The rapid rate of desorption from from the powdered samples suggests that adsorption is also limited to the outer surfaces. In spite of the labyrinthine microporosity of PVG, the distribution of $Fe(CO)_5$(ads) as well as the sampling depth of the DRIFT technique, ca. 20-40 microns, limits the reactions examined in these experiments to $Fe(CO)_5$(ads) onto the outermost surfaces of the support. The PVG surface consists of free and hydrogen bonded silanol groups (128), and small, but variable amounts of hydrogen bonded water. Lewis acid sites, principally B_2O_3, are also present on the surface (118), but no spectroscopic evidence was obtained in these experiments that suggests

preferential adsorption onto these sites. Rather, the adsorption of $Fe(CO)_5$ is a random process that leads to uniform impregnation of the outer surfaces of the PVG sample without disruption of the molecular integrity of the adsorbate.

The electronic spectrum of $Fe(CO)_5$ in n-hexane consists of overlapping, intense MLCT and intraligand transitions with a maximum at 210 nm, and ligand field transitions which appear as shoulders at 285 and 245 nm (50). The spectrum of $Fe(CO)_5$(ads) exhibits a progressive increase in the UV. The band maxima, > 230 nm, and the ligand field transitions which appear as shoulders in the solution spectrum, are masked by intense absorptions due to PVG that occur at $\leq$ 290 nm. However, lower energy ligand field transitions indicative of ligand substitution, or visible absorptions indicative of dimeric or trimeric clusters are not detected. Diffuse Reflectance FTIR spectra of $Fe(CO)_5$(ads) exhibit intense ν_{CO} bands at 2026 and 2004 cm^{-1} and a weak band at 2114 cm^{-1}. Relative to the gas phase spectrum, where the bands appear at 2033 and 2012 cm^{-1}, adsorption shifts the bands to lower frequency and inverts their relative intensities. Jackson and Trusheim (99,100) report similar shifts when the complex is adsorbed onto silica gel. While the reasons for the shift of the adsorbed complex to lower frequency are unclear, the similarity of

the $Fe(CO)_5$(ads) spectrum with the spectrum of the complex in n-hexane, which exhibits bands at 2023 and 2000 cm^{-1}, suggests that the interaction of $Fe(CO)_5$ with the PVG surface is small and comparable to weak solvent effects. The weak band at 2114 cm^{-1} is assigned to the totally symmetric v_1 mode. Although forbidden under D_{3h} symmetry, a weak band at 2115 cm^{-1} does appear in the infrared spectrum of crystalline $Fe(CO)_5$ due to a decrease in the site symmetry of $Fe(CO)_5$ to C_2 (19b). A reduction in the local symmetry from D_{3h} to C_{2v} is also expected to activate the v_1 mode. Bein and Jacobs (129) report the occurance of a weak v_1 band at 2115 cm^{-1} when the complex is adsorbed onto NaY, HY, and Linde L zeolites, and suggest that its occurrence is due to molecular distortions imposed by the support. Consequently, the appearance of a weak band at 2114 cm^{-1} in the $Fe(CO)_5$(ads) spectrum is attributed to a perturbation of molecular symmetry when the complex is adsorbed onto PVG. In spite of the apparent distortion, the similarity with solution spectra establish that $Fe(CO)_5$ physisorbs as a monomeric unit without disruption of its primary coordination sphere. Therefore, changes in photochemical reactivity are not a consequence of molecular changes, but rather a consequence of the chemical nature of the support and its dimensionality.

The electronic spectrum following sublimation of $Fe_2(CO)_9$ onto PVG exhibits visible absorption bands at 605 and 440 characteristic of $Fe_3(CO)_{12}$ and an intense UV absorbance. The spectrum, particularly the appearance of the 605-nm band, indicates a thermally activated disproportionation of the dimer. Reaction 5 was further confirmed by the DRIFT spectrum of PVG loaded with $Fe_2(CO)_9$ which exhibited absorptions attributable to $Fe_3(CO)_{12}$ and $Fe(CO)_5$ but not an 1820 cm^{-1} band that is characteristic of $Fe_2(CO)_9$.

$$(5).\ 2Fe_2(CO)_9 \longrightarrow Fe_3(CO)_{12} + Fe(CO)_5 + CO$$

Disproportionation of $Fe_2(CO)_9$ on PVG, which has also been observed on silica gel (99) and in solutions containing weak ligands at room temperature (59,60), indicates that PVG does not act as an inert support. Rather, the surface silanol groups and/or chemisorbed water are capable of acting as weak ligands thereby influencing the thermal reactions of adsorbates.

The UV-visible spectrum of $Fe_3(CO)_{12}$ adsorbed onto PVG via solution impregnation is identical to that observed for the complex in n-hexane. The ability to desorb the complex intact indicates that $Fe_3(CO)_{12}$ is reversibly physisorbed on PVG without disruption of the coordination sphere or metallic frame of the cluster.

The DRIFT spectrum of the complex sublimed onto PVG is also identical to the solution spectrum, confirming no substitution or declusterification products are formed upon adsorption. The absence of bands in the bridging carbonyl region of the DRIFT spectrum, and the similarity with the solution spectrum, indicate that the adsorbed complex possesses D_3 symmetry, which is the major isomeric form found in fluid solution (49). No spectral evidence was obtained for formation of the anionic hydrido cluster, $H\text{-}Fe_3(CO)_{11}^-$, on PVG which is in agreement with the results reported by Basset's group for adsorption of the complex on silica gel (29). These results reflect the low reactivity of the surface silanol groups of silica supports towards the metallic frame of the cluster.

B. Formation of Atomic Iron Via Photolysis of $Fe(CO)_5$(ads).

The photochemistry of $Fe(CO)_5$(ads), regardless of surface coverage, initially parallels that found in fluid solution. UV photolysis induces CO dissociation and the formation of a surface confined photoproduct that absorbs at 370 nm. The maintainance of an isosbestic point during the first few percent of reaction, and the regeneration of $Fe(CO)_5$(ads) following exposure to CO, suggest that the photoproduct is a sub-carbonyl species.

Poliakoff and Turner (68-70,132) report that $Fe(CO)_4$ generated in low temperature matrices exhibits absorptions centered at 325 nm and 770 nm, whereas $Fe(CO)_4Q$, where Q represents occupation of the vacant coordination site by a matrix atom or molecule, exhibits only a 370 nm absorption. While both species can thermally backreact with added CO to regenerate $Fe(CO)_5$(ads), the similarity of the photoproduct spectrum with that of $Fe(CO)_4Q$ species, particularly the absence of a near-IR band, suggests occupation of the vacated coordination site by a surface functionality on PVG. However, occupation of the vacant coordination site does not necessarily imply formal coordination of the tetracarbonyl to the PVG surface. Recent measurements of the activation energies of the reactions of $W(CO)_5$(ads) with various ligands indicate that the $W(CO)_5$-PVG interaction energy, $\leq$ 7 kcal/mole, is considerably less than that expected for formal coordination to the surface (120c,123). Clearly, the $Fe(CO)_5$-PVG interaction may differ, yet this molecule remains highly reactive. Exposure to weak ligands, L, such as pyridine for example, leads to rapid formation of $Fe(CO)_4L$ complexes. Thus, the primary photoprocess, reaction 1, leads to a surface-bound tetracarbonyl, $Fe(CO)_4$(ads), where the interaction with the PVG surface stabilizes the primary product, but not at the expense of subsequent thermal reactivity. The quantum yield of the reaction, within

experimental error of unity, is in agreement with that previously reported in both solution (54) and the gas phase (64).

Continued 254-nm photolysis of samples containing < 10^{-6} moles of $Fe(CO)_5$/gram leads to the evolution of 4.9 ± 0.1 moles of CO evolved/mole of $Fe(CO)_5$(ads). The loss of an isosbestic point and the general decline in absorbance throughout the near-UV and UV regions following more prolonged photolysis, indicates the primary photoproduct undergoes secondary photochemistry to form more highly unsaturated sub-carbonyl fragments. This is consistent with the photosensitivity of $Fe(CO)_4$ reported by Poliakoff and Turner (68,69,72,132) in low-temperature matrixes and Ouderkirk and Weitz (65,66) in the gas phase. UV-visible spectra recorded during photolysis give no indication of the formation of dimeric or trimeric clusters. The absence of H_2 evolution, as well as the reformation of $Fe(CO)_4$(ads) when the decarbonylated photoproduct is exposed to CO, establish the formation of zerovalent iron on the PVG surface, and in a number of experiments, the product exhibits a line spectrum equivalent to that of atomic iron generated in a low temperature matrix (72). The rapid regeneration of the surface-bound tetracarbonyl following addition of 1 atm of CO, and the slower regeneration of the pentacarbonyl, parallel the results reported by Ouderkirk

and Weitz (66) following addition of CO to a cell containing photogenerated, vapor phase $Fe(CO)_x$ (x = 2, 3, 4) fragments. These authors suggest that the difference between the reaction rates can be attributed in part to the higher reactivity of 12 and 14-electron $Fe(CO)_2$ and $Fe(CO)_3$ species relative to the 16-electron uncomplexed $Fe(CO)_4$ species. The slow regeneration of the pentacarbonyl in the PVG matrix is consistent with formation of a 18-electron surface-bound tetracarbonyl which is not as reactive as free $Fe(CO)_4$.

Basset and coworkers (35,36) report that thermal decomposition of $Fe(CO)_5$ or $Fe_3(CO)_{12}$ on hydroxylated silica yields zerovalent iron particles in addition to small amounts of an iron oxide. While the temperature dependence of the FMR linewidth needs to be determined in order to characterize the particle size distribution, the large room temperature linewidth, $5.0\pm0.5 \times 10^3$ Gauss, recorded following prolonged 254-nm photolysis of $Fe(CO)_5$(ads), suggests formation of iron particles $\leq$ 15 Å (36). The formation of smaller iron particles following photochemical decomposition of $Fe(CO)_5$ on PVG, relative to the particles formed following thermal decomposition on hydrated silica gel, agrees with the results of Nagy, van Eenoo, and Derouane (16) who investigated the thermal and photochemical decomposition of $Fe(CO)_5$ supported on HY zeolites. Photochemical decomposition resulted in

formation of zerovalent iron particles smaller than 9 Å, as compared to the 15 Å particles formed following thermal decomposition. The smaller particle size was attributed to a strong electronic interaction between the subcarbonyl intermediates and the zeolite surface relative to the corresponding system prepared thermally. The formation of small particles of atomic iron on PVG, which possesses dilation symmetry and a Hausdorff dimension of 1.74±0.12 (119), appears to be related to the relatively low dimensionality of the surface. This offers some $Fe(CO)_5$ adsorption sites where the site dimensionality curtails agglomerization. However, although the fractal dimension of PVG is less than that of silica gel, 2.94±0.06, attributing the difference in particle size solely to the smaller dimensionality of the PVG surface is premature since thermal decomposition of $Fe(CO)_5$(ads) was accomplished at temperatures $\geq$ 250 °C where adsorbate mobility is expected to be greater.

C. Mechanism of $Fe_3(CO)_{12}$ Formation.

In contrast to the formation of small particles of atomic iron at low surface coverages, UV photolysis of $Fe(CO)_5$(ads) at higher surface loadings, i.e., $\geq 10^{-6}$ moles/gram leads to the formation of $Fe_3(CO)_{12}$(ads). The low quantum yield of disappearance for $Fe_3(CO)_{12}$ adsorbed onto PVG, 7.4×10^{-2}, establishes that the trimer, once

formed, is relatively photochemically inert and does not undergo additional reactions with relatively high efficiency. The large increase in absorbance in the near-UV that obscures the 440-nm shoulder of $Fe_3(CO)_{12}$ suggests additional photoproducts. Subtraction of the $Fe_3(CO)_{12}$ spectrum, as well as the decline in absorbance in the near-UV when the sample is exposed to 1 atm of CO, indicate the presence of $Fe(CO)_4$(ads). Jackson and Trusheim (99,100) report that an analogous species formed on silica gel reacts thermally with a short-lived dinuclear intermediate to form $Fe_3(CO)_{12}$. Although optical spectra recorded in our experiments failed to reveal the presence of other mononuclear or dinuclear species, the dependence of ϕ_T on irradiation time, Figure 47, is consistent with the proposed mechanism. The intially small value of ϕ_T, which is independent of loading, is suggestive of formation of precursor complexes that either thermally or photochemically react to form the stable trimer. The observed stoichiometry of the photoreaction, Figure 46, in which considerably more CO is evolved than can be accounted for by formation of $Fe_3(CO)_{12}$, indicates a complex reaction mixture. Indeed, DRIFT experiments establish the presence of a number of mononuclear and polynuclear cluster intermediates.

1. DRIFT Experiments Under CO.

DRIFT spectra of the terminal CO region following 350-nm photolysis of $Fe(CO)_5$(ads) under various CO pressures indicate the formation of at least two spectrally distinct species that rapidly react with CO at different rates to regenerate $Fe(CO)_5$(ads). The rates of the backreactions depend on CO pressure, being ca. ten times more rapid under 400 torr than under 0.4 torr for both species. The species exhibiting bands at 2073 and 2048 cm^{-1} appears first. Although the slower rate of decay indicates that this is the more stable species, it is formed in limited amounts. Continued photolysis leads to preferential formation of a second, more reactive component exhibiting a single band at 2062 cm^{-1}. The latter species decays rapidly, but its decay pathway does not lead to additional formation of the 2073 and 2048 cm^{-1} species. The ability of both species to react with CO to regenerate $Fe(CO)_5$(ads) confirms that they are subcarbonyl species. These results, together with the previously discussed UV-vis data, suggest that the primary photoproduct, $Fe(CO)_4$, reacts quickly with the surface silanol sites or chemisorbed water on the PVG surface to yield spectrally distinct $Fe(CO)_4$ complexes characterized by a band at at 2062 and bands at 2073 and 2048 respectively.

Jackson and Trusheim (100) report that $Fe_3(CO)_{12}$(ads) is the sole reaction product when $Fe(CO)_5$ physisorbed onto silica gel is irradiated at temperatures between 200 and 300 K. At temperatures between 100 and 150 K, UV photolysis yields, in addition to $Fe_3(CO)_{12}$, a second product that exhibits poorly resolved, yet reproducible IR bands between 1960 and 1940 cm^{-1}. The latter species was assigned to the product, $Fe(CO)_4(SiO_2)$, arising from the addition of the primary photoproduct $Fe(CO)_4$, to either a surface silanol or bridging siloxane group. Ballivet-Tkatchenko and Coudurier (17) investigated the adsorption and thermal decomposition of of $Fe(CO)_5$ and $Fe_2(CO)_9$ on HY zeolites. Upon adsorption of these complexes into this matrix, CO was evolved, and the authors assigned IR bands at 2112, 2040, 1985 and 1950 cm^{-1} to a zeolite bound iron subcarbonyl, ZOH-$Fe(CO)_4$, which reversibly reacted to form $Fe_3(CO)_{12}$(ads). No species exhibiting bands below 2000 cm^{-1} were observed following ambient temperature photolysis of $Fe(CO)_5$ on PVG. However, species exhibiting bands in the region above 2000 cm^{-1} which react with CO and behave as subcarbonyl species are observed. Their relatively higher energy CO stretching frequencies, as compared to the $Fe(CO)_4$ adducts mentioned above, suggest that at least partially oxidized $Fe(CO)_4$ species are responsible for the 2073-2048 and 2062 cm^{-1} adsorptions. $Fe(CO)_4$ photogenerated from $Fe(CO)_5$ has been reported by

Wrighton (133) to undergo an oxidative addition reaction with R_3SiH in fluid solution at room temperature. Sweany (134) reports that UV photolysis of $Fe(CO)_5$ in a low temperature Ar matrix containing 10% H_2 results in formation of $Fe(CO)_4$ and an oxidative addition adduct $Fe(CO)_4H_2$. The former species exhibited bands at 1994 and 1974 cm^{-1}, while higher frequency bands at 2122, 2051 and 2043 cm^{-1} were assigned to the latter. The more stable species which exhibits bands at 2073-2048 cm^{-1}, following photolysis of $Fe(CO)_5$ on PVG, is assigned to H-$Fe(CO)_4$-OSi, where the primary photoproduct has undergone an oxidative addition reaction with a surface silanol site on the glass. When these sites are consumed, preferential formation of the more reactive species, assigned to H-$Fe(CO)_4$-OH, occurs by oxidative addition of chemisorbed H_2O to $Fe(CO)_4$. Although the PVG has been pretreated under conditions which dramatically reduce the amount of chemisorbed H_2O, the DRIFT spectrum of calcined PVG does reveal the presence of small amounts of adsorbed H_2O. Infrared absorptions from non-carbonyl modes in these $Fe(CO)_4$ oxidative addition adducts are weak and are correspondingly not detected. These adducts are expected to be unstable and may decompose via reductive elimination to form either unstable, uncomplexed $Fe(CO)_4$ species, or by irreversible redox reaction to ionic hydridoironcarbonyl species or cationic iron carbonyl complexes; neither of which are detected as intermediates

or stable products.

DRIFT spectra recorded following photolysis of $Fe(CO)_5$(ads) under 4 and 0.4 torr CO indicate that while the H-$Fe(CO)_4$-OSi adduct is formed in amounts similar to the 400 torr experiment, formation of H-$Fe(CO)_4$-OH is less favored. In addition to the oxidative addition adducts, DRIFT spectra now reveal the presence of an additional stable photoproduct exhibiting an absorption at 2053 cm^{-1}. This spectral feature is assigned to $Fe_3(CO)_{12}$ based on the DRIFT spectrum of $Fe_3(CO)_{12}$ sublimed onto PVG which exhibits a major absorption at 2053 cm^{-1}. Thus, a thermal or photochemical reaction pathway from the reactive H-$Fe(CO)_4$-OH adduct to the relatively unreactive polynuclear metal carbonyls is opened by lack of sufficient CO. The appearance of weak adsorptions in the bridging carbonyl region at 1790 and 1820 cm^{-1}, which are assigned to the dimeric species $Fe_2(CO)_8$ (2068, 1790 cm^{-1}) and $Fe_2(CO)_9$ (2066, 1820 cm^{-1}), confirm this pathway. These assignments are consistent with the peak positions of the bridging carbonyl bands reported by Poliakoff and Turner (69,70,74) for each dimer in low temperature matrices and with the work of Jackson and Trusheim (100) who examined the photolysis of silica adsorbed $Fe(CO)_5$ at subambient temperatures. Although formation of $Fe_3(CO)_{12}$ was observed to be inhibited under higher CO pressures it was

observed to form under 4 torr of CO.

2. DRIFT Experiments in Vacuo.

Examination of the series of difference spectra following 2 pulse excitation of $Fe(CO)_5$(ads) with the 355-nm second harmonic of a Q-switched Nd:Yag laser, Figure 50, reveals immediate formation of a 2056 cm^{-1} band which decays slowly over the 540 second time interval. As discussed previously, bands in the 2053 and 2059 cm^{-1} region are indicative of trimer formation. However, UV-vis spectra and gas phase analysis of a PVG sample impregnated with $Fe_3(CO)_{12}$ which was stored in the absence of light and air, indicate negligible decay of the trimer over a period of several hours. The formation of at least two trimeric species is postulated, one being $Fe_3(CO)_{12}$, (2053 cm^{-1}), which was assigned in the low pressure CO experiments. The slowly decaying trimeric cluster species which exhibits a band shifted to slightly higher frequency, (2056 cm^{-1}), is tentatively assigned to an incompletely formed $Fe_3(CO)_x$ ($x < 12$) species, where its vacant coordination sites are bound to surface functionalities on PVG. The difference spectra illustrating the photoproduct decay forty seconds following excitation shows the rapid decay of the H-$Fe(CO)_4$-OSi adduct, (2073-2048 cm^{-1}). No spectral evidence was obtained for formation of the reactive H-

$Fe(CO)_4$-OH adduct, (2062 cm^{-1}), since this species undergoes either a photochemical or thermal reaction to form more highly unsaturated intermediates from which the polynuclear clusters arise. Minor bands in the bridging carbonyl region at 1790 and 1823 cm^{-1} due to $Fe_2(CO)_8$ and $Fe_2(CO)_9$, respectively, are also observed to decay within 40 seconds following excitation. The formation of polynuclear clusters was facilitated by two pulse excitation, relative to the results obtained following single pulse excitation.

Comparison of a series of difference spectra following cw irradiation of $Fe(CO)_5$(ads) in vacuo, Figure 51, reveal both similarities and differences relative to the pulsed experiments. The spectrum obtained immediately following excitation reveals immediate formation of an unreactive trimeric cluster, (2059 cm^{-1}) which is consistent with the pulsed experiments. The difference spectra obtained 100 seconds following excitation exhibits the 2059 cm^{-1} band with a higher frequency shoulder at 2066 cm^{-1}. In addition, a severe decline in the 1790 and 1820 cm^{-1} intensities occurs after 100 seconds. These spectral changes are due to the rapid decay of the dimeric $Fe_2(CO)_8$ (2068, 1790 cm^{-1}) and $Fe_2(CO)_9$ (2066 1820 cm^{-1}) clusters which is consistent with the high reactivity of $Fe_2(CO)_8$ reported by Koerner von Gustorf (135) and the disproportionation reaction of

$Fe_2(CO)_9$ observed on both silica gel (99) and PVG at room temperature (see above). As with the pulsed experiments, spectral evidence for the formation of the reactive H-$Fe(CO)_4$-OH adduct is not obtained. However, the rapid decay of the H-$Fe(CO)_4$-OSi adduct noted in the pulsed experiments is not observed in the cw experiments. Rather, the decay of the bands at 2073-2048 cm^{-1} attributed to $Fe(CO)_4$-OSi is apparent in the spectrum obtained 200 seconds following excitation, as compared to 40 seconds following pulsed excitation. Although the faster rate of decay in the pulsed experiments may arise from a higher level of CO after pulsed photolysis versus cw photolysis, decay of H-$Fe(CO)_4$-OSi in the cw experiments is observed only after decay of the dimeric clusters. The time dependence of the photoproduct decay suggests that the dimeric $Fe_2(CO)_8$ and $Fe_2(CO)_9$ clusters decay to $Fe(CO)_5$ via H-$Fe(CO)_4$-OSi. The final spectrum obtained 600 seconds following excitation indicates the slow decay of a 2059 cm^{-1} band previously assigned to an incompletely formed trimeric cluster.

3. DRIFT Experiments Under Trimethylphosphine.

A cw photolysis of $Fe(CO)_5$(ads) under 100 torr trimethylphosphine results in formation of an extensive series of photoproducts. No spectral evidence of formation of trimeric clusters were observed in these

experiments. At short irradiation times the spectra consist mainly of adsorptions due to $Fe(CO)_4(P(CH_3)_3)$ (2047, 1969, and 1940 cm^{-1}) and $Fe(CO)_3(P(CH_3)_3)_2$ (1885 cm^{-1}). The assignments were based on the IR band positions of the correspondingly substituted triphenylphosphine complexes in hydrocarbon solution (90). The additional peaks at 2020, 2004, 1998 and 1845 cm^{-1} are difficult to assign to known stable complexes. These bands are tentatively assigned to the monosubstituted phosphine analog of $Fe_2(CO)_9$, $Fe_2(CO)_8(P(CH_3)_3)$. Complexes such as these have not been isolated from substitution reactions of $Fe_2(CO)_9$ with phosphines and other ligands. Instead, disproportionation of the complex into $Fe(CO)_4L$ and $Fe(CO)_5$ occurs. The decay of the bands assigned to $Fe(CO)_2(CO)_8(P(CH_3)_3)$ at 2020, 2004, 1998, and 1845 cm^{-1} following short irradiation times is observed to result in an increase in intensity of bands attributed to $Fe(CO)_4(P((CH_3)_3$ at 2047, 1969, and 1940 cm^{-1}. The decay of the bands assigned to $Fe_2(CO)_8(P(CH_3)_3)$ to $Fe(CO)_4(P(CH_3)_3$ is consistent with the disproportionation of $Fe_2(CO)_9$ in the presence of weak ligands, L, in fluid solution, to $Fe(CO)_4L$ and $Fe(CO)_5$ (59,60). Continued irradiation results in a nearly proportionate increase in all bands, however, those for $Fe(CO)_3(P(CH_3)_3)_2$ and $Fe_2(CO)_8(P(CH_3)_3)$ are somewhat favored. Following 1.6 seconds cw irradiation, the major photoproduct exhibits a

band at 1788 cm^{-1}. This band is tentatively assigned to the bridging carbonyl stretch of a dinuclear $Fe_2(CO)_7(P(CH_3)_3)_2$ species. At this point the bands due to $Fe(CO)_3(P(CH_3)_3)_2$ complex dominate the spectrum. At the longest photolysis times, 6.4 seconds, several absorption bands begin to exhibit shoulders. Analysis by spectral subtraction methods results in observation of a peak at 1815 cm^{-1} tentatively assigned to $Fe(CO)_2(P(CH_3)_3)_3$. The assignments of the reactive, decaying complexes $Fe(CO)_3(P(CH_3)_3)$ (1950, 1920 cm^{-1}) and $Fe(CO)_2(P(CH_3)_3)_2$ (1855 cm^{-1}), each of which is probably complexed by the glass and/or its adventitious ligands, is somewhat tenuous. However, this experiment allows us to postulate the presence of several reactive intermediates and reveals the enormous propensity of the photoproducts to undergo secondary photochemical reactions, with evidence for multiple carbonyl ligand loss even at the shortest photolysis times.

4. Proposed Mechanism For $Fe_3(CO)_{12}$ Formation.

Few reports have appeared in the literature regarding the photochemistry of supported $Fe(CO)_5$ due, for the most part, to the experimental difficulties imposed by the opacity of many traditional oxide supports. The most active researchers have been Jackson and Trusheim (99,100) who circumvented the problem by investigating the photochemistry of $Fe(CO)_5$ supported on

transparent silica gel. Their results proved conclusively that ambient temperature photolysis of $Fe(CO)_5$ at sub-monolayer coverages results in formation of $Fe_3(CO)_{12}$. At surface coverages greater than monolayer, photolysis yields $Fe_2(CO)_9$. Since the enviroment of the $Fe(CO)_5$ residing in these molecular overlayers approximates that of a three-dimensional liquid phase, the formation of $Fe_2(CO)_9$ is consistent with that previously observed in photolysis of pure liquid $Fe(CO)_5$ (58). Two mechanisms were proposed for the formation of $Fe_3(CO)_{12}$, both of which involve the participation of surface silica groups as weak ligands. The first postulates photochemical formation of an unobserved mobile $Fe(CO)_4$ species, intermittently bound as $Fe(CO)_4$-SiO_2, which subsequently undergoes a stepwise thermal trimerization to yield the $Fe_3(CO)_{12}$ cluster. The second involves thermal or photochemical formation of $Fe(CO)_3$ from uncomplexed $Fe(CO)_4$. This highly coordinatively unsaturated intermediate was postulated to react thermally with adsorbed $Fe(CO)_5$ to yield the reactive, dinuclear intermediate, $Fe_2(CO)_8$. A thermal reaction of $Fe_2(CO)_8$ with either uncomplexed $Fe(CO)_4$ or adsorbed $Fe(CO)_5$ resulted in formation of $Fe_3(CO)_{12}$. Neither $Fe(CO)_4$, $Fe(CO)_3$, or $Fe_2(CO)_8$ were spectroscopically observed following photolysis at room temperature. In a subsequent investigation, the photochemistry of silica supported $Fe(CO)_5$ was examined

at sub-ambient temperatures. At temperatures > 200 K, the only significant photoproduct observed was $Fe_3(CO)_{12}$. Photolysis at temperatures between 100 and 150 K resulted in formation of $Fe_3(CO)_{12}$ and the appearance of IR bands between 1960-1940 cm^{-1} which were assigned to $Fe(CO)_4(SiO_2)$. Photolysis between 10 and 50 K resulted in the appearance of two bands in the bridging carbonyl region at 1860 and 1820 cm^{-1}. These bands disappeared as the cell was warmed to 300 K, leading to an increase in intensity of bands due to $Fe(CO)_5$ and $Fe_3(CO)_{12}$. The band at 1820 cm^{-1} was assigned to $Fe_2(CO)_9$ while the band at 1860 cm^{-1} remained unassigned. A new mechanism was proposed which involved formation of a unidentified dinuclear intermediate via thermal reaction of uncomplexed $Fe(CO)_4$ with the immobile $Fe(CO)_4(SiO_2)$ species. This dinuclear intermediate then reacts rapidly with adsorbed $Fe(CO)_5$ to form $Fe_3(CO)_{12}$.

While the facile photochemical formation of $Fe_3(CO)_{12}$ is observed on both silica gel and PVG, the trimer is not the sole photoproduct following ambient temperature photolysis on PVG. Instead, the electronic spectrum reveals, in addition to bands characteristic of $Fe_3(CO)_{12}$, a significant near-UV absorbance which cannot be attributed to the trimer. The decline in this absorbance following addition of CO confirms the presence of subcarbonyl species on PVG following ambient

temperature photolysis. DRIFT experiments also reveal the presence of reactive mononuclear and polynuclear intermediates following ambient temperature photolysis. The myriad of photoproducts spectroscopically observed on PVG can be attributed to the unique surface properties of PVG. Kubokawa and Anpo (121) have demonstrated the ability of PVG to kinetically stabalize photogenerated intermediates and work in our laboratory reveals that photolysis of Group VI hexacarbonyls adsorbed onto PVG yields the corresponding pentacarbonyls, which have spectroscopically quantitated lifetimes of $\geq$ 43 hours in vacuo (120c,122). The lower dimensionality of PVG (119) relative to silica gel may also place geometrical constraints on the photoproducts, thereby curtailing agglomerization and allowing their observation at ambient temperatures.

The observation of IR bands in the 1960-1940 cm^{-1} region, which have been assigned by several authors (17,68,70,100,129) to a $Fe(CO)_4(SiO_2)$ species, are not observed on PVG. Rather, photolysis of $Fe(CO)_5$(ads) under CO leads to the appearance of bands at 2073-2048 and 2062 cm^{-1} which were assigned to H-$Fe(CO)_4$-OSi and H-$Fe(CO)_4$-OH, respectively. While their relatively short lifetimes may prevent their observation at ambient temperature, in the low power, sealed cell experiments of Jackson and Trusheim (99,100) who recorded spectra on a

relatively slow dispersive spectrophotometer, these adducts should be observable in the low temperature experiments by these investigators where they observe the $Fe(CO)_4(SiO_2)$ species. The assignment of the band at ca. 2060 cm^{-1} to $Fe_3(CO)_{12}$ may be an incorrect assumption since it is possible that this band comprises adsorptions from the $H\text{-}Fe(CO)_4\text{-}OSi$ and $Fe(CO)_4\text{-}OH$ at subambient temperatures. As the sample is warmed to room temperature $Fe_3(CO)_{12}$ may indeed be the sole contributor to this band. From analysis of the results obtained by Jackson and Trusheim we conclude that $H\text{-}Fe(CO)_4\text{-}OSi$ and $H\text{-}Fe(CO)_4\text{-}OH$ are more stable than the $Fe(CO)_4(SiO_2)$ species. However, this latter species may still be an important, undetected intermediate in cluster and $Fe(CO)_5$ formation from the former two species. A new mechanism for $Fe_3(CO)_{12}$ formation is proposed which is consistent with our observations on PVG. The mechanism is first presented in a series of reactions and then in terms of a diagram which more clearly illustrates the interconversions amongst the different intermediates.

1. $Fe(CO)_5(ads) \longrightarrow Fe(CO)_4 + CO$
2. $Fe(CO)_4 + PVG \longrightarrow \underline{H\text{-}Fe(CO)_4\text{-}OSi} + \underline{H\text{-}Fe(CO)_4\text{-}OH}$
3. $\underline{H\text{-}Fe(CO)_4\text{-}OH} \longrightarrow Fe(CO)_n\ (n\leq 3) + CO + H_2O(ads)$
4. $\underline{Fe(CO)_3} + Fe(CO)_5(ads) \longrightarrow \underline{Fe_2(CO)_8}$
5. $\underline{Fe_2(CO)_8} + CO \longrightarrow \underline{Fe_2(CO)_9}$
6. $\underline{2Fe_2(CO)_9} \longrightarrow \underline{Fe_3(CO)_{12}} + \underline{H\text{-}Fe(CO)_4\text{-}OSi} + 2CO$

7. $\underline{Fe_2(CO)_8} + Fe(CO)_5(ads) \longrightarrow \underline{Fe_3(CO)_{12}} + CO$

In the above reaction scheme, the underlined species have been spectroscopically identified. Reaction 1 represents the primary photoprocess, i.e., formation of $Fe(CO)_4$. This process is independent of surface loading and excitation intensity. This is followed by a rapid reaction of $Fe(CO)_4$ with the surface silanol groups and chemisorbed H_2O on the PVG surface, reaction 2, to yield the two oxidative addition adducts, H-$Fe(CO)_4$-OSi and H-$Fe(CO)_4$-OH. The rapid decline of both UV-vis and DRIFT bands assigned to these oxidative addition adducts confirm their ability to thermally backreact with either photoejected or added CO to regenerate $Fe(CO)_5$(ads). The absence of the more reactive H-$Fe(CO)_4$-OH in the CO free experiments, in which polynuclear cluster formation is observed, indicates it is this species which gives rise to the more highly coordinatively unsaturated species from which these clusters arise. The loss of the isosbestic point following continued photolysis of $Fe(CO)_5$(ads) at surface loadings, $\leq 10^{-6}$ moles/gram, indicates that the surface-bound tetracarbonyl has undergone secondary reactions to form other photoproducts. This secondary photochemistry yielding $Fe(CO)_3$ and possibly $Fe(CO)_2$ is described by reaction 3. The secondary photoproducts were identified in the DRIFT trapping experiments with trimethylphosphine where

$Fe(CO)_3(P(CH_3)_3)_2$ is found to be a major product even at the shortest irradiation times while more extensive photolysis yields $Fe(CO)_2(P(CH_3)_3)_3$.

The thermal reaction of $Fe(CO)_3$ with nascent $Fe(CO)_5$ on PVG to form the reactive $Fe_2(CO)_8$ cluster is shown in reaction 4. Poliakoff and Turner (74) have generated $Fe_2(CO)_8$ via UV photolysis of matrix isolated $Fe_2(CO)_9$ and have suggested as its structure a labile, carbonyl bridged species containing a formal iron-iron double bond. An alternate pathway to this dinuclear intermediate might involve dimerization of uncomplexed, mobile $Fe(CO)_4$ with the surface bound H-$Fe(CO)_4$-OH. The absence of bands in the near-IR region of the electronic spectrum, coupled with the absence of bands below 2000 cm^{-1}, tend to discredit this pathway since the absence of these spectral features suggests that uncomplexed $Fe(CO)_4$ is not an important intermediate. Consistent with high reactivity of $Fe_2(CO)_8$ in solution reported by Koerner von Gustorf (135), DRIFT spectra (Figure 51) show that the 2068 and 1790 cm^{-1} bands assigned to $Fe_2(CO)_8$ decay occur within 100 seconds following excitation. During the same time interval following excitation, the bands at 2066 and 1820 cm^{-1} assigned to $Fe_2(CO)_9$ are also observed to decay. Reactions 5 and 6 illustrate decay pathways for the dimeric clusters consistent with the photoproduct decay sequence observed in the DRIFT experiments. Rapid

recombination of the reactive $Fe_2(CO)_8$ dimer with photoejected CO forms $Fe_2(CO)_9$, which is unstable on PVG at room temperature, and subsequently disproportionates to yield $Fe_3(CO)_{12}$ and $Fe(CO)_5$(ads). After the decay of the dimeric cluster species, the spectral change 200 seconds following excitation is dominated by the decay of the 2073-2048 cm^{-1} bands assigned to H-$Fe(CO)_4$-OSi which indicates that their decay to $Fe(CO)_5$(ads) occurs via this adduct.

The last reaction illustrates formation of $Fe_3(CO)_{12}$ via a reaction between dimeric $Fe_2(CO)_8$ and a monomeric species. This reaction must proceed at a high rate since spectra recorded immediately following excitation indicate the presence of $Fe_3(CO)_{12}$. Obvious candidates for the mononuclear species include uncomplexed $Fe(CO)_4$, both H-$Fe(CO)_4$-OSi and H-$Fe(CO)_4$-OH, and $Fe(CO)_5$(ads). However, the lack of spectral evidence obtained for uncomplexed $Fe(CO)_4$ indicates that this species is not an important intermediate. The higher mobility of $Fe(CO)_5$(ads) relative to the oxidative addition adducts suggests that $Fe(CO)_5$(ads) will have a much greater probability of encountering $Fe_2(CO)_8$ than the surface-bound adducts. Hence, in the final step leading to $Fe_3(CO)_{12}$, the reactive dinuclear $Fe_2(CO)_8$ intermediate is postulated to react rapidly with the more mobile $Fe(CO)_5$(ads). A summary of the observed interconversions

is shown in Figure 69 where underlining designates those species either directly observed or inferred from spectroscopic characterization of the products formed in the trapping experiments.

D. Photochemical Reactions of $Fe(CO)_5$(ads) With Olefin Complexes.

1. DRIFT Experiments.

A 350-nm irradiation of $Fe(CO)_5$(ads) in the presence of olefins results in formation of iron carbonyl-olefin complexes. Under 100 torr of ethylene, cw irradiation of $Fe(CO)_5$(ads) leads to a reversible reaction sequence affecting the growth and decay of at least four species. The spectrum recorded immediately following 0.4 second 350-nm cw excitation (Figure 62) exhibits bands at 2087, 2074, 2059, 2048, 2015 and 1989 cm^{-1}. The bands at 2087, 2015 and 1984 cm^{-1} agree with the reported spectrum of $Fe(CO)_4(C_2H_4)$ in methylcyclohexane at 298 K (96) and are assigned to this species. The bands at 2074 and 2048 cm^{-1} show similar decay rates, and are reminiscent of the bands observed in both the CO and in vacuo DRIFT experiments where they have been assigned to the more stable oxidative addition adduct $H\text{-}Fe(CO)_4\text{-}OSi$. At slightly longer photolysis times, 1.6 seconds, a species exhibiting bands at 2059 and 1989 cm^{-1} is observed to form in significant amounts. These bands are equivalent

Photochemical and Thermal Reactions of Iron Carbonyls on PVG

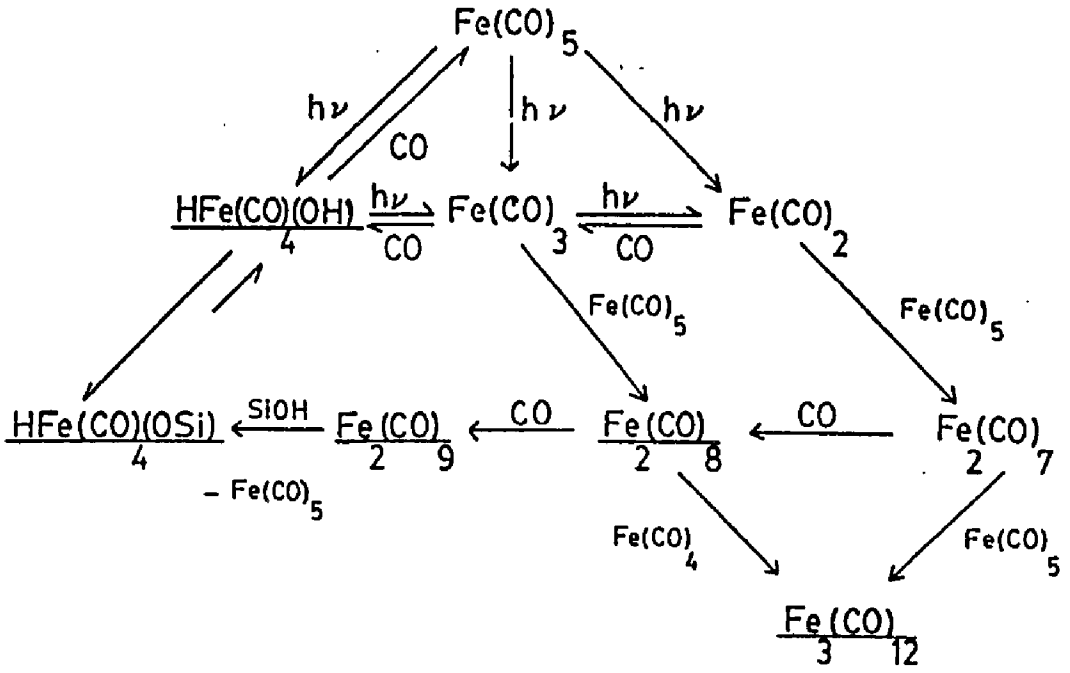

Figure 69. Summary of observed photochemical and thermal reactions for $Fe(CO)_5$(ads.) with or without added CO.

to the reported IR spectrum of $Fe_2(CO)_6(C_2H_4)$ in methylcyclohexane at 273 K (96) and are assigned to this dimer. The dimer decays within 20 seconds following excitation and the increase in the intensities of bands at 2087, 2074 and 2048 cm^{-1} during this time interval suggest that it decays to H-$Fe(CO)_4$-OSi and $Fe(CO)_4(C_2H_4)$. During the next 40 second time interval, i.e., 60 seconds following excitation, the decay is dominated by $Fe(CO)_4(C_2H_4)$.

As pure $Fe(CO)_4(C_2H_4)$ is a liquid boiling slightly higher than $Fe(CO)_5$, the subsequent loss of $Fe(CO)_4(C_2H_4)$ is due to diffusion of this species out of the infrared sampling area and not by chemical reaction. The loss at still longer times of H-$Fe(CO)_4$-OSi is either by thermal backreaction with photoejected CO to regenerate $Fe(CO)_5$(ads) or by a slow thermal reaction with C_2H_4 to form the quickly diffusing $Fe(CO)_4(C_2H_4)$. The species exhibiting the band at 2041 cm^{-1} remains unassigned.

In contrast to the complexity of spectra obtained under 100 torr of ethylene, irradiation of $Fe(CO)_5$(ads) under 100 torr of 1-pentene yields a simpler, but somewhat different array of photoproducts. The spectrum recorded immediately after 0.4 second, 350-nm cw excitation exhibits absorptions at 2081, 2068, 2051, 2012 and 1973 cm^{-1} (Figure 64). The bands at 2081, 2012 and 1973 cm^{-1} are assigned to $Fe(CO)_4(1\text{-}C_5H_{10})$ based on the

infrared spectrum of this complex in 3-methylpentane at 298 K (96). In addition to the relatively slow decay of this species (by diffusion), a rapid decay of bands at 2058 and 1971 cm^{-1} occurs. These bands are assigned to the dimeric $Fe_2(CO)_6(1\text{-}C_5H_{10})_2$ complex since they agree with the IR spectrum of the complex in 1-pentene at 195 K (96). Extended photolysis, 1.6 seconds, results in increased formation of two spectrally distinct, slowly decaying species exhibiting bands at 2068 and 2051 cm^{-1}. These bands are tentatively assigned to partially oxidized π - allyl hydride complexes, $Fe(CO)_3(\pi^3\text{-}C_5H_9)\text{-}L$, where L can be a hydride or surface functionality on PVG. These tentative assignments are based on the peak position of the highest energy band (2059 cm^{-1}) of $H\text{-}Fe(CO)_3(\pi^3\text{-}C_5H_9)$ formed by photolysis of $Fe(CO)_5$ in the presence of 1-pentene in methylcyclohexane at 77 K (96). In contrast to the DRIFT experiments under 100 torr of ethylene, formation of $H\text{-}Fe(CO)_4\text{-}OSi$ does not occur under 100 torr of 1-pentene. Moreover, both UV-visible and DRIFT spectra confirm that in the presence of olefins formation of $Fe_3(CO)_{12}$ does not occur following 1.6 seconds photolysis of $Fe(CO)_5$(ads) in the presence of olefins.

Wrighton and Mitchener (96) have reported the low temperature photochemistry of $Fe(CO)_4$(olefin) complexes in hydrocarbon solution and compared their results for

olefins containing allylic hydrogens with those without allylic hydrogens. Following irradiation of $Fe(CO)_4(C_2H_4)$ in an alkane matrix at 77 K, the infrared spectrum exhibits a band at 2132 cm^{-1} due to photoejected CO along with three bands at 2041, 1963 and 1957 cm^{-1} attributed to the 16 electron $Fe(CO)_3(C_2H_4)$ complex. These spectral features are consistent with that reported by Grevels and coworkers (136) following UV photolysis of $Fe(CO)_4(C_2H_4)$ in an Argon matrix at 77 K. In contrast, UV photolysis of $Fe(CO)_4(1\text{-}C_5H_{10})$, containing allylic hydrogens, in sub-ambient hydrocarbon solution resulted in an infrared spectral pattern consistent with formation of the π-allyl complex, $H\text{-}Fe(CO)_3(\eta^3\text{-}C_5H_9)$. Regardless of the olefin, the primary photoreaction of these complexes is CO dissociation, not loss of olefin. When $Fe(CO)_4$(olefin) complexes were irradiated in a hydrocarbon matrix containing significant amounts of uncomplexed olefin, the IR spectrum exhibited a strong band at ca. 1930 cm^{-1}. This band was assigned to a trans-$Fe(CO)_3(olefin)_2$ complex based on its similarity to the IR spectra of trans-$Fe(CO)_3\text{-}L_2$ complexes, where L = phosphorus ligand (2). On warming the matrix to the softening point (195 K), this feature completely disappears and new IR bands are observed at ca. 2050 and 1970 cm^{-1}. These bands have been assigned to a labile, dinuclear, Fe-Fe double-bonded species, $Fe_2(CO)_6(olefin)_2$, which is a derivative of the well

characterized $Fe_2(CO)_8$ (74,135). The $Fe_2(CO)_6(C_2H_4)_2$ complex is extremely catalytically active, yielding a 60% conversion of 1-pentene to 2-pentene in < 10 seconds, with a turnover rate of at least 3600/minute. Rapid regeneration of $Fe(CO)_4(C_2H_4)$ was observed on warming the hydrocarbon matrix to room temperature and purging with CO.

Comparison of the ambient temperature DRIFT experiments under 100 torr of C_2H_4 (Figure 62) with the photochemistry of $Fe(CO)_4(C_2H_4)$ in subambient hydrocarbon solution (96) reveals both similarites and differences. Photolysis of $Fe(CO)_5$(ads) under 100 torr of olefin results in immediate formation of $Fe(CO)_4(C_2H_4)$ complexes which disappear via diffusion out of the IR sampling region. In contrast to the results reported by Wrighton and Mitchener (96), formation of the 16-electron $Fe(CO)_3(C_2H_4)$ complex was not observed in the photolysis of $Fe(CO)_5$ adsorbed on PVG under 100 torr of C_2H_4. The formation of the catalytically active $Fe_2(CO)_6(C_2H_4)_2$ species, however, is common to both sets of experiments, as is its rapid decay at room temperature to $Fe(CO)_4(C_2H_4)$ in hydrocarbon solution and to $Fe(CO)_4(C_2H_4)$ and H-$Fe(CO)_4$-OSi on PVG. Infrared bands at ca. 1930 cm^{-1} assigned to trans-$Fe(CO)_3(C_2H_4)_2$ are not detected on PVG at room temperature. Their absence is expected, however, since this complex reacts thermally

upon warming the hydrocarbon matrix to 195 K to form the dimeric $Fe_2(CO)_6(C_2H_4)_2$ which is observed on PVG. Also, formation of π-allyl hydride complexes is not observed in the C_2H_4 DRIFT experiments which is consistent with the low temperature photochemistry of $Fe(CO)_4$(olefin) complexes where the olefin does not contain allylic hydrogens. However, irradiation of $Fe(CO)_5$(ads) under 100 torr of 1-pentene (Figure 64) does result in the observation of bands at 2068 and 2051 cm^{-1} which have been tentatively assigned to π-allyl hydride complexes. As with the C_2H_4 DRIFT experiments, no observation of bands at ca. 1930 cm^{-1}, attributed to trans-$Fe(CO)_3(olefin)_2$ is observed. In contrast to the C_2H_4 DRIFT experiments, bands at 2073 and 2048 cm^{-1} due to H-$Fe(CO)_4$-OSi are not detected in the 1-pentene experiments. This suggests that either the reaction of $1\text{-}C_5H_{10}$ with H-$Fe(CO)_4$-OSi is much faster than that of C_2H_4, or that $1\text{-}C_5H_{10}$ is effective in blocking its formation.

2. Photocatalyzed 1-Pentene Isomerization Reaction.

Near-UV irradiation of $Fe(CO)_5$(ads) in the presence of 1-pentene results in isomerization to cis and trans-2-pentenes. The reaction rate increases linearly with photolysis time during the early stages of the reaction, $\leq$ 10 minutes, but is followed by a period in which the

rate of 1-pentene conversion decreases with increasing photolysis time. Qualitatively, the time dependence of the photoinduced isomerization reaction observed for the $Fe(CO)_5$-PVG system agrees with the results reported by Wrighton (76) in fluid solution and Grant in fluid solution (92) and in the gas phase (93). The decrease in the rate of 1-pentene conversion observed on PVG during the latter stages of the reaction can be attributed to several factors. A comparison of Figure 66, which shows the formation of trans/cis-2-pentenes as a function of photolysis time, with Figure 65 reveals that at the 10 minute point where the rate of 1-pentene conversion begins to decrease, the trans/cis ratio increases from 1.58 to 2.67. This suggests that the system rapidly drives toward the thermodynamic ratio of trans/cis-2-pentenes of 4.32 (84), with the rate of product formation decreasing as the system approaches thermodynamic equilibrium. Formation of $Fe_3(CO)_{12}$(ads) during the latter stages of the reaction is indicated by the growth of an absorption band at 605-nm at photolysis times $\geq$ 40 minutes. Wrighton (85) reports that the observed quantum yield for the $Fe(CO)_5$ photocatalyzed 1-pentene isomerization in benzene at room temperature is four times greater than that measured using $Fe_3(CO)_{12}$. Hence, a contributing factor to the rate decrease at photolysis times $\geq$ 40 minutes may be formation of the relatively catalytically inert $Fe_3(CO)_{12}$(ads).

Quantum yield measurements over the portion of the reaction where the extent of 1-pentene conversion is approximately linear with photolysis time gives a quantum yield value of 155±2.0 for the photoinduced $Fe(CO)_5$-PVG 1-pentene isomerization. Although the observed quantum yields for the $Fe(CO)_5$ photocatalyzed 1-pentene isomerization reaction in fluid solution and in the gas phase were found to be > unity, the observed yields were found to be dependent on the intial 1-pentene concentration. Wrighton (79) reports an observed quantum yield value of 429±43 in neat 1-pentene at 20 C using 366-nm cw excitation, while Grant and Whetten (93) report a gas phase quantum yield of 225 using 337-nm pulses (1mJ, 4Hz) from a N_2 laser when the partial pressure of $Fe(CO)_5$ is 400 torr. The high quantum yields observed in solution (79,85,91), in the gas phase (93) and in the $Fe(CO)_5$-PVG hybridized system indicate that the role of the light in these systems is to photogenerate species which are extremely efficient alkene isomerization catalysts at ambient temperature.

In homogeneous catalysis, it is well established that the ligands in the coordination sphere of a metal-centered catalyst influence the rate and product distribution (5,7,86-88). In thermally activated olefin isomerization reactions the product distributions are sensitive to the steric interactions of the coordinated

organic ligand with other ligands in the coordination sphere. Bulky ligands favor formation of the cis-olefin over the trans-olefin. Wrighton (90) has investigated the influence of phosphorus ligands on the trans/cis-2-pentene ratio in the $Fe(CO)_5$ photocatalyzed 1-pentene isomerization reaction. The results obtained for $Fe(CO)_4(PPh_3)$ and $Fe(CO)_3(PPh_3)_2$ in fluid solution are qualitatively the same as for $Fe(CO)_n$ (n = 3,4) species anchored to a phosphinated styrene-divinylbenzene support (101). Although the distribution of 1-pentene and cis and trans-2-pentenes does ultimately reach the thermodynamic ratio after prolonged photolysis, the kinetically controlled intial distribution of products favors formation of the less thermodynamically stable cis-2-pentene isomer. Suib and coworkers (102) have investigated the photocatalyzed 1-pentene isomerization reaction using $Fe(CO)_5$ supported on various inorganic oxides and report the reaction rate and product distribution depend on the type of support used. Prolonged 366-nm photolysis, $\geq$ 18 hours, results in a trans/cis-2-pentene which varies from 2.7 for $Fe(CO)_5$ on Na-Y zeolites to 4.4 for the complex supported on silica gel. It was proposed that the lower percent conversions and trans/cis ratio on zeolites are due to the electrostatic field effects that the iron carbonyl species encounter on the zeolite surface and the role of the zeolite pore system in providing a mechanism for the

photoisomerization to take place (16,129).

The photoproduct distribution obtained for the photocatalyzed $Fe(CO)_5$ 1-pentene isomerization on PVG, particularly the low trans/cis-2-pentene ratios, which ranged from 1.50 to 2.67 during the intial stages of the reaction (Figure 66), indicates preferential formation of the less thermodynamically stable cis-2-pentene isomer. The trans/cis-2-pentene ratio is low, $\leq$ 2.7, during the first 10 minutes of photolysis and then steadily increases until a limiting value of 3.40 is reached after one hour of photolysis. These results are consistent with the product distribution observed by Wrighton (90,101) for mononuclear iron carbonyl complexes containing bulky phosphorous ligands in their coordination sphere. Although the exact nature of the factors affecting the product distribution on PVG are unclear, several explanations can be proposed based on existing data. Since surface hydroyxl ligands and/or chemisorbed H_2O molecules on the PVG surface can coordinate to the catalytically active intermediates, the low trans/cis ratio may be due to the influence of a surface ligand of PVG in the coordination sphere of the active catalyst. Although the steric bulk of the surface silanol groups and chemisorbed H_2O molecules are small relative to the triaryl phosphine ligands used in Wrighton's work, the fact that these ligands are attached

to a highly irregular surface suggests they will impose steric constraints when in the coordination sphere of the active catalyst. An alternative explanation for the dependence of the trans/cis ratio as a function of photolysis time arises from the growth and decay of the catalytically active photoproducts observed in the DRIFT experiments under 100 torr of 1-pentene. Wrighton (96) has described the high catalytic activity of the dimeric $Fe_2(CO)_6(C_2H_4)_2$ complex which yields a 60% conversion of 1-pentene to 2-pentene in < 10 seconds. The 1-pentene analog of this species, $Fe_2(CO)_6(1\text{-}C_5H_{10})_2$ exhibiting bands in the DRIFT experiments at 2058 and 1973 cm^{-1} (Figure 64), is observed immediately following 0.4 seconds excitation and decays completely within 40 seconds. In contrast, bands at 2068 and 2051 cm^{-1}, which have been assigned to the π-allyl complexes, $Fe(CO)_3(\eta^3\text{-}C_5H_9)\text{-}L$, where L is a hydride or surface functionality on PVG, are favored by more extensive photolysis. Moreover, these complexes exhibit a slow decay which is incomplete even 100 seconds after excitation. As shown in Figure 4, the mechanism proposed by Wrighton (79) for the $Fe(CO)_5$ photocatalyzed 1-pentene isomerization reaction involves the generation of a coordinatively unsaturated alkene complex, $Fe(CO)_3$(alkene), which undergoes an oxidative addition reaction to form the catalytically active π -allylhydride intermediates. The rapid formation and decay of $Fe_2(CO)_6(1\text{-}C_5H_{10})_2$ suggests that this highly

catalytic species may be the dominant catalyst during the intial stages of the reaction. The low trans/cis-2-pentene ratio observed for photolysis times $\leq$ 10 minutes, may be due to steric constraints imposed by this dimeric intermediate. Since the DRIFT data indicate that the π-allyl intermediates are favored by extensive photolysis and undergo a slow, incomplete decay, they may be the dominant catalytic species during the latter stages of the reaction. The higher trans/cis-2-pentene ratio observed for photolysis times > 10 minutes, may be attributed to these species since they are less sterically hindered than the dinuclear Fe-Fe double bonded intermediate. Also, the influence of the pore structure of PVG on the product distribution can not be neglected since substrate transformations occuring in the 70 ± 21 Å pores may have additional geometrical constraints imposed on them due to the low dimensionality of the support.

E. Methane Formation Via Photochemical Decomposition of $Fe_3(CO)_{12}$(ads).

In contrast to the photochemistry of $Fe(CO)_5$(ads) where the reaction products are dependent on surface loadings, the photochemistry of $Fe_3(CO)_{12}$ is independent of surface coverage. The UV-vis spectrum of a PVG sample impregnated with $2.2\pm.2 \times 10^{-8}$ moles of $Fe_3(CO)_{12}$/gram

PVG exhibits well resolved bands in the visible region at 605 and 440 nm along with a strong featureless UV absorbance. UV-vis spectra recorded during 350, 312 or 254-nm irradiation reveal a steady decline in the visible and UV bands of the physisorbed trimer with increasing photolysis time. The quantum yield value for trimer disappearance, 7.4×10^{-2}, indicates a relatively inefficient reaction, which is consistent with the results obtained by Jackson and Trusheim (100) who report that 355-nm irradiation of $Fe_3(CO)_{12}$ adsorbed on silica gel with a Q-switched Nd:Yag laser (ca. 20mJ/pulse) results in negligible trimer decomposition. The absence of new bands appearing in the near-UV and UV regions indicates that photodecomposition of $Fe_3(CO)_{12}$ on PVG does not result in formation of $Fe(CO)_5$(ads) or monomeric subcarbonyl species. Instead, the evolution of CO and H_2 concurrent with the decline in $Fe_3(CO)_{12}$(ads) absorbance, indicates that decarbonylation of the trimer is accompanied by oxidation of the iron atoms. Oxidation is confirmed by the inability of the photoproduct to thermally backreact with added CO and the absence of a FMR signal due to zerovalent iron particles.

In addition to H_2 and CO evolution, continued photolysis results in significant CH_4 evolution. Methane formation has been observed following the thermal and photochemical decomposition of supported mononuclear and

polynuclear metal carbonyls. Ballivet-Tkatchenko and Courdier (17) have investigated the thermal decomposition of $Fe_3(CO)_{12}$ adsorbed on HY zeolites. A progressive thermal treatment of the complex in vacuo reveals simultaneous evolution of CO, CO_2, and H_2 at 200 °C while at 250 °C methane formation is observed. In the thermal decomposition of Group VI hexacarbonyls supported on silica, Brenner (137) reports that heating the samples to 200 °C in vacuo resulted in irreversible oxidation of the metal with evolution of CO, CO_2, H_2 and CH_4. In a subsequent study, Brenner (42) examined the thermal decomposition of mononuclear and polynuclear metal carbonyls adsorbed on alumina. The formation of CH_4 was postulated to occur by the direct hydrogenation of carbonyl ligands, where the source of hydrogen is the surface hydroxyl groups of the alumina support.

Simon and Gafney (120c) have investigated the formation of methane following 254-nm photolysis of Group VIB hexacarbonyls adsorbed on PVG. Deuteration of the PVG prior to adsorption of $W(CO)_6$ was followed by 254-nm photolysis. Mass spectroscopic analysis of the gas phase reveals that CD_3H and CD_2H_2 are evolved. This study confirms the suggestion by Brenner that the ultimate source of hydrogen for methanation is either the chemisorbed H_2O or surface silanol groups present on the PVG surface. However, ^{13}C isotopic labelling studies

unequivocally establish that the carbon source for methanation is not coordinated CO. Mass spectroscopic studies of the gaseous effluent, following 254-nm photolysis of $W(^{13}CO)_6$(ads) (90% enriched), confirms only $^{12}CH_4$. These experiments establish that the carbon source for methane is not coordinated CO, but a carbonaceous impurity present on PVG. While an exact identification of the impurity has not been made, obvious possibilities include partially reduced carbonates, such as H_2CO_3 and HCO_3^-. These are reasonable postulates since the mass spectra establishes that the highest m/e ratio, 44, corresponds to CO_2, i.e., the only gaseous products detected up to a m/e of 368 are H_2, CO, CH_4, and CO_2. Indeed, elemental analysis of PVG indicates that there is 0.72% of a carbon oxide in PVG which is probably incorporated into the silica network. If this impurity is the carbon source for CH_4, an upper limit for CH_4 formation can be calculated. Since 3.02 grams of PVG were used in this particular experiment (Figure 59), the maximum amount of CH_4 that can be formed is ca. 10^{-2} moles, which is well above the total amount of 3.12×10^{-5} moles of CH_4 formed during 3000 minutes of 254-nm irradiation.

As shown in Figure 59, the time dependence of gas evolution indicates that significant amounts of H_2 are evolved prior to formation of CH_4. Thus, during 254-nm

photolysis of $Fe_3(CO)_{12}$(ads), extensive metal oxidation is required for CH_4 formation. This is consistent with previous results obtained for supported mononuclear and polynuclear metal carbonyls following both thermal and photochemical activation, which suggest that a metal oxide species mediates CH_4 formation. However, in the photochemically activated $Fe_3(CO)_{12}$-PVG system, the number of moles of CH_4 formed/mole of complex adsorbed is 139 ± 4, which is much larger than the values for methane formation previously reported for thermal activation of supported polynuclear metal carbonyls. For example, Basset and Chauvin (138) have reported that thermal decomposition of $Os_6(CO)_{18}$ and $Ir_4(CO)_{12}$ supported on alumina yields 0.30 and 0.38 moles of CH_4/mole of cluster, respectively. Brenner and coworkers (42), who have examined the thermal decomposition of polynuclear metal carbonyl clusters supported on alumina, report that the number of moles of CH_4 evolved per metal atom for $Fe_3(CO)_{12}$, $Ru_3(CO)_{12}$, and $Os_3(CO)_{12}$ are 0.021, 0.091, and 0.073, respectively.

Calculating the number of moles of electrons needed to form the total amount of H_2 and CH_4 observed during photolysis suggests a mechanism involving a catalytic cycle in which the metal undergoes a series of reversible redox reactions. If one assumes that each Fe atom is oxidized to a +3 oxidation state, since the ultimate

product appears to be Fe_2O_3, the total number of moles of electrons available for reduction is equal to 2.0×10^{-6}. Assuming that six electrons are needed for each mole of CH_4 produced, and that Fe is the only reductant present, 2×10^{-4} moles of electrons are needed to form the 1.28×10^{-5} moles of H_2 and 1.88×10^{-4} moles of CH_4 produced during 3000 minutes of 254-nm irradiation. This clearly establishes that the zerovalent Fe present on PVG at the onset of photolysis is not capable of supplying the equivalents of electrons required to produce the amounts of H_2 and CH_4 observed. Thus one is forced to the conclusion that the metal center undergoes a series of reversible redox reactions.

Several catalytic schemes have recently been proposed for methane formation during thermal activation of metal carbonyls. Shriver and coworkers (139), for example, have investigated the homogeneous reduction of CO to CH_4 by homonuclear and heteronuclear metal carbonyls. Their mechanism involves protonation of the carbonyl ligand, followed by loss of H_2O to yield a coordinated carbide intermediate. This species was postulated to undergo further protonation to yield methane. Brenner and coworkers (42,137), on the other hand, have proposed a mechanism for methane formation which involves oxidation of mononuclear sub-carbonyl species by the surface silanol groups of alumina or

silica supports. In this mechanism, catalytic activity is sustained by H_2, which serves as a reductant and regenerates the reduced metal center. The capability of H_2 to sustain catalytic activity by reducing the metal may offer an explanation for the enhanced methane formation observed following photochemical activation of $Fe_3(CO)_{12}$(ads). During the thermal activation of supported metal carbonyls, it is well established that a dynamic sintering of metallic particles to higher size occurs, particularly at temperatures > 473 K. In contrast, photochemical activation avoids sintering, yielding high metal dispersions even at relatively high metal loadings. The higher Fe metal dispersion in the photochemically activated $Fe_3(CO)_{12}$-PVG system, relative to thermal activation, may result in an increased accessibility of the reducing H_2 molecule to the oxidized Fe atom. This would sustain catalytic activity, resulting in increased methane formation. However, Figure 59 reveals a more complex situation; a sharp decline in H_2 evolution after 3000 minutes of photolysis is accompanied not by a sharp decline in CH_4 evolution, but only a slight decrease in CH_4 formation. Thus, H_2 reduction of the metal may account for some regeneration of the active center, but our data suggest that it is not sufficient to account for the propogation of the reaction sequence leading to CH_4 formation.

A full mechanistic interpretation for the photochemically activated methanation reaction on PVG obviously requires further investigation. However, some conclusions can be drawn. First, a photogenerated metal oxide species appears to mediate methane formation since, as noted above, the 2×10^{-4} moles of electrons required to form the 1.28×10^{-5} moles of H_2 and 1.88×10^{-4} moles of CH_4 far exceeds that available from the metal complex. Second, previous deuteration studies (120c) indicate that the source of hydrogen for methane formation is either the chemisorbed water or surface silanol groups present on the PVG surface. Third, mass spectroscopic measurements following 254-nm photolysis of isotopically labeled $W^{13}(CO)_6$ (120c) clearly establish that the carbon source for methane formation on PVG is not the coordinated carbonyl ligands. Rather, the carbon source is an impurity on PVG, most likely a partially reduced carbonate species, that is capable of adding hydrogen to form methane.

F. Photochemically Induced High Resolution Optical Density Changes Using $Fe(CO)_5$-PVG.

Impregnation of PVG with $Fe(CO)_5$ followed by exposure to light produces high resolution optical density changes in the glass. These optical changes are of little use, however, unless they could be "fixed",

i.e., made permanent and insensitive to further light exposure. Fixing was accomplished by gently heating the glass to ca. 200 C which volatilizes the unreacted $Fe(CO)_5$ from the PVG and stabilizes the photoproduct through further oxidation. The mechanism involved in producing the optical changes using $Fe(CO)_5$ adsorbed on PVG has been reported by Borelli and Morse (103c). Photolysis results in CO dissociation yielding a coordinatively unsaturated species which reacts with the surface silanol groups on PVG. Subsequent heating oxidizes the surface coordinated subcarbonyl species leaving a form of iron oxide bound to the glass. While an exact identification of the magnetic phase was not made by these researchers, magnetic susceptibility measurements reveal the presence of both superparamagnetic and single domain ferrimagnetic particles. Since the phase is ferrimagnetic, two possibilities that exist in the iron-oxide system are Fe_3O_4 and Fe_2O_3. Electron microscopy indicates the particle size distribution of the magnetic phase to be relatively uniform over the 50-100 Å range.

Further heating to ca. 900 °C collapses the porous structure of the glass producing the consolidated state. Although consolidation produces a 30% volume shrinkage, no loss of resolution in the light induced optical patterns is observed (see Figure 68). The resolution in

these experiments has been shown to be ca. 1 micrometer illustrating the potential of these materials for durable, photomask applications.

Conclusion

The adsorption, spectral properties, photochemical and photocatalytic reactions of iron carbonyls adsorbed onto Porous Vycor Glass have been investigated. Characterization of the adsorbed photoproducts by both spectroscopic and physical measurements has established that UV photolysis of $Fe(CO)_5$(ads) leads intially to formation of the primary photoproduct, $Fe(CO)_4$, with a quantum yield of approximately unity. The tetracarbonyl reacts quickly with the surface silanol groups and chemisorbed H_2O on the PVG surface to yield two spectrally distinct oxidative addition products, H-$Fe(CO)_4$-OSi and H-$Fe(CO)_4$-OH, independent of surface loading. The secondary photochemical and thermal reactions of the oxidative addition products were found to be dependent on surface loading. At surface loadings $< 10^{-6}$ moles $Fe(CO)_5$(ads)/gram, continued photolysis leads to formation of zerovalent particles of atomic iron. While the large linewidth of the ferromagnetic resonance signal (FMR) at room temperature suggests formation of a iron particle $\leq$ 15 Å, further experiments to determine the temperature dependence of the FMR resonance are needed to investigate the particle size distribution of the atomic iron.

At higher loadings, $\geq 10^{-6}$ moles $Fe(CO)_5$(ads)/gram, UV photolysis leads to formation of the $Fe_3(CO)_{12}$ cluster. Both spectroscopic and physical measuresments establish that trimer formation arises from secondary thermal reactions of the photogenerated adsorbates. Time resolved FTIR spectra recorded after excitation with both pulsed and cw lasers, as well as trapping experiments with CO and trimethylphosphine, have allowed postulation of a mechanism for $Fe_3(CO)_{12}$ formation in which the intermediates leading to trimer formation are highly unsaturated. The photoproduct decay sequence indicates the principal intermediate involved in trimer formation, $Fe(CO)_3$, arises from secondary photochemical reactions of the least stable oxidative addition product, H-$Fe(CO)_4$-OH.

The photochemical and thermal reactions of $Fe(CO)_5$(ads) in the presence of ethylene and 1-pentene have also been investigated. DRIFT spectra recorded following cw laser excitation have revealed the presence of catalytically significant monomeric and dimeric iron carbonyl-olefin complexes. In addition, the 1-pentene isomerization reaction was used as a probe reaction to investigate the photocatalytic properties of the $Fe(CO)_5$-PVG hybrid system. UV irradiation of $Fe(CO)_5$(ads) resulted in significant isomerization of 1-pentene to cis and trans-2-pentenes. The time dependence of the

reaction, as well as the high quantum yield value, parallel that observed for the $Fe(CO)_5$ photocatalyzed 1-pentene isomerization in both solution and gas phase. The product distribution for the $Fe(CO)_5$-PVG hybrid system resembles that observed for $Fe(CO)_5$ species which contain bulky ligands in their coordination sphere. This illustrates the potential for creating novel, more selective catalysts via photoactivation of hybrid catalysts using iron carbonyl precursors.

The photochemistry of $Fe_3(CO)_{12}$(ads) was also investigated. The adsorbed cluster was found to be photochemically inert relative to $Fe(CO)_5$(ads). In contrast to the monomer, UV photolysis of $Fe_3(CO)_{12}$(ads) resulted in extensive metal oxidation and methane evolution. A comprehensive interpretation for the photochemically activated methanation reactions observed on PVG will require spectroscopic observation, probably via diffuse reflectance FTIR, of the carbonaceous intermediates involved.

The potential for using the $Fe(CO)_5$-PVG system to create high optical density changes in the glass was also investigated. The high resolution obtained in these experiments suggests that refining and improving this and other systems may be a fruitful area of research.

References

(1) Bailey, D.C.; Langer, S.H. Chem. Revs., 1981, 81, 109.

(2) Wender, I.; Pino, P., Eds. "Organic Synthesis Via Metal Carbonyls," Interscience: New York, 1968.

(3) Braterman, P.S., "Metal Carbonyl Spectra," Academic Press: New York, 1975.

(4) (a) Manassen, J.; Whitehurst, D.D. "Progress in Catalysis," Basolo, F.; Burwell, R.L., Jr., Eds.; Plenum Press: New York, 1973: p. 177.
(b) Michalska, Z.M.; Webster, D.E. CHEMTECH, 1975, 5, P.117.

(5) Cotton, F.A.; Wilkinson, G. "Advanced Inorganic Chemistry," Interscience: New York, 3rd ed., 1972, Chapter 24, p.770.

(6) Nakamura, A.; Tsutsui, M. "Principles and Applications of Homogeneous Catalysis", Wiley: New York, 1980.

(7) Parshall, G.W. "Heterogeneous Catalysis, Homogeneous Catalysis", Wiley: New York, 1980.

(8) "Transition Metal Mediated Organic Synthesis", Slocum, D.W.; Hughes, O.R., Eds., Ann. N.Y. Acad. Sci., Vol. 53., 1980.

(9) Wrighton, M.S. Chem. Revs., 1974, 74, 401.

(10) Strohmeier, W.; Gerlach, K. Chem. Ber., 1961, 94, 398.

(11) Wrighton, M.S.; Ginley, D.S. J. Am. Chem. Soc., 1975, 97, 2065.

(12) (a) Geoffroy, G.L.; Gray, H.B.; Hammond, G.S. J. Am. Chem. Soc., 1975, 97, 3933.
(b) Geoffrey, G.L.; Bradley, M.G.; Pierantozzi, R. Adv. Chem. Ser., 1978, 167, 181.

(13) Taqui Khan, M.M.; Martell, A.E. "Homogeneous Catalysis in Metal Complexes," Academic Press: New York, 1974, Vols. 1 and 2.

(14) Avnir, D.; Farin, D. Nature, 1984, 308, 261

(15) (a) Pfeifer, P.; Avnir, D. J. Chem. Phys., 1983, 79, 3558.
(b) Avnir, D.; Farin, D.; Pfeifer, P. ibid., 1983, 79, 3566.

(16) Nagy, N.B.; Eenoo, M.V.; Derouane, E.G. J. Catal., 1979, 58, 230.

(17) Ballivet-Tkatchenko, D.; Coudurier, G. Inorg. Chem., 1979, 18, 558.

(18) (a) Yawney, D.B.W.; Stone, F.G.A. J. Chem. Soc. A., 1969, 502.
(b) Knight, J.; Mays, M.J. J. Chem. Soc., Chem. Commun., 1970, 1006.

(19) (a) Bigorgne, M. Organomet. Chem., 1970, 24, 211.
(b) Cataliotti, P.; Foffani, A.; Marchetti, L. Inorg. Chem., 1971, 10, 1594.

(20) (a) Brenner, A. Chem. Commun., 1979, 251.
(b) Brenner, A.; Burwell, R.L., Jr., J. Catal., 1978, 52, 353.

(21) Jermyn, J.W.; Johnson, T.J.; Vansant, E.F.; Lunsford, J.H. J. Phys. Chem., 1973, 77, 2964.

(22) Angell, C.L.; Schaffer, P.C. J. Phys. Chem., 1966, 70, 1413.

(23) Phillips, J.; Clausen, B.; Dumesic, J.A. J. Phys. Chem., 1980, 84, 1814.

(24) Bartholmew, B.H.; Boudart, M. J. Catal., 1972, 25, 173.

(25) Bette, J.; Kinoshita, K.; Roulsis, K.; Stonehart, P. J. Catal., 1973, 29, 160.

(26) Pope, D.; Smith, W.L.; Eastlake, M.J.; Moss, R.L. J. Catal., 1971, 22, 72.

(27) Hunt, C.E. J. Catal., 1971, 23, 93.

(28) Farmery, K.; Kilner, M.; Greatrex, R.; Greenwood, N.N. J. Chem. Soc., A, 1969, 2339.

(29) Hugues, F.; Basset, J.M.; Taarit, Y.B.; Choplin, A.; Primet, M.; Rojas, D.; Smith, A.K. J. Am. Chem. Soc., 1982, 104, 7020.

(30) Ugo, R.; Psaro, R; Zanderighi, G.M.; Basset, J.M.; Theolier, A.; Smith, A.K. Fund. Res. Homogeneous Catal., 1979, 3, 579.

(31) Besson, B.; Moraweck, B.; Smith, A.K.; Basset, J.M.; Psaro, R.; Fusi, A.; Ugo, R. J. Chem. Soc., Chem. Commun., 1980, 569.

(32) (a) Smith, A.K.; Besson, B.; Basset, J.M.; Psaro, R.; Fusi, A; Ugo, R. J. Organomet. Chem., 1980, 192, C31.
(b) Psaro, R.; Ugo, R.; Zanderighi, G.M.; Besson, B.; Smith, A.K.; Basset, J.M. ibid., 1981, 213, 215.

(33) Deeba, M.; Gates, B. J. Catal., 1981, 67, 303.

(34) Watson, P.L.; Schrader, G.L. J. Mol. Catal., 1980, 9, 125.

(35) Hugues, F.; Besson, B.; Bussiere, P.; Dalmon, J.A.; Basset, J.M.; Olivier, D. Nouv. J. Chim., 1981, 5, 207.

(36) Hugues, F.; Bussiere, P.; Dalmon, J.A.; Basset, J.M.; Olivier, D.; Commereuc, D.; Chauvin, Y.; Bonneviot, L. Preprints VII. Int. Cong. Catal., Tokyo, 1980, paper A. 51.

(37) Dorman, J.L.; Gibout, P.; Suran, S.; Sella, C. Physica, 1977, 86-88 B, 1431.

(38) Kunding, W.; Ando, K.J.; Lindquist, R.H.; Constabain, G. Czech. J. Phys., 1967, 17, 467.

(39) Dumesic, S.A.; Topse, H.; Khammouna, S.; Boudart, M. J. Catal., 1975, 37, 503.

(40) Che, M.; Richard, M.; Olivier, D. J. Chem. Soc., Faraday I, 1980, 76, 1526.

(41) Brenner, A.; Hucul, D.A. Inorg. Chem., 1979, 18, 2836.

(42) Brenner, A.; Hucul, D.A. J. Am. Chem. Soc., 1980., 102, 2484.

(43) McVicker, G.B.; Vannice, M.A. J. Catal., 1980, 63, 25.

(44) (a) Donohue, J.; Caron, A. Acta. Crystallogr., 1964, 17, 663.
(b) Hanson, A.W.; ibid., 1962, 15, 930.

(45) (a) Sheline, R.K.; Pitzer, K.S. J. Am. Chem. Soc., 1950, 72, 1107.
(b) Cataliotti, R.; Foffani, A.; Marchetti, L. Inorg. Chem., 1971, 10, 1594.

(46) (a) Brill, R. Z. Krissallogr., Kristallphys., Kristallchem., 1927, 65, 85.
(b) Powell, H.M.; Ewen, V.G. J. Chem. Soc., 1939, p. 286.

(47) Wei, C.H.; Dahl, L.F. J. Am. Chem. Soc., 1969, 91, 51.

(48) (a)Turner, J.J., Poliakoff, M., J. Chem. Soc., Chem. Commun., 1970, 1008.

(49) Johnson, B.F.G. J. Chem. Soc., Chem. Commun., 1976, 703

(50) Lundquist, R.T.; Cais, M. J. Org. Chem., 1962, 27, 1167.

(51) Dartiguenave, M., Dartiguenave, Y.; Gray, H.G. Bull. Soc. Chim. Fr., 1969, 12, 4223.

(52) Gray, H.B.; Levenson, R.A.; Tyler, D.B. J. Am. Chem. Soc., 1978, 100, 7888.

(53) (a) Stolz, I.W.; Dobson, G.R.; Sheline, R.K. J. Am. Chem. Soc., 1962, 84, 3589.
(b) ibid., 1963, 85, 1013.

(54) Koerner Von Gustorf; Grevels, E.F. Top. Current Chem., 1969, 13, 366.

(55) Graham, W.A.G.; Jetz, W. Inorg. Chem., 1971, 10, 4.

(56) Chisolm, M.H.; Massey, A.G.; Thompson, N.R. Nature (London), 1966, 211, 67.

(57) Dewar, J.; Jones, H.O. Proc. R. Soc. London, Ser. A, 1905, 76, 558.

(58) Braye, E.H.; Huebel, W. Inorg. Synth., 1966, 8, 178.

(59) Schubert, E.H.; Sheline, R.K. Inorg. Chem., 1966, 5, 1071.

(60) Koerner Von Gustorf, Henry, M.C.; DiPetro, C. Z. Naturforsch. B, 1966, B21, 42.

(61) Cotton, F.A. Prog. Inorg. Chem. 1976, 21, 1.

(62) Birenewaig, F.; Shamai, H.; Shvo, Y. Tetrahedron Lett. 1979, 2947.

(63) Dawson, P.A.; Peake, B.M.; Robinson, B.H.; Simpson, J. Inorg. Chem., 1980, 19, 465.

(64) (a) Nathanson, G.; Gitlin, B.; Rosan, A.M.; Yardley, J.T. J. Chem. Phys., 1981, 74, 361.
(b) Nathanson, G.; Gitlin, B.; Rosan, A.M.; Yardley, J.T. ibid., 1981, 74, 370.

(65) Ouderkirk, A.J.; Wermer, P.; Shultz, N.L.; Weitz, E. J. Am. Chem. Soc., 1983, 105, 3354.

(66) Ouderkirk, A.J.; Weitz, E. J. Chem. Phys., 1983, 79, 1089.

(67) Hallam, H.E., Eds. "Vibrational Spectroscopy of Trapped Species," Wiley: London, 1973

(68) Poliakoff, M.; Turner, J.J. J. Chem. Soc., Dalton, 1973, 1351.

(69) Poliakoff, M.; Turner, J.J. J. Chem. Soc., Dalton, 1974, 2276.

(70) Davies, B.; McNeish, A.; Poliakoff, M.; Turner, J.J. J. Amer. Chem. Soc., 1977, 99, 7573.

(71) Barton, T.J.; Grinter, R.; Thomson, A.J.; Davies, B.; Poliakoff, M. J. Chem Soc., Chem. Commun., 1977, 841.

(72) Poliakoff, M.; Turner, J.J. J. Chem. Soc., Faraday II, 1974, 70, 93.

(73) Mann, D.M.; Broida, H.P. J. Chem. Phys., 1971, 55, 84.

(74) Poliakoff, M.; Turner, J.J. J. Chem. Soc., A, 1971, 2403.

(75) Austin, R.G.; Paonessa, R.S.; Giordano, P.J.; Wrighton, M.S. Adv. Chem. Ser., 1978, 168, 189.

(76) Graff, J.L.; Sanner, R.D.; Wrighton, M.S. J. Am. Chem. Soc., 1979, 101, 273.

(77) Tyler, D.R.; Levenson, R.A., Gray, H.B. J. Am. Chem. Soc., 1978, 100, 7888.

(78) Asigner, F.; Fell, B.; Schrage, K. Chem. Ber., 1965, 98, 372.

(79) Schroeder, M.A.; Wrighton, M.S. J. Am. Chem. Soc., 1976, 98, 551.

(80) Faltynek, R.A. Inorg. Chem., 1981, 20, 1357.

(81) Mirbach, M.J.; Mirbach, M.F.; Saus, A.; Topalsavoglou, N.; Tuyet, N.P. J. Am. Chem. Soc., 1981, 103, 7590.

(82) Garner, F.; Krausz, P.; Dubois, J.E. J. Organometal. Chem., 1979, 170, 195.

(83) Wrighton, M.S.; Ginley, D.S.; Schroeder, M.A.; Morse, D.L. Pure Appl. Chem., 1975, 41, 671.

(84) Bond, G.C.; Hellier, M.J. J. Catal., 1965, 4, 1.

(85) Wrighton, M.S.; Graff, J.L.; Reichel, C.L.; Sanner, R.D. "Transition Metal Mediated Organic Synthesis" Slocum, D.W.; Hughes, O.R., Eds., New York Academy of Science: New York, 1980; Vol. 333, p. 188.

(86) Stone, F.G.A.; West, R., Eds. "Advances in Organometallic Chemistry," Academic Press: New York, 1979, Vol. 17.

(87) Kochi, J.K. "Organometallic Mechanisms and Catalysis," Academic Press: New York, 1978.

(88) Forster, D.; Roth, J.F., Eds. "Homogeneous Catalysis," American Chemical Society: Washington D.C., 1974, Adv. Chem. Ser. No. 132.

(89) Henrici-Olive, G.; Olive, S. Angew. Chem., Int. Ed. Engl., 1971, 10, 105.

(90) Graff, J.L.; Sanner, R.D.; Wrighton, M.S. Organometallics, 1982, 1, 837.

(91) Swartz, G.L.; Clark, R.J. Inorg. Chem. 1980, 19, 3191.

(92) Whetten, R.L.; Fu, Kejian; Grant, E.R. J. Am. Chem. Soc., 1982, 104, 4270.

(93) Whetten, R.L.; Fu, Kejian; Grant, E.R. J. Chem. Phys., 1982, 77, 3769.

(94) Mitchener, J.C.; Wrighton, M.S. J. Am. Chem. Soc., 1981, 103, 975.

(95) Chase, D.B.; Weigert, F.J. J. Am. Chem. Soc., 1981, 103, 977.

(96) Mitchener, J.C.; Wrighton, M.S. J. Am. Chem. Soc., 1983, 105, 1065.

(97) De Paoli, M.A. J. Macromol. Sci., 1981, A16, 251.

(98) Burdett, J.K. Coord. Chem. Rev., 1978, 27, 1.

(99) Trusheim, M.R.; Jackson, R.L. J. Am. Chem. Soc. 1982, 104, 6590.

(100) Trusheim. M.R.; Jackson, R.L. J. Chem. Phys., 1983, 87, 1910.

(101) Sanner, R.D.; Austin, R.G.; Wrighton, M.S.; Honnick, W.D.; Pittman, C.U. Inorg. Chem., 1979, 18, 928.

(102) Suib, S.L.; Kostapapas, A.; McMahon, K.C.; Baxter, J.C.; Winiecki, A.M. Inorg. Chem., 1985, 24, 858.

(103) (a) Borelli, N.F.; Morse, D.L. Appl. Phys. Lett., 1983, 43, 992.
(b) Borelli, N.F.; Morse, D.L.; Scheurs, J.W.H. J. Appl. Phys., 54, 3344.

(104) Hood, H.P.; Nordberg, M.E. U.S. Pat. 2,215,039.

(105) Nordberg, M.E. J. Am. Ceram. Soc., 1944, 27, 299.

(106) Elmer, T.H.; Fehlner, A. Corning Glass Company, private communication, 1977 and 1978.

(107) Elmer, T.H.: et. al. J. Am. Ceram. Soc., 1970, 53, 171.

(108) Sakairo, T. Hyomen, 1971, 9, 115.

(109) Pierce Chemical Company., Rockford Ill., General Catalogue (1976-1977), p. 215.

(110) Spatorico, A.L. J. Appl. Polym. Sci., 1975, 12, 1601.

(111) Iler, R.K. "The Chemistry of Silica," Wiley-Interscience: New York, 1979, p. 551.

(112) Hockey, J.A. Chem. Ind. 1965, 57.

(113) Davydov, V.Y. Trans. Faraday Soc., 1964, 60, 2254. Russ. J. Phys. Chem., 1964, 38, 1108.

(114) Kiselev, A.V. "The Structure and Properties of Porous Materials," D.H. Everett and F.S. Stone, Eds., Butterworth: London, 1958, p. 195.

(115) (a) Janowski, V.F.; Heyer, W. Z. fur Chemie, 1979, 19, 1.
(b) All, K.G. J. Organometall. Chem., 1975, 87, 203.

(116) Basu, A.; Gafney, H.D.; Perettie, D.T.; Clark, J.B. J. Phys. Chem., 1983, 87, 4532.

(117) Goonatillake, H.W., Ph.D Thesis, City University of New York, January, 1986.

(118) Hair, M.L.; Chapman, I.D. J. Am. Ceram. Soc., 1966, 49, 651.

(119) Evan, U.; Rademan, K.; Jortner, J.; Manor, M.; Reisfeld, R. Phys. Rev. Letters, 1984, 52, 2164.

(120) (a) Kennely, T., Ph.D Thesis, City University of New York, June, 1980.
(b) Wolfgang, S.W., Ph.D Thesis, City University of New York, Feb., 1983.
(c) Simon, R., Ph.D Thesis, City University of New York, Feb., 1983.

(121) Anpo, M.; Yun, C.; Kubokawa, Y. J. Catal., 1980, 61, 267.

(122) Simon, R.; Gafney, H.D.; Morse, D.L. Inorg. Chem., 1983, 22, 573.

(123) Simon, R.; Gafney, H.D.; Morse. D.L. Inorg. Chem., 1985, 24, 2565.

(124) Dieter, T., Ph.D Thesis, City University of New York, September, 1985.

(125) Schubert, E.H.; Sheline, R.K. Inorg. Chem., 1966, 5, 1071.

(126) Ross, S.; Olivier, J.P. "On Physical Adsorption," Wiley-Interscience: New York, 1964, Chapter 2, Section 1, p. 31.

(127) (a) Hatchard, C.G.; Parker, C.A. Proc. Roy. Soc., Ser. A., 1956, 235, 518.
(b) Calvert, J.G.; Pitts, J.N. "Photochemistry," Wiley: New York, 1971.

(128) (a) Cant, N.W.; Little, L.H. Can. J. Chem., 1965, 43, 1252. (b) Cant, N.W.; Little, L.H. ibid., 1964, 42, 802.

(129) Bein, T.; Jacobs, P.A. J. Chem. Soc., Faraday Trans., 1983, 79, 1819.

(130) Herpui, A. "Theorie de Magnetisme," PUF: Paris, 1968, p. 437.

(131) Che, M.; Richard, M.; Olivier, D.; J. Chem. Soc., Faraday I, 1980, 76, 1526.

(132) Poliakoff, M.; Chem. Soc. Reviews, 1978, 7, 527.

(133) Wrighton, M.S.; Schroeder, M.A. J. Organomet. Chem., 1977, 128, 345.

(134) Sweany, R.L. J. Am. Chem. Soc., 1981, 103, 2410.

(135) Filscher, I.; Hildenbrand, K.; Koerner von Gustorf, E. Agnew. Chem., Int. Ed. Engl., 1975, 14, 54.

(136) Ellerhorst, G.; Gerhartz, W.; Grevels, F.W. Inorg. Chem., 1980, 19, 67.

(137) Brenner, A.; Hucul, D.A.; Hardwick, S.J. Inorg. Chem., 1979, 18, 1478.

(138) Smith, A.K.; Theolier, A.; Basset, J.M.; Ugo, R.; Chauvin, Y.; Commereuc, D.; J. Am. Chem. Soc., 1978, 100, 2590.

(139) (a) Drezdou, M.A.; Whitmire, K.H.; Bhattacharyya, A.A.; Hsu, W.L.; Nagel, C.C.; Shore, S.G.; Shriver, D.F. J. Am. Chem Soc., 1982, 104, 5630.
(b) Whitmire, K.H.; Shriver, D.F. J. Am. Chem. Soc., 1981, 103, 6754.